UNIVERSITEIT VAN PRETORIA
UNIVERSITY OF PRETORIA
YUNIBESITHI YA PRETORIA

Performance characteristics of a deep tilling rotavator

Moses Okoth Marenya

Submitted in partial fulfilment of the requirements for the degree

Philosophiae Doctor

in the

Faculty of Engineering, Built Environment and Information Technology

University of Pretoria

Pretoria

September, 2009

UNIVERSITEIT VAN PRETORIA
UNIVERSITY OF PRETORIA
YUNIBESITHI YA PRETORIA

SUMMARY

Performance characteristics of a deep tilling rotavator

Supervisor: Professor H. L. M. du Plessis

Department: Civil and Biosystems Engineering

Degree: Philosophiae Doctor

The continued increase in the price of fossil-based fuels and lubricants has resulted in tremendous increase in the cost of land preparation. This has resulted in considerable increase in the cost of food. The situation is worsened by the prevalent use of the conventional tillage system in the preparation of seedbeds; particularly for deep tillage. This system of tillage escalates land preparation costs because it requires a series of operations using passive tillage tools to realise an acceptable tilth quality. It also ties down capital in the form of additional machinery and tillage tools; thus increasing significantly the cost of land preparation. Therefore, it is necessary to design better tillage tools that are capable of reducing the number of tillage operations required for the realization of seedbeds of acceptable tilth quality.

The rotavator is one of the tillage tools with the capability for realizing the desired soil tilth quality with significantly reduced number of tillage passes. In comparison to passive tools, the rotavator has a superior soil mixing and pulverisation capability. When rotated in the down-cut direction, it generates a forward thrust that aids traction under difficult field conditions. However, no documented analytical models capable of predicting the performance of rotavators fitted with commercially available blades was found in literature. In addition, there is dearth of information on the behaviour of the magnitude of the horizontal thrust forces generated for a down-cut rotavator for different set tillage depths.

This study was undertaken to develop an analytical model that is capable of predicting the torque requirements of a rotavator fitted with commercially available L-shaped blades. In developing the proposed model, an analytical approach based on the limit equilibrium

analysis was used. An interactive computer program was developed, in MATLAB (*Version 7, Mathworks Inc., USA*), to solve the proposed model. The proposed model was verified by comparing the model and measured torque requirement at predetermined rotavator blade angular positions from the horizontal for a down-cut rotavator.

Field experiments were conducted in a sandy loam soil, using two instrumented research equipment. The research equipment were calibrated in a laboratory and field-tested prior to conducting the field experiments. A torsional shearing apparatus was used to characterize the soil by determining the soil shear strength and soil-metal friction parameters. The rotavator operational parameters, necessary for analyzing its performance, were recorded using an instrumented tool-frame carrier. The experiments were conducted in the down-cut direction of rotation, in the 200 mm – 500 mm set tillage depth range.

The study findings indicated that there was an optimum set tillage depth for each rotavator configuration and operational conditions at which the resultant horizontal thrust generated was greatest. This unique depth was influenced by the bite length. The validation of the proposed model showed that the predicted and measured torque requirements, at different angular blade positions from the horizontal, correlated reasonably well for all the set tillage depths. As the depth of tillage increased, however, the curve for the measured torque requirements exhibited a cyclic behaviour after the peak torque requirements value had been recorded. The cyclic behaviour was probably due to the re-tilling and the instability of the tool-frame carrier, which increased with the set tillage depth.

The knowledge contributed by this research will afford the designers of active tillage tools a better understanding of the operations of the rotavator, particularly in deep tillage. The modelling approach, and instrumentation technique used in this research, can be extended to analyze the performance of rotavators fitted with other types of commercial blades.

Key terms: rotavator, deep-tilling, soil-failure modelling, tillage performance, soil shear strength, soil-metal friction, bite length, kinematic parameter, down-cut rotavator, power, specific energy

ACKNOWLEDGEMENTS

I wish to express my sincere appreciation to the following organizations and individuals who made the realization of the work reported in this thesis possible.

- The University of Nairobi, Kenya, for giving me a study leave to pursue these studies.
- Log Associates, a firm of consulting engineers, based in Nairobi, Kenya and her staff. The financial and moral support you accorded me during my extended absence from the office is greatly appreciated.
- The Department of Civil and Biosystems Engineering, University of Pretoria for funding the research. This support is gratefully acknowledged and appreciated.
- The following persons are gratefully acknowledged for their assistance during the course of this study.

    a) Prof H. L. M. du Plessis, my supervisor for his guidance, support and availing the funds for the research component of this study.

    b) Mr. D. Gouws, formerly the Workshop Manager, Agricultural Engineering Workshop, Department of Civil and Biosystems Engineering, University of Pretoria. His role in the instrumentation of the research equipment, used in this study, was vital.

    c) Messrs J. Nkosi, W. Morake and D. Sithole; Technical Assistants in the Agricultural Engineering Workshop, University of Pretoria. They all played important roles during field work undertaken for data collection.

    d) Dr. T. Yu; for introducing me to MS Visio and MATLAB software packages that were used extensively in this work.

    e) My family, children, relatives and friends for their support, encouragements; and for enduring my absence from their lives for such a long period of time.

In memory of my dear mother, the late Mama Meresia Odundo Orony-Marenya (Nyar Aol)

Table of Contents

LIST OF FIGURES

LIST OF TABLES

NOMENCLATURE

τ_{max} = maximum shear stress at soil-soil failure surface (kPa)

ρ = angle that the rupture surface makes with the horizontal (degrees)

σ_n = normal stress (kPa)

ϕ = soil internal friction angle (degrees)

ψ' = the angle formed by the positive direction of the tangent at the given point of the cycloid and the positive direction of the abscissa (degrees)

γ = unit weight (or bulk density) of the soil (kN/m^3)

β = angle that the tool makes with the horizontal during an instantaneous time moment (degrees).

$\overline{z}_c$ = depth from the top of the failed soil wedge (m)

N_γ, N_c, N_q = factors dependent on soil frictional strength, soil geometry and tool to soil strength properties (dimensionless)

N_c' = cohesion N-factor (dimensionless)

τ_f = maximum frictional stress at the soil-tool interface (kPa)

V_{cir} = peripheral velocity of the rotor blades (m/s)

τ_o = soil property related to static component of the static shear strength (kPa)

τ_i = soil property related to the dynamic component of soil shear strength, proportional to the operating speed (kPa (ms^{-1})$^{-1}$)

N_q' = surcharge N-factor (dimensionless)

α_{c_2} = the angle at the second blade make with the maximum crest height (degrees)

$\frac{2\pi}{z}$ = the angle between any two adjacent blades on a flange on the rotor (rad.)

α_{c_1} = the angle the first blade makes with the maximum crest height, h_c (degrees)

τ_{max} = maximum shear stress at failure (kPa)

A = effective area of the grouser head or the flat steel plate of the torsional shear apparatus in contact with the soil (m^2)

a, b = regressions coefficients, which were all significant at 1 % level (Stafford & Tanner, 1983a, 1983b)

A_1 = area of the span in contact with the soil, 'area abed, in Fig. 3.16' (m^2),

A_2 = area of the triangular rupture surface, 'area abc or def in Fig. 3.16' (m^2)

A_3= areas of the rectangular rupture surface 'area bcfe in Fig. 3.16' (m^2)

C_a = soil metal adhesion factor (kN/m^2)

C_c= soil cohesion (kN/m^2)

d = depth of tillage (m)

$d_1 \ldots d_n$ = distance covered in respective plots during a test run

d_c = critical tillage depth (m)

d_e = effective depth of transverse failure (m)

D_f = Resultant draft force (N)

d_i = instantaneous depth of wire from soil surface

d_z = average depth to the centroid of failure wedge (m)

E_{rot} = power required for the rotary work (kW)

$f(v)$ = function containing the soil inertial term (kN)

F_d = draft force under dynamic conditions (kN)

F_n = the applied 'constant' normal load (kN)

F_s = static draft force component (kN)

g = gravitational acceleration, ≈ 9.81 (m/s^2)

h_c = the peak crescent height at the bottom of the cut furrow (m)

H_{dc}= draft for a blade operated at deep tillage depth (kN)

H_l = draft for the lateral soil failure (kN); Godwin and Spoor (1967) model

H_s = draft for a blade operated at a shallow tillage depth (kN)

H_t = draft for crescent above the critical depth (kN); Godwin and Spoor (1977) model

k = ratio of critical depth to width (dimensionless)

k_1, k_2, k_3 = constants for both soils at all soil water contents (Stafford & Tanner, 1983a)

K_i = tine inclination factor (dimensionless, Hettiaratchi and Reece (1967) model)

K_o = ratio of the horizontal and static vertical stress, $K_o = (1 - \sin\phi)$

L = length of the span of the blade in contact with the soil (m)

L_b = the bite length (m)

L_{ps} = the length of the blade to the point of action of the soil-blade resistance force P_s (m)

L_{tr} = tilling route length (m)

M = the maximum torque or the maximum resisting moment (kNm)

z_n = number of blades of the rotavator that pass through the soil in time t

N_a = an additional factor comprised in soil cutting forces, which accounts for the acceleration forces in the soil with varying tool speeds, but a fixed soil strength

N_a = an additional factor comprised in the soil cutting force, which accounts for the acceleration forces in the soil for varying tools speed, but a fixed soil strength (dimensionless)

N_{ca} = a dimensionless factor that dependent on the soil-metal adhesion

N_{ca} = a dimensionless factor that depends on soil-metal adhesion

N_γ, N_c, N_q = a dimensionless factors depend on soil frictional strength, soil geometry, and tool to soil strength properties

P = total force (kN)

P_1 = force applied to the centre wedge (kN)

P_2 = force applied to the side crescent of the soil (kN)

P_o = geostatic stress (Pa)

P_r = soil resistance force due to the penetration resistance (kN)

P_{rot} = rotary power required to process the soil (kW)

P_s = soil resistance force due to the span and leg of the L-shaped blade (kN)

q = surcharge pressure vertically acting on the soil surface (kNm^{-2})

Q = the normal acting force on the soil-soil interface of the failed soil wedge (N)

Q_s= force upon face of tip of the span (kN)

R = rotor radius (m)

R_{cr}= reaction force acting on the side of the centre wedge (kN)

r_i = inner radius of the annulus shear ring head with grousers (m)

r_o = outer radius of the annulus ring head with grousers (m)

t = time of rotation of the rotor through angle α (s).

t_1 = time taken by the leading blade to turn through angle α_{c1}(s)

t_2 = time taken by the second blade to turn through angle α_{c2} (s)

t_b = time during which the blades rotate through an angle, equal to the angle between the adjacent blades on the same side of a flange (s)

t_{bt} = thickness of the cutting edge of the span of the blade (m)

t_i = time of rotation of a blade through angle, α_i from the horizontal (s)

T_{meas} = experimental torque requirement values at different angular position of the tip of the cutting blade during soil processing (kNm)

T_{mod} = model generated torque requirements values at different angular positions of the tip of the cutting blade during soil processing (kNm)

T_{pr} = instantaneous time moment torque requirement due to force P_r (kNm)

T_{ps} = instantaneous time moment torque requirement due to force P_s (kNm)

T_{total} = total instantaneous time moment torque requirement (kNm)

V = instantaneous peripheral velocity of the tool along the cycloidal path, (m/s)

V_{ac} = actual soil chip volume processed by a single blade (m^3)

V_f = forward travel speed (m/s)

V_f = forward travel speed of the tractor for rotary tillage or the speed of the tool for a passive tillage implement (m/s)

V_i = the instantaneous peripheral velocity of the tool along the cycloidal path, (m/s.)

V_s = sliding velocity of the blade (m/s)

V_{wsv} = total volume of the soil tilled in time, t (m^3)

w = tool width (m)

α = the angle of rotation of the blade from the horizontal position (degrees)

α_i = the angle the blade turns through in time, t_i (rad)

α_r = the intercept on the vertical axis for predicted versus measured torque linear regression

β = rake angle (degrees)

γ = soil bulk density (kN/m^3)

δ = soil-metal friction angle (degrees)

ϑ = thickness of cross-section of the cut soil slice (m)

ω = rotor speed (rad/s)

CHAPTER 1

INTRODUCTION

1.1 Background

The rotavator (derived from *rotary* cultivator) or rotary tiller is a tillage tool primarily comprising L-shaped blades mounted on flanges, which are attached to a shaft that is driven by the tractor power-take-off (PTO) shaft. It is an active tillage tool that processes the soil at a speed that is different from the forward travel speed of the tractor. With respect to depth of tillage, the rotavator is unique in that during its operation, the actual depth of tillage for each blade changes throughout the rotational path of the cutting blade.

Historical records have traced the cultivation of land, in Europe, with active tillers back almost 170 years when steam engine tractors were introduced in agriculture (Bernacki, Haman & Kanafojski, 1972). Since their original design in the 1840s, along with the application of steam power to agriculture (Spence as cited by Hendrick & Gill, 1971a), they have been devices that inspired both enthusiasm and controversy. The controversy still exists but a number of inherent advantages of tillage tools that transmit power directly to the soil require that they be considered as an alternative to tools that are drawn through the soil (Hendrick & Gill, 1971a).

The entry of the rotavator in agriculture is relatively recent in comparison to hand tools and animal-drawn tillage tools. The delayed entry of rotavators is attributed to the lack of suitable sources of power, prior to the development of the steam powered tractor. The original rotavators were intended for deep land preparation as an alternative to the drawn or passive tillage tools. They were heavy machines that expended excessive energy per unit mass of processed soil at the intended depths of operation. These rotavators suffered frequent mechanical breakdowns during tillage operations (Bernacki

et al., 1972). The combination of the excessive power demand and frequent breakdowns led to their rejection as an alternative to the passive tools for primary land preparation.

In tillage, rotavator blades may be rotated on vertical-axis or horizontal-axis rotor shafts (Figure1.1). The resulting texture of rotavator-tilled soil is a function of the soil condition, blade kinematics and soil flow dynamics (Kinzel, Holmes & Huber, 1981). The soil flow dynamics depends on whether the rotor axis of the cultivator is horizontal or vertical; and on the direction of rotation of the blades. For the horizontal rotor axis, the blades may be rotated in the down-cut or up-cut direction; while for the vertical axis, the direction of rotation may be clockwise or anti-clockwise. In general, rotavators work on the horizontal axis rotor; and seldom on a vertical or series of vertical axis rotors (Bukhari, Bukhari, Leghari & Memon, 1996).

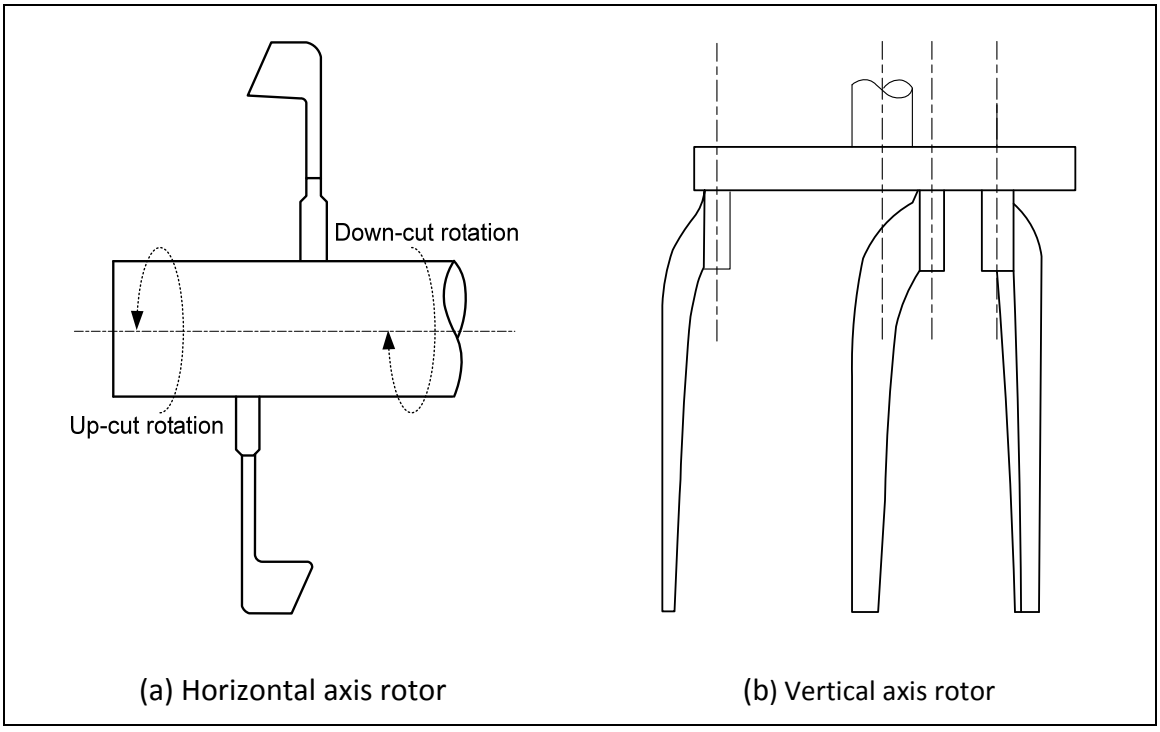

Figure 1.1: Illustrations of horizontal and vertical axis rotavators (Bernacki *et al.*, 1972)

Down-cut rotavators may exert a forward force/thrust to the tractor driveline while the up-cut ones pull the tractor rearwards (Bernacki *et al.,* 1972). The forward thrust, generated by the down-cut rotavator, though possibly detrimental to the tractor driveline, offers the following advantages in tillage (Manian & Kathirvel, 2001; Shinners, Wilkes & England, 1993):

- The thrust force generated by the rotavator blades can be used as traction aid and contributes significantly to the reduction of the rolling resistance of the tractor.
- Reduced draught of rotavators results in less wheel slip at the tractor tyre - soil interface, thus improving field productivity and efficiency.
- Reduced draught of rotavators allows the use of lighter tractors, thus reducing the soil compaction levels and the purchase price of tractors required to operate the tillers.
- Reduced draught of rotavators allows tillage operations to be performed in more difficult traction conditions.

In addition to the aforementioned advantages, the rotavator also mixes and pulverizes the tilled soil well; resulting in a good clod size distribution. The number of tillage passes required to achieve an acceptable tilth quality, using rotavators, is also significantly reduced (Destan & Houmy, 1990) in comparison to the series of operations that would result in the same tilth quality with the use of passive tools. .

In situations with limited traction conditions and/or where thorough mixing of the tilled soil layer is a requisite, the down-cut rotavator is the preferred tillage implement. This preference is due to its ability to generate a forward thrust that aid in traction under such conditions, and the attainment of a well-mixed tilled soil layer. Consequently, the down-cut rotavator is applied widely in the preparation of paddy rice fields in the Asian subcontinent. Paddy rice fields are characterized by limited traction conditions, and the resultant tilled soil needs to be well-mixed.

In spite of these advantages, the down-cutting rotavator is not the implement of choice for land preparation due its perceived excessive specific energy requirements. To date, the application of the rotavator in crop production systems, that require the manipulation of the soil at deeper depths, has been hindered by its excessive energy demands. Because of this, all the commercially available rotavators are presently designed for shallow tillage. This view has been controversial and a number of studies have been conducted with the object of comparing the energy demands for the

realization of an acceptable seedbed. According to Manian and Kathirvel (2001), the view of the excessive energy consumption by rotavators only holds when the energy consumption of the rotavator is compared to the energy consumed by individual passive tillage tools, without considering the quality of the resultant tilth and the number of tillage operations required under conventional tillage. When the total energy demand for producing an acceptable tilth is considered, the series of passive tillage operations needed to realise the same tilth consumes more specific energy than the rotavators (Manian & Kathirvel, 2001; Prasad, 1996). The series of tillage operations for passive tools also require more time and additional resources, thus increasing the production costs of crops.

With such desirable characteristics, there is need to find ways of utilizing the rotavator in the preparation of land for other crops, besides rice and vegetables. In particular, the forward thrust generated could be useful in other land preparation conditions where high traction is required, such as the deep tillage for the rehabilitation of compressed arable land layers and the incorporation of soil amendment materials due to it its superior mixing ability. In Africa, crops that can greatly benefit from the use of rotavators include horticultural crops, orchards, and perennial tree crops such as coffee that require periodical rehabilitation of soils they stand on. The need for rehabilitation arises from the compaction of the root-zone layer due to the numerous surface operations inherent in perennial crop production systems. Also there may be a need to retrieve plant nutrients that might be leached beyond the reach of root zone.

According to Hendrick and Gill (1971a, b, c), power requirements of rotavators might be reduced by considering the relationships between the tiller design and its operational parameters. These parameters include the direction of rotation of the blades, depth of tillage, ratio of peripheral to the forward speed (λ) and the soil condition.

1.2 General hypothesis and model

From the profitable farming perspective, the rotavator hold immense potential for reducing the cost of production of crops especially if methods for reducing its perceived

excessive power requirements in deep tillage can be found. One way of doing this is to carry out studies that would establish the effects of the rotavator design parameters and soil conditions on its performance. Practically, this can be accomplished by designing and fabricating a deep-tilling rotavator with requisite instrumentation to obtain information on the soil-tool interaction system that can be used to study its performance.

In tillage, the performance of tools is determined by their specific draft and energy requirements, and the quality of work. Whereas there is no precise definition of the quality of work, it is generally evaluated by the clod size, the evenness of the operative depth and percentage of plant residue covered after a tillage operation (Srivastava, Goering & Rohrbach, 1993). Though numerous attempts have been made to quantify the performance of rotavators, little is known about how the rotavator design parameters and soil conditions influence the energy requirements and the quality of work due to the empirical nature of the studies on performance (Marenya, du Plessis & Musonda, 2003).

In order to understand the influence of tool design parameters and the influence of soil conditions on performance, Gill and Vanden Berg (1967) emphasized that mathematical description of a tillage process can be accomplished only when all the elements of the tillage process are expressed in a quantitative sense. They gave a hypothetical model to illustrate the factors involved in influencing the desired quality of operation and resulting forces from the design point of view. The hypothetical model they presented considered the initial soil conditions, shape and the manner of movement of the tool as input factors; and tool forces and the final soil condition as output parameters.

In this study, a similar model, in the form of a block diagram (Figure 1.2), is proposed as a basis for gauging the performance of an experimental deep tilling rotavator, fitted with L-shaped blades. The ASAE Standards (2000) defines deep tillage as any tillage operation undertaken at depths in excess of 300 mm. The block diagram includes additional factors, such as the direction of rotation of the blade, bite length and operational depth.

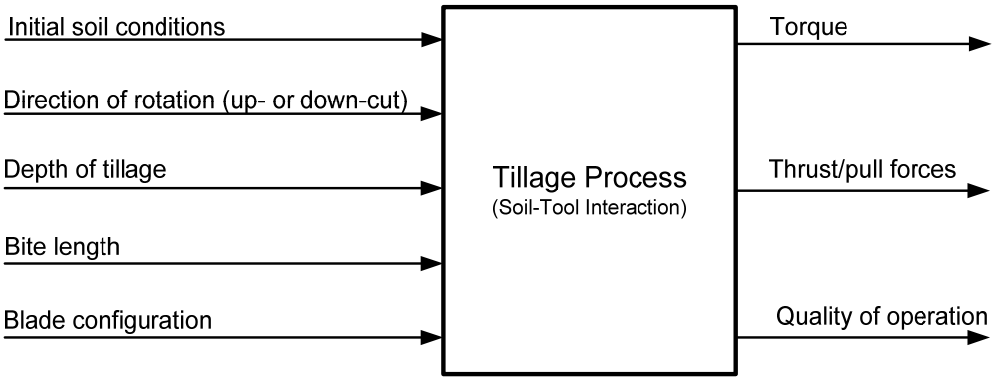

Figure 1.2: Proposed block diagram for the rotavator tillage process model

CHAPTER 2

LITERATURE REVIEW

During rotavator tillage operations various factors affect its energy requirements. These factors (Figure 1.2) can be divided into three categories, *viz*. the soil condition, operational conditions and rotavator configuration. One of the ways for evaluating the performance of such a tillage tool is by determining the tool's total energy requirements. An estimation of the total energy requirements for a tillage tool, such as a rotavator, can be obtained by determining the energy requirements resulting from each group of these factors and their interaction with the tool.

In attempts to quantify the energy requirement of tillage tools, a number of models have been developed that relate the input and output parameters depicted in Figure 1.2 Such models predict the forces acting on soil tillage tools in relation to tool geometry, soil physical properties and the nature of soil disturbance ahead of the tool (Godwin & O'Dogherty, 2006). Therefore, the purpose of this chapter was to review the existing literature on soil parameters, tool geometry and soil-tool interaction models in order to develop a basis for the quantification and prediction of rotavator tillage energy requirements.

2.1 Soil parameters

The soil physical, mechanical and soil dynamic properties, have significant influence on the energy requirements of tillage tools. This is because these properties affect the soil strength, which has to be overcome by a tillage tool during a soil tillage operation (Gill & Vanden Berg, 1967). In this section, the pertinent soil physical and soil dynamic properties, which affect energy requirements of tillage tools, are discussed.

2.1.1 Soil physical properties

The physical condition of a soil greatly influences the energy/power requirement and performance of tillage tools (Ros, Smith, Marley & Erbach, 1995). Soil physical properties

include the soil water content (or moisture content), bulk density, texture, temperature, colour, and pore (void/porosity) space. The soil water content, bulk density and soil texture affect mechanical behaviour and strength of a soil (Gill & Vanden Berg, 1967).

The soil water content of agricultural soils is commonly expressed as the ratio of mass of water contained in the mass of dry material (dry-basis soil water content). There are many methods for determining the soil water content (Erbach, 1987; Gardner, 1986), but the usual way involves the placing of a weighed soil sample in a ventilated oven at a temperature of between 100^{o}C and 110^{o}C until the sample mass becomes constant (Gardner, 1986). Camp and Gill (1969) and Smith (1964) reported that shear strength parameters of fine grained soils decreased with increasing soil water content. However, in the same study, it was also observed that the soil bulk density was concurrently decreasing as the soil water content was increased. Thus, soil water content is a vital parameter in tillage since it influences many parameters that affect the energy requirements of tillage tools.

Soils at same mechanical and environmental conditions, but different textures, behave differently (Gill & Vanden Berg, 1967). Presence of water in void space of soils, for example, can have major impacts on the mechanical behaviour of the soils, owing to its influence on soil strength defining parameters such as the soil shear and soil metal friction parameter (Chancellor, 1994; Spoor & Godwin, 1977). Therefore, in a tillage study, it is important to know not only how much water is present in a soil, but also how this presence affects its engineering or mechanical behaviour. The soil water content is correlated to the soil engineering properties such as strength, compressibility, swelling potential, clay mineralogy, and stress-strain history (Gitau, Gumbe & Biamah, 2006).

Bulk density of a soil is a function of soil water content at any given amount of compactive effort (Marenya & Nyakiti, 2000). As the soil wetness increases, the soil moisture weakens the inter-particle bonds, causing swelling and reducing internal friction making the soil more workable and compactable (Hillel 1980). However, as the soil wetness nears saturation, the fractional volume of expellable air is reduced and the soil can no longer be compacted to the same degree as before, with the same

compactive effort. The optimum moisture content is the point at which the soil wetness is just enough to expel all the air from the soil, and the corresponding density is the maximum dry density. Mouazen and Ramon (2002) reported that draft force of a subsoiler was increased with wet and dry bulk densities where it decreased with soil moisture content. Draft force changed linearly with moisture content where it was a quadratic function of wet bulk density and a cubic function of dry bulk density respectively.

Mechanical behaviour of a soil is directly influenced by changes that occur in its bulk density (Gitau, *et al*., 2006). Soil water content is known to affect the soil bulk density. Changes in the levels of the soil water content within different depth ranges in a soil influenced soil bulk densities within such depth ranges (Chancellor, 1994). Ayers (1987) studied the effect of soil moisture content and density effect on soil shear strength parameters of three coarse grained soils during tillage operations. The author concluded that the soil cohesion and friction angle of the three coarse-grained soils increased with increasing soil density. Therefore, in any tillage study, particularly one aimed at the quantification of energy requirement by tillage tools, it is imperative that the soil bulk density is maintained constant throughout the depth of the test layer.

2.1.2 Soil shear strength and soil failure

The strength of a soil is its ability or capacity at a particular condition, to resist or endure an applied load (Gill & Vanden Berg, 1967). The strength of soil to be tilled maybe described by evaluating the parameters involved in the soil's yield conditions on application of a load. In tillage, soil yielding or failure is achieved through a combination of tillage and traction forces. The combined force system can cause the soil to fail or yield by shear, compression, tension and/or plastic flow (Johnson, Grisso, Nichols & Bailey, 1987; Gill & Vanden Berg, 1967; Schafer, Bochop & Lovely, 1963).

Yield or failure conditions in agricultural soils are much more complex than in many engineering materials. This is due to the fact that the conditions of these soils may vary from a near liquid state (like in rotavator-puddled clay soil) to a brittle state. Shear failure and fracture for brittle materials have a clear meaning. Fracture by shear is also

observed in agricultural soils (Gill & Vanden Berg, 1967). In some cases, however, fracture is not apparent in soils which may exhibit plastic flow and permanent deformation. The stress state that causes soil fracture or plastic flow is a measure of the soil's shear strength. Shear failure is, therefore, some function of the stress state at which failure occurs (Johnson *et al*., 1987).

Yielding of agricultural soils can be approximated using the Mohr-Coulomb failure criterion (Johnson *et al*, 1987; Gill & Vanden Berg, 1967). The criterion postulates that failure occurs when the maximum shear stress of a material on any plane reaches some critical value that is equal to the shear strength of the given material. Gill and Vanden Berg (1967) traced the history of the original Coulomb theory from its postulation to straight line failure envelope of the Mohr failure theory. This failure envelope is expressed as:

$$\tau_{\max} = C_c + \sigma_n \tan\phi \qquad \ldots (2.1)$$

where:

τ_{max} = maximum shearing stress at failure (kPa)

C_c = soil cohesion (kPa)

σ_n = normal stress (kPa)

ϕ = angle of internal friction of soil (deg.)

In classical soil mechanics, Equation (2.1) is referred to as the Mohr-Coulomb equation. This equation represents shear failure at a point within a soil mass. Therefore, the criterion of shear failure using this expression must be carefully distinguished from the distribution of shear point failures i.e., the shear plane or surface (Gill & Vanden Berg, 1967). The application of this equation is limited to effective stress cases and does not apply when the total stresses are considered (Chancellor, 1994).

Gill and Vanden Berg (1967) referring to Equation (2.1) stated that: "*while the straight line envelope of Mohr theory does not rigorously represent shear yield in all soil conditions, the theory has been close enough so the extent that this equation has, almost universally, been accepted as a law. One confusing factor is the fact that* C_c *and* ϕ *are so*

firmly entrenched that they are often referred to as real physical properties of the soil. In reality they are only parameters of the assumed yield equation; and their logical existence can be explained only by an interpretation of the equation, and not from the physical nature of the soil itself."

From Equation (2.1), it is evident that the magnitude of the soil shear strength depends on the soil-soil friction and the soil cohesion. The soil cohesive parameter (C_c) represents the maximum shear stress value of the soil when the normal stress is equal to zero. The cohesive parameter depends only on the strength of the *in situ* bonds between soil particles. Therefore, C_c is constant, irrespective of the magnitude of the normal stress applied to a body of soil. The shear stress associated with soil–soil friction, on the other hand, results from the sliding of soil over soil, and is therefore directly influenced by the magnitude of the normal load. Stafford and Tanner (1983) reported a linear relationship between the maximum shear strength and the normal stress applied.

Both the cohesion (C_c) and the coefficient of internal friction ($\tan\phi$) are influenced by soil water content, porosity and grain size distribution of the soil material (Spoor & Godwin, 1977; Chancellor, 1994; Gitau *et al*., 2006). In general, C_c and $\tan\phi$ increase with decrease in porosity, whereas cohesion at any given density increases with soil water content reaching a maximum at some intermediate level and decreasing thereafter as the soil water content increases (Chancellor & Vomicil, 1971; Stafford & Tanner, 1983a). Although a similar observation was made by Wells and Treesuwan, (1978), a study by Kuipers and Kroesbergen (1966) indicated a decrease of the cohesion value with increasing soil water content. This disagreement in the behaviour of soil cohesion could be due to the differences in the ranges of the soil water content levels studied by respective researchers. In addition, it is probable that the textures of the soil studied by these researchers were different resulting in the reported differences in the variation of soil cohesion with soil water content. In general, soil cohesion increases with soil water content, reaching a peak value and thereafter, decrease with further increase in soil water content (Gitau *et al*. 2006; Ayers, 1987). The magnitude of this variation is affected by the soil texture and the soil bulk density (Ayers, 1987).

2.1.3 Soil-metal friction

With any given tillage tool, soil failure does not only occur in the shear mode along the internal rupture planes during tillage but, also at the boundary between the tool surface and the soil. The force to be overcome at the boundary between the tool surface and the soil is called friction force. For agricultural soils sliding against common materials used for making tillage tools, the relationships found by numerous investigators (Koolen & Kuipers, 1983; Hendrick & Bailey, 1982; Gill & Vanden Berg, 1967;) appear to be neither simple nor consistent across soil type and conditions.

The relationship for determining frictional stress considered capable of accounting for the complexities and inconsistencies associated with the agricultural soils (Chancellor, 1994; Stafford & Tanner, 1977) takes the form that is similar to Equation (2.1), and is expressed as:

$$\tau_f = C_a + \sigma_n \tan\delta \qquad \text{... (2.2)}$$

where:

C_a = adhesion stress between the soil and the tillage tool (kPa)

δ = angle of soil-metal friction (degrees)

σ_n = normal stress (kPa)

τ_f = maximum frictional stress at the soil-tool interface (kPa)

Like in the case of shear strength, Equation (2.2) indicates that the maximum frictional shear stress at the soil-tool interface is determined by adhesion and soil-metal friction. There are many factors that influence the magnitude of the resultant frictional shear stress at the soil-tool interface. Chancellor (1994) listed some 12 factors that affect the magnitude of the maximum frictional stress at the soil-tool interface. In tillage, for a given soil, the pertinent factors influencing the magnitude of τ_f include level of the normal stress, soil water content, soil porosity or density, sliding velocity, the maximum value of the normal stress during the course of the test history, and sudden changes (increase or decrease) of normal stress.

From Equation (2.2), the normal stress significantly affects the value of the maximum frictional shear stress. A study by Stafford & Tanner (1983b) reported that for most soils, frictional stress tends to change linearly with normal stress level. However, cases in which small increments in the coefficient of friction μ, ($\tan\delta$ in Equation 2.2) occurred with the increase of normal stress for a given soil/moisture condition were reported in the same study. Cases of small decrease in μ values have also occurred with constant normal stress for different soil/moisture condition (Soehne as cited by Chancellor, 1994). Therefore, the application of this Equation (2.2) must be accompanied by explicitly quantified soil condition, in particular the level of the soil water content.

The level of the soil water content, like in the case of soil shear strength, affects the maximum frictional stress at the soil-tool interface. For many soils (Stafford & Tanner, 1977; Stafford & Tanner, 1983b) the coefficient of friction rise to a maximum value at some intermediate soil water content, with lower values of the coefficient at lower and higher soil water content levels. This effect is more pronounced with fine grained soils than with coarse-grained soils (Robinson, Schafer, & Johnson, 1988).

Soil water content also has a significant effect on adhesion, with adhesion increasing as the soil water content increases from low to intermediate values (Stafford & Tanner, 1977). During tillage, the soil-to-tool bonding depends on the soil water tension. It is, therefore, expected that more fine-grained soils would exhibit greater adhesion at certain soil water contents than would be the case for coarse-grained soils. It has been observed that at very high soil water contents that would produce positive pore water pressure under load, tension would decrease thus reducing adhesion (Neal, 1966), and may even increase to effect lubrication (Chancellor, 1994; Srivastava, *et al.,* 1993).

Soil density or porosity has an insignificant effect on the coefficient of friction, but significantly affects the adhesion component of the frictional shear stress (Stafford & Tanner, 1977). The adhesion shear stress tends to increase as the porosity is reduced, i.e., as the soil density increases. In a study by Butterfield and Andrawes (1972) using pure sand at 36 % and 44 % porosity, the coefficient of friction on six different surfaces, at higher porosity, were 66 % that at the lower porosity.

2.1.4 Dynamic soil strength components

Gill and Vanden Berg (1967) defines the soil dynamic properties as those properties of the soil that become manifest through soil movement. From this definition, if a block of soil starts moving on a flat surface, the resultant friction angle is a dynamic property of soil as it does not appear unless soil starts moving over the flat surface. Also, when loose soil is compacted, its bulk density and shear strength increases; therefore, soil shear strength is another dynamic property of soil.

The soil dynamic properties are affected by the both the soil water content and the soil texture (McKyes, 1985). Based on the soil texture alone, soils can be classified as cohesive on non-cohesive, or as frictional and non-frictional. Measurements have shown that for the purely frictional soils (sandy), the shear strength of the soil does not vary a great deal with shear rate (Stafford & Tanner, 1983a). For such a soil, the inertial force involved in accelerating the soil is the important factor as the operating speed of the tillage tool increases. On the other hand, purely cohesive soils (clay soils) exhibit marked changes in shear strength. Increasing the shear rate at sufficiently high tools speed resulted in the shear strength forces nearly outweighing the inertial forces for clayey soils (McKyes, 1985).

The possible causes for the increases in soil strength with increasing operating tillage tool speed has been studied by many researchers (El-Domiaty & Chancellor, 1970; Aref, Chancellor & Nielson, 1975; Fleniken, Henfer & Weber, 1977, Koolen & Kuipers, 1983; Stafford & Tanner,1983a, 1983b; Glancey, Upadhyaya, Chancellor & Rumsey, 1996; Zhang & Kushwaha, 1999). Zhang and Kushwaha (1999) reported that three mechanisms accounting for the draft increase with increase in operating tool speed were; the soil inertial effect, the soil strength rate effect, and the wave propagation effect. The last effect has been reported on extensively by many Russian researchers (Azyamova 1963; Katsygin, 1964; Vetrov & Stanevski, 1972), who reported inverse decrease in draft requirements with increasing the operating tillage tool speed beyond some limits. This observation was attributed to the fact that tool speed increased faster than the increase in the wave of soil stress propagation. Theoretically, the plastic zone of soil in front of

the tool decreased or even disappeared, thus the soil cutting resistance decreased. The significance of these finding is the existence of an optimum operating speed for set soil conditions and blade configuration at which the draft requirement, and therefore energy requirements of passive tillage tools was optimal.

Equations (2.1) and (2.2) describe the stresses interacting on a failure plane within the soil body and on the soil-tool interface, respectively. These two failure criteria are static in nature, and in tillage, they do not account for the effect of speed of the tool. There are a number of studies (El-Domiaty & Chancellor, 1970; Aref *et al.*, 1975; Fleniken, Henfer & Weber, 1977; Koolen & Kuipers, 1983; Stafford & Tanner, 1983a; Glancey *et al.*, 1996) reported in literature indicating that the strength of a soil is a function of the deformation rate. Therefore, the overall soil strength overcome by a tillage tool consists of the static (from Mohr-Coulomb failure criterion) as well as dynamic components. By taking the dynamic component of the soil strength into account, Glancey *et al*. (1996) formulated a general expression for the maximum shear strength of a soil under the influence of a tillage tool as:

$$\tau_{\max} = \tau_o + \tau_i V_f \qquad \ldots (2.3)$$

where:

$\tau_{\max}$ = maximum shear stress at failure (kPa)

τ_o = soil property related to static component of the static shear strength (kPa)

τ_i = soil property related to the dynamic component of soil shear strength, proportional to the operating speed (kPa $(ms^{-1})^{-1}$)

V_f = forward travel speed of the tool (ms^{-1})

In a study of the draft force requirements, Stafford (1979) developed the expression:

$$F_d = F_s + f(v) \qquad \ldots (2.4)$$

where:

F_d = draft force under dynamic conditions (kN)

F_s = static draft force component (kN)

$f(v)$ = function containing the soil inertial term (kN)

In 1983, Stafford and Tanner (1983a, 1983b) conducted studies on the effect of rate of change on soil shear strength and the soil-metal friction on a clay and sandy clay loam soil. The results of these studies indicated that the soil-metal friction angle increased logarithmically with speed over a wide range of tool velocity and soil water content; and could be fitted by the following logarithmic expression.

$$\delta = a + b\log V_s \quad \text{... (2.5)}$$

where:

$\delta =$ soil-metal friction angle (deg.)

V_s = sliding velocity of the blade (ms^{-1})

a, b = regressions coefficients, which were all significant at 1 % level

For the shear strength, Stafford and Tanner (1983a) found a logarithmic relationship between deformation rate and the cohesion component for the two soils over a wide range of soil water content for tool velocities in the 0.0015 – 5 m/s range. The fitted logarithmic expression for this case was of the form:

$$C_c = k_1 + k_2 \log(1 + k_3 v) \quad \text{... (2.6)}$$

where:

k_1, k_2, k_3 = constants for both soils at all soil water contents.

2.2 Tillage tool parameters

2.2.1 Blade configuration

Many types and shapes of blades have been developed for rotavators (Kepner, Bainer & Barger, 1978). Currently, some of the commercially available blade configurations include the L-shaped, the C-shaped, the C-L hybrid, the hook-shaped or pick-type blades, and the hoe-type (Salokhe, Hanif & Hoki., 1993). Because these blades have different soil-tool interaction systems, they affect both the power performance and the quality of work of rotavators. The development of rotavator blades is an on-going process and new

blades, particularly in the Asian subcontinent and Japan, where the rotavator is widely used in the preparation of paddy rice fields, has been reported in the recent past (Shibusawa, 1993; Salokhe *et al.,* 1993).

The blade configuration influences the performance of rotavators. Studies of the effects of the blade configuration on performance of rotavators have been investigated by many researchers (Beeny & Khoo, 1970; Shibusawa, 1993; Salokhe *et al.*, 1993; Lee, Park, Park & Lee 2002). Salokhe, *et al.* (1993) investigated the performance characteristics of three types of blades, *viz*, 'C', 'C-L' and 'L' shaped blades in terms of power requirements and the puddling[1] quality of a tractor-driven rotavator in a wet clay soil. They conducted field tests at different speeds at an average tillage depth of 100 mm in a saturated soil, with the wetness maintained at a standing water level of 40 mm. Results of their experiments indicated that the torque requirements for the L-shaped blade was significantly higher than for the other two types of blades, and that the C-shaped blade required the least torque. On the quality of work, which they quantified in terms of the percent reduction in the bulk density of the tilled soil and the puddling index, the C-shaped blade gave better results.

Baloch, Bukhari, Kilgour and Mughal (1986) evaluated the performance of new slashers, old (used) slashers and 'L' shaped blades in terms of the work rate, fuel consumption and specific energy consumption in a soft and a hard soil. The results indicated that the old slasher blades gave the highest field capacity, consumed less fuel and demanded less power in both soft and hard soils at different speeds. Comparison of the L-shaped and new slasher blades, showed that the L-shaped blades performed better in both soft and hard soils at low and high rotor speeds, using the stated performance parameters.

Beeny and Khoo (1970) investigated the performance of different shaped blades for rotary tillage in a wet rice soil. The blades studied were of the 'L-', C- and I-shapes. The results obtained indicated a relatively high specific work requirement for the L-shaped

[1] the process of churning soil and water in a flooded field so as to form a homogenous mixture such that the soil particle remain in suspension during the time of planting (Gupta & Visvanathan, 1993b)

blade, compared with the other two types over the same range of operating regimes. The L-shaped blade, on average, required about 30 % more energy for the specific work than the I- and C-shaped blades. The study also indicated that the L-shaped blades gave the greatest forward thrust/push to the tractor, followed by the C-shape and the I-shape respectively. This thrust may be worth paying for in difficult traction conditions such as those prevalent in the paddy rice fields.

From the findings of Beeny and Khoo (1970) it appeared that a 'hybrid' blade from the C- and L-shaped parent shapes, might give better performance results. Consequently, Beeny (1973) developed two modified blades and conducted a study under typical swampy rice field conditions to compare the performance of these specially designed blades. He referred to these blades as the 'power' blade, which was essentially a L-shaped blade with an extended blade length and 'speed' blade, which was a 'hybrid' between the 'power' blade and C-shaped blade. The study found that the fitting of 'speed' blades effected a saving of about 25 % in brake horse power (bhp) of the tractor over those fitted with the 'power' blade. However, the 'power' blade gave greater forward thrusts compared to the 'speed' blade. The author hypothesised that the power saved could be utilized by increasing the working width of a rotavator fitted with 'speed' blades by 25 % and that this would increase the forward thrust of the 'speed' blade fitted rotavator by 25 %. This hypothesis was not verified.

A remarkable reduction of specific power demanded by an up-cut rotavator as a function of blade configuration was reported by Shibusawa (1993). In this study, he observed the dynamics of the rotavator tilled-soil and the blade kinematics and noted tremendous amounts of re-tillage occurring as the depth of tillage increased. He surmised such re-tillage to be the main source of high energy expenditures associated with deep rotary tillage. From the observations, Shibusawa (1993) hypothesised that significant reduction in energy and power requirement for deep tilling rotavators can be realised if re-tillage could be avoided.

In a study that investigated the minimum tillage characteristics by rotavator blades, Lee *et al.* (2002) used three types of blades, *viz,* two general-purpose rotary blades, used

with tractors and power tillers; and a levelling rotary blade for tractor use in wet paddy fields. Of the three types of rotary blades used in this study, the rotary blade for the power tiller was considered most satisfactory for strip tillage on the basis of its low torque requirement and the highest ratio of soil breaking.

2.2.2 Direction of rotation

The direction of rotation of the rotor is a basic rotavator design parameter that has a significant influence on the power performance and the quality of work of rotavators (Hendrick & Gill, 1971a). For the horizontal axis rotavators, the direction of rotation influences the power demand; and determines whether a thrust force or pull force will be exerted on the tractor. In general, for the same design dimensions and operational conditions, the energy required for only processing the soil in up-cut rotation is less than the requirement for down-cut rotation (Lee *et al*., 2003; Salokhe & Ramalingam, 2001; Shibusawa, 1993; Hendrick & Gill, 1971a). However, this may not be true for the total energy required, which includes the energy required for the forward propulsion of both the tractor and the rotavator in addition to the energy required to till the soil.

The difference in specific energy demand for tilling the soil between the up- and down-cut rotavator has been attributed to the resultant soil-blade dynamics and the difference in the soil failure process, between the down- and the up-cut rotary tillage (Hendrick & Gill, 1971a; Kataoka & Shibusawa, 2002). When down-cut rotation is used, each blade cuts an increment of undisturbed soil while entering from the surface. With the up-cut rotation; the soil increment is cut from the bottom upward. For the up-cut rotation, after the initial entry of the blade into the soil, the blade for subsequent cuts operates from an area that had been tilled by the preceding blade.

The direction of rotation also affects the manner in which soil failure occurs during the rotary tillage operation. Up-cut rotation causes the blades to operate towards an unconfined area (the soil surface) with more of the soil failing in tension and shearing than in the case of down-cut process (Kataoka & Shibusawa, 2002). Reversing the direction of rotation also changes the geometry of the soil-tool system (Thakur & Godwin, 1990); even where the other operational parameters are constant. The

significant differences observed in the energy requirements for tilling the soil between the down- and up- cutting directions can therefore be attributed to the different soil-tool systems and the different soil failure processes taking place during up-or down-cutting tillage.

The segment in which the majority of energy is expended during a complete rotation of a rotavator is different for the up-and down-cut directions of rotation. When the down-cut direction is used, the majority of the energy is expended in the first quadrant (between 0 and 90 degrees). For the up-cut direction, the cutting is mainly in the fourth quadrant and occurs between 270 and 360 degrees (Hendrick & Gill, 1971a). These differences in the segments where the majority of energy is expended during rotary tillage for the up- and down-cut directions may possibly influence the energy requirements.

Lee *et al*., (2003) measured the tilling torque variation through 180^{o} for a rotavator fitted with three different types of blades for the down- and up-cut directions and reported a 20-30 % higher torque requirement during the down-cut for all blade shapes. Salokhe and Ramalingam (2003) working in Bangkok clay, evaluated the draft and power requirements of rotavators equipped with up-cut and down-cut blades. The study reported less PTO power consumption for the up-cut direction than for the down-cut direction of rotation for all passes and forward speeds.

Whereas the magnitudes of the thrust or pull forces exerted on the tractor by a down-cut or up-cut rotavator have significant influence on the total energy, there is almost lack information on the impact of the direction of rotation, the soil condition and other rotavator design factors on the magnitude of forward thrust or pull forces generated by rotavators during the tilling process. What is acknowledged in literature is the fact that the use of the down-cutting rotavator under difficult traction conditions, such as in the paddy rice fields, aid in traction. This is attributed to the forward thrust generated while processing the soil in the down-cut (concurrent) direction of rotation (Shinners *et al.,* 1993; Maniam & Kathirvel, 2001).

2.2.3 Depth of tillage

As with any other tillage tool, the depth of operation has significant influence on the power requirement and performance of a rotavator (Gosh, 1967; Hendrick & Gill, 1971b; Shibusawa, 1993). Hendrick and Gill (1971b) reported that increasing the depth of operation, while holding other rotavator design parameters and soil conditions constant, resulted in increased energy requirement for both directions of rotation. From the previous research work reviewed by Hendrick & Gill (1971b), there was no consensus on the relationship between depth and energy requirements.

In most cases, specific energy requirement increases at an increasing rate with the depth of tillage (Shibusawa, 1993) although some studies (Beeny & Khoo, 1970) have shown a linear relationship between increments in these two factors for same soil conditions for a given rotavator. This increasing rate of the specific energy requirement with depth has been the main reason for restricting the rotavator to be operated at shallow depths of tillage. A combination of deep depth of tillage, with increasing blade rotational velocity, results a rapid increase in specific energy (Hendrick & Gill, 1971b).

While the energy demand increased with depth, the specific energy requirements, i.e., energy per unit volume of tilled soil, decreases. The degree of the decrease in the specific energy requirements has been shown to be greatly influenced by the direction of rotation of the rotor (Shibusawa, 1993). Furlong (as cited by Hendrick & Gill, 1971b) reported a ratio of 3:2 for the increase in soil-volume-tilled to the increase in the specific energy requirements for a down-cut rotavator. Hendrick & Gill, 1971b citing the findings of Furlong stated that this ratio is unaffected by the speed of the rotor.

Until the study by Shibusawa (1993) the reason behind the rapid increase in specific energy of rotavators with increase in working depth had remained unclear. The author reported that a tremendous amount of re-tillage occurred during rotavator tillage for a rotavator fitted with commercial blades, and that as the depth increased, the amount of soil being re-tilled increased significantly. This resulted in rapid increase of the total specific energy requirements of the rotavator. Using special blades, that avoided re-tillage, the author reported a 50 percent reduction in specific energy requirements for

both up-and down-cut rotavator tillage operations at depths of 300 mm or greater. From this study it is evident that avoiding re-tilling is a plausible means of reducing the specific energy requirement of rotavators.

Specific energy requirements of rotavators have also been reported to be influenced by the ratio of the tillage depth to the radius of the rotor (Shibusawa, 1993; Hendrick & Gill, 1971b). However, relationship between the rotavator radii with the energy requirement is unclear (Hendrick & Gill, 1971b). Shibusawa (1993) reported that for a given direction of rotation, a smaller radius rotor required less energy when this ratio is less than unity. Hendrick and Gill (1971b), after reviewing a number of past researches, concluded that the optimum rotor diameter-to-depth ratio appeared to be in the range of 1.1 to 1.4 since this is the range in which the minimum specific energy requirement occurs.

In general, when the depth of tillage is greater than the rotor radius, the up-cut rotavators require 20 to 30 percent less specific power (Salokhe & Ramalingam, 2001). When the tillage depth is less than the rotor radius, the rotavator tends to throw more soil forward, resulting in significant re-tillage (Hendrick & Gill, 1971b; Shibusawa, 1993; Lee *et al*., 2003) and hence the higher energy requirements for down-cutting rotavators.

2.2.4 The rotavator kinematic parameter, λ

The kinematic parameter, λ is the ratio of the blade peripheral velocity to the forward travel velocity of the tractor. It is perhaps the most important rotavator operational parameter for quantifying this tool's tillage performance because it influences both the energy requirements and the resultant tilth quality of a rotavator (Hendrick & Gill, 1971c). Being a ratio of the blade peripheral velocity to the forward travel velocity, λ can be varied in the following ways: (1) changing the rotor radius, (2) changing the rotor velocity, and (3) changing the machine travel velocity. In practice the rotor radius for a rotavator of given configurations remains unchanged and the manufacturer only provides means of varying the ratio between the tractor PTO and the rotor velocity as a means of changing the λ. This provision is usually by means of suitable gearing mechanism (Manian & Kathirvel, 2001).

Changing of λ has a significant influence on the performance of a rotavator since this changes the bite length or tilling pitch, which affects the volume of the soil cut per revolution by the rotavator blades. From the findings of Beeny and Greig (1965), larger values of λ mean more cutting by the blade per unit volume, which increases the specific work of the rotavator. This effect holds whether λ is increased by increasing rotor radius, R; the rotational speed, ω; or by decreasing the forward travel speed V_f while holding the other operational parameters constant. However, decreasing λ does not necessarily decrease the specific power requirement, except within certain limits. Beeny and Greig (1965) showed that increasing the forward travel velocity beyond the point of providing adequate clearance angle, caused the specific power to increase drastically.

Interesting observations have been reported on the influence of λ on the power or specific energy requirement. Depending on the parameter(s) that is being changed to change λ, the accompanying changes in the specific energy or power requirements are significantly different (Hendrick & Gill, 1971c). Kisu *et al.* (as cited in Hendrick & Gill, 1971c) reported that when λ is changed by holding V_f constant and decreasing the rotational rotor velocity ω, the power required decreases to a minimum value and then increases as the clearance angle approaches zero. In the same study, when λ was changed by holding ω constant and increasing V_f, the specific power requirement decreased up to a point and thereafter remained constant.

From a review of independent past studies by Hendrick and Gill (1971a, 1971b, 1971c), Hendrick (1980), Beeny and Khoo (1970) on the effect of λ on the specific energy requirements of rotavators, there appear to be an optimal value of λ at which the rotavator of a given rotor radius should be operated. When R and ω are held constant and V_f is increased (i.e., decreasing λ), the specific energy or power required initially decreases to a minimum value and then increases. Similar observations were reported for the case of changing λ by holding R and V_f, and then varying the rotational velocity, ω, of the rotor. The optimal λ value appears to be influenced by the direction of rotation (Dalin & Pavlov as cited by Hendrick & Gill, 1971c). Hendrick (1980) suggested a practical lower limit of the ratio of rotor tip speed to forward speed, i.e. velocity ratio, to be 2.5. Lisunov as cited in Hendrick & Gill (1971c) found the optimum value of λ to be 2.4. At

low velocity ratios, the backside of the blades would contact uncut soil resulting in drastic increase in the specific energy requirements (Hendrick, 1980).

After comprehensively reviewing research literature of past studies on the effect of λ on the specific energy or power requirements, Hendrick and Gill (1971c) made the following general conclusions:

- Decreasing λ by increasing forward travel speed, results in an increase in the power requirement, but a reduction in the specific power (provided the geometry of the soil-tool system is not significantly varied).
- Decreasing λ by decreasing angular velocity of the rotor, decreases the power requirement and the specific power.
- Increasing λ results in a greater value of the ratio between cutting area and the volume of the soil slice cut.

2.3 Modeling energy requirements of tillage tools

In Figure 1.2 (see §1.2), it is the tillage process or soil-tool interaction that interfaces the input parameters and output performance indicators used for assessing the performance of a tillage tool. Therefore, any model that aims to predict the energy requirements of tillage tools must be capable of developing relationships for the interaction process between a soil in a given state or condition, and a given tillage tool during tillage. Over the years, a number of analytical, empirical and numerical models have been developed for predicting the energy requirements of different tillage tools (Kushwaha, Chi & Shen, 1993; Marenya, du Plessis & Musonda, 2003). These models have been developed using the empirical, analytical, and numerical modeling approaches for both the passive and active tillage tools.

Analytical models have been extensively used, for the past six or so decades, for predicting the draft and energy requirements of narrow passive tillage tools (Payne, 1956; O'Callaghan & Farrelly, 1964; Hettiaratchi & Reece, 1967; Godwin & Spoor, 1977; McKyes & Ali, 1977; Perumpral, Grisso & Desai, 1983; Swick & Perumpral, 1988; Zeng & Yao, 1992). On the other hand, a number of empirical models have been developed for

the active tillage tool, particularly the rotavator. The absence of the application of analytical methods for the prediction of the energy requirements of active tillage tools, including the rotavator was attribute to the complex manner of movement of these tillage tools(Marenya *et al.*, 2003).

The application of the numerical methods such as the Artificial Neural Network (ANN), Discrete Elements Methods (DEM), Finite Element Methods (FEM), and Computational Fluid Dynamics (CFDs) for the modeling of tillage tools energy requirements only became feasible with the advent of powerful computers (Kushwaha *et al.*, 1993) and appearance of improved computing software. Among these approaches, FEM was applied earlier than the other numerical methods in the analysis of the cutting process of simple passive tillage tools (Yong & Hanna, 1977). The results of the FEM soil cutting process available in literature (Yong & Hanna, 1977; Chi & Kushwaha, 1989, 1990, 1991a, Kushwaha & Shen, 1995; Fielke, 1999; Mouazen & Nemenyi, 1999) indicate that this method produced acceptable results. In addition, FEM has showed more flexibility to simulate tillage operations under different tools shapes.

In an extensive review of literature on analytical and numerical models Kushwaha *et al*., (1993) stated that FEM not only calculated the soil forces but also provided a progressive failure zone, soil acceleration field, and stress distribution on the tool surface. This means that FEM models can be used to better understand the soil tool interaction during tillage operations. However, this method has a serious limitation because all FEM models require a constitutive relation relationship of a material, which for agricultural soils, is not yet fully understood. This shortcoming of FEM eliminated the need for further analysis and discussion of the FEM models in this study.

The application of CFDs technique in the analysis of the soil-tool interaction for the prediction of the tillage tool energy requirements is a recent development. This technique, like the FEM, requires the use of powerful computers and specialized software for their successful implementation. Karmakar and Kushwaha (2005a) applied this technique to simulate the flow of soil around a simple tool using a vertical blade in rectangular flow domain. The soil was treated as a Bingham viscoplastic material in

respect to its non-Newtonian rheology. The free-surface simulation of an open channel visco-plastic soil flow indicated soil deformation patterns, and the effect of speed on the failure front propagation. Soil deformations, as the flow of a visco-plastic material with yield stress, were observed to possess "plastic flow" and "plug flow" patterns at different tool travel speeds. In a related study, Karmakar and Kushwaha (2005b) reported that soil pressure on the tool surface increased with the tool operating speed, with the pressure being greatest at the tool tip.

From the literature review presented in this section, there was no documentation in literature, on the application of the ANN and DEM for modeling techniques for the predicting the energy requirements of both passive and active tillage tools. Therefore, the remainder of this section is devoted to the analysis of some of the past analytical models because they may be useful in the development of an analytical model for the prediction of rotavator torque requirements.

2.4 Analytical soil failure models

There are many analytical prediction models available, that could be used for predicting the forces on the tillage tool (Kushwaha, *et al.*, 1993). These models have been developed for simple rectangular blades passively drawn through the soil (Marenya *et al*., 2003). Depending on the depth-to-width ratio (*d/w*) for such tools, three categories of these blades have been distinguished, viz., wide blades ($d/w < 0.5$); narrow tine or chisel ($1 < d/w < 6$); and very narrow (knife) tines ($d/w > 6$). Depending on the blade category, both 2 – and 3 – D models have been developed using the analytical approach (Godwin & O'Doherty, 2006). All the 2-D models reviewed are of the static type while the 3-D models comprise both static and dynamic analytical models. In static models, the effect of the travel speed of the tool is not considered. In the subsequent subsections, detailed analysis of the existing analytical models is presented.

2.4.1 Two-dimensional models

The critical soil cutting models were first developed, in the early 1960's, for 2-D soil cutting caused by a wide blade based on Terzaghi's passive earth pressure theory. Based

on this theory, a failure zone was assumed to exist ahead of a cutting blade and the soil in the failure zone was assumed of be in the critical failure state. The slope-line theory was then applied to predict the soil forces. The calculations of the shape of the slope-line and the failure areas were cumbersome, at that time, as the proposed solution used the finite difference method (Kushwaha, *et al.*, 1993), which is highly iterative.

According to Kushwaha *et al*., 1993, to obtain a simpler solution, a semi-empirical failure zone, was earlier suggested by Terzaghi (1943) for 2-D soil failure that consisted of a Rankine passive zone and a complex shear zone, bounded by part of a logarithmic spiral curve, was developed (Figure 2.1). The resulting force, P on the blade was calculated by assuming static equilibrium along the boundary and determining the position of O to provide a minimum value (Hettiaratchi *et al.*, 1966).

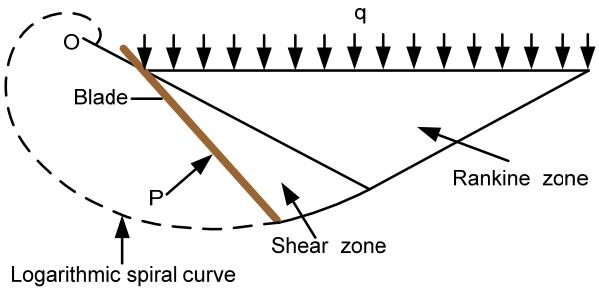

Figure 2.1: Logarithmic spiral failure zone

2.4.1.1 Reece model

Reece (1965) hypothesized that the mechanics of earthmoving by a blade is similar, in many respects, to the soil bearing capacity of shallow foundations as described by Terzaghi (1959). Using this theory and the mathematical force expression developed by Osman (1964), he proposed the following expression, popularly known as Reece's earthmoving equation (Equation 2.7), for describing the force required to cut the soil by a tool.

$$P = \left(\gamma g d^2 N_\gamma + C_c d N_c + C_a d N_a + q d N_q\right) w \qquad \ldots (2.7)$$

Equation (2.7) is widely accepted by many researchers (Hettiaratchi & Reece, 1967; Godwin & Spoor, 1977; McKyes & Ali, 1977; Perumpral *et al*., 1983) for predicting the

draft force of wide blades. This equation takes into account the effect of the soil bulk density, soil cohesion, soil frictional strength, geometry of cut soil, tool to soil adhesion and friction angle, tool operating depth, and tool width; all of which contribute to total soil resistance that must be overcome in tillage operations by a blade. However, it does not include the speed of the blade, which is known to have effects on the draft force (Perumpral, Grisso & Desai, 1983; McKyes, 1989).

Based on the logarithmic spiral failure zone (Figure 2.1), Hettiaratchi and Reece (1974) developed charts for determining the different N-factors contained in Equation (2.7). These N-factors were functions of the blade rake angle, soil internal friction and the soil-metal friction. To compensate for this shortcoming of Reece's equation, McKyes (1985) proposed another model (Equation 2.8) that basically was the same as the Reece (1965) model, with an additional term that accounted for the effect of tool speed on the draft force requirements.

$$\left.\begin{aligned} P &= \left(\gamma g d^2 N_\gamma + C_c d N_c + C_a d N_{ca} + q d N_q + \gamma V_f^2 N_a\right) w \\ N_a &= \frac{\tan\rho + \cot(\rho+\phi)}{\left[\cos(\beta+\delta) + \sin(\rho+\delta)\cot(\rho+\phi)\right]\left[1+\tan\rho\cot\beta\right]} \end{aligned}\right\} \quad \ldots (2.8)$$

2.4.2 Static three-dimensional models

2.4.2.1 Payne model

From literature, it is evident that the first analytical 3-D model for predicting the force requirements of a simple inclined tillage tool was developed a Payne (1956). The model adapted quasi-static Mohr-Coulomb soil mechanics using both the passive retaining wall and the bearing capacity theories by studying the soil failure patterns in a series of field and laboratory tests. By observing the upward displacement of soil ahead of the tillage tool, Payne (1956) assumed a failure zone for tines with a width-to-depth ratio of less than 1:1.

Further experiments done by Payne and Tanner (1959) in a follow-up study, showed that the shape of the failure zone changed with the geometry of the tool such as rake angle, depth and width. In this latter work by Payne and Tanner (1959), no equations were

developed for evaluating the draft force. In another related study, Osman (1964) improved the model proposed by Payne (1959) by introducing factors such as soil properties, tool rake angle and tool-surface roughness, to the force equation, using the dimensional analysis techniques.

2.4.2.2 O'Callaghan and Farrely model

Based on the work of Payne (1956), O'Callaghan and Farrely (1964) undertook extensive field experiments for three soil conditions. Based on the observation made from the extensive field measurement undertaken, a soil failure model shown in Figure 2.2 was proposed.

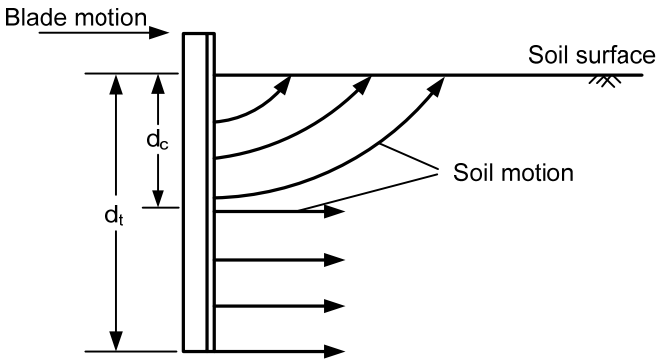

Figure 2.2: Schematic illustration of the crescent and lateral failure zones observed by O'Callaghan and Farrely (1964)

Based on Figure 2.2 and Terzaghi's passive earth pressure theory, O'Callaghan and Farrely (1964), proposed a model consisting of a crescent failure above the critical depth, d_c and lateral failure below the critical depth. The d_c was assumed to be equal to the width of the tool for a smooth blade and half the tool width for a free surface with normal restraint. Depending on the depth at which the tool was operated at, they proposed two equations for predicting its (blades') draft force by applying Terzaghi's method (Terzaghi, 1959). For shallow blades, operated above the d_c, the draft prediction equation, which only accounts for the crescent failure, was given by Equation (2.9).

$$H_s = w\left(C_c d N_c + \gamma d^2 N_\gamma\right) \quad \text{... (2.9)}$$

When the blade was operated at a depth greater than d_c, the total force required for both the crescent and lateral failure was predicted by Equation (2.10).

$$H_{dc} = \frac{C_c w(d - kw)}{\tan\phi}\left[\tan^2\left(\frac{\pi}{4} + \frac{\phi}{2}\right)e^{\pi\tan\phi} - 1\right] + H_s \qquad \text{... (2.10)}$$

In this model, the effect of two side crescents for the failure above the d_c plus the forces due to adhesion and soil interface friction were not included in the equations developed for the prediction of the blade draft force. In addition, the effect of the gravity term, in Equation (2.7), was considered negligible owing to the small masses of soil involved. Comparison between the model and test data, were generally good for a vertical blade. However for hard soil, the model under-predicted the draft force. The slight disparity between the test data and the predicted draft force for hard soils was attributed to the lack of incorporating all the identified soil resistance elements in the model.

2.4.2.3 Hettiaratchi and Reece model

After developing the two dimensional model discussed above (§2.4.1.1), Hettiaratchi and Reece (1967) developed a three-dimensional (3-D) soil failure model. This model was, in some respects, similar to the earlier model developed O'Callaghan and Farrely (1964) since the soil failure configuration was divided into forward failure, ahead of the soil-tool interface; and traverse failure, i.e., the horizontal transverse movement of the soil away from interface (Figure 2.3).

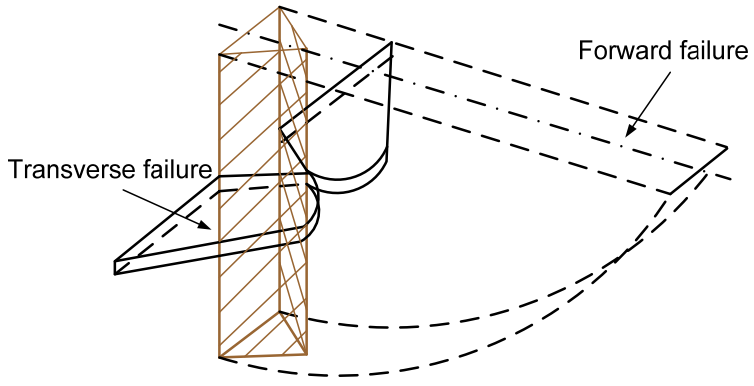

Figure 2.3: Failure zone of the Hettiaratchi and Reece model (Hettiaratchi & Reece, 1967)

The total force comprised was calculated as the sum of the force for forward failure and the transverse failure. The force due to the forward failure was found using the 2-D

equation (Equation (2.7), §2.4.2.1) while the force due to the transverse failure was calculated similar to that derived by O'Callaghan and Farrelly (1964) with an additional component to account for the gravitational component. The resultant model was as follows:

$$P_f = \left(\gamma d N_\gamma + C_c d N_c + q d N_q\right) \quad \text{... (2.11a)}$$

$$P_{trans} = \left[\gamma\left(d_e + \frac{q}{\gamma}\right)^2 w N_{s\gamma} + C_c w d_e N_{sc}\right] K_i \quad \text{... (2.11b)}$$

$$H = P_f \bullet \sin\left(\alpha + \beta\right) + P_{trans} \bullet \sin\alpha + C_a d \cos\alpha \quad \text{... (2.11c)}$$

$$V = P_f \bullet \cos\left(\alpha + \delta\right) + P_{trans} \bullet \cos\alpha + C_a d \quad \text{... (2.11d)}$$

This model included the soil and soil-metal frictional properties as well as the tool geometry, including the rake angle, depth and width. The model has been found to over-predict the draft force (Grisso & Perumpral, 1985).

2.4.2.4 Godwin-Spoor model

Godwin and Spoor (1977) studied the soil failure patterns with narrow tillage tines; and proposed a 3-D crescent failure above the critical depth and a 2-D horizontal failure pattern below the critical depth. For the 3-D crescent failure, a failure model was proposed as a parallel centre wedge flanked with two side crescents (Figure 2.4). The lateral failure below the critical depth was similar to earlier horizontal failure models proposed by O'Callgahan and Farrelly (1964) and Hettriaratch and Reece (1967). The model included an addition parameter, r, the rupture radius. They defined r as the total forward distance of soil failure on the surface from the tool face.

The total force was calculated as the sum of the forces due to the three sections. The centre wedge force was calculated using Equation (2.7). This 2-D expression was also used to calculate the force for small elements cut from the side crescents (Figure 2.3) as:

$$dP_q = \left(\gamma d_c^2 N_\gamma + C_c d N_c + q d_c N_c\right) \bullet \frac{r d\eta}{2} \quad \text{... (2.12a)}$$

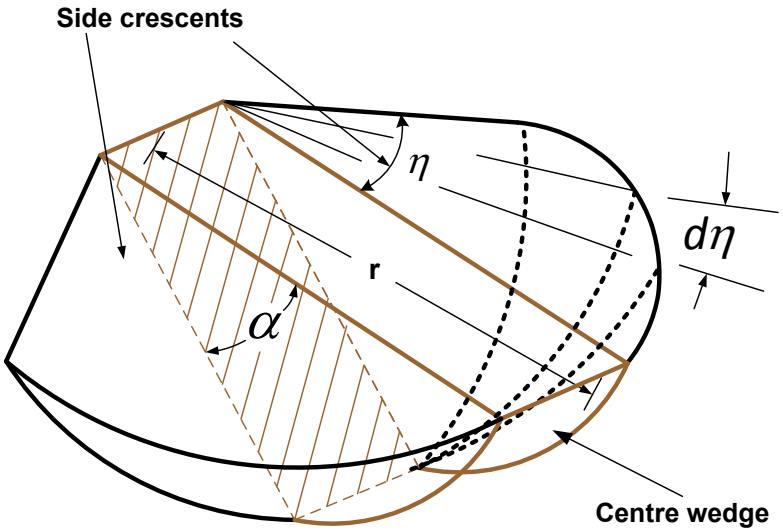

Figure 2.4: Failure zone of the Godwin and Spoor model (Godwin & Spoor, 1977)

The total applied force due to the side crescents was obtained by integration. The integration was simplified by assuming that the failure boundary on the top surface was circular. The draft (H_t) and vertical (V_t) forces for the 3-D crescent failure, above the critical depth was then given as:

$$H_t = \left[\gamma d_c^2 N_\gamma + C_c d_c N_c + q d_c N_q\right] \bullet \left[w + r\sin\eta\right]\sin\left(\alpha+\beta\right) + C_a w d_c \left[N_a \sin\left(a+\delta\right) + \cos\alpha\right] \quad \text{... (2.12b)}$$

$$V_t = -\left[\gamma d_c^2 N_\gamma + C_c d_c N_c + q d_c N_q\right] \bullet \left[w + r\sin\eta\right]\cos\left(\alpha+\delta\right) - C_a w d_c \left[N_a \cos\left(\alpha+\delta\right) + \sin\alpha\right] \quad \text{... (2.12c)}$$

The extended angle, η in Equation (2.12b & 2.12c) was calculated as:

$$\eta = \cos^{-1}\left(\frac{d_c \cos\alpha}{r}\right) \quad \text{... (2.12d)}$$

The lateral draft soil failure force was given as:

$$H_l = w\left[C_c N_c^{'}\left(d - 2d_c\right) + 0.5\left(1-\sin\phi\right)\gamma w N_\gamma^{'}\left(d^2 - d_c^2\right)\right] \quad \text{... (2.12e)}$$

The total draft force for deep blade was given as:

$$H = 2H_t + H_l \quad \text{... (2.12f)}$$

The application of this model required prior knowledge of *r*. However, *r* was affected by the blade rake angle and depth. Therefore, in order to test and verify this model, Godwin and Spoor (1977) developed a graph using the data from Payne (1956) and Payne and Tanner (1959); and Reece (1967) to determine the distance ratio (rupture distance over depth, i.e., *d/w)* and the tool rake angle. According to Shen and Kushwaha (1998), the determination of *r* was difficult.

2.4.2.5 McKyes and Ali model

McKyes and Ali (1977) developed an analytical model for narrow blades. Like was the case in the Godwin and Spoor (1977) model, a failure wedge was proposed ahead of the cutting blade (Figure 2.5). The model was similar to that of Godwin and Spoor (1977) as it consisted of a centre wedge and two side crescents. However, the bottom surfaces of both the centre wedge and the side crescents of this model were different from that of Godwin and Spoor (1977) (see Figures 2.3 & 2.4). In this model, the failure shape of the centre wedge's bottom was assumed to be a plane, while the two side crescents were assumed to be a straight line.

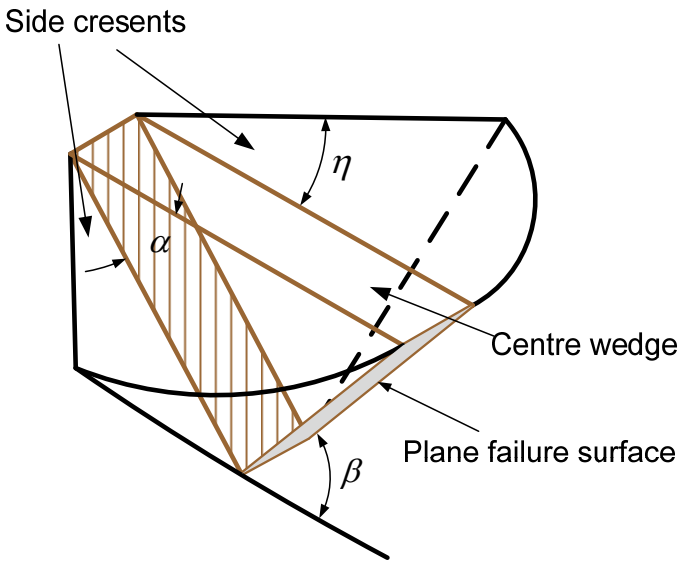

Figure 2.5: Single wedge failure zone of the McKyes and Ali model (McKyes & Ali, 1977)

Unlike the foregoing models, that used the 2-D slip-line theory to evaluate the forces, this McKyes and Ali (1977) model proposed a new approach to overcome the shortcoming of the cumbersome slip-line theory. In this model, the forces on each

section were determined by applying the mechanics of equilibrium directly rather than using the equation and *N*-factors of the 2-D soil failure (Kushwaha *et al.*, 1993). The assumed flat bottom plane of the centre wedge and the straight line at the bottom of the side crescents enabled the defining of the direction of the reaction forces at the bottom of the failure zone.

The total draft force expression developed (Eqn. 2.13a) for the failure wedge shown in Figure 2.5 consisted of the force contributions from the centre wedge and the two side crescent wedges (McKyes, 1989, pp 198), and was given as:

$$P = \left[\gamma d^2 N_{\gamma H} + C_c d N_{cH} + q d N_{qH} + C_a N_{ca} \right] w \qquad \text{... (2.13a)}$$

Equation (2.13a) is similar to the Reece (1965) equation but with N-factors re-evaluated for the 3-D soil failure. The expressions for the N-factors in this case were as follows:

$$N_{\gamma H} = \frac{\frac{r}{2d}\left[1 + \frac{2r}{3w}\sin\eta\right]}{\cot(\alpha+\delta) + \cot(\beta+\phi)} \qquad \text{... (2.13b)}$$

$$N_{cH} = \frac{\left[1 + \cot\beta\cos(\beta+\phi)\right]\left[1 + \frac{r}{w}\sin\eta\right]}{\cot(\alpha+\delta) + \cot(\beta+\phi)} \qquad \text{... (2.13c)}$$

$$N_{qH} = \frac{\frac{r}{d}\left[1 + \frac{r}{w}\sin\eta\right]}{\cot(\alpha+\delta) + \cot(\beta+\phi)} \qquad \text{... (2.13d)}$$

The rupture distance r, used in Equations (2.13b) to Equation (2.13d) was calculated as:

$$r = d\left(\cot\alpha + \cot\beta\right) \qquad \text{... (2.13e)}$$

The N-factors in Equation (2.13b) to Equation (2.13d) are all a functions of angle β. The angle β was calculated by minimizing the factor $N_{\gamma H}$, which was the factor for the gravity term in the draft equation. The angle β, obtained by the minimization, of $N_{\gamma H}$ was thereafter used to calculate the remaining N-factors. McKyes (1989) developed sets

of charts for determining the N-factors in the above expression. However, since the advent of good computing power and software, it is now easier to write simple computer programs to determine the N-factors. Kushwaha *et al.* (1993) stated that this model was easier to use than the Godwin and Spoor (1977) model, and that it does not require prior knowledge of the rupture distance, r.

2.4.2.6 Perumpral, Grisso and Desai model

Perumpral *et al.* (1983) developed another 3-D for narrow tillage tools. In this model, the weight of the soil due to the two side failure crescents of the Godwin and Spoor (1977) and McKyes and Ali (1977) were replaced by two reaction forces (R_{cr}) acting on the center wedge as shown in Figure 2.6. The model assumed that soil heaved ahead of the blade and that the failure wedge's slip bottom was a straight line, similar to that of the McKyes and Ali (1977) model.

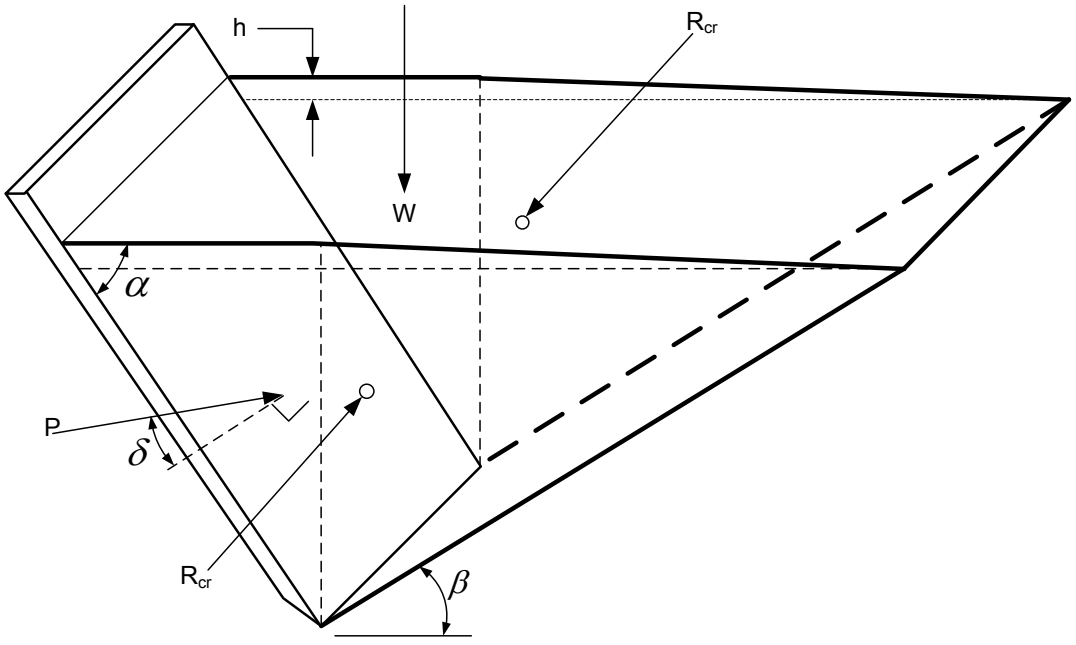

Figure 2.6: Failure zone of Perumpral *et al* model (Perumpral *et al.*, 1983)

The total draft force was calculated by considering the equilibrium of all the forces acting on centre wedge. The final force equation was given as:

$$P = w\left[\gamma d^2 N_\gamma + C_c d N_c + C_a d N_a\right] \quad \text{... (2.14a)}$$

The N-factors in Equation (2.14a) were given by the following expressions

$$N_\gamma = \frac{\frac{A}{wd^2}\left[2K_o d_z \sin\phi + w\sin(\phi+\beta)\right]}{\sin(\alpha+\beta+\phi+\delta)} \quad \ldots (2.14b)$$

$$N_c = \frac{\cos\phi\left[\frac{2A}{wd}+\frac{1}{\sin\beta}\right]}{\sin(\alpha+\beta+\delta+\phi)} \quad \ldots (2.14c)$$

$$N_a = \frac{-\left[1+\frac{h}{d}\right]\cos(\alpha+\beta+\phi)}{\sin(\alpha+\beta+\delta+\phi)} \quad \ldots (2.14d)$$

The coefficient of earth pressure, K_o and the average depth to the centroid of the failure wedge, d_z from the soil surface were given by the following equations:

$$K_o = 1-\sin\phi \quad \ldots (2.14e)$$

$$d_z = \frac{1}{3}(d+h) \quad \ldots (2.14f)$$

The angle β was determined by minimizing the total force P in Equation (2.14a). A computer program was developed that minimized the total force and determined the failure plane angle, β. The average depth at which the centroid of the failure wedge was located from the soil surface was found to be a function of failure plane angle, β.

2.4.3 Dynamic three dimensional models

2.4.3.1 Swick and Perumpral model

Swick and Perumpral (1988) modified the Perumpral *et al* (1983) model and proposed a dynamic 3-D soil cutting model that incorporated the tool dynamic effects. The model formulation included soil shear rate effects, soil inertial forces and soil-tool interaction parameters. The soil failure zone for this model was similar to that of McKyes and Ali (1977) model; and consisted of a centre wedge and two side crescents, with a straight rupture plane at the bottom (Figure 2.7).

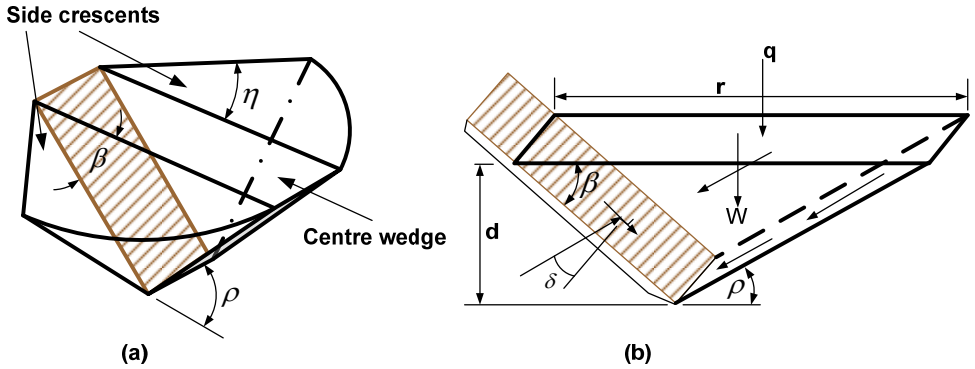

Figure 2.7: Failure zone of the Swick and Perumpral model (Swick & Perumpral, 1988)

In this model, the centre and the side sections were considered separately. Forces acting on the centre wedge are shown in Figure 2.7(b). Swick and Perumpral (1988) observed that the approach of Godwin and Spoor (1977) and McKyes and Ali (1977), in which the extreme outer points of the crescent sides were assumed to lie in a vertical plane passing through the forward tip of the tool, over-predicted the size of the side crescents. Therefore, based on the observations from the soil bin tests, Perumpral and Swick (1988) proposed the extended angle η as a function of the rupture angle distance, *r* and the rake angle β ; and was expressed as (Kushwaha *et al.*, 1992):

$$\eta = \frac{\sin^{-1}\left(-6.03 + 0.46r + 0.0904\sin\beta\right)}{r} \qquad \text{... (2.15a)}$$

The force equation, for this model, was derived in the same manner as the McKyes and Ali (1977) model but, with an acceleration force added, to account for travel speed effect. Based on the equilibrium equations for the centre wedge, the force on the centre wedge was given as:

$$P_1 = \frac{\dfrac{C_a d\cos\left(\beta+\phi+\rho\right)}{\sin\beta} + \left(\dfrac{\gamma dr}{2} + qr\right)\sin\left(\phi+\rho\right) + \left(\dfrac{C_c d}{\sin\phi} + F_{acc}\right)\cos\phi}{\sin\left(\beta+\phi+\rho+\delta\right)} \qquad \text{... (2.15b)}$$

The expression for the acceleration force, F_{acc}, was given as:

$$F_{acc} = \frac{\gamma d V^2 \sin\beta}{g\sin\left(\beta+\rho\right)} \qquad \text{... (2.15c)}$$

The forces on the side crescents was derived by considering the equilibrium of a small slice crescent and then integrating this force for the entire side crescent (Figure 2.8). The force on one side of the crescent was given as:

$$P_2 = \frac{\left\{\left[\frac{\left(\gamma dr^2 + qr^2\right)\sin\left(\phi+\rho\right)}{\sin\left(\beta+\phi+\delta+\rho\right)}\right] + F_{acc2}\cos\phi\left(\frac{\eta}{2}+\frac{\sin 2\eta}{4}\right) + C_c dr\cos\phi\sin\eta\right\} w}{\sin\left(\beta+\phi+\rho+\delta\right)} \quad \text{(2.14d)}$$

The side crescent acceleration force, in this case, was given as:

$$F_{acc2} = \frac{\gamma dr V^2 \sin\beta}{2g\sin\left(\beta+\rho\right)} \quad \text{... (2.15e)}$$

The total force, for the centre wedge and the two side crescents was expressed as:

$$P = P_1 + 2P_2 \quad \text{... (2.15f)}$$

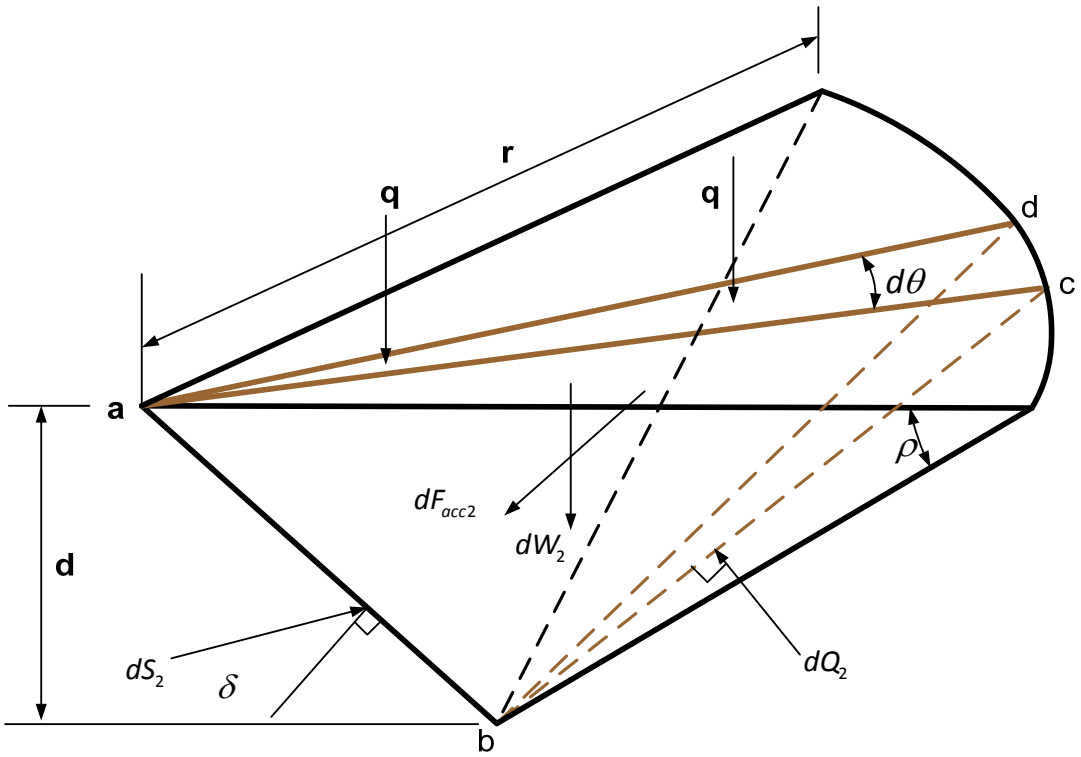

Figure 2.8: A side portion of the idealized failure wedge considered for the model and failure forces (Swick & Perumpral, 1988)

The force, P is a function of rupture angle ρ (Figures 2.7 & 2.8). Since the tool movement creates a passive condition, Swick and Perumpral (1988) used the Passive Earth Pressure Theory to determine the rupture angle. According to this theory, passive failure occurs when the resistance to the soil wedge is minimal. The wedge creating the minimum resistance was determined, in this case, by minimizing the total force (Equation (2.15f)) with respect to the rupture angle, using a numerical procedure. This model gave reasonable draft force predictions for the narrow tools tested.

2.4.3.2 Zeng and Yao model

Zeng and Yao (1992) proposed a soil cutting dynamic model to predict forces on wide and narrow blades. The model incorporated shear rate effects on soil shear, soil-metal friction and inertial effects. The failure zone of was similar to that of McKyes and Ali (1977). The soil failure zones of this model were as shown in Figure 2.9.

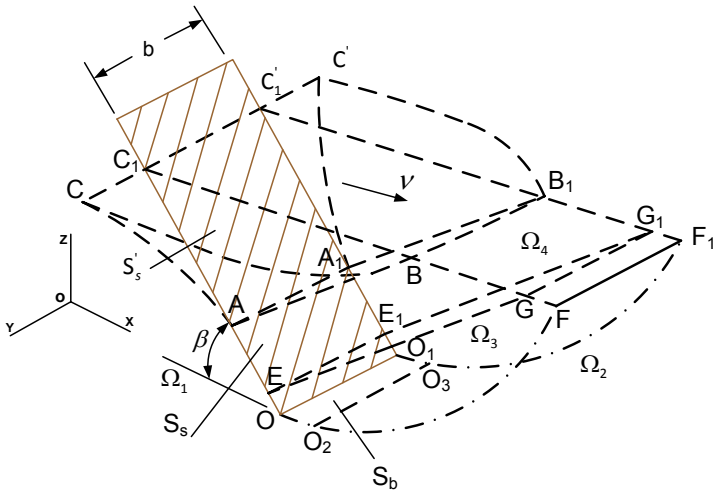

Figure 2.9: Failure zone of the Zeng and Yao model (Zeng & Yao, 1992)

There were two main differences between this model and the one proposed by McKyes and Ali (1997). The first difference was that this model required prior knowledge of the failure shear strain for the determination of the position of shear failure boundary shown in Figure 2.9. Secondly, the total draft force, P_X, for this model comprised five components, namely: the compressive force of the soil, P_G; inertia force of the soil in acceleration, P_A; bottom-wedge cutting force, P_C; frictional force along the cutting board

surface, P_F; and soil shear strength force, P_{SH}. The total draft force was expressed as follows:

$$P_x = P_G \sin\beta + \left(P_{SH} + P_A\right)\cos\beta_1 + P_F \cos\beta + P_C \quad \text{... (2.16)}$$

Comparison between the measured and predicted draft force produced acceptable results (Zeng & Yao, 1992). Some significant features of this model were that: soil-metal friction and shear strength were not influenced by shear rate; the model was not applicable for soils that flow plastically.

2.5 Rotavator performance prediction models

2.5.1 Empirical models

Extensive and comprehensive literature reviews on rotavators or rotary tillers have been undertaken by a number of researchers (Marenya, *et al.*, 2003; Hendrick & Gill, 1971a, 1971b, 1971c; Thakur & Godwin, 1989). The findings from these reviews indicated that no fundamental research capable of producing soil-tool mechanics has been undertaken for active tillage tools (Marenya, *et al.*, 2003). This is because all the literature reviewed by the above researchers indicate, that all the torque prediction models developed in the past, were empirically-based. The use of the empirical models for the prediction of rotavator torque requirement was probably due to the perceived complexity in the manner of the movement of a rotavator blade during tillage operations. However, empirical models lack the wide applicability, afforded by analytical models; and are therefore of limited use to designers of tillage tools.

2.5.2 Analytical models

There are very few analytical models that have been proposed for predicting the performance of rotavators (Marenya *et al.,* 2003). The few studies found in literature only modelled some aspects of energy requiring components; and did not use any of the known blades types in the model development. Details of some of the models found in literature that model some different aspects of performance of rotavators are discussed in the subsequent paragraphs.

Thakur and Godwin (1989) have presented the conceptual mechanism of soil failure by a wire under two different situations, i.e., when working through a semi-infinite homogeneous soil mass, and working close to an open wall. They surmised that the soil failure mechanism of a wire, cutting a varying thickness of the soil slice as in rotary tilling can be considered asymmetrical. In a follow-up study, Thakur and Godwin (1990) observed that, in general, soil shear failure planes developed towards the free curved face at an angle of $(45 - \phi/2)^{o}$ with the direction of the major principal stress, while cutting a full soil slice. They developed an analytical model by considering the soil resistance force to failure and reaction due to local shear failure. The model was applied to predict various force components for various bite lengths and depths of tillage. The relation between observed and predicted sets of data returned a high correlation coefficient of 0.94.

Shibusawa (1993) developed a model based on the trochoidal motion of the blade and the sliding motion of the soil over the blade that was capable of avoiding re-tillage in the up-cut direction. It was observed during this study, that significant amount of re-tillage occurred with down-cut rotavators; particularly for set tillage depths greater than 350 mm. Based on this model, a new blade, that enabled maximum backward throwing of the soil, sufficient to avoid re-tillage, was designed, fabricated and tested. On testing the new blade at tilling depths greater than 300 mm, it was found that the energy required in both directions of rotation was about half that demanded by rotavators fitted with conventional blades.

Gupta and Visvanathan (1993b) developed an analytical model for predicting the power requirement of a rotavator in saturated soil. The model was based on the predicted behaviour of saturated soil under impact and pure shear loading. In this model it was assumed that the power required by a rotavator is used for cutting the soil, throwing the cut soil slices by centrifugal action of the blades, overcoming soil-metal friction and overcoming parasitic forces. In this model, all the energy requirements were expressed in terms of torque requirements. The application of this model showed that for saturated clay under rotavator tillage, the power requirement consisted of 0.34 to 0.59 % for cutting, 30.5 to 72.4 % for throwing out cut slices by centrifugal action of rotary

blades, 0.96 to 2.45 % for overcoming soil-metal friction, 0.62 to 0.99 % for soil-soil sliding friction, and 23.1 to 64.6 % for idle power. This model was however, not based on any of the standard rotavator configurations, which makes its suitability for wider application questionable.

2.6 Summary and conclusion from the reviewed literature

The power performance and quality of work of rotavators is affected by many factors including the blade configuration, direction of rotation, depth of tillage, ratio of the peripheral speed to the forward travel speed (λ), and the soil condition. Irrespective of the direction of rotation, when other rotavator operational factors and the soil condition are held constant, increasing the depth of operation increases the specific energy requirements. In most cases the specific energy requirements increases at an increasing rate with depth of tillage but some studies reported a linear relationship between increments in these two factors for the same soil conditions for a given rotavator. Consequently, there is no consensus on the specific energy requirements of rotavators with the increase in depth of tillage.

The direction of rotation of a rotavator has significant influence on the power performance and the quality of work. For the horizontal axis rotavators, the direction of rotation influences the power demand and determines whether a thrust force or a pull force will be exerted on the tractor. In most studies cited in reviewed literature, the magnitude of the push/pull forces were not measured and were therefore not included in the calculations of the rotavator's power requirements. There are two reasons why the magnitude of the push/pull forces should be recorded. First, it would ensure that the calculations of the specific energy requirements takes into account the influence of the push/pull forces. The secondly reason is that it would allow for the quantification of the magnitude of the push forces that may be detrimental to the tractor's operation. The measurement and determination of the resultant horizontal force would enable the correct determination of total power requirement for a given rotavator operated under specified operational and soil conditions.

The soil physical condition has a marked influence on the power performance and the quality of work of rotavators. The soil condition is affected by the soil water content, which has significant influence on other soil strength properties. Pertinent soil parameters that must be monitored for the quantification of tillage tool's performance include the soil water content, soil bulk density, soil shear strength and the soil-metal friction parameters.

There was no documentation in literature, on the application of the ANN and DEM for modelling techniques for the predicting the energy requirements of both passive and active tillage tools. This is attributed to the difficulty of modelling soil-tool interaction and soil failure by these methods, during dynamic processes such as tillage operations. On the other hand the application of the analytical models for the prediction of energy requirements for passive tillage tools has been extensive, and has produced acceptable results for predicting the energy requirements of passive tillage tools. Furthermore, since the behaviour of the rotavator blade, at an instantaneous time moment resembles that of a wide passive blade, the analytical models that have been used to predict the energy requirements of passive tillage tools can, form a basis for the development of an energy requirements prediction model, for rotavators.

There are many models that have been developed for the prediction of the draft force for a passive blade. However, for the rotavator, only empirical models have been proposed, for the different cutting blades in different soils. Empirical models, by nature are limited in applicability, and can therefore not be used to design blades that may result in improved performance of rotavators. From the review of literature presented in this chapter, the development of analytical models for prediction of torque requirement of rotavators is necessary, if better rotavator blades are to be developed.

2.7 Justification

The literature reviewed revealed that numerous studies have been undertaken on the passive tillage tools. The literature reviewed also indicated that only a limited number of studies have been undertaken on active tools. Furthermore, the studies undertaken for

predicting the rotavator torque requirements were empirically-based, thus having limited applicability. Therefore, there is need for the development of analytical models based on the actual rotavator blade configurations for the accurate prediction performance of rotavators.

As a tillage tool, the rotavator has a number of advantages over the passive tillage tools. However, its adoption as an alternative to the passive tools has been hampered by its perceived excessive power requirement, particularly in deep tillage. Owing to its capability for significant reduction in the number of tillage operations necessary for achieving the required tillage tilth, this tool offers great potential for the reduction of the land preparation costs. Land preparation costs using the conventional tillage system is becoming prohibitively expensive owing to the escalating cost of fossil-based fuels and oils. Therefore, there is need to characterize the performance of the rotavator over a wider range of tillage depths. In addition, there is need to quantify the behaviour of the resultant thrust force generated when the rotavator is operated in the concurrent and counter-current directions of rotation, at different tillage depths.

Therefore, a study on performance characteristics of a deep tilling rotavator was proposed.

2.8 Hypotheses

The hypotheses of this study were as follows:

- The existing analytical models for passive blades can be adopted and modified to form a basis for formulating a model that can be used to model the performance indicators of a rotavator fitted with a standard commercially available rotavator blade
- The performance of a rotavator can be quantified through the measurement of its torque requirements and the resultant horizontal thrust force generate during its operation.

- There exists an optimum depth at which the resultant horizontal thrust force generated is greatest for a down-cutting rotavator of given design dimensions and operational conditions.

2.9 Objectives

The objectives of this study were to:

1 Design, fabricate and test an instrumented experimental deep-tilling setup to measure rotavator performance, including the thrust forces generated and the corresponding instantaneous rotavator operational parameters including, set tillage depth, instantaneous depth, rotational and forward travel speed and forward distance travelled.

2 Design, fabricate and test an instrumented soil strength characterisation apparatus capable of measuring the soil strength properties at different depths.

3 Quantify the field performance of an experimental deep-tiling rotavator over a wide range of set tillage depths based on the measured torque requirements and the resultant horizontal thrust forces generated.

4 Develop an analytical model that uses the soil dynamic parameters to predict the torque requirements of a rotavator fitted with commercially available rotavator blades.

5 Compare the predicted and the measured torque requirements of a rotavator fitted with a commercially available rotavator blade type.

CHAPTER 3

MODELING ROTAVATOR TORQUE AND POWER REQUIREMENTS

3.1 Introduction

The changing location of the tip of a rotavator as it processes the soil is one of the key parameters that must to be considered when developing a mathematical model for its torque requirements. For a rotavator fitted with cutting blades of given a configuration, the instantaneous location of its tip is determined by the kinematics of the rotavator. This change in depth, as the blade processes the soil, results in continuous change of the torque requirements from the initiation to the end of the soil cutting process. Rotavator kinematics affects the choice of the renovator's design and operational parameters, which in turn have a marked effect on its torque requirements.

With the exception of the direction of rotation, which affects the shape of the cut soil slice, all the other rotavator input parameters (Figure 1.2) can be held constant for a given setup. For the two possible directions of rotation on a horizontal rotor (Figure 1.1a), two mathematical models can be developed for predicting the variation of torque requirements with the angle of rotation or instantaneous depths for a chosen cutting blade configuration. This arises because the soil-tool interactions for the down- and up-cutting directions of rotation are different.

In this study, only the down-cut direction was considered for modelling the rotavator torque requirements. The down-cut direction of rotation was preferred because of the following reasons:

- reverse rotational rotavators are uncommon
- the forward thrust generated by a down-cut rotavator aids in traction
- the instantaneous behaviour of the blade is similar to that of an inclined passive blade, therefore the existing force prediction models can be modified in the development of their torque and specific energy prediction models.

The first part of this chapter analyzes the kinematics of a down-cutting rotavator. The remainder of the chapter is devoted to the development of an analytical model for predicting the force, torque and energy requirements for a down-cutting rotavator fitted with L-shaped blades.

3.2 Rotavator kinematics

Rotavators execute combined rotational and forward motion during tillage operations. The path of motion of each point on the rotavator tine depends on the circumferential and forward travel velocities, as well as the direction of rotation. An understanding of the rotavator kinematics is necessary for the analysis of its operations (Hendrick & Gill, 1971a). Kinematics is the study of motion without, reference to the force(s) causing the motion (Meriam & Kraige, 1987).

3.2.1 Equation of motion and the cutting trajectory of the tiller blade

In rotavators, the forced rotation of the rotor shaft, with working tools fixed to it, participates in two motions, namely, the rotary motion around its axis with velocity V_{cir} and forward travel speed, V_f, associated with the prime-mover e.g. a tractor. For deriving the equation of motion, a stationary system of co-ordinates (Figure 3.1) is considered.

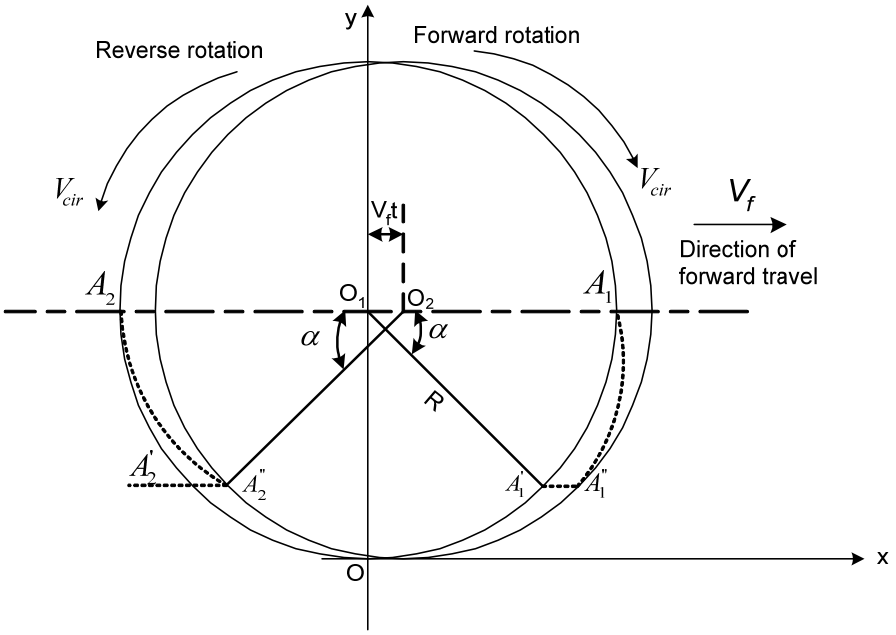

Figure 3.1: Diagram for the determination of the equation of motion (Sineokov & Panov, 1978).

Let the rotor of radius, *R*, turn through an angle, α, from its original position in time, *t* (Figure 3.1). The point A_1, for the case of down-cut rotation; and point A_2, for the case of the up-cut rotation, corresponding with the tip of the tiller blade, take positions A_1' and A_2', respectively, for a stationary system. In practice, the system is not stationary and a point on the rotor tiller travels along a path that is a combination of the forward travel speed and the rotor rotational speed. In this case, the distance from the rotational axis to the point of interest points, A_1' and A_2', move a distance equal to V_f*t,* and take positions A_1'' and A_2'', respectively. The co-ordinates of these points are expressed (Hendrick & Gill, 1971a; Bernacki *et al*., 1972 and Sineokov & Panov, 1978) as:

$$\left.\begin{aligned} x &= V_f t \pm R\cos\alpha \\ y &= R\left(1-\sin\alpha\right) \end{aligned}\right\} \quad \text{... (3.1)}$$

where:

α = the angle of rotation of the tiller blade with respect to its initial position (rad.)

t = is the time of rotation of the rotor through angle α (s).

Equation (3.1) determines the absolute trajectory of motion of rotavator blades with a horizontal axis of rotation. Geometrically, this trajectory is a trochoid or curate cycloid (Figure 3.2) depending on the distance of the point from the rotor axis (Hendrick & Gill, 1978; Bernacki *et al*., 1972; Bosoi *et al*., 1988; and Sineokov & Panov, 1978).

While Equation (3.1) could be used for design purposes, the parameter most frequently used, both as a design and use parameter, is the dimensionless ratio of the rotor peripheral velocity (V_{cir}) to the machine forward travel velocity (V_f) called the kinematic parameter, λ, (Hendrick & Gill, 1971c). This dimensionless ratio is expressed as:

$$\lambda = \frac{V_{cir}}{V_f} = \frac{R\omega}{V_f} \quad \text{... (3.2)}$$

where:

R = rotor radius (m)

ω = angular velocity of the rotor (rad/s)

V_f = forward travel velocity (m/s).

V_{cir} = peripheral velocity of the rotor blades (m/s)

Substituting the value of λ into Equation (3.1) gives the trajectory of motion of the tiller blades as:

$$\left.\begin{aligned} x &= R\left(\frac{\alpha}{\lambda} \pm \cos\alpha\right) \\ y &= R\left(1-\sin\alpha\right) \end{aligned}\right\} \quad \text{... (3.3)}$$

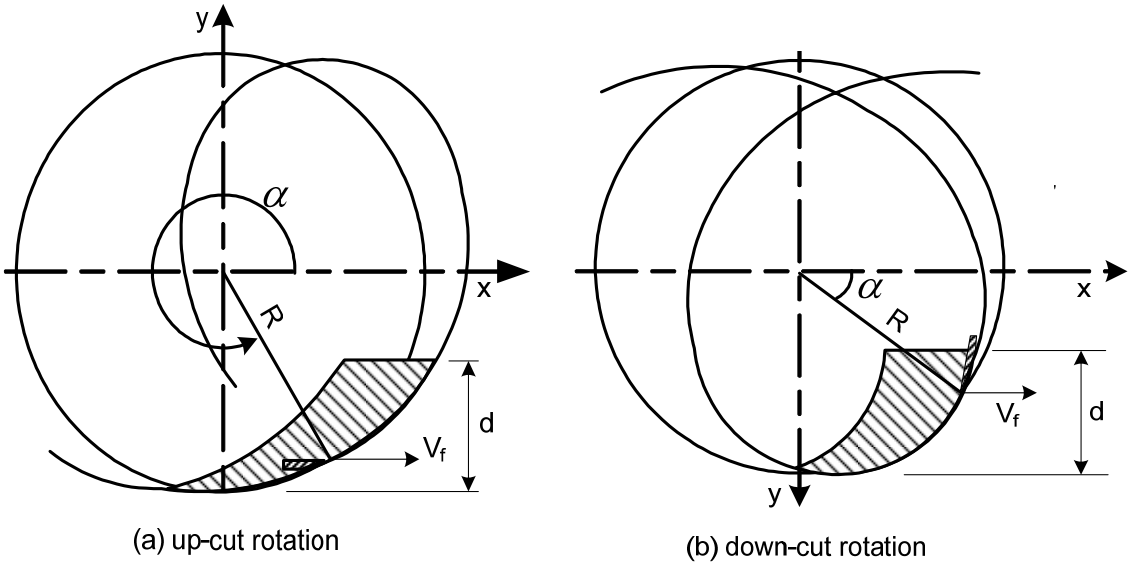

Figure 3.2: Trajectories of working elements and thickness of shapes of the soil slices cut by rotavator blades during up- and down-cut tillage (Hendrick & Gill, 1971a)

Equation (3.3) shows that the variation of the trochoidal shape is affected only by λ, characterising the working regime of rotavators. Figure 3.3 presents the dimensions and form of the cut slices of soil as determined by trajectories of two successively working tines and their direction of rotation. From Figure 3.3, the direction of rotation of the blades, relative to the travel direction, also influences the rotavator working regime.

The tilling speed or the absolute velocity of the tiller blades is obtained by differentiating Equation (3.1) with respect to time. Therefore,

$$\left.\begin{aligned} v_x &= \frac{dx}{dt} = V_f \mp R\omega\sin\omega t = V_f \mp V_{cir}\sin\omega t \\ v_y &= \frac{dy}{dt} = -R\omega\cos\omega t = -V_{cir}\cos\omega t \end{aligned}\right\} \quad \text{... (3.4)}$$

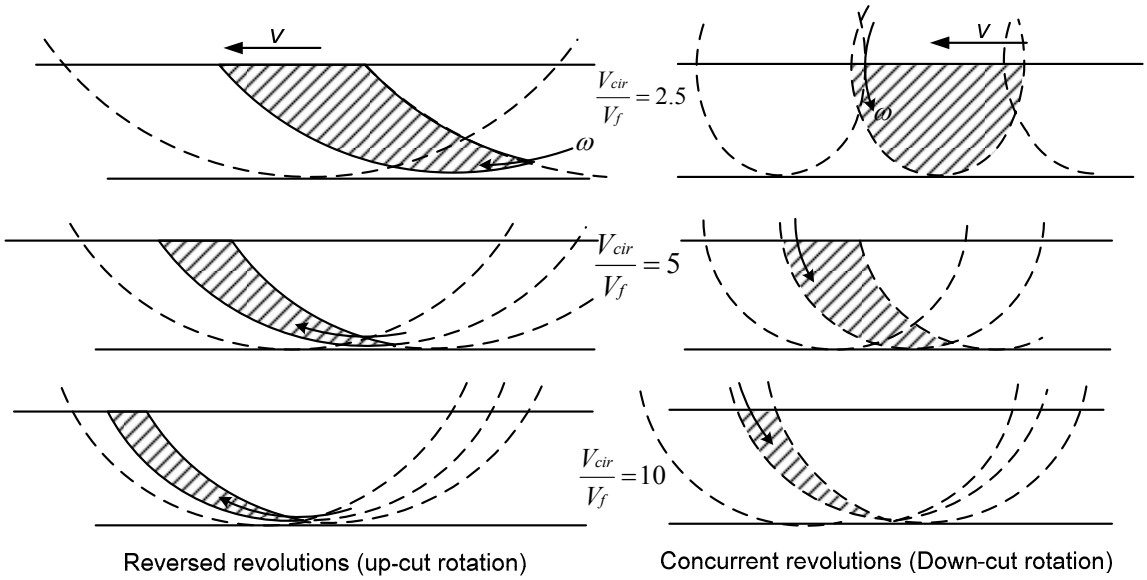

Figure 3.3: Shapes of slices for down-cut and up-cut rotation as a function of the ratio of the peripheral speed to forward speed. *Rω/Vf=λ.* Number of blades operating in one plane z = 3 (Bernacki *et al.*, 1972)

The modulus of the absolute velocity, V_a, of the rotor blade tip (Sineokov & Panov, 1978) is given by:

$$V_a = \sqrt{V_x^2 + V_y^2} = \sqrt{V_f^2 \pm 2V_f V_{cir} \sin \omega t + V_{cir}^2} \quad \text{... (3.5)}$$

Inserting λ and $\alpha = \omega \cdot t$ into Equation (3.5) gives,

$$V_a = V_f \sqrt{\lambda^2 \pm 2\lambda \sin \alpha + 1} \quad \text{... (3.6)}$$

Equation (3.6) shows that the absolute velocity of the rotor blade tip is variable and is influenced by the angle of rotation of the blade in relative motion. The tilling speed is directed along the tangent to the absolute trajectory of motion of the blade (Sineokov & Panov, 1978; Meriam & Kraige, 1987).

3.2.2 The bite length

The bite length or blade delivery is determined by considering the process of soil cutting by two adjacent blades in one vertical plane and mounted on the same side of the flange (Figure 3.4).

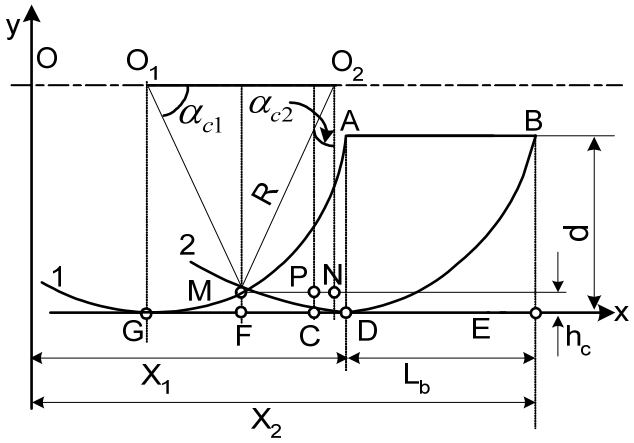

Figure 3.4: Determination of the bite length and the undisturbed peak crest heights (Sineokov & Panov, 1978)

With reference to Figure 3.4, the trajectory of Blade 1 is displaced with respect to that of the adjacent Blade 2 along the horizontal line through a certain value, L_b, called the bite length (Sineokov & Panov, 1978). The value of L_b is given by:

$$L_b = V_f t_b \qquad \text{... (3.7)}$$

where:

t_b = time during which the blades rotate through an angle, equal to the angle between the adjacent blades on the same side of a flange (s).

If the number of blades in one plane of rotor flange is z, then the angle between adjacent blades, in radians, is equal to $\frac{2\pi}{z}$. In such a case, the time t_b is given by $t_b = \frac{2\pi}{z\omega}$ and the bite length, L_b is expressed as:

$$L_b = \frac{2\pi V_f}{z\omega} \text{ or } L_b = \frac{2\pi R}{\lambda z} \qquad \text{... (3.8)}$$

Equation (3.8) shows that the bite length is a constant quantity that is dependent on the rotavator radius, R, the number of blades on the same side of a flange, z and the kinematic parameter, λ. The value of the bite length is one of the principal technological parameters of rotavators (Chamen *et al.*, 1979) and determines the degree of chopping of the processed soil (Sineokov & Panov, 1978).

3.2.3 Furrow bottoms produced by rotavators

During tillage operations, rotavators produce furrow bottoms with peaks of undisturbed (untilled) soil (Figure 3.4). These undisturbed peaks are dependent on the direction of rotation and the ratio of the peripheral to the forward travel speed. The non-uniformity of the furrow bottoms can be excessive and be agronomically undesirable. Therefore, in the design of rotavators, selection of parameters that will ensure the occurrence of minimum height of undisturbed peaks, are important.

In developing the expression for the determination of the peak crescent height, h_c, many researchers (Sineokov & Panov, 1978; Bosoi *et al*., 1988; Hendrick & Gill, 1976) considered paths of adjacent tiller blades revolving in one vertical plane (Figure 3.4). The height of peaks, h_c is equal to the ordinate of point M, which is the point of intersection of two adjacent cycloids. This peak height is given by:

$$h_c = R\left(1-\sin\alpha_c\right) \qquad \text{... (3.9)}$$

The angle of rotation of the tiller radius that corresponds to maximum peak height of the crests formed first (Blade 1) is:

$$\alpha_{c_1} = \sin^{-1}\left(1-\frac{h_c}{R}\right) \qquad \text{... (3.10)}$$

where:

α_{c_1} = the angle the first blade makes with the maximum crest height (rad.)

The angle of rotation (Figure 3.4) of the adjacent blade (Blade 2) corresponding to the point of intersection of the cycloids (M), which give the peak height at the bottom of the furrow, is given by (Sineokov & Panov, 1978)

$$\alpha_{c2} = \frac{2\pi}{z} + \pi - 2\alpha_{c1} \qquad \text{... (3.11)}$$

where:

α_{c_2} = the angle at the second blade make with the maximum crest height (rad.).

$\frac{2\pi}{z}$ = the angle between any two adjacent blades on a flange on the rotor (rad.)

z = the number of blades in the same vertical plane.

By the time the adjacent blade (Blade 2) reaches the point of intersection, M, the centre of the rotor will have moved a horizontal distance equal to $\overline{O_1O_2}$. This distance is equal to V_f*t, which is equal to the bite length (or blade delivery) L_b. Since $t = \alpha/\omega$, where α is the angle turned at ω *rad/s* in time t, the distance $\overline{O_1O_2}$ may be expressed as:

$$\overline{O_1O_2} = V_f t = V_f \left(\frac{2\pi}{z\omega} + \frac{\pi - 2\alpha_{c1}}{\omega} \right) \quad \text{... (3.12)}$$

The same distance $\overline{O_1O_2}$ may be expressed in terms of the rotor radius as:

$$\overline{O_1O_2} = 2R\cos\alpha_{c1} \quad \text{... (3.13)}$$

Since Equation (3.12) and Equation (3.13) represent the same point, and because $\cos\alpha_{c1} = \sqrt{1-\sin^2\alpha_{c1}}$, it follows that Equation (3.13) may be expressed as:

$$2R\sqrt{(1-\sin^2\alpha_{c1}} = \frac{V_f}{\omega}\left(\frac{2\pi}{z} + \pi - 2\alpha_{c1} \right) \quad \text{... (3.14)}$$

Given that $\alpha_{cr} = \sin^{-1}\left(1-h_c/R\right)$ and since for small values of $\alpha_{c1}, \sin\alpha_{c1} \approx \alpha_{c1}$, with acceptable levels of accuracy. Also recalling that $R\omega = V_{cir}$ and $V_{cir}/V_f = \lambda$, after substituting these values in Equation (3.14) and making the necessary transformations (Sineokov & Panov, 1978), results in Equation (3.15).

$$\lambda = \frac{\left(\frac{\pi}{z} \pm \frac{\pi}{2}\right) \mp \sin^{-1}\left(1 - \frac{h_c}{R}\right)}{\sqrt{2\frac{h_c}{R} - \frac{h_c^2}{R^2}}} \quad \text{... (3.15)}$$

The $\pm$ and $\mp$ in Equation (3.15) takes care of the direction of rotation of the rotor. Equation (3.15) combines the rotavator principal parameters λ, R and z, with the peak crest height, h_c.

The relations given above, do not permit easy manual determination of the absolute peak crest height, h_c (Sineokov & Panov, 1978), and the use of the geometric relations in Figure 3.4 is recommended for the determination of the absolute value of the peak height of the crest, h_c, by considering the path of the points on adjacent loci (Hendrick &

Gill, 1976) to have a rolling radius equal to $\frac{V_f}{\omega} = \frac{R}{\lambda}$. Using this approach, the angle between the rotor radius, drawn from O_2 to the point M, and the vertical in Figure 3.4 is denoted as α_{c2}. This angle, from the triangle O_2MN, can be expressed as,

$$\sin \alpha_{c2} = \frac{\overline{MP} + \overline{PN}}{R}$$

From symmetry of the position of the crest in Figure 3.4 with respect to the two adjacent cycloids, $\overline{MP} = \frac{L_b}{2}$, where L_b is the bite length or the blade delivery.

The length $\overline{PN}$ (Sineokov & Panov, 1978) is given by:

$$\overline{PN} = \frac{V_f}{\omega}\alpha_{c2} = \frac{R}{\lambda}\alpha_{c2}$$

The value of $\sin \alpha_{c2}$ can therefore be expressed as:

$$\sin \alpha_{c2} = \frac{\frac{L_b}{2} + \frac{R}{\lambda}\alpha_{c2}}{R} \quad \text{... (3.16)}$$

Putting $\sin \alpha_c = \alpha_c$ for small angles, and making the necessary transformation gives:

$$\alpha_{c2} = \frac{\pi}{z(\lambda - 1)}.$$

Hence the crest height is given by:

$$h_c = R\left[1 - \cos\left(\frac{\pi}{z(\lambda \mp 1)}\right)\right] \quad \text{... (3.17)}$$

If the maximum peak crest height, h_c, is dictated by agronomic requirements, the kinematic parameter λ can be calculated from:

$$\lambda = \frac{\pi}{z\cos^{-1}\left(1 - \frac{h_c}{R}\right)} \pm 1 \quad \text{... (3.18)}$$

The crest-shaped nature of the furrow bottoms produced by rotavators is one of the tiller's important indices of performance. The height of ridges can be used as means of determining the effective tilling depth of rotavators (Hendrick & Gill, 1976), even though the exact agronomic significance of the peak crest height has not been investigated.

In practice, the peak crest height, $h_{c,}$ may be less than the theoretically determined h_c using Equation (3.17), due to crumbling away or breaking loose of the untilled soil, though it is uncut by the rotor blade (Sineokov & Panov, 1978). The actual crest height may therefore be approximately given by:

$$h_{ac} = \frac{h_c}{k_c} \quad \text{... (3.19)}$$

In Equation (3.19), k_c is the coefficient allowing for reduction of the crest height due to breakage of the peak crest height as the tillage operation progresses. Values of k_c depend on the soil type, and average k_c values have been given by Sineokov and Panov (1978) as 2.0 for sandy loam, 1.5 saturated sandy-loams and 1.0 for heavy sandy-loam.

3.2.4 Side surface area of the soil chip

The soil chip cut by the blades of rotavators is best looked at in terms of the area of the side surface, thickness, and the volume. The three constitute the chips of soil slices cut by rotavator blades.

Based on the geometric relation of Figure 3.4, the area of the surface ABM can approximately be given as:

$$A_{ABM} = L_b d \quad \text{... (3.20)}$$

The crest area, A_{cr}, which is the area under GMC (Figure 3.4), must be taken into consideration, for accurate determination of the side surface area. Using the equality of the areas under BEC and ADG, the side surface area, A_{AMB} is given as:

$$A_{ABM} = A_{ABCG} - A_{cr} = L_b d - A_{cr} \quad \text{... (3.21)}$$

The crest area, A_{cr} is equal to twice the area under CFM. This area is equal to half the crest area and can be determined from:

$$A_{CFM} = \int_{t_1}^{t_2} yx dt = \int_{t_1}^{t_2} R(1-\sin\omega t)(V_f - V_{cir}\sin\omega t)\, dt \quad \text{... (3.22)}$$

where:

t_1 = time taken by the leading blade to turn through angle α_{c1}

t_2 = time taken by the second blade to turn through angle α_{c2}

Changing the limits of integration and noting that $t = \frac{\alpha}{\omega}$, and that $dt = \frac{d\alpha}{\omega}$, A_{CFM} can be expressed as:

$$A_{CFM} = \int_{\alpha_1}^{\alpha_2} R(1-\sin\alpha)\left(V_f - V_{cir}\sin\alpha\right)\frac{d\alpha}{\omega} \quad \text{... (3.23)}$$

Integrating Equation (3.23) and taking limits of integration as $\alpha_1 = \pi/2$ and $\alpha_2 = \alpha_c$ gives

$$A_{CFM} = \frac{R^2}{\lambda}\left(-\frac{\pi}{2} + \alpha_c + \cos\alpha_c\right) + R^2\left(\cos\alpha_c - \frac{\pi}{4} + \frac{\alpha_c}{2} - \frac{1}{4}\sin 2\alpha_c\right) \quad \text{... (3.24)}$$

The angle α_c (Figure 3.4) is obtained from the expression $\alpha_c = \frac{\pi}{2} - \alpha_{c1} = \frac{\pi}{2} - \frac{\pi}{z(\lambda - 1)}$.

3.2.5 Chip thickness

The thickness of the soil cut by blades of a rotavator varies continuously from a maximum value to zero for a down-cut rotating rotor, and from a minimum (zero) to a maximum for an up-cut rotating rotor. The chip thickness must be known when calculating the tilling power of rotary blades. In general many methods, based on geometry of the cut soil slice have been presented for approximately determining the thickness of the chip (Sineokov & Panov, 1978).

In the first approximation approach (Sineokov & Panov, 1978), the thickness is the distance between two adjacent trajectories, measured in the radial direction from the centre of the rotor (Figure 3.6). In this case; the thickness ϑ is expressed as,

$$\vartheta = L_b \cos\alpha \quad \text{... (3.25)}$$

where:

L_b = is the bite length

α = the angle of rotation of the blade.

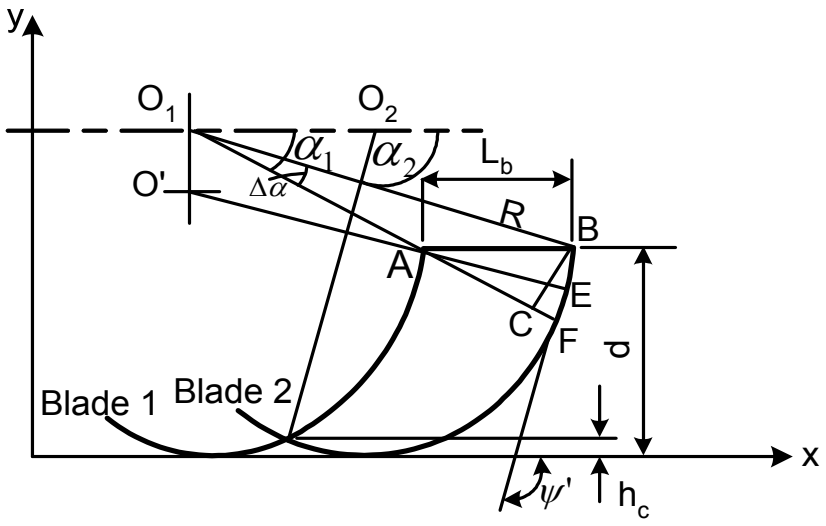

Figure 3.6: An illustration for determination of the soil chip thickness (Sineokov & Panov, 1978)

The maximum sizes of the chip thickness in this case comprise the angle $\alpha = \alpha_1$, i.e. the angle turned through at the beginning of blade tilling and is calculated (Sineokov & Panov, 1978) using:

$$\vartheta_{\max} = L_b \cos\alpha_1 = \frac{L_b}{R}\sqrt{2Rd - d^2} \quad \text{... (3.26)}$$

where:

d = depth of tillage

ϑ_{max} = equal to the length $\overline{AE}$

Equation (3.26) underestimates the value of maximum thickness of the soil chip by a value equal to the length $\overline{CF}$ (Figure 3.6). Secondly, the equation is only applicable for kinematic parameter (λ) values in excess of 10, when the tilling trajectory of the blades is almost circular (Sineokov & Panov, 1978). For such high values of λ, the rotational velocity for most rotary tillage operations is too high and is associated with high power expenditure, accompanied with excessive pulverisation of the tilled soil, both of which, are undesirable.

The second approximation was presented by Kaneve (as cited in Sineokov & Panov, 1978). In this method, the section CF is taken into consideration and gives the soil thickness as:

$$\vartheta = L_b \cos\alpha + R\left(1-\cos\Delta\alpha\right) \quad \text{... (3.27)}$$

where:

$$\Delta\alpha = \sin^{-1}\left(\frac{L_b}{R}\sin\alpha\right)$$ (see Figure 3.6)

The third method (Sineokov & Panov, 1978), which is more accurate, is based on the geometry of Figure 3.6. In this latter approach, the thickness of the soil chip is obtained by measuring the section $\overline{AE}$ as a straight line, drawn from the instantaneous centre of the rotor O, i.e. along the normal to the external cycloid.

The thickness, ϑ of the chip is then given by:

$$\vartheta = L_b \sin\psi' \quad \text{... (3.28)}$$

where:

ψ' = the angle formed by the positive direction of the tangent at the given point of the cycloid and the positive direction of the abscissa.

The angle ψ ' (Sineokov & Panov, 1978) is obtained from:

$$\tan\psi' = \frac{dy}{dx} = \frac{-V_f\cos\alpha}{V_{cir} \mp V_f \sin\alpha} \quad \text{... (3.29)}$$

From Equation (3.29) the angle ψ' may be expressed as:

$$\psi' = -\tan^{-1}\left(\frac{\lambda\cos\alpha}{1\mp\lambda\sin\alpha}\right) \quad \text{... (3.30)}$$

Substituting ψ' into Equation (3.28) gives the soil chip thickness, ϑ, as:

$$\vartheta = L_b \sin\left(-\tan^{-1}\left(\frac{\lambda\cos\alpha}{1\mp\lambda\sin\alpha}\right)\right) \quad \text{... (3.31)}$$

In some cases (Sineokov & Panov, 1978) it may be sufficient to use the concept of average thickness of the soil chip. In such an approach, the average thickness of the chip

is expressed as $L_{bav} = L_b \cos\frac{\alpha_k}{2}$, where $\alpha_k = \alpha_2 - \alpha_1$. The angle, α_k, being the difference between the angles turned through by the blade at the beginning and the end of the soil cutting process. Expressing the angles α_1 and α_2 in terms of depth of tillage, *d*, and the peak crest height, h_c, (Sineokov & Panov, 1978) gives the average cut soil thickness as:

$$\vartheta_{av} = L_b \cos\frac{1}{2}\left[\left(1-\frac{h_c}{R}\right) - \sin^{-1}\left(1-\frac{d}{R}\right)\right] \quad \text{... (3.32)}$$

3.2.6 Volume of the soil chip

Figure 3.7 shows the dimensions of a soil block chipped-off by a down-cut rotavator blade. The width of the chip, *w*, is the distance between adjacent blades along the rotor shaft axis. The volume of the chip can be approximately determined (Hendrick & Gill, 1971a; Sineokove & Panov, 1978) as:

$$V_{chip} = L_b dw \quad \text{... (3.33)}$$

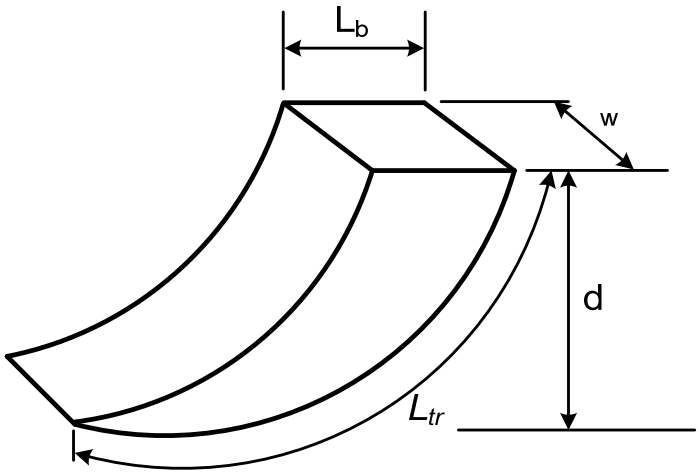

Figure 3.7: The main dimensions of a soil chip cut by a down-cutting rotary blade (Hendrick & Gill, 1971a)

For accurate determination of V_{chip}, it is necessary to take the volume of the crest into account (Figure 3.4). The volume of the crest is given by:

$$V_{crest} = A_{cr} w \quad \text{... (3.34)}$$

where:

$A_{cr} = 2A_{CFM}$ (A_{CFM} is given by Equation (3.24)

Therefore the actual volume, V_{ac}, of the soil is

$$V_{ac} = V_{chip} - V_{crest} \quad \text{... (3.35)}$$

3.2.7 Length of the tilling route

The length of the tilling route, L_{tr}, (Figures 3.7) is the length of the cycloid section from the point of intersection of the blade trajectory with the soil surface to the point of intersection of two adjacent trajectories at the maximum peak crest height (point M in Figure 3.4). An elemental arc of the trajectory is given by

$$dL_{tr} = \sqrt{dx^2 + dy^2} \quad \text{... (3.36)}$$

Substituting the values of the first derivative of the equation of motion (see Equation 3.3) of the rotor blade end point gives:

$$dL_{tr} = V_f \sqrt{1 \mp 2\lambda \sin \alpha t + \lambda^2} \quad \text{... (3.37)}$$

From Equation (3.37) the tilling route L_{tr} is given by:

$$L_{tr} = \int_{\omega t_1}^{\omega t_2} dl dt$$

Changing limits of integration with respect to angle of rotation $\alpha_i = (\omega \cdot t_1)$, $\alpha_e = (\omega \cdot t_2)$ and $dt = \dfrac{d\alpha}{\omega}$ gives the tilling route length as:

$$L_{tr} = R \int_{\alpha_i}^{\alpha_e} \sqrt{1 \mp 2\lambda \sin \alpha + \lambda^2}\, d\alpha \quad \text{... (3.38)}$$

Equation (3.38) can be expressed (Sineokov & Panov, 1978) as:

$$L_{tr} = \frac{R}{\lambda} \sqrt{1 + \lambda^2} \int_{\alpha_i}^{\alpha_e} \left(1 \mp \frac{2\lambda \sin \alpha}{1 + \lambda}\right)^{\frac{1}{2}} d\alpha \quad \text{... (3.39)}$$

Integration of Equation (3.39) belongs to elliptic integrals (Sineokov & Panov, 1978) and can be evaluated using numerical methods. The approximate values of the integral can be obtained by expressing the function under integration in Taylor series form. For the first three terms (Walters & Owen, 1996), Equation (3.39) takes the form:

$$L_{tr} = R\sqrt{1+\lambda^2}\left[(\alpha_e - \alpha_i) \mp \frac{\lambda}{1+\lambda^2}\left(\alpha_e^2 - \alpha_i^2\right) - \frac{\lambda^2}{6\left(1+\lambda^2\right)}\left(\alpha_e^3 - \alpha_i^3\right)\right] \quad \text{... (3.40)}$$

The angle α_i correspond (Figure 3.8) to the beginning of blade cutting and is determined from the relation $\alpha_i = \sin^{-1}\left(1 - \frac{d}{R}\right)$ and the angle α_e, correspond to the end of the soil cutting process by the blade.

The value of α_e is obtained from Figure 3.8 as:

$$\alpha_e = \frac{\pi}{2} + \alpha_{ie} \quad \text{... (3.41)}$$

From the foregoing analysis, it is evident that the length of the tilling route depends on the rotor radius, *R*, the kinematic parameter, λ, tilling depth, *d*, number of cutting blades on the same side of a flange, *z*, and the direction of rotation (the $\pm$ sign in Equation (3.40)).

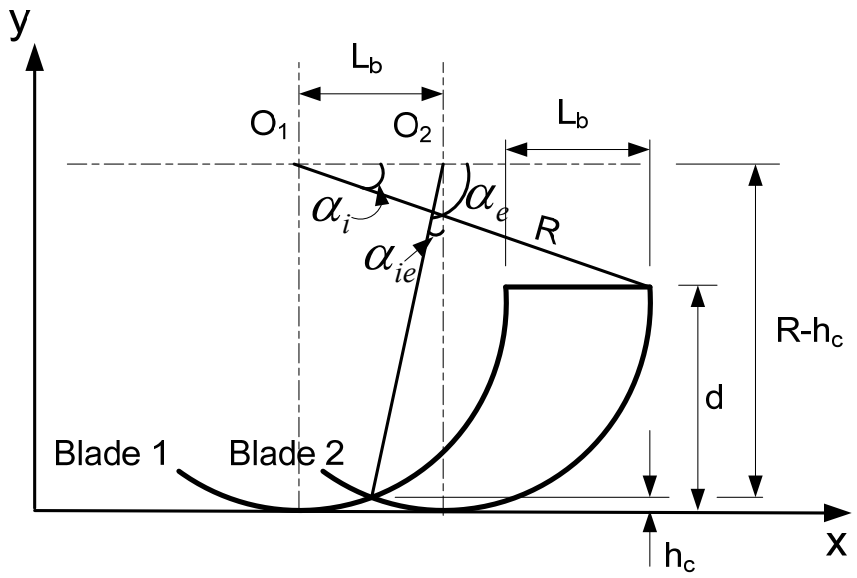

Figure 3.8: Determination of the start and end angles of soil cutting by a blade in a down-cut operation

3.3 Identification of torque requirement sources

The configuration and dimensional details of the blade used in this study is as shown in Figure 3.9.

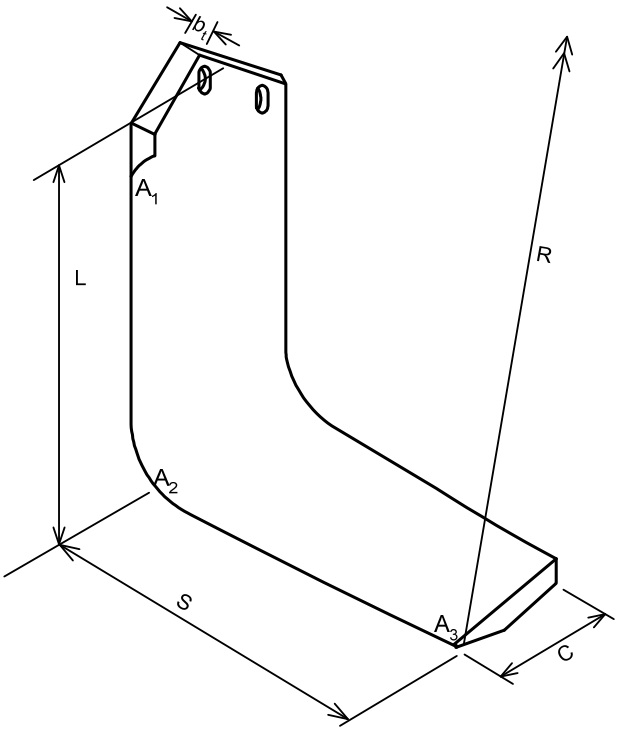

Figure 3.9: Line drawing of the standard 'L-shaped' blade (*C – chord of the blade, 80 mm at tip and 100 mm at the L–S intersection; L – vertical section (stem or leg), 100 mm; S – horizontal section (span), 130 mm;* b_t *– thickness of the blade, 7 mm; R – radius of the rotor, 500 mm;* $\overline{A_1A_2}$ *– cutting edge of the leg;* $\overline{A_2A_3}$ *– leading edge of the leg*)

A hypothetical soil-tool interaction of a down-cutting rotavator fitted with an L-shaped blade is shown in Figure 3.10, for a given depth of tillage and kinematic parameter, λ. The width of the soil slice (*w*) corresponds to the span of the blade (Figure 3.9), and it was assumed that the face FEDF separated from the uncut soil body breaks away in a vertical manner.

For a down-cut direction of rotation at a given kinematic parameter λ, the length of cut, L_{tr} (Figure 3.10) is dependent on the set depth of tillage. The set depth of tillage determines the angle at which the cutting edge of the blade comes into contact with the soil surface and the angle at which the blade stops the soil cutting process.

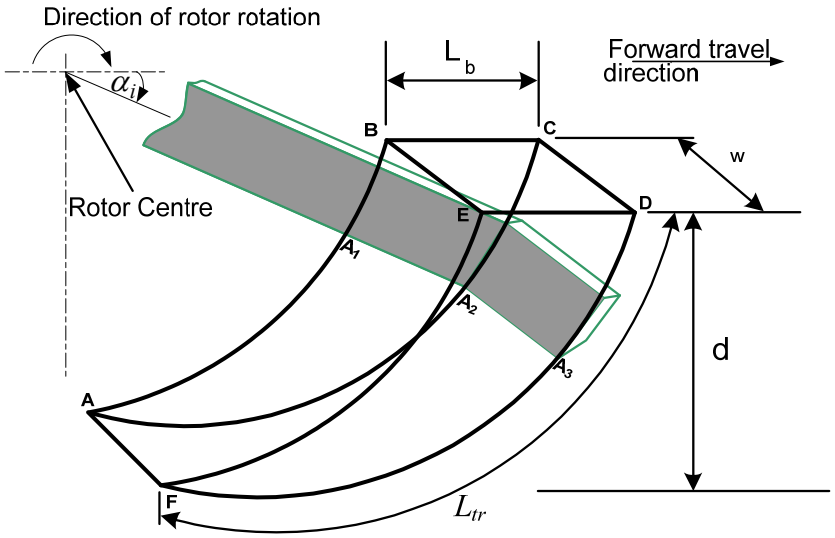

Key:
Face ABEF - Previously cut surface by the span of the preceding blade
Face ABCA - Soil surface in being cut by the leg of the cutter
Face ACDF - Soil surface cut by the blade of the cutter
Face FEDF - Soil surface sheared from the un-cut soil body

Figure 3.10: The soil-tool interaction for a down-cutting rotavator fitted with an L-shaped blade (L_{tr} *= length of cut; w = width of the blade; d = depth of tillage;* L_b *= bite length*)

3.4 Proposed analytical model for rotavator torque requirements

In processing the soil using the standard L-shaped blade, two of its distinct parts come into contact with the soil, *viz.*, the vertical section (also called the leg or stem), and the horizontal section (also called span). In terms of torque requirements, the stem requires torque for cutting and separating the cut soil slice along face ABCA (Figure 3.10), and for overcoming the soil-metal friction on the backside of the leg in contact with the uncut soil mass body. The span requires torque for overcoming soil shear strength, soil-metal friction (on the inside), cutting by the leading edge, and the acceleration and throwing of the cut soil slice.

The proposed analytical model in this section is based on forces that need to be overcome by the L-shaped blade when cutting the soil. From the blade configuration and its interaction with the soil (Figure 3.9 and Figure 3.10), torque is required to overcome the following soil and soil-tool interaction forces:

- soil-metal friction on the backside of the leg in contact with uncut soil body

- soil forces due to the soil-tool interaction by the span of the blade
- penetration resistance of the cutting edge of the span from the time the blades comes into contact with the soil to the time the cutting action ends (Figure 3.10).

3.4.1 Length of the blade in contact with the soil

The first parameter calculated in order to derive an expression for the torque requirement due to the soil-metal friction by the leg of the blade was the length of the leg in contact with the un-cut soil mass at different instantaneous tillage depths for a single blade. This is because in rotary tillage the length of the leg of the blade in contact with the soil varies from zero(before the blade enters the soil body) to a maximum value equal to the set depth of tillage after the blade has turned through an angle $\alpha = \pi/2$ from the horizontal (Figure 3.11). At this latter angle, the blade is vertical and the length in contact with soil is equal to the set tillage depth.

The length of the leg of the blade in contact with the soil was calculated by first, determining the co-ordinates of the tip of the cutting edge of the span, (x_i, y_i) at the at different instantaneous time moments. The coordinates of the tip of the blade for a down-cutting rotavator was obtained by modifying Equation (3.1). The modified expression takes the form:

$$\left.\begin{aligned} x_i &= V_f t_i + R\cos\alpha_i = V_f t_i + R\cos(\omega t_i) \\ y_i &= R(1-\sin\alpha_i) = R(1-\sin(\omega t_i)) \end{aligned}\right\} \quad i=1, 2, 3, \ldots, n \qquad \ldots (3.42)$$

where:

i = position of the blade along the cutting path of the blade

α_i = the angle the blade turns through in time, t_i (rads)

t_i = time of rotation of the blade though angle, α_i, from the horizontal(sec.)

From the coordinates of instantaneous depth along the cutting path of a blade, the length of the leg of the blade in contact with the soil is obtained from the geometric relations (Figure 3.11). The length of the blade in contact with the soil in Figure (3.11) at point P_i is obtained by using the geometric relation as follows:

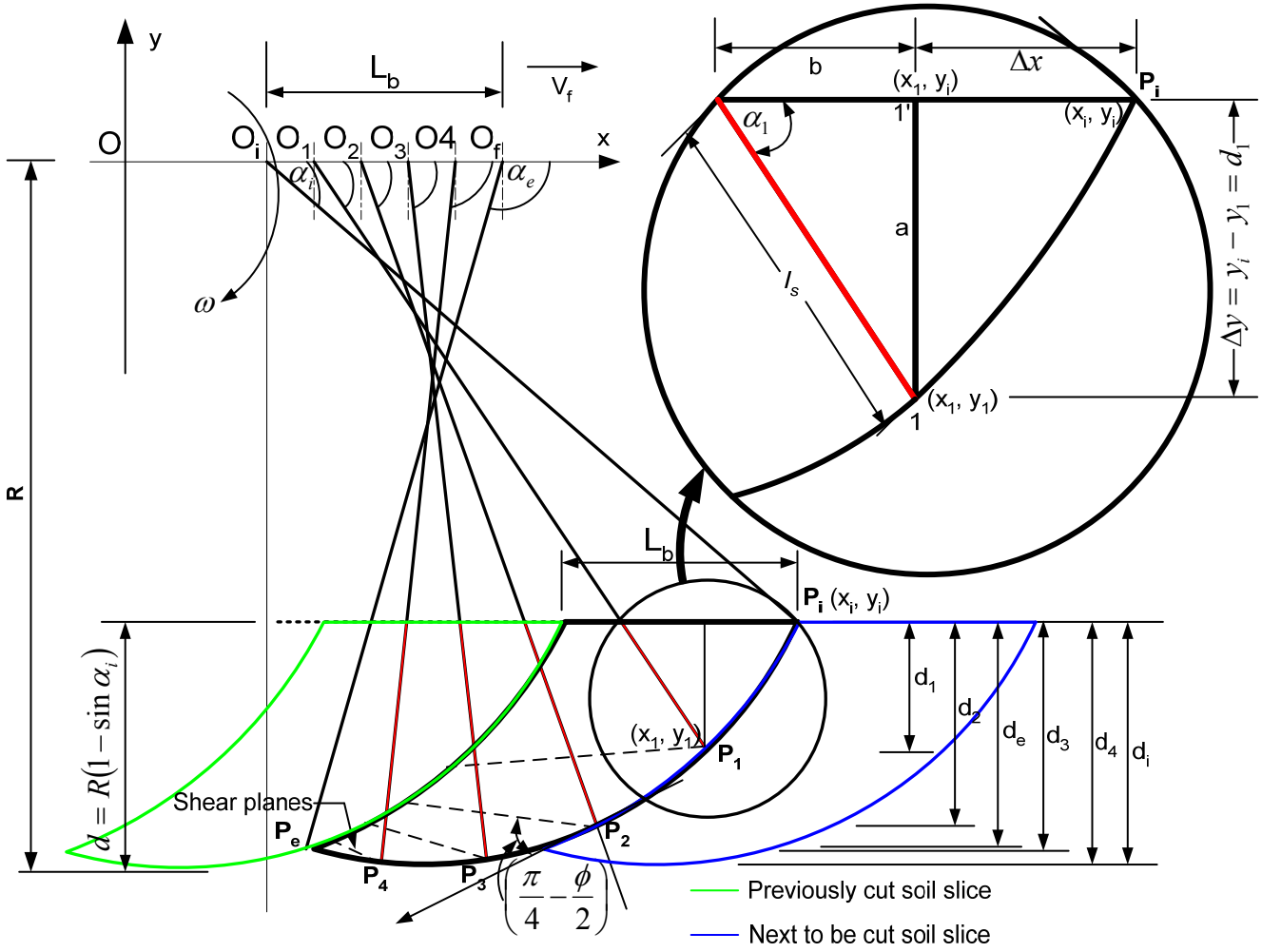

Figure 3.11: Theoretical shear planes in a soil slice at different positions for a down-cutting blade: α_i – the angle at which the blade comes into contact with the ground surface and starts cutting the soil; α_e – angle at which the cutting edge of blades exits the soil; *1*; *2*; *3*; *4* …, *n* – the position of the blade at various positions where shear planes are assumed to occur

1. Determine the coordinates (x_i, y_i), of the point at which the blades comes into contact with the horizontal ground surface
2. Allow the blade to advance to a second point along the cutting path, say position 1, in time $t_1 = \frac{\alpha_1}{\omega}$. Determine the coordinates of the blade at this new location. In this case t_1 is the time required to move from point *i* to point *1* at a constant rotor speed, ω.
3. The depth of the blade at the new location *d* is given by:

   $$d_1 = \Delta y = y_i - y_1 \quad \text{... (3.43)}$$

4. The length of the blade in contact with the soil (see Figure 3.4, magnified part) is then obtained as:

   $$l_s = \frac{\Delta y}{\sin \alpha_1} = \frac{d_1}{\sin \alpha_1} \quad \text{... (3.44)}$$

The above procedure was then repeated for all the locations of interest of the cutting edge of the blade, at pre-determined time intervals, and the length of the backside of the leg of the blade in contact with the uncut vertical soil mass determined. A similar expression was used for the other positions of the tip of the cutting end of the span.

3.4.2 Torque requirements due to the span of the blade

From Figure 3.10, torque is required by the span of the L-shaped blade for the following:

- Accelerating the cut soil by the span of the blade
- Overcoming the soil-metal friction and adhesion on the span of the blade
- Overcoming the soil-soil friction on the shear plane
- The continuous penetration resistance by the tip (cutting edge) of the span in the form of the tip reaction.

The first step in development of the mathematical model for torque requirements for the span was to make a number of assumptions. The first assumption made was that during an instantaneous time movement, the span of an L-shaped blade behaves like an inclined passive tillage blade. Secondly, given that the width of the span of the blade is greater than its depth (Figure 3.9), its instantaneous moment in time behaviour when

processing the soil is analogous to that of a wide blade. This wide blade consideration implies that the 'end effect' which has considerable influence on the soil-tool interaction forces for narrow tillage passive tools is negligible and can be ignored. The third assumption was that the heaving of soil in front of the tool was negligible, and was also ignored in the resultant failed soil wedge. With these assumptions, the assumed shape of the soil failure wedge by the span at an instantaneous time moment is as shown in Figure 3.12.

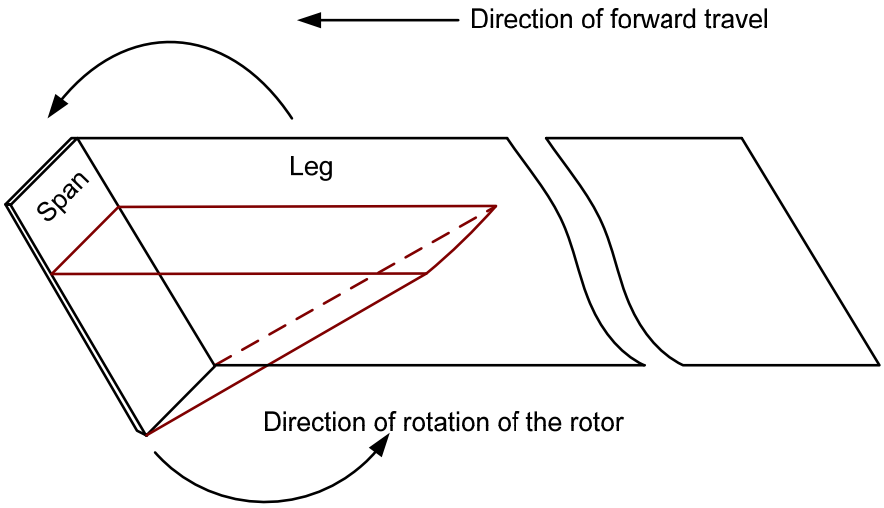

Figure 3.12: The assumed instantaneous time moment soil failure wedge in front the span

The next step was the identification of the soil-tool interaction forces on the different planes that would enable the development of a soil-tool interaction forces model that would enable the prediction of torque requirements. In this regard, 3-D soil failure approach was chosen. Three dimensional analytical resistance models are better suited to explain soil resistance induced by separation-mechanism of inclined tillage blades. This is because the 3–D resistance models predict soil resistance reasonably well by analytically representing forces involved in the soil-tool interaction with 3–dimensional soil failure geometries whereas 2–D analytical models and the empirical models are unable to do this.

Among the 3–D resistance models, Perumpal-Desai-Grisso model (Perumpal, Grisso & Desai, 1983) based on the limit equilibrium analysis was chosen in this study as the basic

model, from which soil-tool interaction forces for the span was developed. The torque requirements were to be derived from the force prediction model by determining the distance of the point of action of the resultant force to the centre of the rotor. This 3–D analytical model was appropriate in this case as:

- it allows a relatively simple soil failure shape without relying on experimental results; and
- its proposed failure shape is close to the one created by the span of the L-shaped blade (Figure 3.13) used in this study as shown in the right side of Figure 3.13(b), which also shows the failure geometry of McKyes model (McKyes 1985) for comparison. The confinement of the soil wedge supported by the span by the leg of the L-shaped blade (Figure 3.12), and span being a 'wide blade' (Koolen & Kuipers, 1983) makes the Perumpral-Desai-Grisso model soil failure shape an appropriate approximation of the soil failure shape for the span at instantaneous time moments. An idealised soil failure wedge within the soil slice cut by a down–cutting rotavator is presented in Figure 3.14.

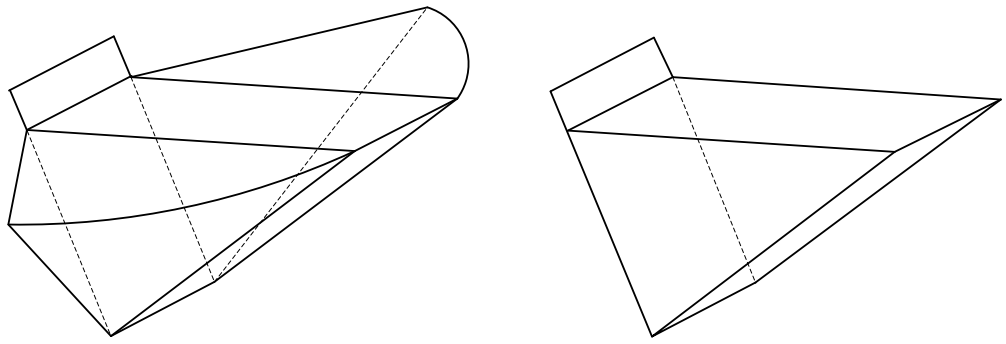

(a) McKyes model failure shape

(b) Centre portion of Perumpral, Griso and Desai model failure shape

Figure 3.13: Outlines of soil failure shapes of McKyes and Perumpral-Grisso-Desai models for inclined blades

However, Perumpral-Desai-Grisso model needed to be modified and expanded such that it could predict the dynamic soil-tool interaction forces for a 'wide blade' moving in a trochoidal path with a non-uniform resultant velocity. The proposed model also needed to incorporate the L-shaped blade configuration, specifically the inclusion of the leg since

the Perumpral-Desai-Grisso model is based on an inclined rectangular plate without sides, such as the leg part of the L-shaped blade. Further modifications of this static model were also necessary to account for the dynamic nature of the soil-tool interaction in rotavator tillage. To this end, the centre wedge of Swick-Perumpral model for predicting the soil-tool interaction (Swick & Perumpral, 1988) was used to introduce the terms that accounted for the acceleration force. The centre wedge of the Swick-Perumpral model resembles the assumed idealised soil failure shape (Figure 3.14 and Figure 3.15) supported by the span of the L-shaped blade.

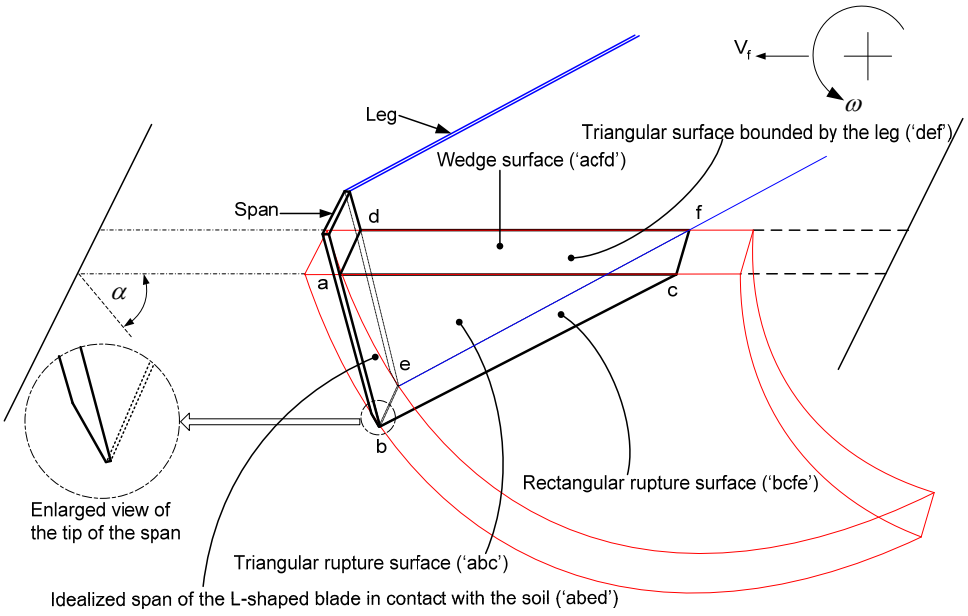

Figure 3.14: Geometric boundaries of the idealised separation failure wedge within the soil slice cut by the span of an L-shaped blade at an instantaneous depth for a down-cutting blade

Based upon the soil failure wedge, all the forces acting on the different surfaces are identified as shown in Figure 3.15. These forces contribute to the total force due to the wedge, designated as P_s; which act at an angle δ, normal to the surface of the span. The description of the all identified force components, per wedge surface, is as follows:

- Rectangular surface abed:
  - Adhesion force, F_{ad} due to adhesion between the span and the soil

- Soil-metal friction force on the interface between the soil and the span of the blade
- The force exerted on the span by the tool in the instantaneous direction of movement, P_s

- Triangular surface abc:
  - Equal and opposite reaction normal forces, R
  - Cohesion force, CF_2 due to soil cohesion between the soil particles.
  - Friction force, SF_2, between soil particles, i.e., soil-soil friction

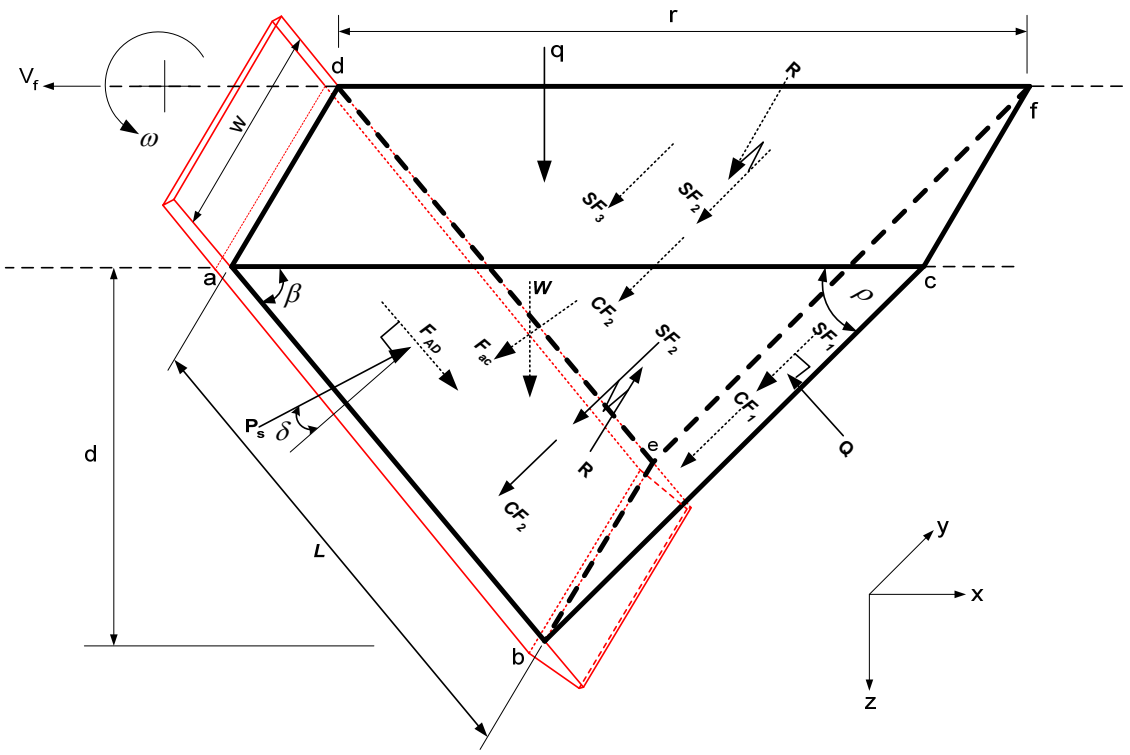

Figure 3.15: Breakdown of the soil-tool interaction forces on an idealised soil wedge for the span at an instantaneous time moment for a down-cutting rotavator tillage operation

- Rectangular rupture surface bcfe:
  - The normal acting force, Q
  - Cohesion force, CF_1 due to cohesion between soil particles
  - Friction force, SF_1 due soil-soil friction between the soil particles on this plane

- Triangular surface def:
  - Equal and opposite reaction normal forces, R
  - Cohesion force, CF_2 due to soil cohesion between the soil particles
  - Friction force, SF_3, due to soil-metal friction between the leg and the soil

Other additional forces identified due to the failed soil wedge were:

- Acceleration force F_{ac}; a body force resisting the acceleration of the wedge
- Gravitational force, W, due to the weight of the wedge
- Surcharge force, F_q, due to the heaving of the soil in front of the span.

The angles used in Figure 3.15 are as defined below:

β: angle that the tool makes with the horizontal during an instantaneous time moment (degrees). This is also called the rake angle.

ρ: angle that the rupture surface makes with the horizontal (degrees)

δ: soil-metal friction angle (degrees)

ϕ : soil internal friction angle (degrees)

In order to include the contribution of the leg to the resistance in the soil separation process, a soil-metal friction force (SF_3) on the triangular failure surface 'def' has been included. This is different from Perumpral-Desai-Grisso model, which includes only the cohesion force on the triangular surfaces 'abc' and 'def'. The inclusion of this force eliminates the need to separately include the leg part of the L-shaped blade (Figure 3.12) in the instantaneous idealised soil failure shape, as shown in Figure 3.15. Owing to the dynamic nature of the rotavator tillage, additional forces for the acceleration and the weight of the soil wedge have also been included.

Calculation of the each force component

With the exception of the acceleration force component, the calculation of the identified force components for the span is described below. The calculations are based on the 2–D drawing of the idealized soil failure wedge (Figure 3.16).

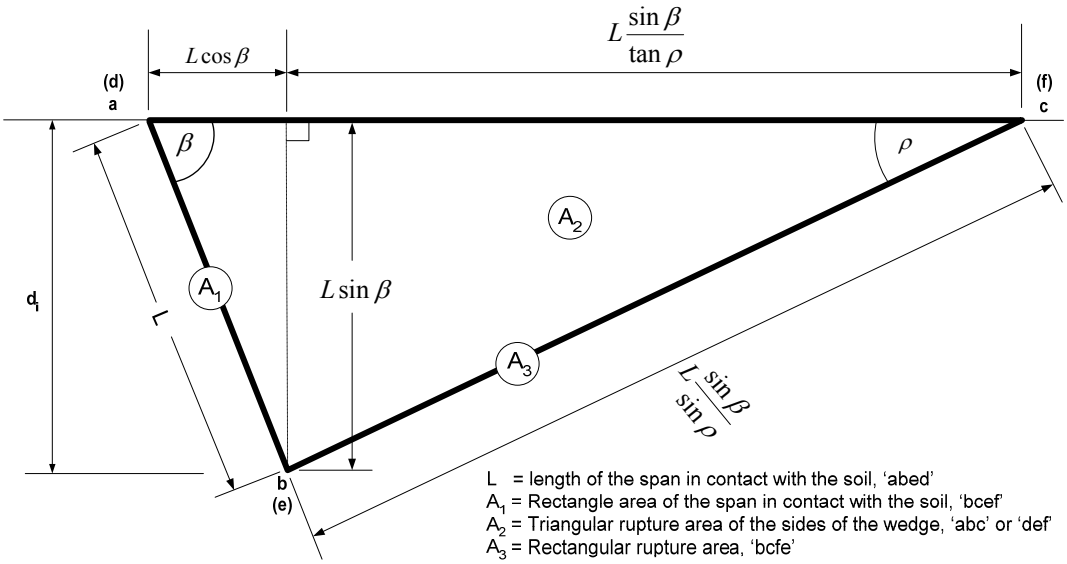

Figure 3.16: Dimensions of the soil failure wedge for calculating the force components

The expressions for the respective forces were obtained as:

- *The adhesion force*. The force of adhesion on the surface, F_{ad}, resisting the movement of the wedge on the span is given by:

$$F_{ad} = C_a \times A_1 = C_a \times w \times L$$

where:

C_a = soil metal adhesion factor (kN/m^2)

A_1 = area of the span in contact with the soil, 'abed' (m^2)

L = length of the span in contact with the soil (m)

- *Weight of the soil wedge*. The expression for weight of the failed soil wedge, *W*, obtained as:

$$\begin{aligned} W &= \gamma \times w \times A_2 \\ &= \gamma \times w \times \frac{1}{2} \times (L \times \sin\beta) \times \left(L \times \cos\beta + \frac{L \times \sin\beta}{\tan\rho} \right) \\ &= \frac{1}{2} \times \gamma \times w \times L^2 \times \sin\beta \times \left(\cos\beta + \frac{\sin\beta}{\tan\rho} \right) \end{aligned} \quad \text{... (3.47)}$$

where:

γ = unit weight of the soil (kN/m^3)

A_2 = area of the triangular rupture surface, abc or def (m^2)

- *Cohesion force acting on rectangular failure surface bcfe*. This was calculated as:

$$CF_1 = C_c \times A_3 = C_c \times w \times \left(L \frac{\sin\beta}{\sin\rho} \right) \quad \text{... (3.48)}$$

where:

C_c= soil cohesion (kN/m^2)

A_3= areas of the rectangular rupture surface bcfe (m^2)

- *The soil-soil friction force* was calculated as:

$$SF_1 = Q \tan\phi \quad \text{... (3.49)}$$

- *The combined soil-metal friction force on the triangular surface def, SF_3.*

It was assumed that this force component at any depth d_i may be approximated using the maximal earth pressure theory (McKyes, 1989). The soil-blade interaction and the assumed idealized earth pressure distribution on leg part of the blade are shown in Figure 3.17.

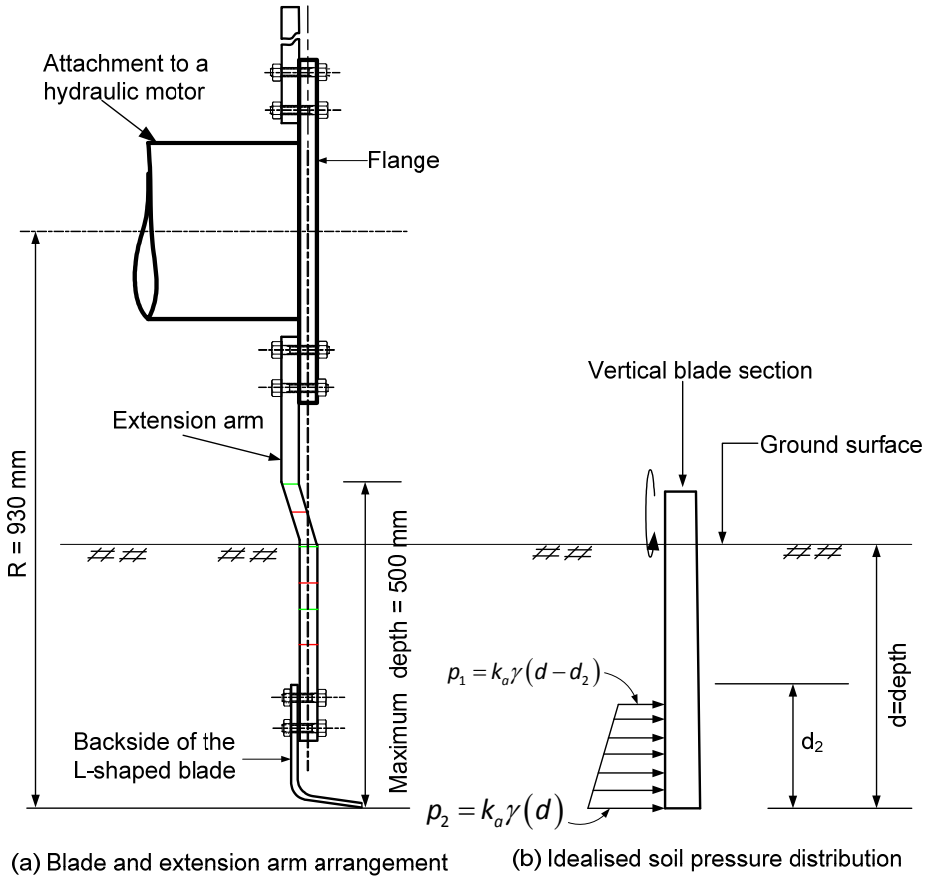

Figure 3.17: Idealised soil pressure distribution on the backside of the leg of the L-shaped blade

The maximum earth pressure for the distribution shown in Figure 3.17(b) at any depth d_i was approximated as:

$$p_{\max} = k_a \gamma d \quad \text{(kPa)} \qquad \text{... (3.50)}$$

The value of k_a was determined using the Rankine earth pressure theory. The value of k_a was determined using the following expression.

$$k_a = \frac{1-\sin\phi}{1+\sin\phi} = \tan^2\left(45 - \frac{\phi}{2}\right) \qquad \text{... (3.51)}$$

Because only the backside of leg was considered to be in contact with the soil during cutting (Figure 3.17a), the average soil pressure, p_{ave}, contributing to the combined adhesive-cohesive force, was taken as the average of p_1 and p_2 (Figure 3.17b), i.e., $P_{ave} = 0.5k_a\gamma(2d - d_2)$. It was assumed that the area of the leg contributing to this force was A_2 (Figure 3.16).

The total friction and adhesion force at an instantaneous during at instantaneous time moment was calculated as:

$$\begin{aligned} SF_3 &= A_2\left(C_a + p_{ave}\tan\delta\right) \\ &= 0.5\left(L\sin\beta\right)\left(L\cos\beta + \frac{L\sin\beta}{\tan\rho}\right)\left(C_a + p_{ave}\tan\delta\right) \\ &= 0.5L^2 \times \sin\beta\left(\cos\beta + \frac{\sin\beta}{\tan\rho}\right)\left(C_a + p_{ave}\tan\delta\right) \end{aligned} \qquad \text{... (3.52)}$$

- *Soil-soil frictional force acting on the triangle surface abc, SF_2.* This was calculated by first determining the reaction force R on the surface. The reaction force R is given by $R = \gamma K_o \bar{z}_c A_2$ (Perumpral *et al.*, 1983). The friction force, SF_2 is then calculated from the expression

$$\begin{aligned} SF_2 &= R\tan\phi \\ &= K_o\gamma z_c A_2 \tan\phi \\ &= K_o\gamma\bar{z}_c \tan\phi \times \frac{1}{2}\left(L^2\sin\beta\left(\cos\beta + \frac{\sin\beta}{\tan\rho}\right)\right) \end{aligned} \qquad \text{... (3.53)}$$

where:

K_o = coefficient of lateral earth pressure at rest. In terms of friction angle of the soil, $K_o = (1 - \sin\phi)$

$\bar{z}_c$ = depth from the top the failed wedge, i.e., points *c* or *f* to the centroid of the wedge (see Figure 3.16). The average depth at which the centroid of the wedge is from the surface of the failed soil wedge is $\frac{1}{3} \cdot d_i = \frac{1}{3} \cdot L \sin\beta$ (m)

The acceleration force. The expression for the acceleration force (F_{acc}) obtained in this study was a modified version of the one developed by Swick & Perumpral (1988). The tool velocity under rotavator soil processing is a combination of the forward travel velocity, V_f and the rotational velocity,V_{cir}. For a down-cutting rotavator blade, the instantaneous peripheral speed of any point in a cycloidal trajectory is a function of the rotor speed $V_{cir} = R\omega$, the forward travel speed, V_f, and the distance from the rotational axis to the point of interest. In this study, this peripheral velocity was obtained using the 'instantaneous-centre-technique' proposed by Hendrick and Gill (1974). Using this technique, instantaneous velocity V for a down-cut operation can be calculated as:

$$V = \omega R \sqrt{\left(1 + \frac{1}{\lambda^2} - \frac{2\sin\alpha}{\lambda}\right)} \quad \text{... (3.54)}$$

The modified expression for the acceleration force was of the form:

$$F_{acc} = \left(\frac{\gamma}{g}\right) \times \frac{w \times L \sin\beta \times V_i^2 \times \sin(\beta)}{\sin(\beta + \rho)} \quad \text{... (3.55)}$$

where:

γ = Unit weight of the soil (kN/m^3)

g = gravitational acceleration, ≈ 9.81 (ms^{-2})

w = tool width; which is the span of the L-shaped blade (m)

L = length of the span of the blade in contact with the soil (m)

V_i = the instantaneous peripheral velocity of the tool along the cycloidal path, (ms^{-1}.)

Derivation of the instantaneous total soil resistance force for the span (P_s)

The total soil resisting force (P_s) was determined by solving the equilibrium with the conditions specified in Figure 3.15. This was done by resolving the forces in the vertical (*y*) and horizontal (*x*) directions. Since the forces in the y-direction are opposite in their directions and equal in magnitudes, a 2–D representation in the x–z plane (Figure 3.18) was adequate to determine the total wedge resisting force.

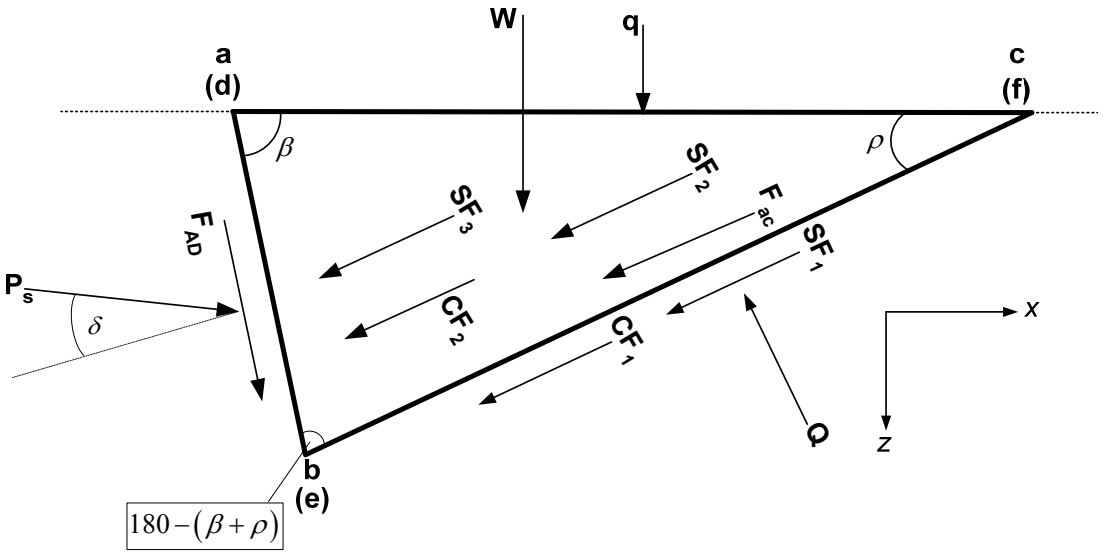

Figure 3.18: 2–D breakdown of the forces on the failed soil wedge

Summation of the component forces in the x- and z- directions that enabled the derivation of the total soil separation resistance due to the span as follows:

Σ of forces in the x-direction (horizontal)

$$\left.\begin{aligned} P_x &= P_s\cos(\beta+\delta) \\ &= -F_{AD}\cos\beta + CF_1\cos\rho + SF_1\cos\rho + F_{ac}\cos\rho + 2CF_2\cos\rho\ldots \\ &\quad + SF_2\cos\rho_2 + SF_3\cos\rho + Q\sin\rho \end{aligned}\right\} \quad \ldots (3.56)$$

Σ of forces in the z-direction (vertical)

$$\left.\begin{aligned} P_z &= P\cos(\beta+\delta) \\ &= W + F_q + F_{AD}\sin\beta + CF_1\sin\rho + SF_1\sin\rho + F_{ac}\sin\rho + 2CF_2\sin\rho\ldots \\ &\quad + SF_2\sin\rho + SF_{3}\sin\rho - Q\cos\rho \end{aligned}\right\} \quad \ldots (3.57)$$

By combining Equation (3.56) and Equation (3.57), the total soil resistance force, P_s, was obtained using the approach of Perumpral *et al.* (1983), and Swick and Perumpral (1988). The resultant equation for the total resistance force obtained was of the following form.

$$P_s = \frac{-F_{AD}\cos(\beta+\phi+\rho)+(W+F_q)\sin(\phi+\rho)+(CF_1+2CF_2+SF_2+SF_3)\cos\phi}{\sin(\beta+\delta+\phi+\rho)} \ldots$$

(3.58)

The derived total separation resistance formula (Equation 3.58) is different from the one by Perumpral *et al.* (1983) only by the inclusion of the wedge weight (W), acceleration force (F_{acc}) and surcharge force (F_q) terms; and the soil-metal friction force SF_3 due to the presence of the leg part of the blade. It is also different from the Swick-Perumpral dynamics model expression for the centre wedge total soil separation resistance for narrow blades (Swick & Perumpral, 1988) due to the inclusion of the SF_2, SF_3, and CF_2 force terms.

In Equation (3.58), both the resistance force Ps and the soil failure angle ρ are unknown. This means that the soil resistance force Ps, the primary target in the above expression cannot be determined directly. The soil failure angle and the resistance force, however, can be determined indirectly by using the passive earth pressure theory that states thet passive soil failure occurs when the resistance is minimum (Perumpal,*et al.*, 1993; Swick & Perumpal, 1988; McKyes, 1989). Consequently, either through an iteration or trial-error method, the soil resistance force P_s or the soil failure angle can be determined finding the minimum resistance value.

In this study, the approach of Perumpral *et al.* (1983) was used to solve Equation (3.58) using a computer program, written in MATLAB. The program calculates the force P_s for different values of the rupture angle as the blades processed the soil. By plotting a graph of P_s versus ρ values, the rupture angle which produces the minimum soil resistance force was selected.

3.4.3 Penetration resistance

During soil cutting by a rotavator, the cutting edge of the span of an L-shaped blade ($\overline{A_2A_3}$, Figure 3.10) continually penetrates the soil between the angles α_i and α_e (see Figure 3.8). This action of the blade requires torque to overcome the penetration resistance offered by the soil when the blade is moving between the two angles for any set depth of tillage. This penetration resistance was considered to be equal to the tip reaction force. The approach used to determine this tip reaction force in this study was based on the research by Thakur and Godwin (1990) in which the soil failure by the tip of the blade was demonstrated with the help of a non-extensible steel wire. The idealised system of force acting on the tip of the wire is given in Figure 3.19.

Figure 3.19 show the conceptual soil failure mechanism by a wire under two different situations, i.e., when working through a semi-infinite homogeneous soil mass, and working close to an open wall. This failure mechanism assumed to resemble the penetration of the soil by the cutting tip of the span of the blade. In the asymmetrical case near the open wall [Figures 3.19(b)], there is a general shear failure of soil towards the open wall and a local shear failure towards the infinite soil mass.

The force acting on the other half thickness of the wire [force RF_1, Fig. 3.19(b)] due to local shear failure towards the undeformed soil can be determined using the solution of Meyerhof (1951) for a wedge-shaped foundation at great depth (Thakur & Godwin, 1989; Thakur & Godwin, 1990). Based on this theory, the stress on the face of the wire for weightless soil is given as:

$$Q_s = C_c N_c^{'} + P_o N_q^{'} \quad \text{... (3.59)}$$

where:

Q_s = force upon face of tip of the span (kN)

$N_c^{'}$ = cohesion N factor

$N_q^{'}$ = surcharge N factor

P_o = geostatic stress (Pa)

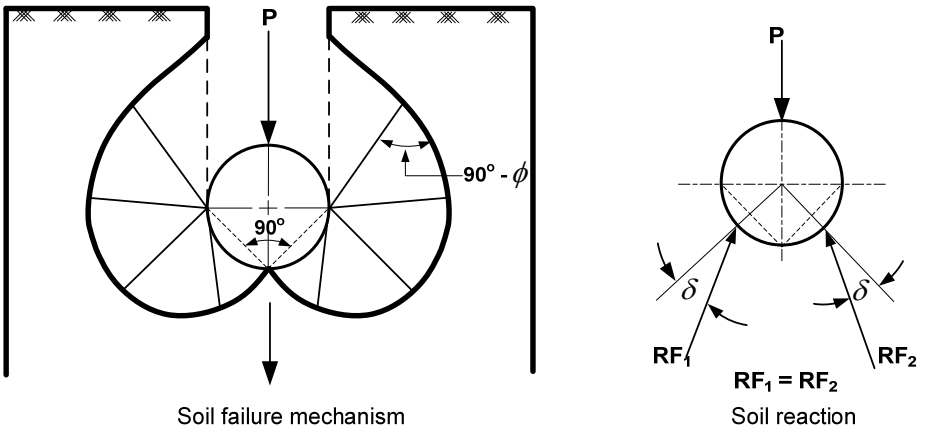

(a) Symmetrical soil failure mechanism in a semi-infinite mass by a rough wedge

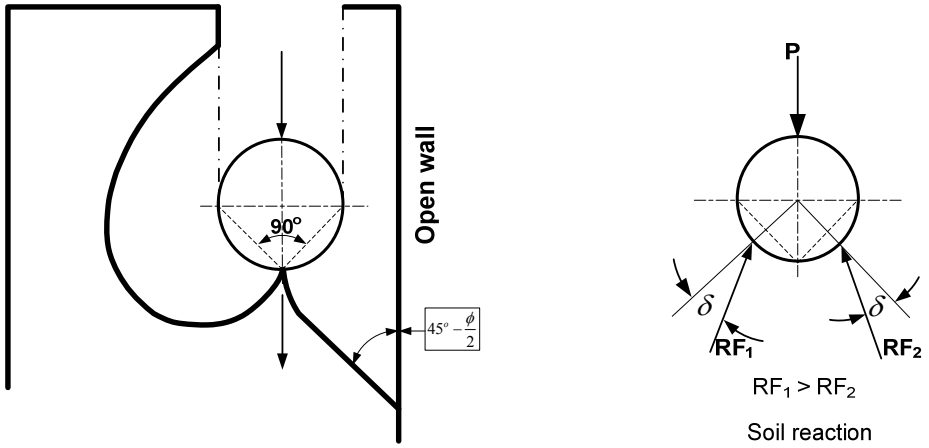

(b) Asymmetrical soil failure mechanism near an open wall

Figure 3.19: Idealized system of force acting on the tip of a wire (Thakur and Godwin (1989), after Meyerhof (1951))

The values of the dimensionless N-factors used in this study were based on the reseach by Meyerhof (1951) on the ultimate bearing capacity of wedge shaped foundations. Thakur and Godwin (1990) used this approach to determine these dimensionless N-factors, and obtained acceptable predicted torque requirement values for the cutting of soil by a rotating wire. For rough edges, the factors are sensibly unaffected by the wedge angle except for semi-angles of approximately less than 30 degrees, when the factors increase rapidly. In general, the N-factors for smooth wedges are much smaller than those for rough wedges. A graph of N-factors plotted by Thakur and Godwin (1990) for a wedge of 45^{o} applicable to the wire (Figure 3.20) was used in this study.

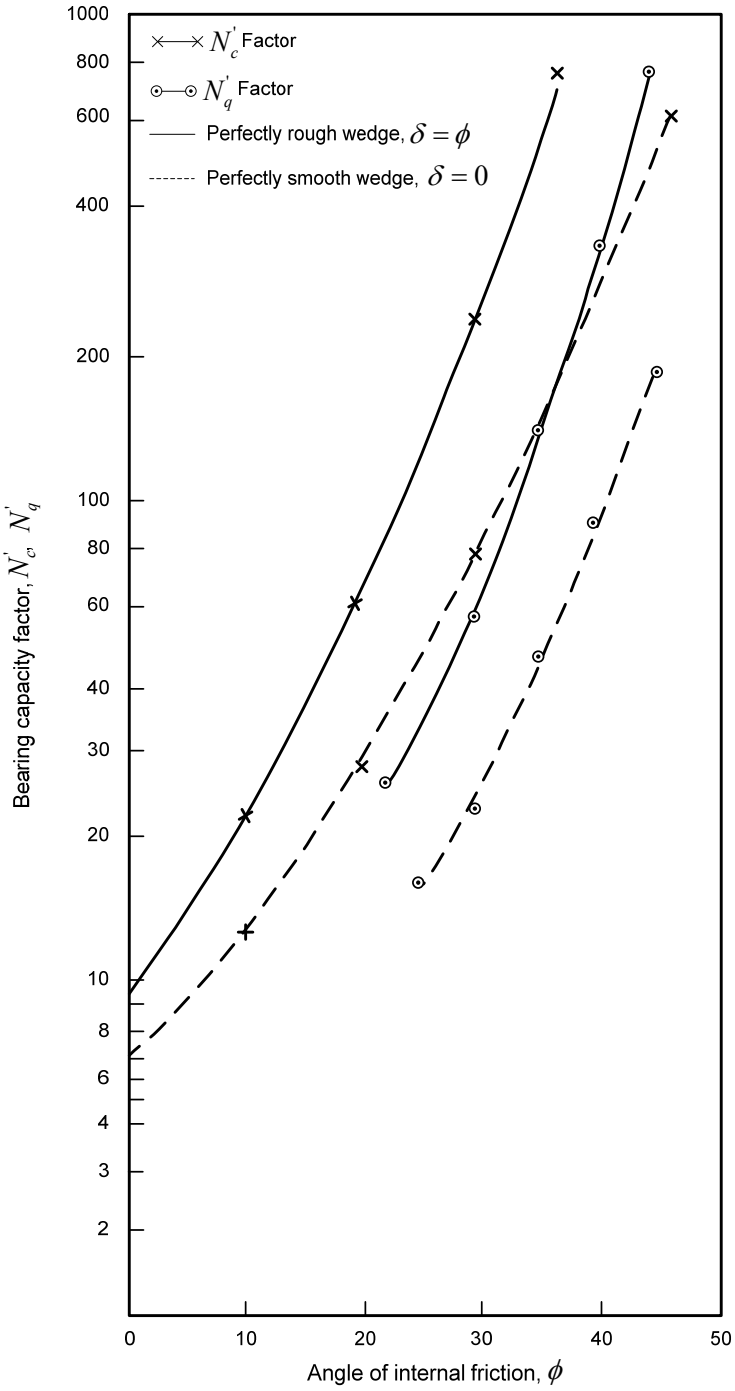

Figure 3.20: Relationship between bearing capacity factors and angle of internal friction for deep wedge shaped footing with included tip angle of 90° (Thakur & Godwin, 1989 after Meyerhof, 1951)

The geostatic stress P_o acting normal to the equivalent free surface is given by Thakur and Godwin (1990) as:

$$P_o = K_o \gamma d_i \qquad \text{... (3.60)}$$

where:

K_o = ratio of the horizontal and static vertical stress, *(K_o = 1 – sinϕ)*

γ = bulk density of the soil (kN/m^3)

d_i = instantaneous depth of wire from soil surface (m)

The total force on a half thickness of the wire, considered equivalent to the thickness of the tip of the cutting edge of the span, is then obtained from the following expression.

$$P_r = \frac{t_{bt}}{2} C_c w N_c' + K_o \gamma z w \frac{t_{bt}}{2} N_q' \quad \text{... (3.61)}$$

where:

C_c = soil cohesion (kN/m^2)

t_{bt} = thickness of the cutting edge of the span of the blade (m)

w = width of the span of the blade (m)

It was assumed that this tip reaction force (penetration resistance) remained constant throughout the soil cutting process by the tip of the blade as shown in Figure 3.21.

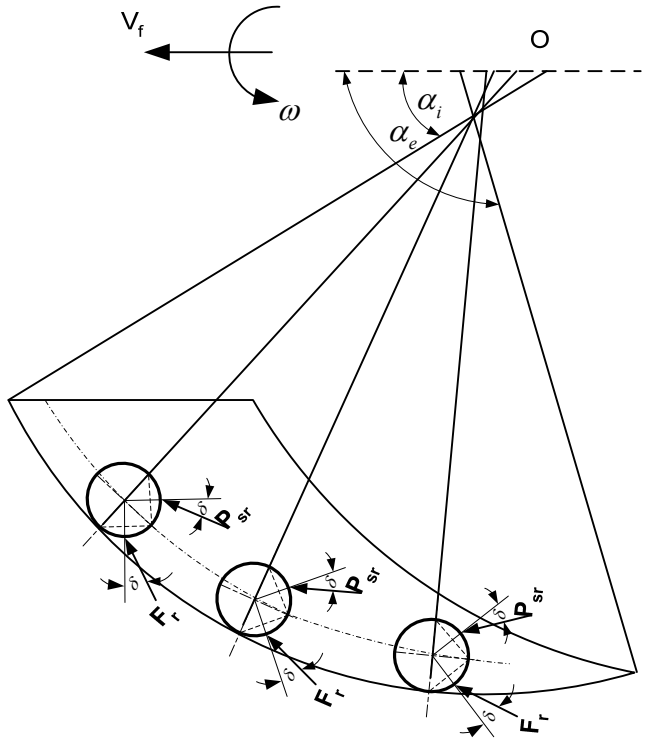

Figure 3.21: Soil reaction with constant tip force Fr and varying soil resistance P_{sr} for different positions of the wire in cutting a full soil slice (Thakur & Godwin, 1990)

3.4.5 Determination of the total torque requirements

The total instantaneous torque requirement for a single L-shaped blade is the sum of the torque due to P_s and P_r. The torque value due to these two forces is the product of the respective force and its distance from the centre of the rotor to its point of action, i.e., the centroid of the instantaneous failed soil wedge (Figure 3.16). The distances at which these two forces act are different. The P_r force acts a distance equal to the radius of the rotor at all instances during soil processing by the blade. The instantaneous time moment point of action of the force P_s is the distance from the centre of the rotor to the centroid of the instantaneous time moment soil wedge on the surface 'abed' (Figures 3.18).

The instantaneous time moment location of the centroid of the failed soil wedge is given as $\bar{z}_i = \frac{1}{3} \cdot d_i = \frac{1}{3} \cdot L \sin\beta$. Given the dependence of the centroid of the soil failed by the L-shaped rotavator blade on the rake angle, β and the dependence of β on the angle turned through by the rotor, α_i, from the horizontal, this parameter changes throughout between α_{cs} and α_{ce} when the blade is processing the soil. For any position of the rotor between angle α_{cs} and α_{ce}, the point of action of the location of force P_s from the centre of the rotor may be expressed as follows.

$$L_{Ps} = R - \frac{2}{3} \cdot \frac{d_i}{\sin\beta} \qquad \text{... (3.62)}$$

The instantaneous time moment torque values for the P_s and P_r may then be expressed as follows:

$$T_{ps} = P_s \cdot \left(R - \frac{2}{3} \cdot \frac{d_i}{\sin\beta} \right) \qquad \text{... (3.63)}$$

$$T_{pr} = P_r \cdot R \qquad \text{... (3.64)}$$

The two instantaneous time moment torque requirement values are added to give the total instantaneous time moment torque requirement as follows.

$$T_{total} = T_{ps} + T_{pr} = P_s \cdot \left(R - \frac{2}{3} \cdot \frac{d_i}{\sin\beta} \right) + \mathrm{P_r} \cdot R \qquad \text{... (3.65)}$$

3.5 Performance of the experimental tiller

The performance of tillage tools is usually determined by their draft or power requirements; and the quality of work (Srivastava, *et al.*, 1993). Quality of work is however, dependent on the types of the tillage tools; and may therefore be an unsuitable measure for the assessment of the performance of different tillage tools since this would require a common criterion. Consequently, the performance of the experimental deep tilling rotavator will be based on its draft and power requirements. Draft and power requirements of tillage tools can be manipulated to give a single performance criterion, which can be used to compare the performance of different tillage tools.

Using the draft and power requirements of tillage tools, the concept of specific energy or specific work has been used extensively (Kepner *et al*., 1978; Srivastava *et al.*, 1993) to determine the performance of different tillage tools; including the performance of rotavators (Beeny & Greig, 1965; Beeny & Khoo, 1970). Specific energy/work is defined as the ratio of the total energy expended during soil processing by a tillage tool to the volume of the soil disturbed (Srivastava *et al.*, 1993). The specific energy or work of a rotavator may be expressed as (Beeny & Khoo, 1970):

$$\text{Specific work} = \frac{\text{Energy expended}}{\text{Volume of the soil worked}} \ (\text{J/m}^3)$$

or

$$\text{Specific power} = \frac{\text{Power input per blade}}{\text{Volume of soil processed per blade}} \ (\text{N.m/s.m}^3) \qquad \ldots. (3.66)$$

The energy expended in Equation (3.65) can be determined from the product of the power and time it takes to work the volume of soil. The rotavator requires draft and rotary power when tilling the soil. The resultant draft was measured by considering the forces recorded on the two lower links and the top link of the tractor. The difference between the sum of the instantaneous time moment forces recorded at the two lower links and the top link gave the resultant thrust or pull force during rotavator operation. The energy required for both is calculated as the product of the power requirements and the time during which that power is utilised.

The rotary power requirement (P_{rot}) may be calculated as the product of the total torque requirements (Equation 3.67) and the speed of rotor. This power requirement may be expressed as:

$$P_{rot} = \frac{\omega T_{total}}{1000} \quad \text{... (3.67)}$$

where:

P_{rot} = power (kW)

ω = rotor speed (rad per second)

The energy required for the rotary work (E_{rot}, in kNm) is then calculated as the product of the rotary power requirements and the time during which the rotary work is done. The total rotary energy expended during this time is calculated as:

$$E_{rot} = \frac{T_{total} \times \omega \times t}{1000} \quad \text{... (3.68)}$$

where

t = time (s)

The draft energy (E_d) is the product of the forward travel speed, the resultant (effective) horizontal draft force and the time. The draft energy component for such a force (E_d in kJ) is calculated as:

$$E_d = \left(V_f \times D_f \times t\right)/1000 \quad \text{... (3.69)}$$

where:

V_f = forward travel speed (m/s)

D_f = Resultant draft force (N)

The total energy expended is then the sum of the rotary and the draft energy expended during the stated time period.

The volume of the soil tilled is determined in two stages. First, the volume of the soil tilled by a single blade is calculated. Thereafter, the total volume of the tilled soil is calculated for the stated time period determined. For a single blade, the volume of the

tilled soil is given by Equation (3.35) as described in §3.2.6. Depending on the number of blades that will pass through the soil in the stated time period, the total volume of the soil worked by the tiller is calculated as:

$$V_{wsv} = z_n V_{ac} \quad \text{... (3.70)}$$

where:

V_{wsv} = total volume of the soil tilled in time, t (m^3)

z_n = number of blades of the rotavator that pass through the soil in time t

V_{ac} = actual soil chip volume processed by a single blade (m^3)

The specific energy/work (*SE*) is then calculated as:

$$SE = \frac{E_r + E_d}{1000 V_{wsv}} = \frac{t\left(V_f D_f + \omega T_{total}\right)}{1000 V_{wsv}} \text{ kN.m/m}^3 \quad \text{... (3.71)}$$

Equation (3.71) can be used to compare the power performance of the experimental deep rotavator with the performance of other tillage tools. The draft component may increase or decrease the magnitude of the specific energy as the resultant draft force may be large or small, and be positive or negative with respect to the forward travel direction of the tractor.

3.6 Chapter summary

The kinematics of a rotavator is crucial in the development of mathematical models for predicting rotavators torque and power requirements. Rotavator kinematics influences the following parameters which have immense effect on its torque input; and thus its specific energy or power requirements.

- the cutting velocity of the tip of the span
- the cross-sectional area and volume of the soil slice,
- the equation of motion which is used to determine the location of the tip of the cutting edge of blade
- the bite length
- the kinematic parameter, λ

- the angle at which the soil processing starts and ends by a blade
- the length of the tilling route

The analytical model for torque requirements developed for a down-cutting rotavator comprises many force elements. By combining the soil resistance forces with the motion of the rotavator blade, two categories of resistance forces that have to be overcome during down-cut rotavator tillage operation have been identified. These are the soil resistance force elements due to the soil-blade interaction; and the soil penetration resistance force. The magnitude of the forces related to the soil failure wedge is greatly influenced by the position of the blade during soil processing and the rotational and forward travel speeds of the rotavator. The penetration force on the other hand acts at a fixed distance, equal to the radius of the rotor, throughout the soil processing; and is independent of the position of the rotor.

From the derived force expressions, the torque and power requirements for a down-cutting rotavator can be calculated. The torque requirements for the blade can be calculated for different rotor positions by locating the point of action of the soil penetration resistance force and soil resistance force due to the span and leg of the L-shaped blade. Using the specific energy requirements expression, the performance of the down-cut rotavator can be compared with other tillage tools.

CHAPTER 4

RESEARCH EQUIPMENT, INSTRUMENTATION AND CALIBRATION

Two instrumented research equipment were developed to measure the required parameters for the realisation of the objectives of this study. The first equipment was the instrumented experimental deep rotavator while the second was an instrumented apparatus for the *in situ* measurement of the soil strength and soil-metal friction parameters. The equipment was mounted on separate tool-frame carriers that were hitched onto separate tractors. The two tool-frame carriers were equipped with appropriate hydraulic systems for controlling their heights during the field trials and transportation, and to operate the soil strength characterisation apparatus. The rotavator was hydraulically driven using a hydraulic motor connected to the tractor PTO shaft. This chapter gives details of the functional components of the research equipment, instrumentation, calibration, and the data acquisition systems (DAS) used to collect the experimental data.

4.1 The instrumented experimental deep tilling rotavator

4.1.1 Functional components

A schematic layout of the developed instrumented experimental deep tiling rotavator mounted on the tool-frame carrier is shown in Figure 4.1. The tiller comprised a tool-frame carrier, the deep tilling rotavator, a variable displacement hydraulic pump, a hydraulic motor, and transducers for measuring the desired outputs. The tiller tool-frame carrier was attached to a tractor through the two lower links and the top link of the tractor. The tiller is driven by a constant displacement hydraulic motor (component 9 in Figure 4.1), which is mounted onto the driving shaft of the rotavator. The hydraulic motor is driven by a bi-directional variable displacement hydraulic pump (*Bosch, Germany,* not shown in Figure 4.1), which is connected to the tractor PTO shaft.

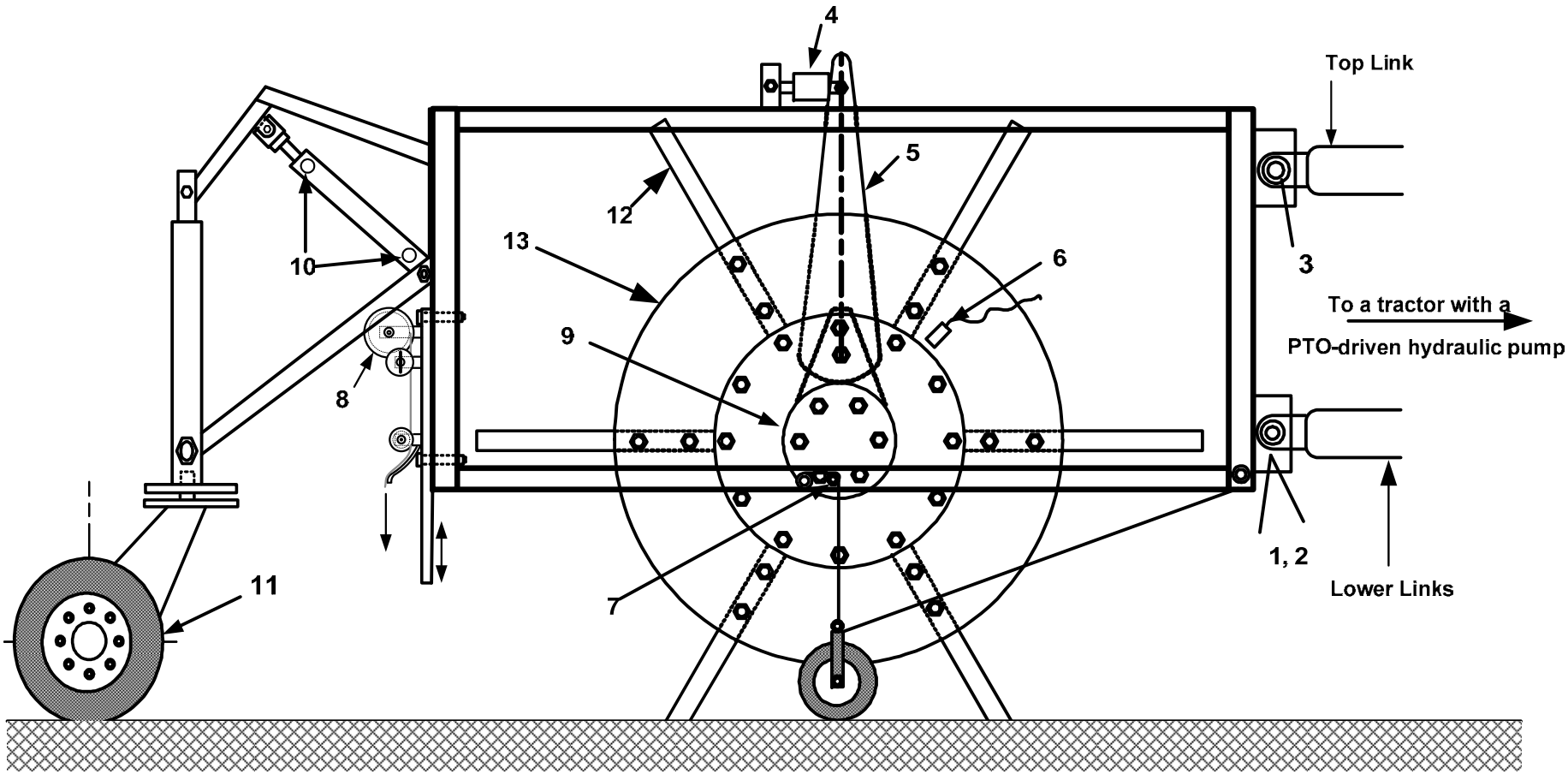

Figure 4.1: Side view of the instrumented experimental deep rotavator (*1, 2 – lower right and left force transducers; 3 –top link force transducer; 4 – torque load cell; 5 – torque arm; 6 – magnetic proximity detector; 7 – cable-extension displacement potentiometer; 8 – integrated optical transducer for measuring distance travelled; 9 – Hydraulic motor connected to a tractor PTO-driven bi-directional variable displacement hydraulic pump, 10 – double acting hydraulic cylinder for lifting; lowering the rear of the tool-frame carrier and the lifting of the swivel wheel, and 11 – two swivel wheels; 12 – Extension arm; 13 – Flange*).

Commercially available standard L-shaped blades were purchased from a local supplier and fitted at the lower end of the extension arms (component 12, Figure 4.1) of the tiller. Such blades give the highest forward thrust forces (Salokhe *et al*., 1993, Chamen *et al.*, 1979), and should be helpful for deep rotary tillage where increased draft forces are likely to result. The blades were secured at the lower ends of 600 mm long steel extension arms of 80 mm wide by 30 mm thick) using a pair of bolts and nuts. The other end of the extension arms were fixed onto a 16 mm thick circular flange (component 13, Figure 4.1) of 800 mm diameter

The design of the experimental tiller allowed for the easy removal and fastening of the extension arms; and hence the number of blades. This was necessary for investigating the effect of the number of blades on the performance of the tiller. The tiller tool –frame carrier had a swing gate on its left side which was used to access the flange for removal and fixing of the extensions arms together with the blades.

The oil for the hydraulic pump was contained in an overheard tank fitted with a valve at the base of the tank. The structure carrying the hydraulic oil tank was mounted on the frame of the tractor to which the rotavator tool-frame was connected via the three-point links (Figs. 4.1 & 4.2). The direction of rotation of the motor and hence direction of the tiller blades could be changed by either changing the inlet and outlet oil pipes into the hydraulic motor or by changing direction of the outlet valve on the pump. Both the inlet and outlet hydraulic oil pipes from the pump to the motor were of 37 mm diameter. The excess/leakage oil was returned to the tank via a 25 mm diameter hydraulic pipe from the hydraulic motor.

The tiller tool-frame is supported by a swivel wheel at the rear and the custom-built tractor three-point hitch system at the front. Both the rear and front parts of the tool-frame can be raised and independently lowered using the tractor standard hydraulic system, with the top link removed for transport. For the front, the lift mechanism of the three-point hitch point was used while for the rear, a double-acting hydraulic cylinder (Figure 4.2) connected to a suitable lifting mechanism that rested on top of the swivel wheel. The hydraulic systems for controlling the height of the tiller tool-frame carrier and for driving the hydraulic pumps via the tractor PTO used separate hydraulic circuits.

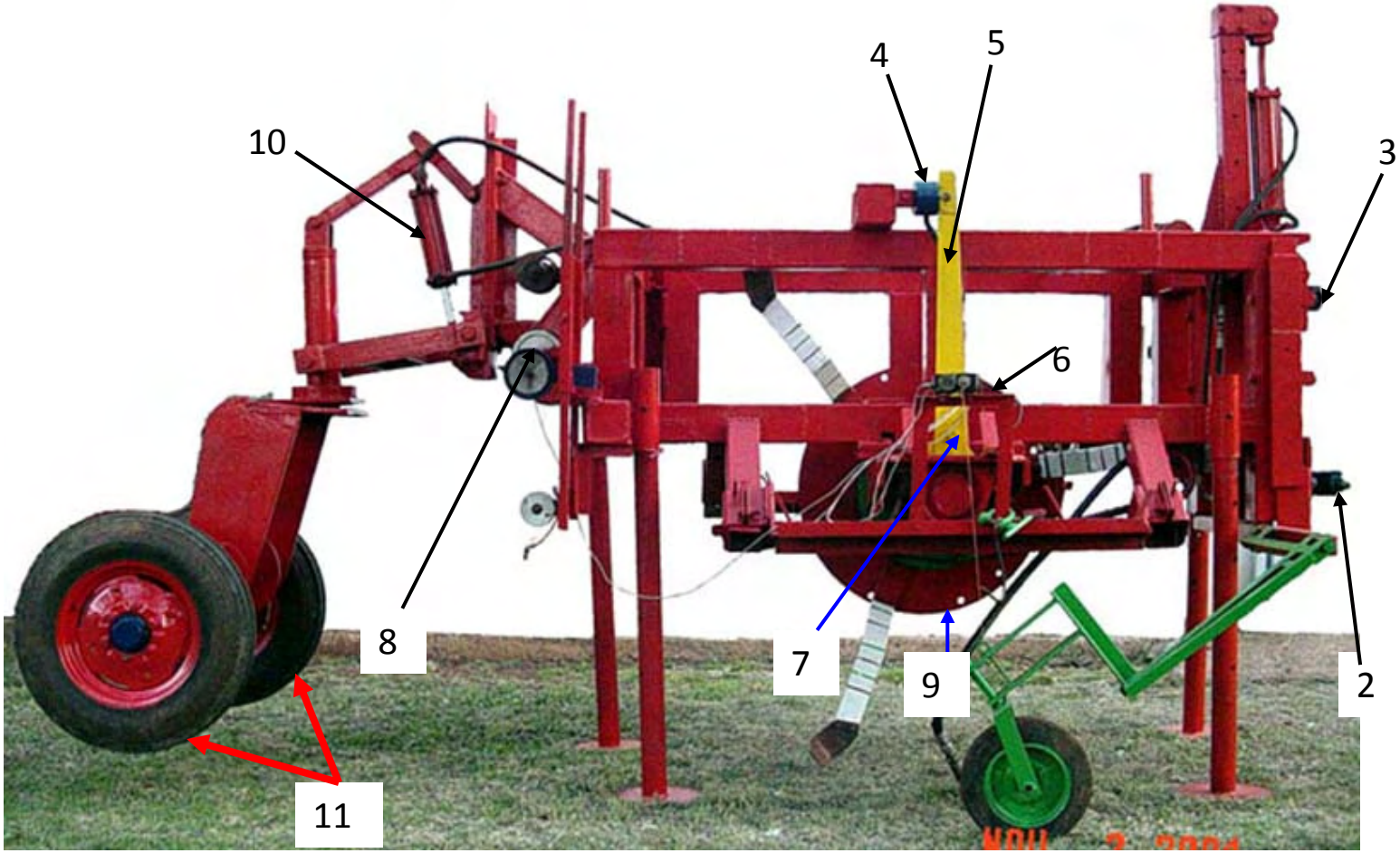

Figure 4.2: The fabricated experimental deep rotavators showing some of the key functional components *(1- left link force transducer (hidden); 2 – Right lower link force transducer; 3 – top link force transducer; 4 – torque load cell; 5 – torque arm; 6 – magnetic pick-up (hidden); 7 - cable-extension displacement potentiometer; 8 – integrated optical transducer; 9 – hydraulic motor (partly hidden); 10 – double acting cylinder; 11 – swivel wheels)*

The tractor hydraulic systems were used to control the height of the tool-frame during transport with the top link removed. For the setting and controlling the depth during the field experiments, the top link was set to a length equal to the length of the two lower links. The equal length of the three links was necessary for keeping the top and lower links parallel during field test. This was done to ensure that only horizontal thrust or pull forces were generated during field tillage experiments. During storage, the rotavator tool-frame was rested on four support legs (Figure 4.2). The support legs were lifted and held in place with metal pins/pegs during field experiments and transportation.

4.1.2 Instrumentation of the experimental deep tilling rotavator

The complexity of the rotavator tillage process necessitates simultaneous measurement of many variables (Romig, 1971) in order to determine its performance. The instrumentation for the experimental rotavator was designed to measure the horizontal force reactions on the three-point hitch of the tractor and the rotor shaft torque variation during tillage. Additional measurements needed to determine the performance of the tiller included the rotor rotational speed, the forward tractor travel speed, the tillage depth, and the soil condition.

The torque applied by the hydraulic motor was measured using a tension/compression load cell of nominal load rating of 2.5kN. The load cell (component 4, Figures 4.1 and 4.2) was connected to an 800 mm long torque arm (component 5). Thrust or pull forces generated was measured by the purpose made strain gauge force transducers connected to the three point hitch system of a tractor (Figure 4.2). Each of the three links had a calibrated force transducer to measure force components in the horizontal directions. The resultant push or pull was the summation of the forces experienced at the two lower links and the top link. The strain gauge force transducers had a nominal force rating of 10 kN (du Plessis, 2004).

The strain gauges for force transduction were bonded (Figure 4.3c) onto a 30 mm square section made of special stainless steel of 1500 MPa yield stress (du Plessis, 2004). The square steel section with the bonded strain gauges was fixed onto the tool-frame carrier

at one end. The free end had of the force transducer had a provision for attaching the links of the three-point tractor hitch system (Figures 4.3b and 4.3c).

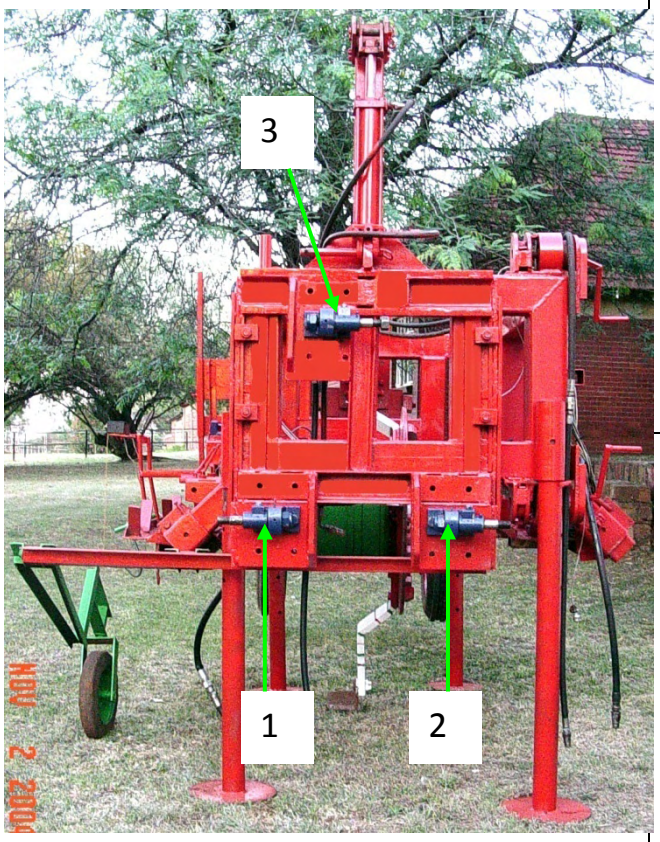

(a) front view of the tiller tool-frame carrier

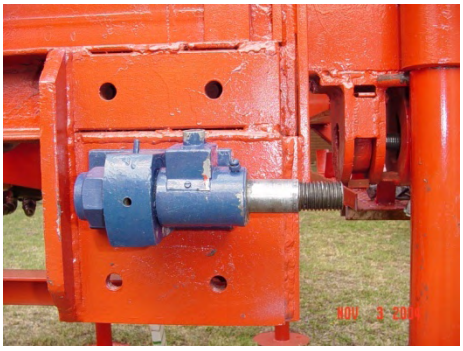

(b) assembled right-hand strain gauge force transducer in position

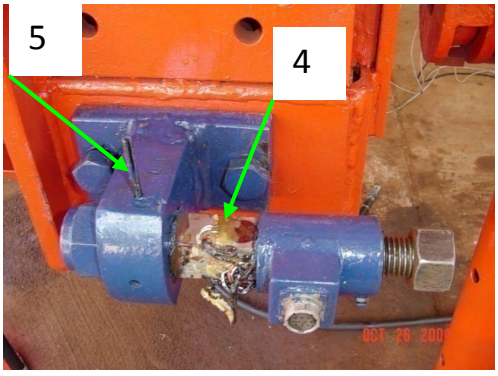

(c) bonded strain gauges (4) on a 30 mm square section of the transducer

Figure 4.3: The strain gauge force transducers *(1, 2 & 3 - strain gauge force transducers; 4 – bonded strain gauge; 5 – restraining pin*)

The assembled force transducer formed a 'cantilever-like' beam when fastened onto the tool-frame (Figure 4.3a). The force transducer comprised two identical strain gauges, one on top and the other at the bottom surfaces of 30 mm square made from special steel (du Plessis, 2004). The strain gauges were fixed (bonded) on these surfaces at 45° (Figure 4.4). With this arrangement of strain gauges, the transducer measured the magnitude of shear forces caused by a push or a pull by a tractor link arm at the free end of the cantilever beam assembly. A straining pin (Figure 4.3b) was used to lock the square steel section in position to ensure that only the horizontal forces were measured.

Depth of tillage was measured as the vertical distance between the soil surface and the lower point of the tip of the blade. The tiller tool-frame depth setting was constrained by the two hydraulic systems used to lower and raise it to the desired depth of operation. The depth measurement transducer was a string-driven ten (10) turn 20-kΩ cable-extension displacement potentiometer (Doebelin, 2004). This depth measurement system could measure up to depth of 1000 mm without appreciable loss of accuracy, which was well beyond the intended experimental tiller's maximum operational depth of 500 mm. Figure 4.4 shows the layout of the transducer used for measuring the depth.

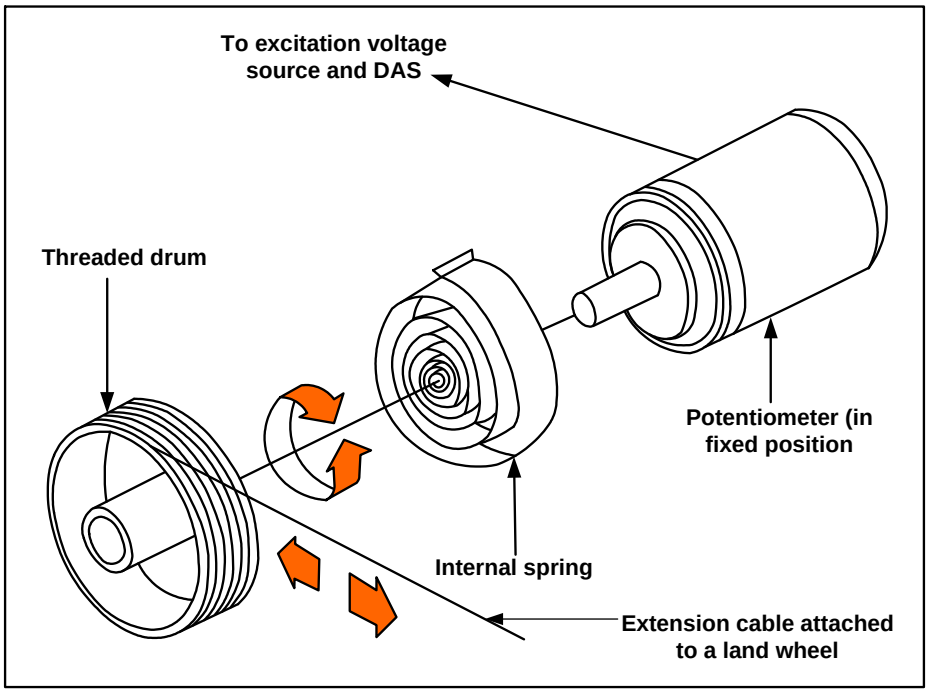

Figure 4.4: An illustration of a 20 kΩ ten-turn cable-extension potentiometer transducer used for measuring the depth of tillage

Rotational speed of the tiller was measured using a proximity magnetic probe. The proximity probe was mounted at an appropriate position on the tiller tool-frame carrier using a flat steel piece extension with a provision for varying the proximity of the probe from the toothed-gear part of the drum housing of the hydraulic motor (Figure 4.5). As the drum rotated the probe generated square wave pulses, corresponding to the crest and trough parts of the geared wheel. The geared wheel fixed onto the rotor drum had 154 teeth and therefore, a complete revolution of the drum generated 154 square-wave pulses.

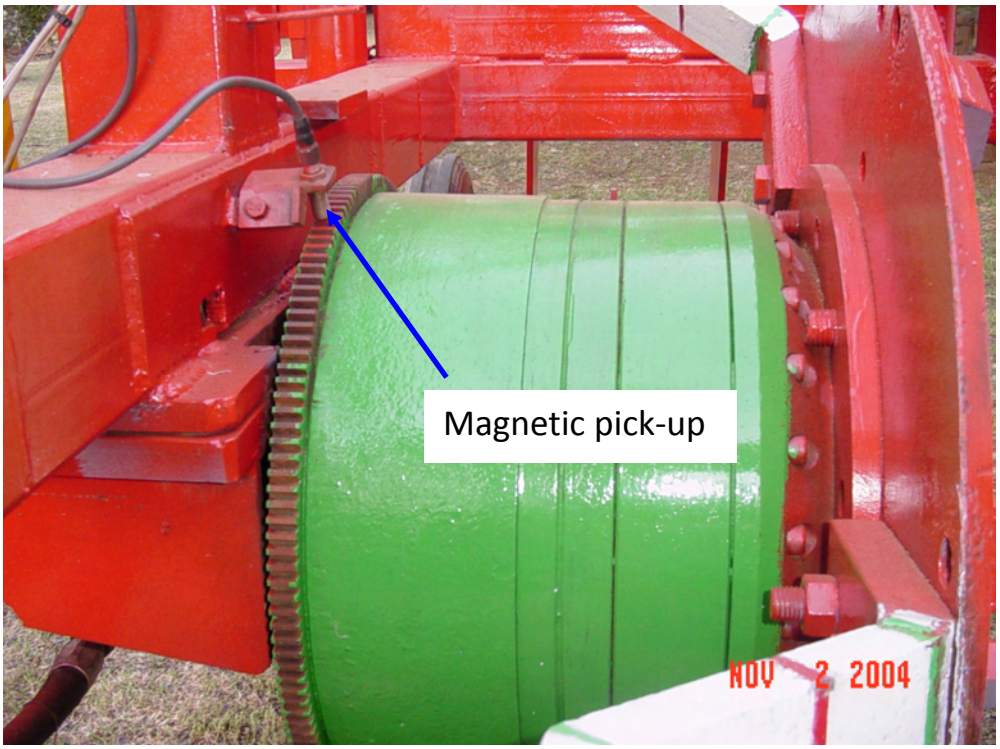

Figure 4.5: The magnetic pick-up proximity probe for the measurement of the rotor speed and the angle turned by the rotor

The true ground speed was measured using an integrated optical sensor mechanism (Figure 4.6). The mechanism was connected to a wire rope (component B, Figure 4.6a). As the tractor travelled forward the tension in the wire rope wound around the rubberised section (component C, Figure 4.6) forced the geared wheel to rotate and in turn drove an integrated optical sensor comprising an enclosed probe (component A, Figure 4.6). The rotation caused the generation of square-wave pulses similar to that generated by the rotor speed proximity probe. The wire had a weight with a provision for inserting a peg to hold it firmly into position on the ground during field trials. The system could measure to the nearest 5×10^{-3} m.

The designed travel speed measurement systems measured the distance covered in a given time interval. The forward travel speed of was determined using the standard distance-speed-time relation. Time measurement was done using the in-built PC clock and the DAS software program (§ 4.3). The travel time was predetermined and set for a known duration before measurements were started. All the measurements for the experimental tiller were then done during this predetermined time interval.

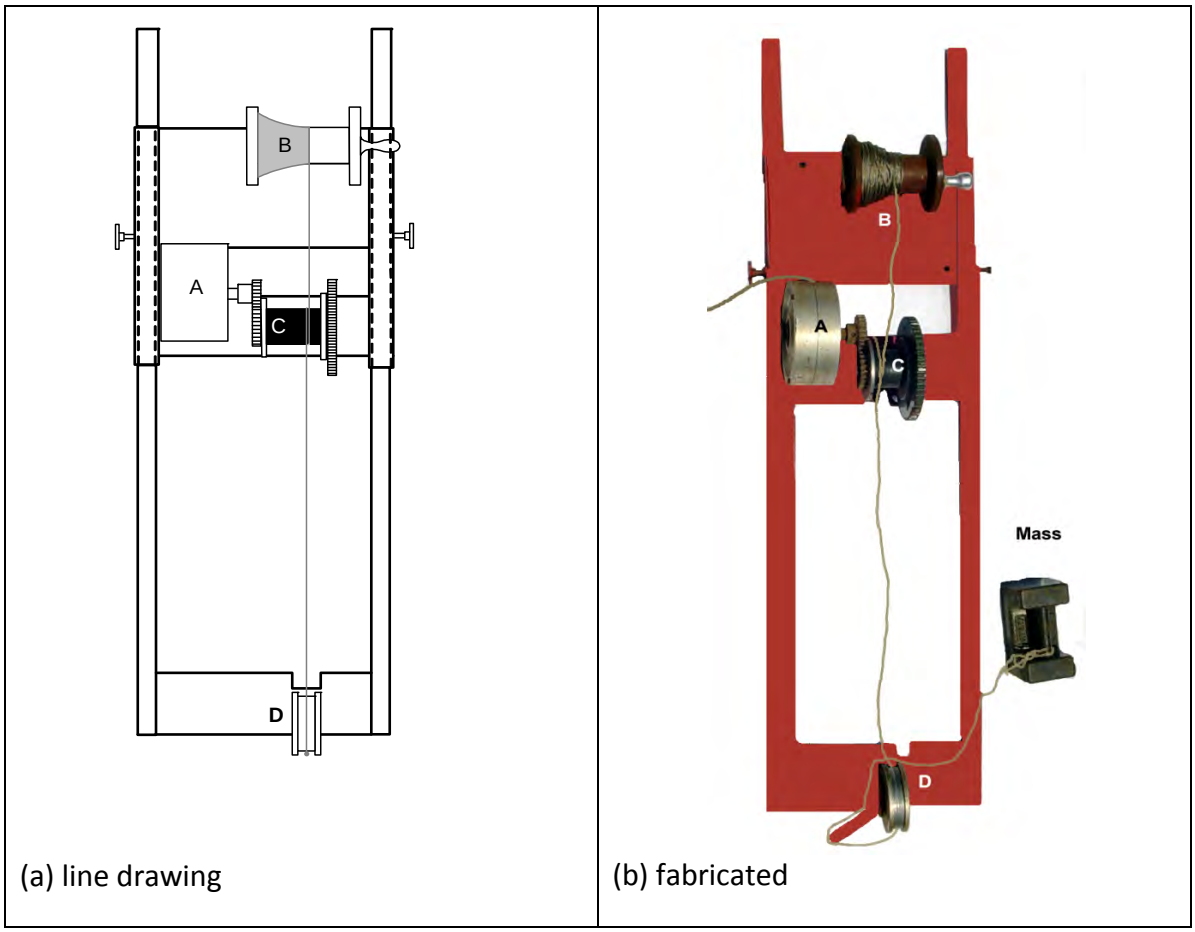

(a) line drawing

(b) fabricated

Figure 4.6: The assembled ground distance measurement system showing its various components *(A – gearing mechanism with an enclosed integrated optical sensor; B – wire rope wound on a braked drum ; C – rubberised surface on a geared wheel for driving A ; D – wire rope guide)*

4.2 Soil characterisation apparatus

4.2.1 Functional components

Much apparatus and many techniques have been development and tested for the *in situ* quantification of the soil strength and soil frictional characteristics (Johnson *et al*., 1987; McKyes, 1989). These *in situ* apparatus and techniques are primarily based on the method of measuring failure by shear in the soil (Johnson *et al*., 1987). In tillage studies, the use of a particular apparatus depends on its convenience and practical utility with respect to the soil condition(s), and the desired purpose of the soil strength data (McKyes, 1989).

After carefully considering the suitability of the devices that have been used for determining the strength of agricultural soils, the torsional shearing device (Schjønning, 1986; Olsen, 1984) was chosen for this study. The choice of the torsional device was influenced by the need for the determination of soil strength parameters at various depths within the 500 mm depth tilled by the experimental rotavator. Further, it was necessary that the same device be used for the determination of the frictional soil/steel parameters at the same depth as that at which the soil shear strength had been determined. These requirements were satisfied by the versatility of a torsional shear device, as its design would allow easy swapping of heads for measuring the soil shear strength and the soil/steel frictional parameters.

The torsional device designed had two load sensing transducers comprising a torque arm force strain gauge transducer and an industrial load cell (Figure 4.7). The load cell was used for recording the applied normal loads while the strain gauge force transducer was used for measuring the applied torque loads.

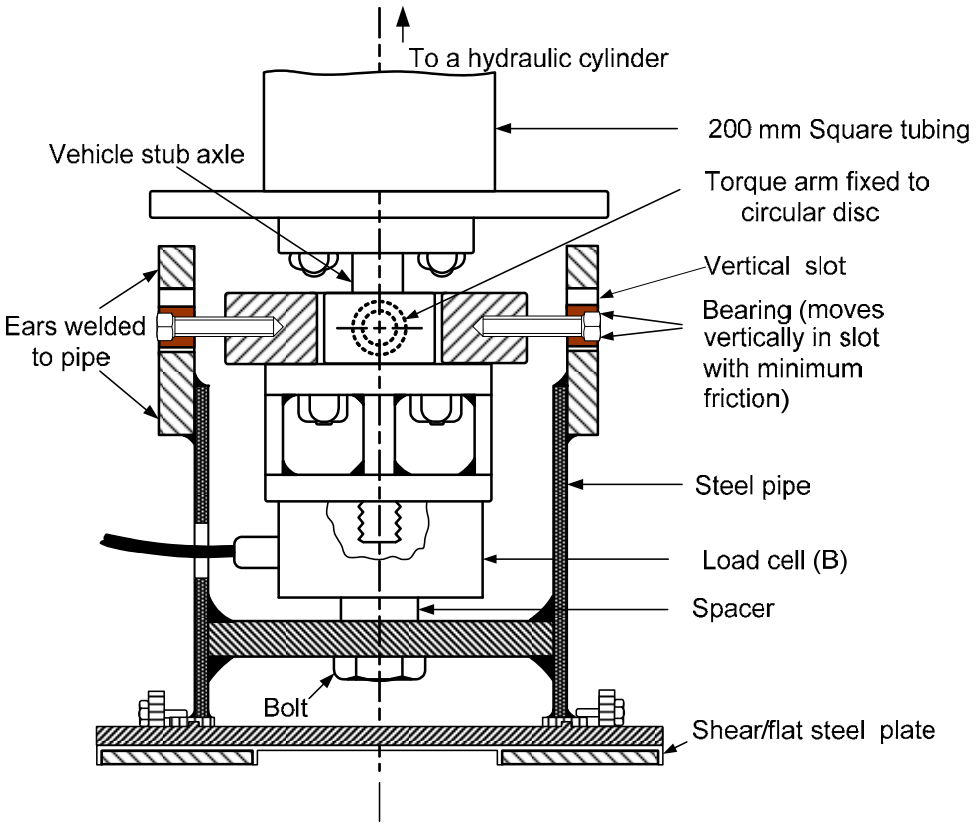

Figure 4.7: Cross-section of the torsional shearing device for the determination of the soil shear strength and soil/steel frictional parameters

Two heads (Figure 4.8a and Figure 4.8b), comprising an annulus head with grousers and other a flat polished circular steel plate annulus, both of internal and external diameters of 130 mm and 300 mm, respectively, were fabricated with suitable attachment mechanism. The annulus with grousered head was used to determine the cohesion and angle of internal friction of the soil at various depths.

For the determination of the steel/soil frictional characteristics, the grousered circular annulus head was replaced with the polished circular flat steel plate made from the same material as that of the grousered head. The surfaces of the two heads, which came in contact with the soil during the determination of the soil strength parameters, are shown in Figures 4.8b and 4.8c.

(a) The assembled torsional shear device with the circular flat plate in position

(b) Grouser head for soil shear strength determination

(c) Flat circular plate for frictional soil/steel characterization

Figure 4.8: The fabricated torsional shearing device for determination of soil shear strength and soil-steel frictional parameters (*A – torque arm; B –normal/vertical load measuring load-cell; C – grouser head; D – double acting hydraulic cylinder*)

To determine the soil strength parameters a normal load and a torque load were applied hydraulically to the torsional shear apparatus. The normal load was measured using a

load cell of 2.5kN nominal rating and the torque load measured using a purpose made strain gauge force transducer connected to the stub axle torque arm (Figure 4.7a). For the application of normal load, an engine operated hydraulic pump (*Robin EH17-20, Fuji Heavy Industries, Tokyo, Japan*) connected to a double-acting hydraulic cylinder was used to apply the load. The magnitude of the load was controlled hydraulically by operating the engine at a constant speed of 4000 rpm by operating the engine at it full throttle, and a given level of opening of the pressure release valve (component C, Figure 4.9). With this set-up, the greater the pre-stress on the control spring, the greater was the normal load applied and vice-versa. During sinkage the vertical load was held constant.

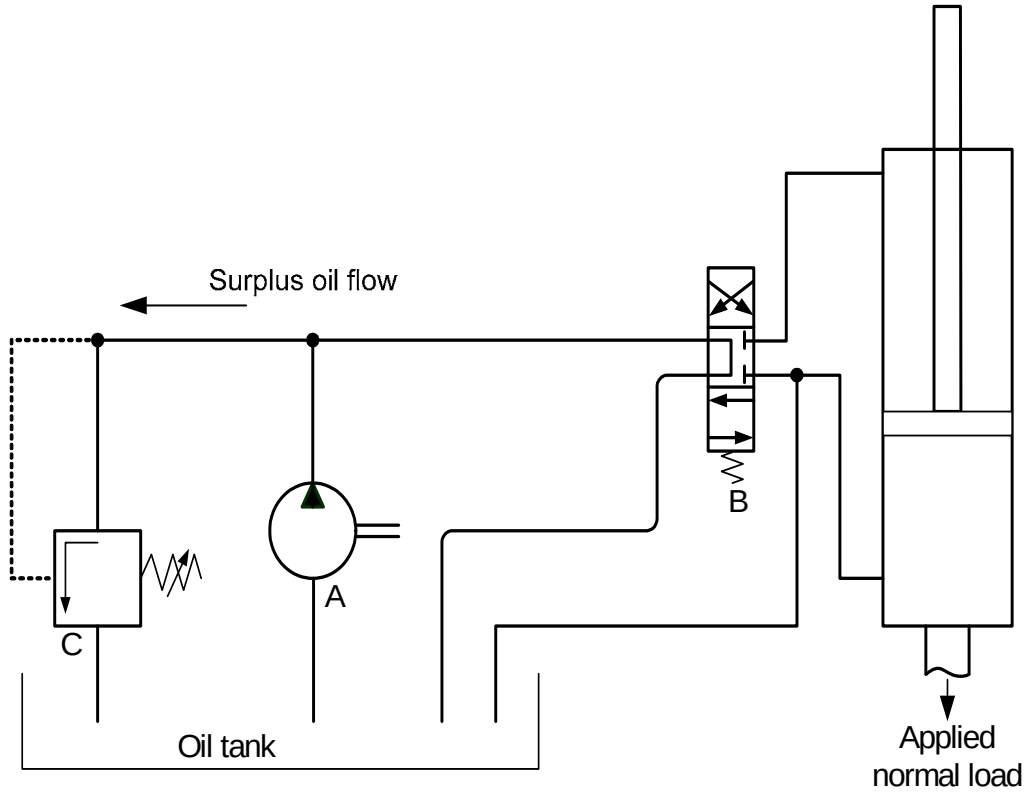

Figure 4.9: The special hydraulic circuit for maintaining a constant normal load for the soil shear and frictional shear strength measurement apparatus during sinkage *(A – engine driven pump; B – directional control valve; C – flow and pressure control valve with surplus oil back to tank; D – double acting hydraulic cylinder)*

The torque load for rotating the head (grouser or friction plate) was applied using the tractor hydraulic system to prevent the interaction between the two hydraulic circuits.

The load was applied slowly by either lifting or lowering the tractor hydraulic control lever thereby inducing the torque hydraulically. Lifting or lowering the hydraulic lever to shear the soil or overcome the soil-metal friction was continued until the stroke of the hydraulic cylinder was completed. During the initial field trials, it was observed that it was easier to apply the load by lowering rather than by lifting the hydraulic lever.

4.2.2 Instrumentation

The torsional shearing apparatus (§4.2.1) was instrumented so that the normal and the shearing (torque) loads required for the determination of the soil shear strength and soil-metal friction parameters could be measured. The maximum normal load that could be exerted hydraulically by the engine powered pump (Figure 4.9) was about 2kN. The normal load cell was suitably connected to a 200 mm square tubing (Figure 4.7) that was connected to a double acting hydraulic cylinder connected to a special hydraulic circuit (Figure 4.9). The circuit had a pressure control valve for maintaining a certain level of load by restricting the amount of oil flowing back to the reservoir.

The torque load for shearing the soil using the grouser head (Figure 4.8b) or for overcoming the soil-metal friction using the flat circular plate (Figure 4.8c) was applied in the form of a torque through the torque arm (components A and D, Figure 4.8a) using the tractor hydraulic system. The applied torque was measured using a bending arm torque transducers. Depending on the direction of motion of the double-acting hydraulic cylinder, the resultant signal was either negative or positive with respect to the off-set values of the strain gauge force transducer. In order record a meaningful response of the torque load applied, the hydraulic application of the load was done at a slow speed such that on average, the complete stroke length of 0.5m was done in about 45 second.

4.3 The data acquisition system

Output signals from the two instrumented systems were recorded using appropriate transducers at suitable measurement rates. The signals were fed to a state-of-the-art commercial data acquisition system (DAS), called Spider8 (*Hottinger Baldwin Messtechnik, Germany*), which was connected to a personal computer (Figure 4.10).

The DAS comprised eight (8) input (measurement) channels and a computer software program, called CARTMAN EXPRESS version 3.1, a MS Windows compatible data acquisition program, for reading the measured information from the transducers and storing the data into a file in the PC's hard disk. Each channel of the Spider8 is equipped with a separate A/D converter which allowed data measuring rates from 1 Hz to 9.6 kHz. Using the DAS's in-built clock interface, the experimental measurement periods were set. The in-built clock system was also useful in the determination of both the rotational and forward travel velocities of the rotavator.

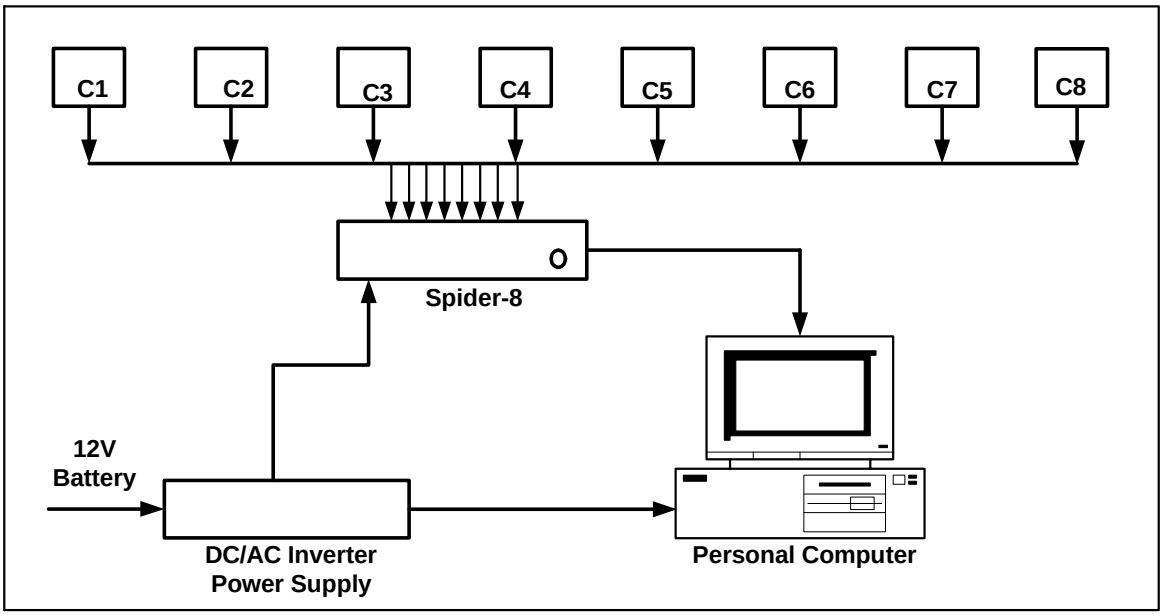

Figure 4.10: Schematic diagram of the DAS (C1 … C8 – measurement channels)

The different transducers for the two research equipment developed; the instrumented experimental deep rotavator and the soil strength characterisation apparatus were connected to the DAS using 15-pin D-type connectors to the various measurement channels (Figure 4.10). The tiller tool-frame had seven (7) transducers comprising three strain gauge force transducers for recording the forces on the two lower links and the top link of the tractor, a load cell connected to the torque arm for measuring the torque, a proximity pick-up sensor for recording the rotational speed of the rotavator, a 20kΩ ten-turn cable-extension potentiometer displacement transducer (Figure 4.4) for sensing the tillage depth and proximity probe for measuring the tractor forward travel speed. The eighth channel on the DAS was not utilized.

For soil characterization, the torsional shear device utilized two of the eight channels available on the Spider8. Channel 1 was connected to the load cell for measuring the normal load and channel two was connected to the strain gauge force transducer for measuring the torque required to fail the soil through shear or friction overcoming the soil-metal interface friction.

Depending on the type of the transducer connected to a channel, the output signal could be one of voltage for all the force measuring transducers and the depth sensor, or a square-wave (frequency) counter for the all the speed measuring transducers. The DAS was connected to the computer via the parallel printer port and the data measured was stored in the hard disk of the PC in a text file format. Output signals from all the channels were recorded at a predetermined rate, e.g. 2.4 kHz for a preset length of time. Output signals from the channels could be monitored as the measurement progressed using the CARTMAN EXPRESS program. This allowed for easy detection and rectification of faults, and ensured that the correct measurements were made.

4.4 Calibration

4.4.1 Calibration of strain-gauge force transducers and load cells

Force measuring strain gauge transducers and the torque load cell were all calibrated outside the respective tool-frames. Calibration of the strain gauge force transducers was done by fixing them horizontally with the measuring planes vertical and horizontal onto a specially designed beam (Figure 4.11). The fixed strain gauge force transducer and the beam formed a ‘cantilever-like’ beam, much like the fastening of the transducers onto the tiller tool-frame carrier. Dead loads of known masses, e.g. Figure 4.11, were then hang onto a specially designed metal bar of known mass. The bar was connected to the free end of the fastened force transducer (Figure 4.11).

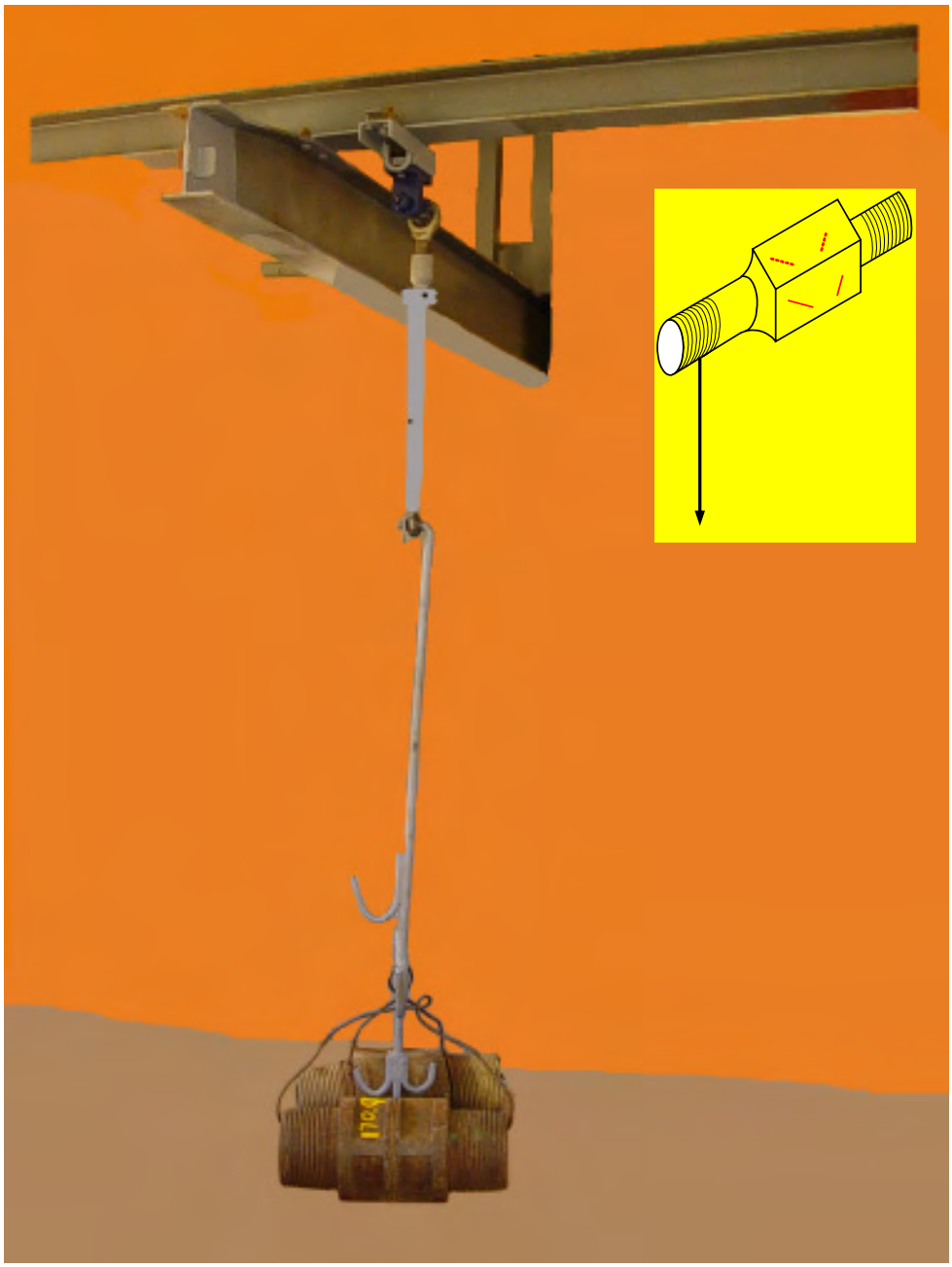

Figure 4.11: Calibrating a strain gauge force transducers for one of the tractor links

The loading was continued to a total mass of about 50 % of nominal load capacity of the force strain gauge transducers. For each added mass, a time of about 20 seconds was allowed to elapse before another weight of known mass was added onto the hanging bar. The process was continued until the target weight of hanging weights was reached. The setup was allowed to stabilise after which the weights were removed one-by-one in the reverse loading order, i.e., the last added weight was removed first until all the weights hang on the bar were removed.

A specially designed hanger (Figure 4.12) was used for the calibration of double acting industrial load cells for measuring the torque on the torque arm on the tiller tool-frame carrier and the normal load on the soil strength characterisation apparatus. A load cell that was being calibrated was thereafter placed under a hanging beam and two dead loads of approximately equal masses were placed on either side of the beam and the cam and arm activated to transfer the load to the load cell. Like was the case with the strain gauge forces transducers, the loading was continued to about approximately 50 % of the nominal load capacity of the load cell.

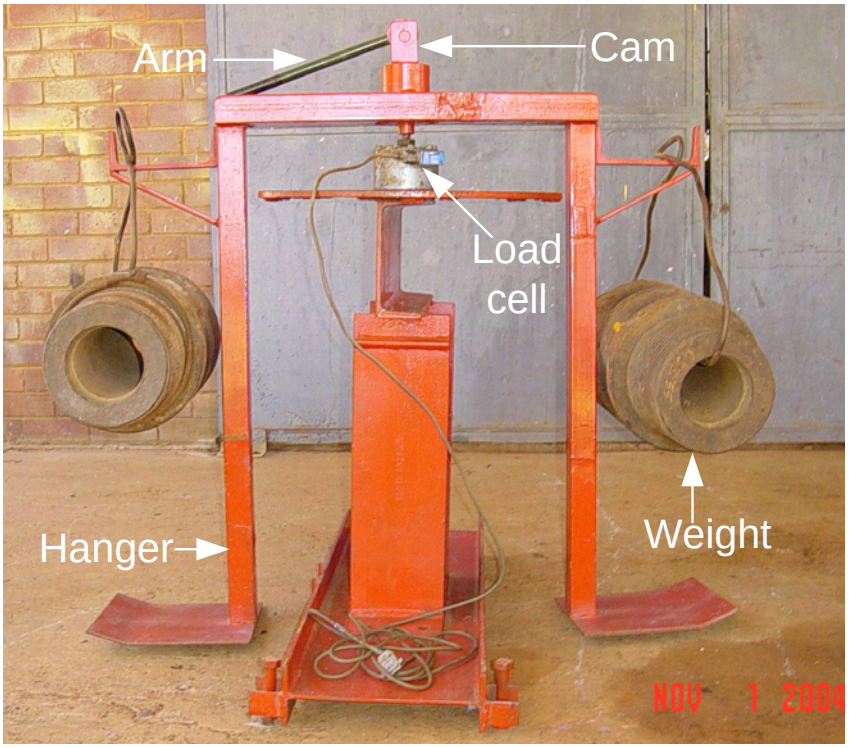

Figure 4.12: Calibrating load a cells in compression using a specially designed hanger

At the end of the loading phase a pair of dead loads placed on the hanging beam was removed and the setup allowed to stabilise before the next pair of weights was removed. The unloading phase was done until all the dead loads were removed. The object of this unloading was to counter-check the magnitude of the voltage response of the force transducers at equal loading levels so as to determine the status of hysteresis[2]

[2] The difference the in output signal for a given input during loading and unloading phases (Bentely, 1995)

of the transducers. Figure 4.13 is a typical plot of the output signal, done in MATLAB graphics mode, for the calibration of the load cells and the strain gauge force transducers. Similar plots were obtained for all the load cells and strain gauge transducers.

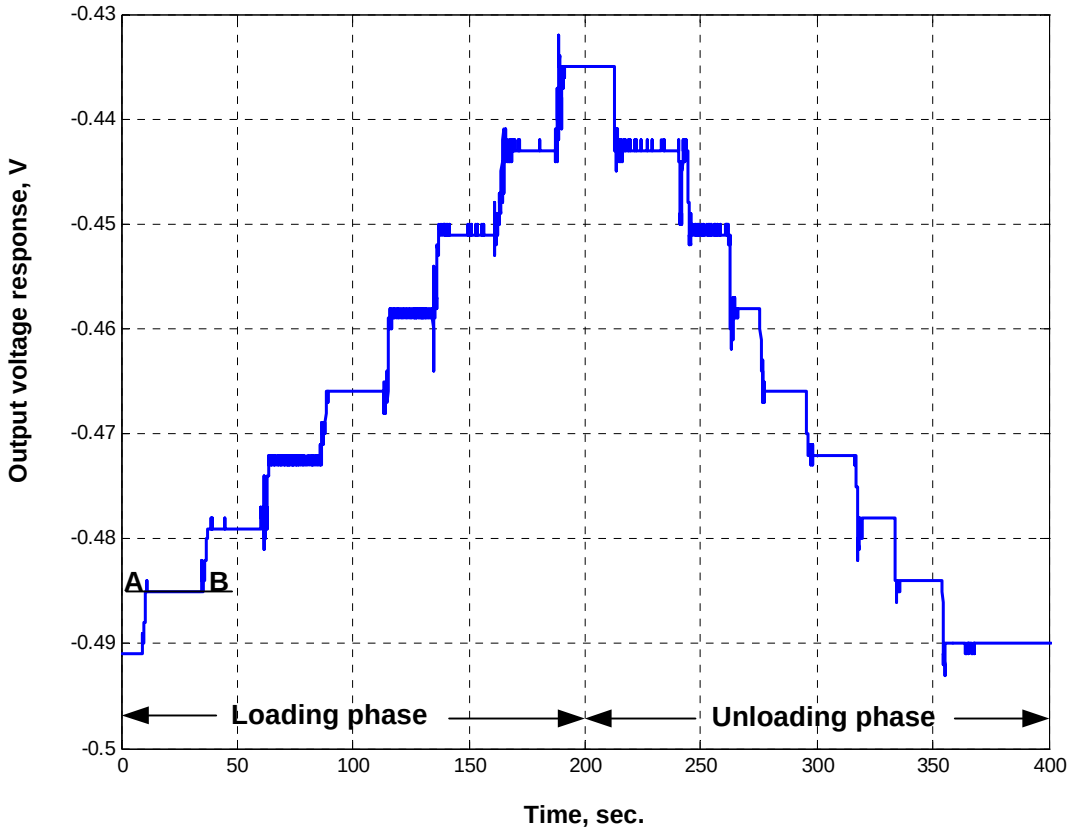

Figure 4.13: Typical calibration output signal for strain gauge force transducers and load cell for the loading and unloading phases

In Figure 4.13, the flat portions such 'A-B' which represent constant voltage levels on the voltage axis indicate the total weight registered by the force strain gauge transducers or the load cells with the passage of time of the transducer being calibrated after addition or removal of a dead load. During the loading phase, the voltage response of the load cells or strain gauge force transducer rises in a '*climbing-up staircase manner*' while during the unloading phase, the voltage response curve falls in a '*climbing-down staircase manner*'. In the case of Figure 4.13 the loading phase lasted about 200 seconds, and a total of 8 known dead loads of approximately equal masses were suspended on the load cell or strain gauge force transducer. The loads were then removed, one at a

time (unloading phase, Figure 4.13) and the set-up was allowed to stabilize before removing the next set of weight(s). This was repeated until the all loads were removed. The first and the last constant dead load recorded was the weight of the bar (Figure 4.11) or the hanger (Figure 4.12) for suspending the dead loads. The mass of the road and the hanger were known.

From plots similar to Figure 4.13, the voltage response values corresponding to known magnitudes of total dead load masses were read of the graph using the MATLAB graphics interactive zoom function. The voltage response was then plotted against the corresponding total dead load weight and the best fit regression line plotted. The resultant regression equation of best-fit lines based on the least-squares technique for all the force and torque transducers was of the form:

$$y = mx + c \qquad \ldots (4.1)$$

where:

y = voltage response for (V)

m = gradient of the best fit regression line (V N^{-1} for force or V$N^{-1}m^{-1}$ for torque)

c = the intercept on the voltage response axis (V)

The best-fit lines were plotted for both the loading and unloading phases of the calibration data. Figures 4.14a and 4.14b are typical best fit lines obtained for a purpose made strain gauge force transducer and an industrial load cell used on the two tool-frame carriers (§4.1 and 4.2).

From plots made and curve fittings results for the transducers, all the regression lines are highly linear with coefficients of determination of 0.99 or greater. The gradients of the fitted regression equations between the voltage response and the applied load were used to determine the calibration factors for the strain gauge force transducers and load cells. Calibration factors determined for load cells and strain gauge force transducers are presented in Table 4.1.

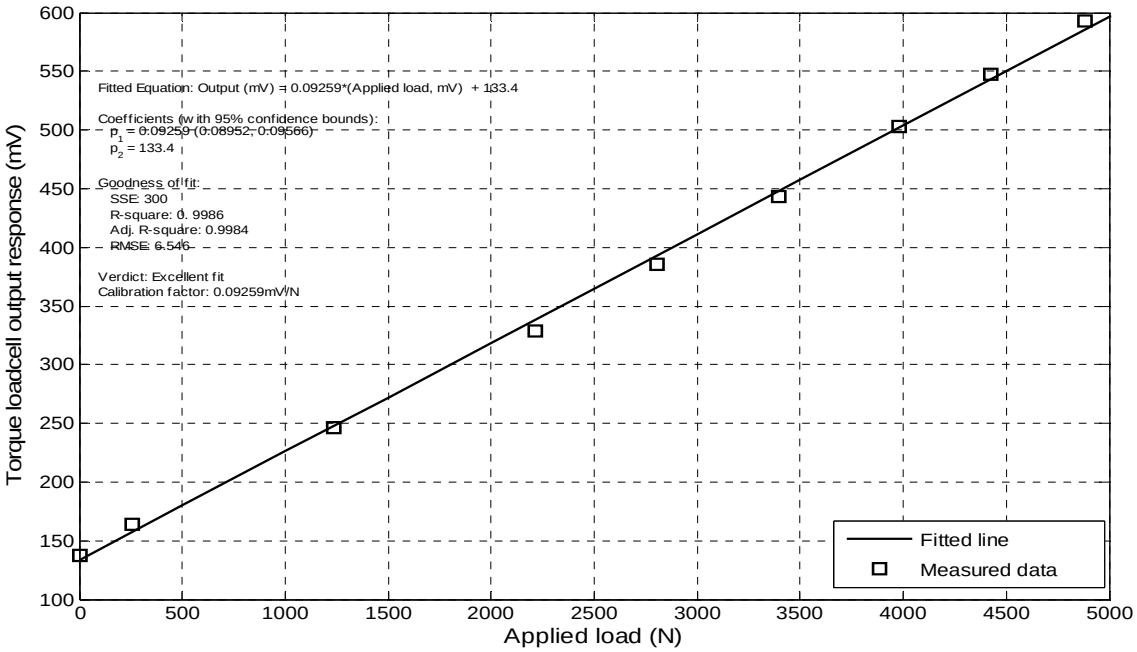

Figure 4.14a: Typical loading phase calibration curve for strain gauge force/torque transducers or force/torque load cell; (calibration curve of the strain gauge torque transducer)

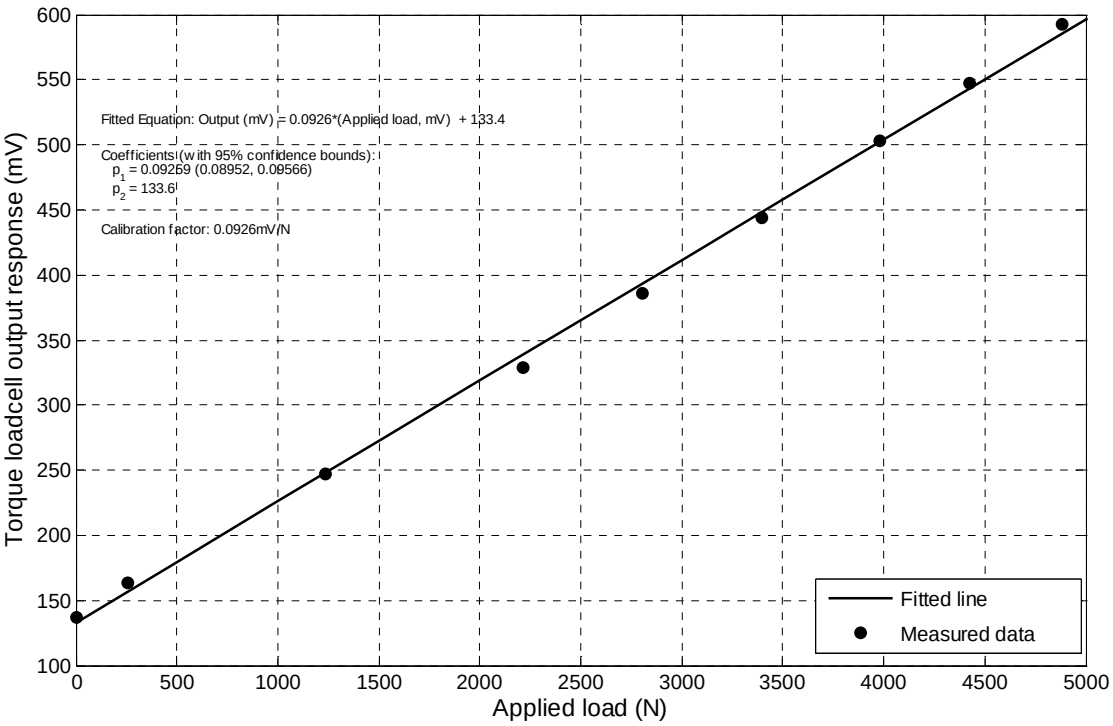

Figure 4.14b: Typical unloading phase calibration curve for strain gauge force/torque transducers or force/torque load cell; (calibration curve of the torque arm strain gauge transducer)

Table 4.1: Calibration results for the force strain gauge transducers and load cells

Component description	(R^2)	Calibration factor
Tiller tool-frame force/torque transducers:		
1. Lower left link strain gauge force transducer	0.9999	4.9020 x 10^4 N/V
2. Lower right link strain gauge force transducer	0.9996	4.4766 x 10^4 N/V
3. Top link strain gauge force transducer[3]	0.9998	6.3434 x 10^4 N/V
4. Torque load cell	0.9996	3.7313 x 10^4 N/V
	0.9999	1.0599 x 10^4 Nm/V
Torsional shearing device transducers		
1. Load cell for the normal load	0.9999	9.523 x 10^3 N/V
2. Strain gauge torque transducer	1.0000	407.997 Nm/V

4.4.2 Other transducers

Depth measurement transducer

The twenty–turn 200kΩ cable-extension potentiometer displacement transducer (Figure 4.4) was used for measuring depth of tillage was calibrated by pulling the string attached through a known distance on a scaled rule and recording the voltage output response using the DAS.

Calibration was done on a flat surface and the string pulled against a scaled metallic rule at 5 mm intervals. The span of calibration was 600 mm, which was beyond the intended depth of tillage operations. A plot of voltage against the distance was made and a regression line of best fit obtained. Figure 4.16 presents the calibration curve for the depth measuring system, together with the calibration factor and the coefficient of determination. The calibration curve is a perfect fit.

Travel distance and forward speed

Calibration of the travel distance was done in two steps. The first step involved the determination of the number of square waves generated by the sealed proximity probe. Ten complete revolutions were made and the number of pulses generated counted and the average number of revolutions determined. The effective circumference of the

[3] New set of strain gauges was fitted for the top link strain gauge force transducer in June 2004 after the initial one with a calibration factor of 6.3434 x 10^4 N/V failed. The bottom calibration factor is for the new top link strain gauge force transducer

section of the geared wheel driven by the wire rope was then determined. The tractor was then driven over known distance and the two distances compared. From the distance travelled, the average speed was obtained using the speed-time-distance relationship.

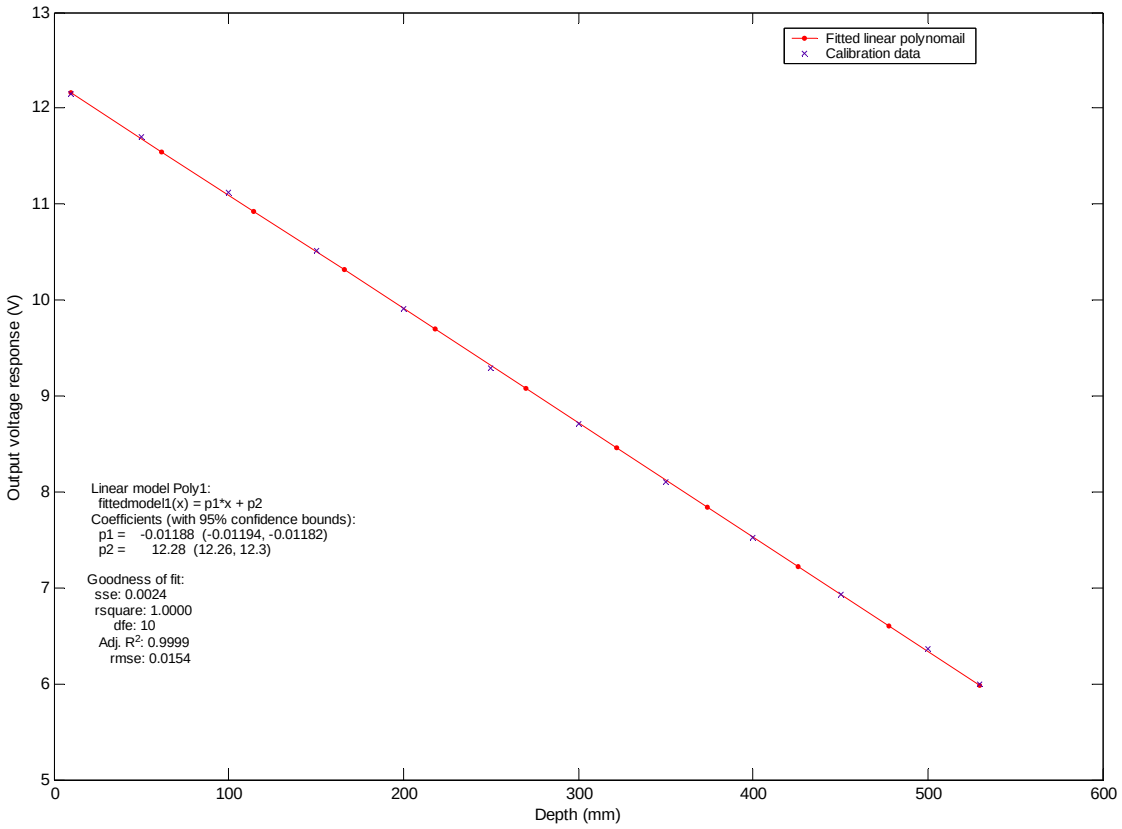

Figure 4.16: Calibration curve for the twenty–turn 200kΩ cable-extension potentiometer displacement transducer for monitoring the depth of tillage

Rotor speed measuring system

Like was the case for the measurement of the distance travelled, the rotor speed was determined using a proximity probe. The number of geared teeth on the drum (Figure 4.5) of the hydraulic motor that rotated at the same speed as the rotor shaft was 154. Thus 154 square waves were generated by the proximity probe for one revolution. The field tests were conducted at a constant tractor engines speed of 2000 rpm. The number of complete revolutions divided by the time taken for doing the tests yielded the rotational speed of the rotor.

4.5 Preliminary field testing of the apparatus

Field testing of the apparatus was done in order to determine the operational limitations of the rotavator and the soil shear strength and soil-metal friction characterisation device. The testing was also aimed at determining the data sampling rates, at which the measurements were to be made for the research equipment.

4.5.1 The experimental deep tilling rotavator

Measurements for the field testing of the equipment developed were carried out in the field under the intended actual experimental conditions. For the tiller, data was simultaneously recorded at a sampling rate of 2.4 kHz for all the eight channels on the tiller tool-frame carrier. The sampling rate for all the channels was determined by the channel that required the highest rate. In this case the rotor speed measured by the magnetic pick-up channel (4.4) required the highest rate. The in-built clock of the DAS was used for setting the timer over which test-runs was done.

Two tractors, connected by a tow bar, were used during the field testing (Figure 4.17). The use of the two tractors was to eliminate slippage, which would affect the performance of the tiller. The leading tractor provided the draft force for the forward travel only, while the tractor to which the rotavator tool-frame carrier was mounted provided the rotary power through its PTO shaft. Depth was the only operational parameter varied during the field testing. The depth of tillage was varied from 200 mm to 450 mm in steps of 50 mm in order to assess the resultant transducers output response. Field testing was done at a constant rotor speed after setting the engines speed of the two tractors. The forward travel speed maintained constant by operating the towing tractor on one forward travel gear, at a time, at a constant engine speed of 1000 rpm.

At the end of each test run, which was done for a specified length of time, the data was exported by the Spider8 interfacing program (*CARTMAN EXPRESS version 3.1, HBM, Germany*) and stored in the hard disk of the on-board computer. A second program, also developed in MATLAB, was used to determine the number of square-waves generated

by the magnetic proximity probe channel and the integrated optical transducer channel for the determination of the rotor speed and forward travel speed, respectively.

Figure 4.17: Setting-up for a tillage test-run *[the swivel wheel at the rear end of the rotavator tool-frame carrier was lifted off the ground during tillage experiments]*

Graphs of the pull/push forces on the tractor three-point link, the torque requirement and depth of tillage were thereafter plotted while still in the field and a visual inspection of the respective output responses effected. The object of the visual inspection was to ascertain the validity of the recorded transducer outputs. Figure 4.18 is a typical plot of the channel output responses for the three strain gauge force transducers and the input torque transducer.

From Figure 4.18 the portion of the various output response section that are constant, correspond to the measurements recorded taken when the rotavator was stationary for initialising the respective channels. The recording of data with the equipment stationary was necessary for the force and torque measuring channels because the 'zero' load value for these channels formed the basis for determining the magnitudes of the loads recorded during tillage tests.

In Figure 4.8, the sudden change in the response of the occurring at data point 4.8×10^4 correspond to the beginning of a test with the rotavator cutting the soil and the towing tractor in forward motion. The part enclosed within the rectangle for data points in the range 7.0×10^4 to 10.0×10^4 is presented in Figure 4.16, which give a better view of the variation of the response signals from the force strain gauge transducers and the load

cell on the torque arm. It was observed that immediately after the initial jump from the recordings taken when the set-up was stationary to recording taken when doing a trial run, the output response for the force transducer channels maintain fairly constant values. Further, by looking at the direction of this sudden jump, the forces in the two lower links oppose the force in top link during the rotavator operation.

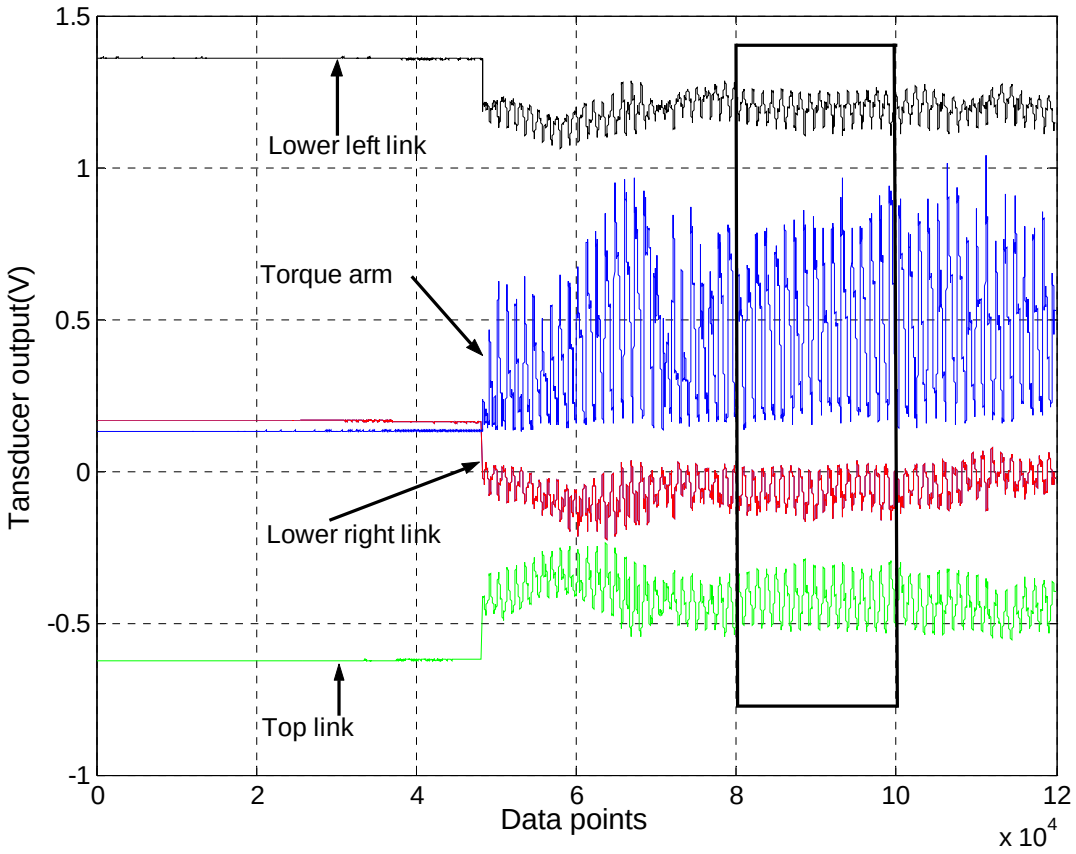

Figure 4.18: A typical plot showing the signal outputs obtained for the tiller strain gauge force transducers and the torque load cell during a down-cutting operation

The output responses the forces push/pull forces on the three-point hitch links and the torque on the torque arm are cyclic in nature (Figure 4.19. The torque link response is in phase with the top link phase and out of phase with the pus/pull force in the left and right lower links of three-point hitch system. In general the torque load fluctuate between zero (initialisation values) and a maximum value during down cut tillage while the push pull forces fluctuate within some confined ranges that are significantly different from their initial values. The cyclic nature observed for all channels corresponded to the

cutting actions by individual blades. This was established by plotting the torque response curve against the angular position of the blade from the horizontal.

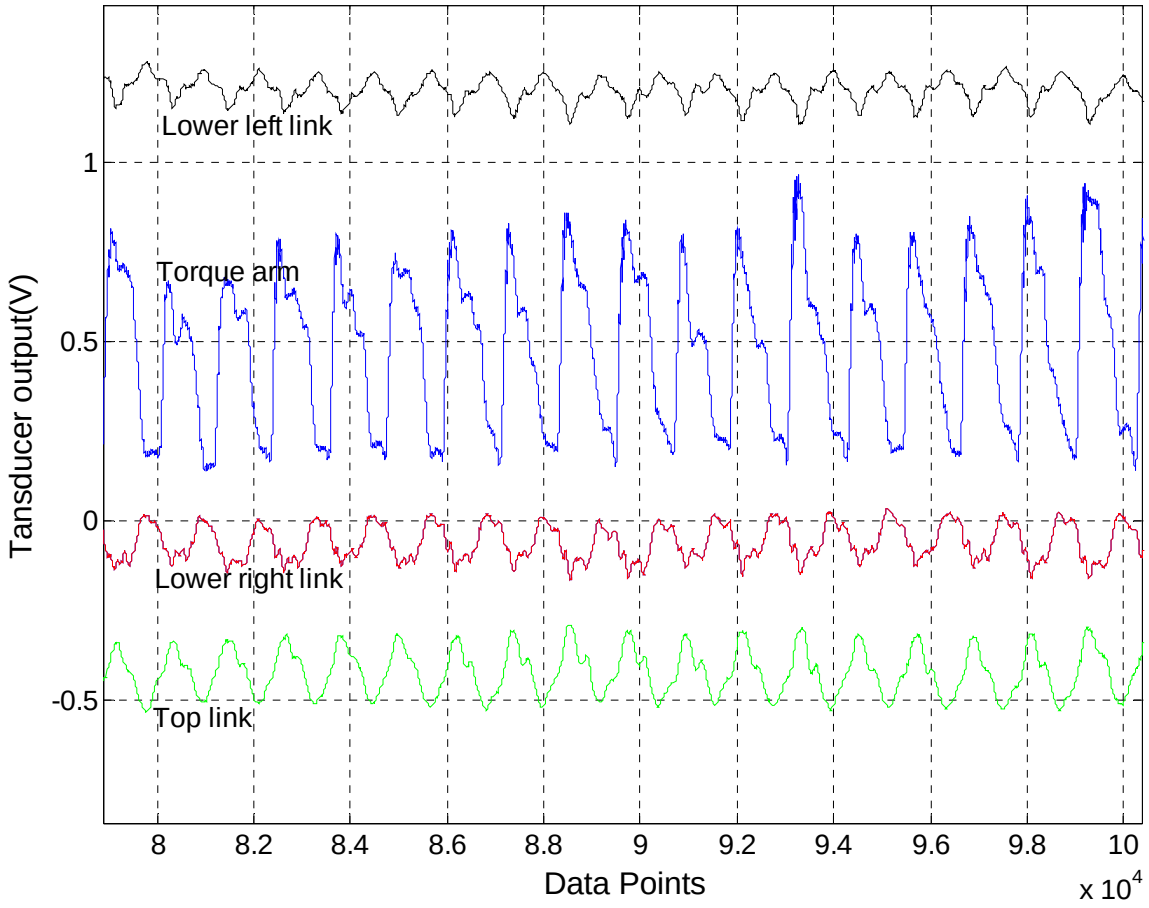

Figure 4.19: Expanded view of the output responses of the three point force transducers and the torque load cell for a down-cutting tillage test run

The magnitudes of the applied forces (on the three links), torque and depth of tillage recorded by the respective channels, were calculated using the respective calibration factors (Table 4.1, § 4.4.1) and the following equation.

$$O = CF \times V \quad \text{... (4.2)}$$

where:

O = magnitude of the applied force (N), torque (Nm) or depth (mm)

CF = calibration factor for the respective transducers

V = the respective voltage output response for a transducer

The rotor rotational speed and the forward travel speed were calculated using another computer program developed in MATLAB. This program also calculated the kinematic parameter, λ, and the bite length, L_b.

4.5.2 The soil strength characterisation apparatus

The torsional shear apparatus was field-tested at a data sampling rate of 60 Hz. The purpose of the preliminary field testing of the shearing device was threefold. First, it was necessary to determine the length of time necessary to record for a set of normal load and torque data using the torsional shear apparatus. Second, since the soil strength characterisation was to be determined at different depths, it was also necessary to determine the maximum depth that this apparatus could be operated at under field conditions. Finally, these tests were done in order to ascertain that the output response signals from the normal load and torque transducers were consistent with the expected outputs. The maximum depth that the shear device could reach was 320 mm.

The tests were done on a levelled ground surfaces at a depth of about 10 mm. Only the grousered ring head (Figure 4.8b) was used for the preliminary field-testing of the shear device. The decision to use only the grousered head at this stage was based on the fact that the procedure for determining of the soil shear strength and the soil-metal friction parameters using this apparatus is based on the same principle (see §4.2.1). During the tests, the desired level of the normal load was set using a digital read-out, connected in series with the load cell for measuring the normal load, via an electrical switch.

Once the normal load was set, the DAS was started and after about 30 seconds, the slow application of the torque load commenced. The torque load was applied for about 60 seconds. The torque load was applied for the full length of the shear device torque load hydraulic cylinder through an angle of about 60°. At the end of a test-run, the voltage output response of the applied normal and torque loads for the shear device were also plotted and visually inspected at the field for every test-run done

A typical plot of the normal and the torque loads voltage output response curves for the shear device is shown in Figure 4.20. Similar output voltage responses were obtained for the grouser head and the flat circular steel plate. Using Equation (4.2), the voltage

responses of the normal and the torque load channels were converted to their normal load and torque equivalents using the respective calibration factors given in Table 4.1 (§4.4.1). Plots of the variation of the normal and torque loads applied with time were thereafter made. .

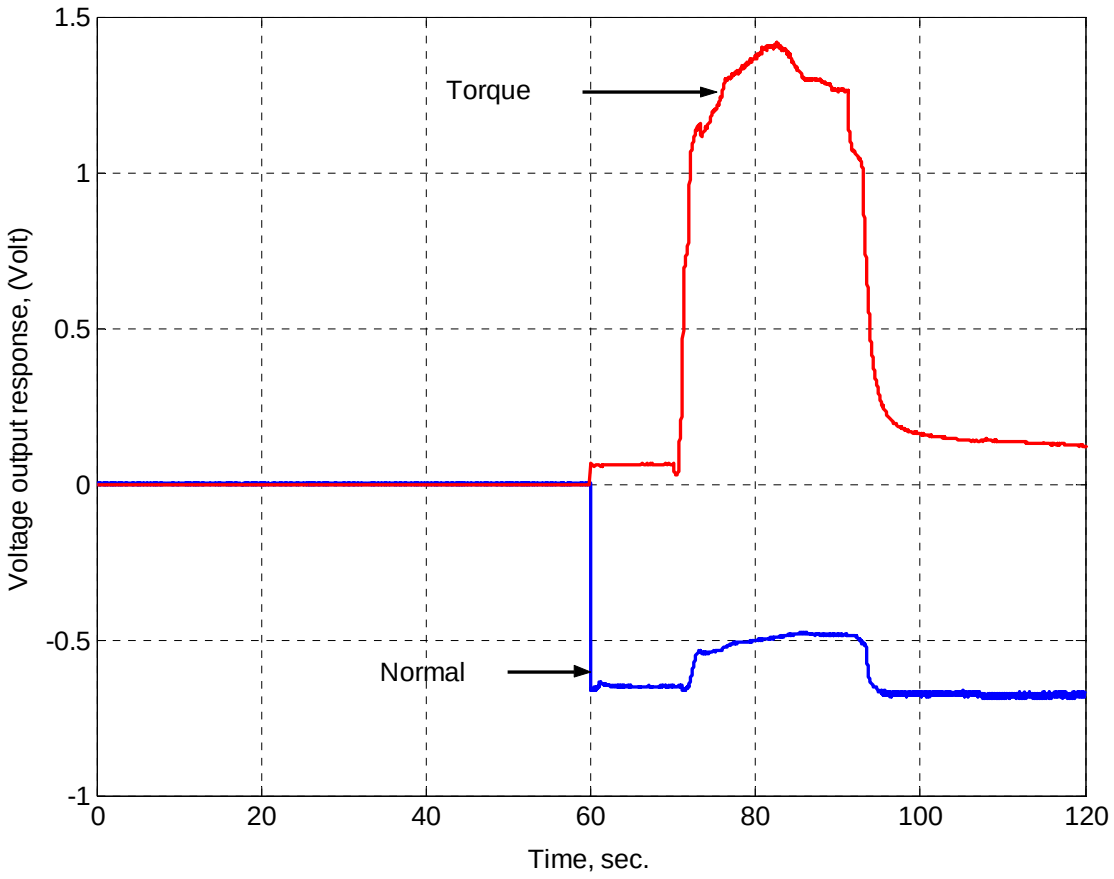

Figure 4.20: A typical plot of the output voltage responses of the shear apparatus showing the variation of the normal and torque loads with time

From Figure 4.20, prior to the initiation of the application of the shearing action by applying the torque load, the normal remains constant. However, with the application of the torque load, there occurred a slight decrease in the magnitude of the normal load. The fall in the normal load continues and only stops at the end of the application of the torque load. The decrease in the normal load voltage response was attributed to the sinkage of the head of the shear apparatus as it turns and penetrates the soil. It was also observed that greater fall in the normal load voltage response occurred if the application of the torque load was applied fast, i.e. in a short span of time. Therefore, all test runs

for the determination parameters of the shear strength and the soil-metal friction were performed at the slowest speed possible with the shearing apparatus.

On completion of the application of the torque load, the DAS was allowed to continue recording with the normal load maintained at the set level. During this session, the normal load returned to its original set value (from time of about 95 seconds to the end, Figure 4.20). With the normal load back to its set value, the shear apparatus tool-frame carrier was shifted laterally about 0.2 m from an already sheared spot and another test-run taken without altering the level of the normal load. This was repeated three times, i.e., three replications, after which the normal load was increased in steps of about 2kN and other test runs undertaken.

CHAPTER 5

RESEARCH METHODOLOGY

The research methodology used included the field testing of the two instrumented apparatus described in Chapter 4, field experimentation to study the effect of tillage depth and bite length on the performance of the rotavator, and the validation the proposed analytical model for predicting the torque requirements for a down-cut rotavator. All the field testing and experimentation were conducted at the Hatfield Experimental Farm at the University of Pretoria in South Africa. This chapter describes the methodology used to achieve the stated study objectives.

5.1 Determination of soil properties

5.1.1 Soil textural classification

Textural classification of the soil was done by collecting adequate soil samples randomly from the designated experimental site. The samples were collected from the top 600 mm, which was beyond likely maximum reach of the experimental deep tilling rotavator. The standard sieve method (Bardet, 1997) was used for the textural classification. The textural classification of the soil at the experimental site was done using the UDSA soil classification system (McKyes, 1989; Gill & Vanden Berg, 1967).

5.1.2 Soil water content

Soil water content was determined using the standard oven drying procedure (Bardet, 1997; Mandal & Divshikar, 1994; Gardner, 1986). The soil samples for the determination of the water content were collected immediately upon the completion of a test-run. At least 10 soil samples of about 40 g were collected in metallic containers for each test-run from different located strata of the soil whose water content was to be determined. This was done to obtain a representative soil water content (Lambe, 1951), for a given condition. The mass of the collected moist soil samples was determined using a scale balance with an accuracy of 0.01 g, and placed in a ‘constant temperature’ oven for

drying at a temperature of about 105 °C for a minimum drying period of 24 hours as described by Bardet (1997).

5.1.3 Soil bulk density

For the determination of the *in situ* soil bulk density, a field density test apparatus based on the principle of the core cutter method (Mandal & Divshikar, 1994) was fabricated, and used to collect soil samples at randomly selected spots within the experimental test area. The fabricated soil sampler had a volume of 820 cm^3. Prior to the collection of the soil samples the experimental site was irrigated for about 48 hours using a sprinkler irrigation system. The ground surface was thereafter levelled at depths of about 100 mm, 200 mm and depths greater than 300 mm using a shovel, after the irrigated area had attained its field capacity.

Soil samples for the determination of the soil water content were collected at the respective depths; at spots adjacent to where the soil samples for the determination of the bulk density were collected. A minimum of five samples were collected using the fabricated core sampler at each depth for a given level of soil water content for the determination of the bulk density of the soil. The collection of the soil samples at the prepared stretches of the levelled ground surface were then repeated after every two days, since the date of the last soil sample collection, until the soil water content dropped to about 8 % or less. The two days lapse was necessary for the test to be done at significantly different soil water contents levels. Initial trial tests had indicated that the soil water contents for soil samples of subsequent days were not statistically significantly different. Thus, field tests were done and soil samples were collected at two day intervals.

5.1.4 Soil shear strength

The torsional (rotational) shear apparatus described in §4.2 working on the principle of the shear ring (McKyes, 1989) was used to determine the soil shear strength parameters. The choice of this apparatus, among the many other possibilities, was based on the fact that in practice, the shear ring is more convenient to operate in the field because it is both manually and hydraulically easier to provide a forcing torque to the

device than to find anchorage and strength needed to apply large horizontal forces to the shear plate. The apparatus was also the most suitable for the determination of the soil shear strength and soil-metal frictional characteristics at the tillage depths that the tiller was to be operated at during test runs as the design allowed the lowering and raising the head of the apparatus hydraulically (see §4.2).

An annulus ring with grousers was attached to the head of the device for the determination of the soil cohesion (C_c) and angle of internal friction (ϕ). A normal load was applied hydraulically as described in § 4.2 and held constant with the help of the special hydraulic circuit (Figure 4.9). After about 60 seconds, a torque load was hydraulically applied, to rotate the head of the soil shearing apparatus (Figure 4.7) and cause soil shear-failure, using a separate hydraulic power system (tractor hydraulic system). The measured data for determining the soil shear strength and soil-metal friction parameters were collected using the DAS described in §4.3.

The data for soil shear strength and soil-metal characterization was sampled at the rate 60 Hz. The data recording was done for a total period of 120 seconds as described in §4.3. At a given depth and soil water content level, a minimum of five (5) sets of normal and torque loads were obtained for the determination of the soil shear strength parameters. For a given level of the normal load, three replications of the torque load were done. This was done by holding the normal load constant at the set level, shifting the apparatus tool-frame carrier a short distance of about 30 cm from a sheared spot.

For each test, graphs of the normal force and the shearing torque were plotted using the interactive plot function in MATLAB. The plots showed the recorded normal force and the applied torque with time (see Figure 4.20). The voltage output response for the normal load and the applied torque were converted to the normal load (N) and torque (Nm), respectively, by multiplying the respective channel of the measured data by the calibration factors. Graphs similar to Figure 4.20 with the y-axis expressed in force and torque units were thereafter produced. From these graphs the maximum torque at which soil failure occurred for a given magnitude of normal load was read-off the using the interactive zoom function of the MATLAB computer program graphics.

Using the maximum torque obtained graphically, the maximum shear stress calculated using the following expression (Johnson *et al*., 1987; Bailey & Weber, 1965):

$$\tau_{\max} = \frac{3M}{2\pi\left(r_o^3 - r_i^3\right)} \quad \text{... (5.1)}$$

where:

τ_{max} = maximum shear stress at soil-soil failure surface (kPa)

M = the maximum torque or the maximum resisting soil moment (kNm)

r_i = inner radius of the annulus ring head with grousers (m)

r_o = outer radius of the annulus ring head with grousers (m)

The normal stress was determined from the expression (McKyes, 1989).

$$\sigma_n = \frac{F_n}{A} \quad \text{... (5.2)}$$

where:

σ_n = normal stress (kPa)

F_n = the applied 'constant' normal load (kN)

A = the effective area of the torsional shear apparatus grouser head in contact with the soil (m^2)

The soil shear strength parameters were determined by plotting a graph the values of the normal stress against the average value of the three maximum shear stress values. The graphs were plotted using the curve-fitting toolbox in MATLAB, and the least-squares fitting procedure applied to obtain the best fit regression line. The internal angle of friction of the soil, ϕ and the soil cohesion are given by the slope and the y-intercept, respectively of such a graph (McKyes, 1989).

5.1.5 Soil-metal friction

Soil-metal frictional parameters were determined by replacing the grouser ring head of the shear device with a smooth circular steel plate of the same internal and external radii as the grouser head (Figure 4.8). Thereafter the same procedure described in §5.1.4 above, for determining the soil shear strength parameters, was used. Like was the case with shear strength parameters determination, the test was repeated three times for a given level of the normal load at a given depth and level of the soil water content. Equation (5.1) was applied to calculate the maximum soil-metal friction resistance force, and the normal stress calculated using Equation (5.2). By plotting a graph the values of the normal stress against the average maximum friction force, the angle of the soil-metal friction and the soil-metal adhesion are respectively given by the slope and the y-intercept of the obtained graph (McKyes, 1989).

5.2 Field experiments

Field experiments were carried out at the experimental site at the Hatfield Experimental Farm, University of Pretoria. The experiments were done in winter because the experimental site is situation in an area that receives summer rainfall. Thus, it was easier to control the levels of the soil water content in winter by irrigating the area where the experiments were to be conducted. After a irrigating, field experiments were carried out on it at predetermined dates. The use of different dates (days), was a natural means of attaining different soil water content levels required for the experimentation. The experiments were only done for assessing the performance of the experimental tiller; and the provision of the data required for the validation and evaluation of the proposed model for a down cutting rotavator.

5.2.1 Experimental layout

The general experimental layout used is presented in Figure 5.1. During the tillage test trials, two tractors were used. The paths cut by individual blades for the down-cutting direction are illustrated in Figure 5.2. Tractor 1, to which the rotavator is connected, was towed by Tractor 2 through a tow bar. Using this layout (Figure 5.1), and the set-up

(Figure 4.17, §4.5.1), experiments were carried out for determining the effect of set tillage depth, forward travel speed, number of cutting blades on the flange and bite length for different soil water content levels on the torque requirements and the push/pull forces generated for a down-cut rotavator.

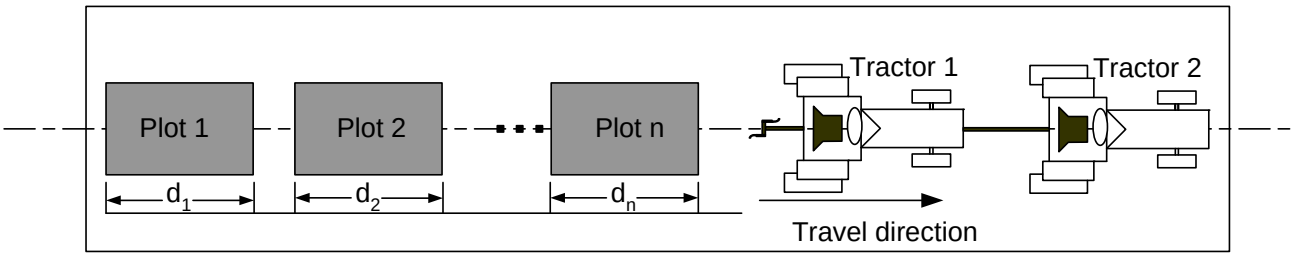

Figure 5.1: Experimental layout (d_1, d_2 … d_n – distance covered in respective plots during a test run)

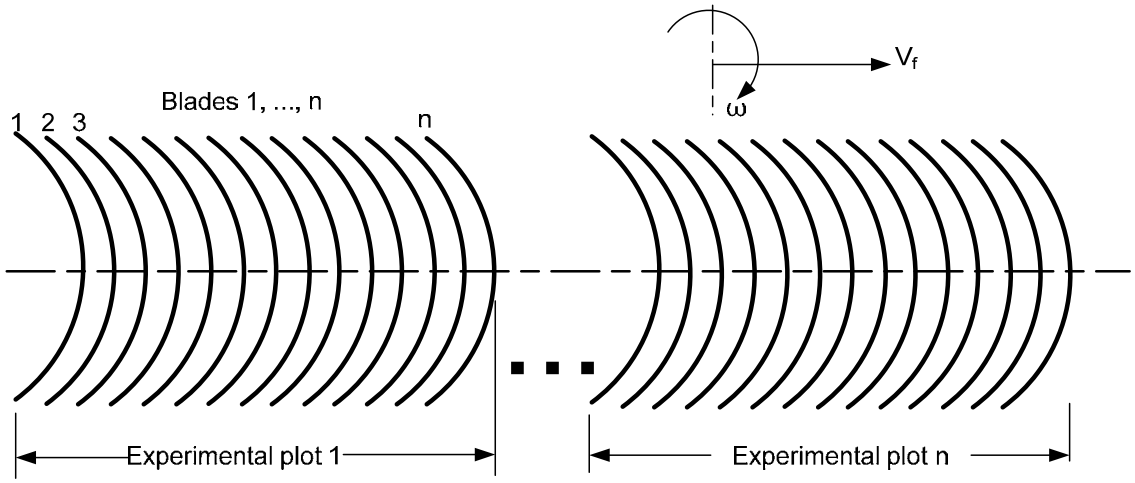

Figure 5.2: Illustrations of the cutting paths by individual blades within experimental blocks for experimental plots 1 … n.

All the field tests with the rotavator, irrespective of the variable whose effect on the performance parameters was being studied, required the same set-up (Figure 4.17). At the commencement of any test trial, for studying the effect of a given parameter on the tiller performance, the tiller tool-frame carrier was lowered to a point (Figure 5.3a) where a tip of a vertically positioned (aligned) blade came into contact with the ground surface. This was considered as the 'zero' or the reference depth. The DAS was then triggered and a test run was made with this set-up for the set length of time. The recorded data obtained at this depth constituted the initial channel values for all the seven channels on the tiller tool-frame carrier. The initial channel values so recorded

were used for referencing changes in the respective transducer values during field experimentation at the desired experimental conditions. In most cases a test run lasted 10 or 20 seconds. However, in severe conditions the time was increased to 30 seconds to allow the equipment to achieve stability.

After completion of the initialisation test-run, the recorded data was exported and stored in a data file in the hard disk of the on-board PC. Subsequent desired set tillage depths (Figure 5.3b) at which test runs were to be made was set by cutting a furrow to that depth. The initial setting of the depth of tillage was done manually, using a metallic tape measure.

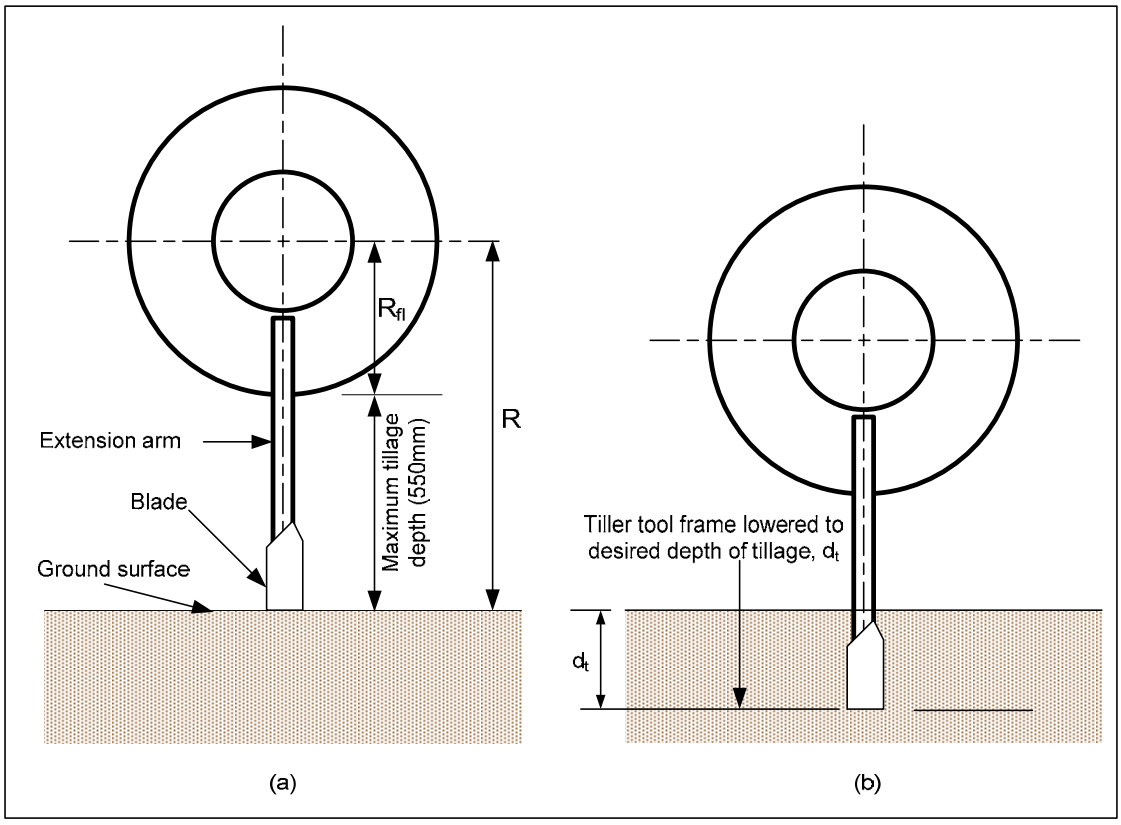

Figure 5.3: Initial and field test-run depth settings during experimentation

At the completion of the depth setting, the set-up was readied for collection of the desired data. The PTO gear was engaged and the engine speed of Tractor 1 (Figure 5.1) set to a constant value of 2000 rpm. A suitable forward travel gear of Tractor 2 was then selected and engaged, and its engine speed set to a constant value of 1000 rpm. The forward travel was then initiated and after about five complete rotations of the rotor,

the DAS was started and the measurement started. The progress of the measurements for a test-run was monitored on the monitor of the on-board PC. At the completion of a run, the data was exported and stored in a data file in the hard disk of the on-board PC for later analysis.

For a given depth and soil condition, three sets of measurement of 20 seconds each was done. Once the forward motion had been initiated for a given depth, Tractor 2 was not halted until after the completion of the third replication. The in-built clock of the DAS software terminated the measurement after the set duration had elapsed. Graphs of the measured data were plotted at the end of a measurement for visual inspection, immediately after the completion of a test-run, before another test run was initiated. The test-runs were repeated for different depths with the same number of blades on the flange for the two forward travel gears.

5.2.2 Effect of tillage depth

Field trial test runs were conducted to determine the effect of the depth of tillage on the torque requirement and the resultant push/pull forces generated on Tractor 1. These tests were done at constant travel and rotational speed of the rotor and the towing tractor, (Tractor 2). Five depths of tillage, namely 250 mm, 300 mm, 350 mm, 400 mm, 450 mm, 500 mm and 550 mm were used. For each set tillage depth, three tillage tests were done.

The setting of the depth at which the tillage test runs was done was achieved by cutting a furrow while the equipment was stationary until the required set tillage depth was reached. Once this depth was reached, the forward motion was initiated by engaging the appropriate forward travel gear of Tractor 2 (Figure 5.1). A minimum of three test plots were then processed without stopping. This was done to ensure that the stability of the experimental set-up was maintained for a set tillage depth. Soil samples were collected as described in §5.1.2 and the standard oven drying method (Bardet, 1997) used to determine the soil water content for the soil tilled at various depths.

5.2.3 Effect of bite length

The bite length was varied in two ways; by changing the forward travel gear ratio of the towing tractor (Tractor 2, Figure. 5.3) or by changing the number of blades on the flange of the rotor. Tractor 2 was only operated in two forward gears; Gear I and Gear II, in the low speed range.

The change in bite length by either operating the rotavator with six (6) or three (3) cutting blades on the same side of the flange, or by operating Tractor on the two forward travel gears for a fixed set of number of blades on the same side of the flange.

After changing the bite length using any of the above two approaches, the field tests using the experimental rotavator were thereafter performed at different depths of tillage (§5.3.1) for the set bite length. A minimum of three tests was done without for each set tillage depth. Again, soil samples were collected randomly at random depths within the tilled layer for each field test for the determination of the soil water content, as described earlier.

5.3 Calculating the bite length and the blade angular position

The bite length was calculated using Equation (3.8). The forward travel velocity and the rotor rotational speed was determined as explained in §4.4.2. The radius of the rotavator, R was 930 mm; and comprised the blade-extension arm length plus the flange distance to the centre of the rotor (Figure 5.3).

The angular blade position from the horizontal was calculated by counting the number of square-waves generated and multiplying this by 2.338, the angle equivalent for one square-wave. This enabled the determination of the torque values (measured and model generated) for the angular position of the tip of the blade during the soil cutting. The ability to determine the angular position is important because the comparison of the measured and model generated torque requirements at different set tillage depths will be done for the same angular positions.

5.4 Data processing and analysis

5.4.1 Experimental data processing

Processing of the field experiment data was done using MATLAB (*Matlab, Version 7, Mathworks, Inc. USA*) and MS Excel (*Microsoft, Inc., USA*). MATLAB was extensively used in the manipulation of the tillage data. The Curve Fitting Toolbox MATLAB was used for the development of regression relationships between the variation of the soil shear and frictional strength parameters with the soil water content for the two depths. The interactive zoom function in MATLAB graphics was used for the determination of the specific values at the points of interest, e.g., the determination of the maximum torque required for the determination of the stress and maximum frictional force values.

For the processing of the data for the rotor and the forward travel speed, a computer program was developed in MATLAB. The program counted the number of the square-wave pulses generated during a test run and converted them to their equivalent rotational or forward travel speed. The program was also used to calculate the kinematic parameter, λ and for the determination of the bite length, for all test runs.

Preliminary data analysis also involved the determination of the average pull/push force generated by the rotavator during the tillage trial and the determination of the mean torque requirements. Owing to the high sampling rate used for capturing the tillage test run data and the many data files to be pre-processed, a third computer program was developed in MATLAB for calculating the average values for reaction forces and torque requirement transducer channels and the depth transducer. The calculated average channel values were then transferred to a special spreadsheet with corresponding columns for the recorded data. The average resultant push/pull force was determined from the summation of the three-point link forces.

MS Excel was used for the manipulation of the soil water content and bulk density determination data. The spreadsheets for the collection and processing of the data for soil water content and the bulk density were prepared in advance.

5.4.2 Statistical data analyses

A combination of graphical and statistical analyses was used to analyse the experimental and model generated data (Chapter 6). Minitab (*version 15, Minitab Inc., USA*) was used to effect the required statistical analysis. The different graphs required for both the model generated and the measured field experiments data is done using MATLAB. The analysis was done for the model input parameters, experimental results, and the validation and evaluation of the proposed model. Different statistical techniques, highlighted below were used as appropriate in effecting the required analysis.

The least squares linear regression technique is used to determine the soil shear and soil metal friction parameters at 95 % confidence interval (or 5 % significance level). MATLAB's Curve Fitting Toolbox is used in analysing all the data to be analyzed using the linear regression technique. For example this technique will be used to fit the normal stress data against the corresponding maximum shear stress for both the soil shear stress and soil-metal friction parameters for the soil at the experimental site. The resulting empirical equals will give the parameters for both the shear stress and soil-metal friction at the specified levels of the soil water content.

Analysis of some of the data required the determination of simple means. The versions of Minitab and MATLAB used to analyse the data in this study were both capable of calculating the simple mean. The mean of the soil bulk density from different depth ranges was a required model input and was also used to define the soil condition. Mean values of the horizontal resultant thrust force generated and the torque requirements for different experimental conditions are also needed in the evaluation of the field performance of the experimental deep-tilling rotavator.

In order to verify, validate and evaluate the model; a significance test is performed (§6.5.3) for the difference between the model and measured torque requirements values for different set tillage depths. The test statistic applicable in this case is the paired Student t-test (Levine, Ramsey & Smidt, 2000; Johnson, 2000; Montgomery & Runger, 2003) Using this approach, it is possible to compare the model generated and measured torque requirement values for the same angular blade positions during soil

processing. Misczak (2005) used this statistical approach in a study that involved the comparison of the measured and predicted torque values for a rotary subsoiler at the same angular positions from the horizontal.

In addition to the t-test, a conformity test was effected between the model generated and measured torque requirement values. This test assessed the degree of agreement between the measured and the model generated torque requirement using the least squares linear regression technique (Equation (5.3)).

$$T_{\text{model}} = \alpha_r + (\beta_r) \times T_{measured} \quad \text{... (5.3)}$$

Equation (5.3) is used (§6.5.3) to evaluate the degree of agreement between the model generated and the measured torque requirement values at different blade angular position. The α_r and β_r in Equation (5.3) are determined for the following null *(H_0)* and alternative *(H_1)* hypotheses:

$$\left.\begin{aligned} H_o : \alpha_r = 0,\ \beta_r = 1 \\ H_1 : \alpha_r \neq 0,\ \beta_r \neq 1 \end{aligned}\right\} \quad \text{... (5.4)}$$

This approach of the least squares regression technique has been used in the past by many researchers (Misczak, 2005; Zhang & Kushwaha, 1995; Swick & Perumpral 1988; Perumpral *et al.*, 1983) to compare the predicted and experimental (measured) data for tillage tools.

CHAPTER 6

RESULTS, ANALYSIS AND DISCUSSION

6.1 Introduction

A mathematical model for predicting torque and power requirements of a rotavator fitted with L-shaped blades was proposed in Chapter 3. Field experiments were done in order to assess the performance of the deep-tilling experimental rotavator for the 200 – 500 mm tillage depth range; and to validate and evaluate the proposed model. Rotavator performance field tests in this tillage depth range were necessary due to the dearth of information on the performance of this tool in deep tillage (see Chapter 2).

6.2 Experimental site soil characteristics

6.2.1 Soil shear strength parameters

Figure 6.1 is a typical graph used in this study for the determination of the soil shear strength parameters for the soil at the experimental site at a given depth and soil water content, using the approach described in §5.1.4. The graph includes a fitted least square linear regression line for the mean of the maximum shear stress values and the respective normal stresses. The graph and the fitted line were generated using MATLAB's graphics and Curve Fitting Toolboxes (MATLAB version 14, *Mathworks Inc., USA*). The least squares fit gives the values for the slope, the *y*-intercept coefficient, and the coefficient of determination (R^2). The 95 % prediction bounds included in this graph is used for the visualization of any outliers in the experimental data obtained. Points located outside such prediction bounds are outliers; and usually have significant effects on the outcome of a least squares regression analysis results. In order that the results are within the state range, all the data points must be located within the stated bounds. The 95 % confidence interval (CI) is recommended for tests involving least square linear regression analysis (Montgomery & Runger, 2003).

In Figure 6.1, the slope and intercept of such graphs define the tangent of the angle of soil internal friction and cohesion (Ayers, 1987; McKyes, 1989), respectively, in the Coulomb's equation (Equation 2.47, §2.2.5). Therefore, the Coulomb's shear stress equation for Figure 6.1 is of the form:

$$\tau = 15.8 + 0.8058\sigma_n \qquad \ldots (6.1)$$

In Equation (6.1), the soil cohesion (C_c) for the soil tested is 15.8 kPa and the internal angle of friction of the soil, ϕ is given by the tangent of the coefficient of the normal stress, σ_n, i.e., $\phi = \tan^{-1}(0.8058) = 38.86^o$.

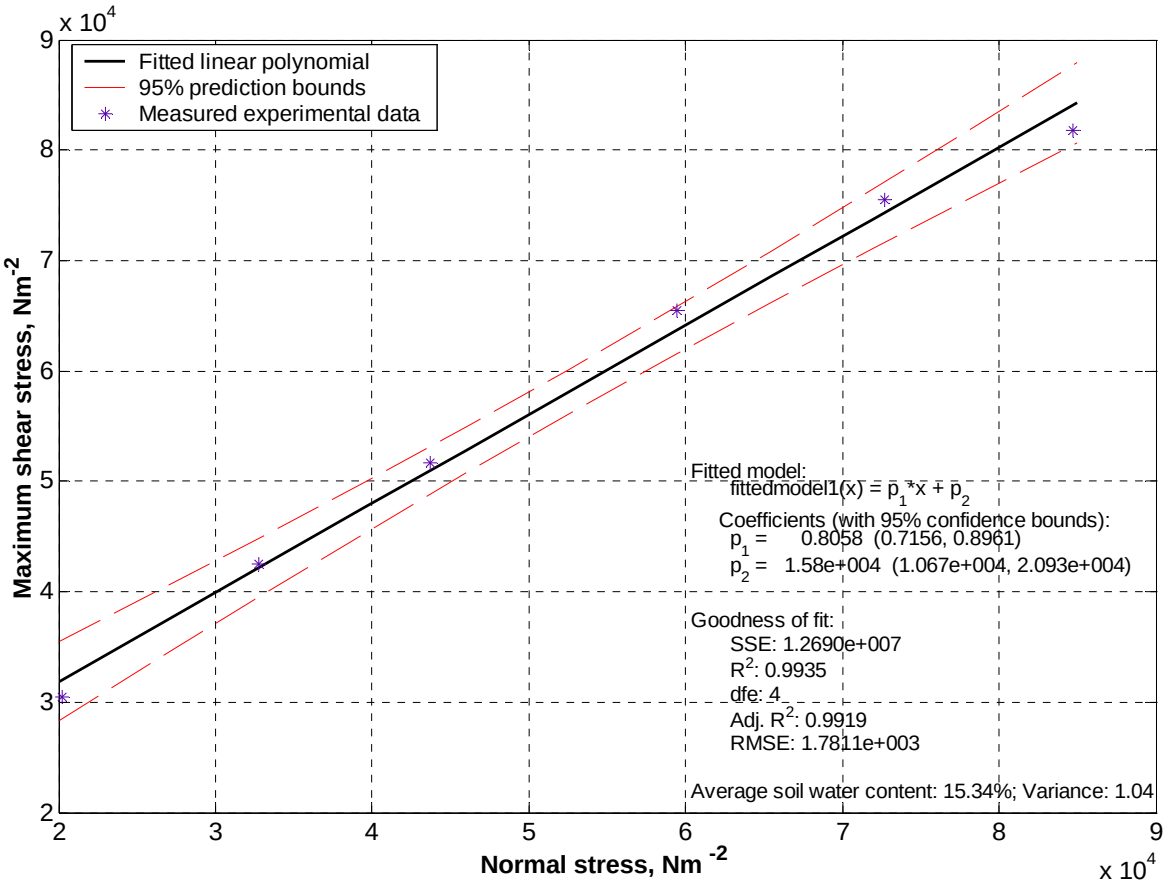

Figure 6.1: A typical graph of the average maximum shear stress versus the normal stress values at the soil-soil failure plane for the determination of soil shear strength parameters

6.2.2 Soil-metal friction parameters

The soil-metal friction parameters were determined using the method outlined in §5.1.5. Figure 6.2 is a typical graph of the average maximum frictional stress versus the normal stress for the soil at the experimental site at a given depth and soil water content. In this case, the slope and intercept for a graph of the average maximum friction shear stress against the normal stress defines the angle of soil-metal friction ($tan\,\delta$) and adhesion (C_a), respectively (Ayers, 1987; McKyes, 1989).

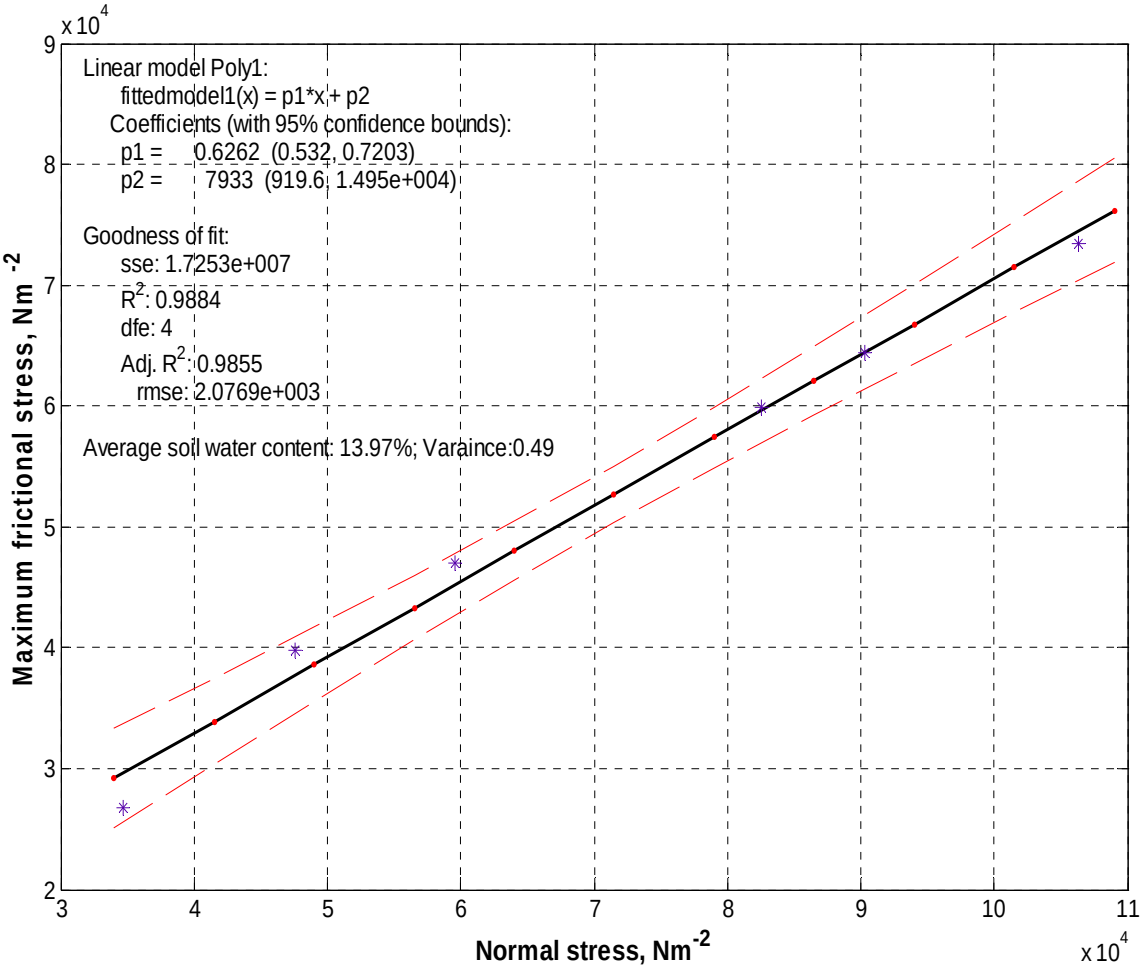

Figure 6.2: A typical plot of the average maximum frictional stress versus normal stress at the soil-metal failure plane (depth of 200 mm and 13.97 % soil water content)

The fitted least square linear regression line and the coefficient of determination (R^2=*0.988*) in Figure 6.2 indicate that a linear relationship fits the average maximum

frictional stress and the normal stress data well. The Coulomb's equivalent expression for the soil-metal friction is of the form (Ayers, 1987; McKyes, 1989):

$$\tau_f = 7.933 + 0.6262\sigma_n \quad \text{... (6.2)}$$

Using the approach of §6.1 and Equation (2.47), the soil-metal adhesion (C_a) at the stated soil condition (soil water content) is 7.933 kN/m^2. From the graph (Figure 6.2), the angle of the soil-metal friction is given by $\delta = \tan^{-1}(0.6262) = 32.06^o$.

From Figure (6.2) it is evident that the least squares linear regression technique can be applied to determine soil-metal friction parameters from the data collected using the torsional shear apparatus (§4.2). The results obtained returned a high value of the correlation coefficient *(R^2 = 0.9884)*. In addition, all the data points for the respective paired normal and soil-metal friction are within the 95 % prediction bounds. The high R^2 value and location of the data points within the 95 % prediction bounds indicated that the parameters obtained were statistically acceptable for the estimation of the soil-metal friction parameters. Therefore, the soil-metal friction parameters could be used with confidence as inputs to the proposed rotavator torque requirements model.

6.2.3 Soil texture and bulk density

Results of the standard sieve analysis obtained using the method described in §5.1.1 indicate that the soil within the top 600 mm contained 25 % clay, 11 % silt and 64 % sand. Using the USDA soil classification textural triangle for soil mixtures, the results indicate that the soil at experimental site is *sandy clay loam* (McKyes, 1989).

Table 6.1 gives a summary of the soil water content and the bulk density of the soil at the experimental site for the different depth ranges determined using the approaches described in §5.1.2 and 5.1.3, respectively. The analysis of variance (ANOVA) performed on the data (Tables 6.2 & 6.3) indicated that the soil bulk density and soil water content within the different depth ranges were statistically different. The respective mean values for the different depths are 11.86 % (± 0.86); 13.77 % (± 1.36) and 16.51 % (±1.52). The corresponding average soil bulk density within the depth ranges are 1804.6 kg/m^3 (±

53.9) for depths less than 150 mm, 1715.0 kg/m^3 (± 71.1) for the 150 – 300 mm, and 1625.0 kg/m^3 (± 25.7), respectively. The difference in the average bulk density and the soil water content is attributed to the drying of the soil which is more pronounced in the shallow depth ranges. The decrease in the soil bulk density with depth was therefore attributed to the increase in the soil water content with depth.

Table 6.1: Summary of the soil water content (swc) and soil bulk density results for different depth ranges at determined 48 hour intervals after stopping irrigation

Depth < 150 mm		150 mm < Depth < 300 mm		Depth > 300 mm	
swc (%)	density kg/m^3)	swc	density (kg/m3)	swc (%)	density (kg/m^3)
10.74	1886.53	11.96	1664.47	15.36	1621.30
11.31	1749.61	12.13	1833.25	15.53	1592.52
11.66	1749.61	14.32	1766.40	15.95	1640.48
11.94	1805.97	14.80	1705.24	16.61	1611.70
12.24	1844.35	14.91	1662.31	17.09	1658.87
13.26	1791.58	14.94	1667.47		

The observed higher values of soil bulk densities for correspondingly lower values of the soil water content (Table 6.1) was attributed to fact that drying of a soil results in more solids (soil) particles occupying the same volume. Since the soil particles are heavier than water, the drying of a soil results in increased mass of the soil occupying the same volume, e.g., the soil bulk density test apparatus used in this study. The systematic decrease in the soil bulk density with deeper depth ranges is due to the systematic differential drying rates of the soil for different depth ranges. The decrease and increase of the soil bulk density and soil water content, respectively, with depth within different depth ranges has been reported by other researchers (Gitau, *et al*., 2005; Girma, 1989) for clay loam soils.

Table 6.2: Summary of ANOVA test performed on the soil bulk density for the different depth ranges

Source	Df	SS	MS	F	p-value
Depth	2	88249	44125	14.57	0.000
Error	14	42390	3028		
Total	16	130639			

Table 6.3: Summary of ANOVA test performed on the soil water content for the different depth ranges

Source	Df	SS	MS	F	p-value
Depth	2	49.25	24.63	22.92	0.000
Error	14	15.04	1.07		
Total	16	64.30			

6.3 Measured forces and torque requirements

One of the specific objectives of this study was to measure the torque requirements and determine the magnitude of the resultant thrust forces generated under field conditions for an experimental deep-tilling rotavator, operated in both the up- and down-cut directions of rotation. Preliminary field tests done for assessing this objective indicated that the up-cut rotary tillage left an open furrow, which was considered undesirable for the preparation of a seedbed. As a result of this observation, no further field tests were done in the up-cut directions for the determination of torque requirements and thrust forces generated for the experimental deep tilling rotavator.

This section, therefore, presents the results of the measured torque and horizontal forces on the tractor three-point links for the experimental deep-tilling rotavator operated in the down-cutting direction of rotation. A typical output of the response curves for the torque and the forces recorded on the top and the two lower tractor links for a given experimental condition is presented in Figure 6.3. Two distinctive sections of the measured torque and horizontal forces on the tractor links are shown in Figure 6.3. Sections A and B, respectively, are for measurements recorded when the rotavator was stationary and when processing the soil.

The torque and force values in section A (Figure 6.3) were expected to be zero. A scrutiny of this section, however, reveals that only the torque and the lower left link force values measured had the expected zero values in this section. The top link and lower right link transducers recorded values that were slightly greater and slightly lower than zero, respectively when the system was not subjected to tilling or soil processing forces. The effect of this 'non-zero' values at no load is however insignificant when

compared to the magnitudes of the average of the forces recorded by the respective channels, during soil processing by the rotavator. The average force and torque requirements recorded when the rotavator is processing the soil, are the parameters used in this study to assess the performance of the experimental deep-tilling rotavator.

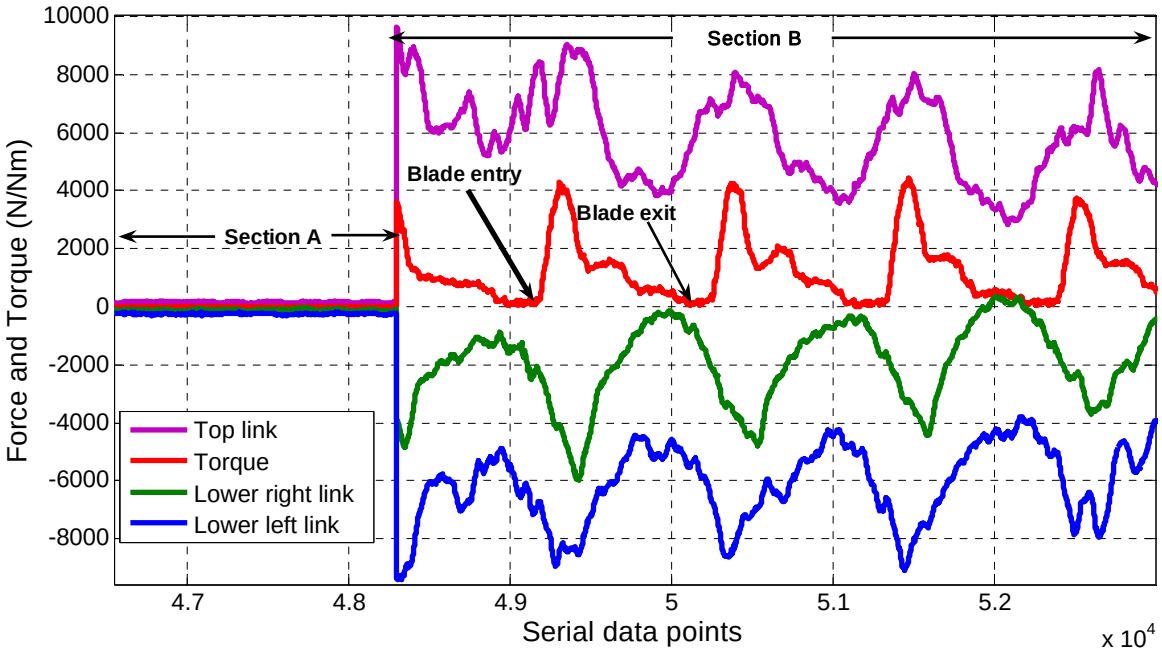

Figure 6.3: A section of the measured torque and horizontal forces on the top and lower links (A – rotavator is stationary; B – rotavator is processing the soil)

A strong association was observed between the values of the torque requirements and the individual horizontal reaction forces on the three links (Figure 6.3). This observation was such that upon the initiation of the soil cutting action by the blade, as the torque requirement, and the horizontal reaction forces at the top and the lower links are also increased with time for individual blade. Considering the processing of the soil by a blade, it is observed that the peak values in torque requirements and the respective horizontal forces measured on the three point links of the tractor occured at the same time.

Considering the torque response curve for a single blade only (Figures 6.5), the measured torque values increased rapidly at the commencement of the soil cutting, reaching a peak and then decreased gradually, to a minimum value at the end of soil cutting process. The rapid increase in torque values at the commencement of soil cutting

is an indication of high resistances offered by the soil to the cutting blade upon the blade entry into the soil. The forces that contribute to this high resistance include the cutting and soil compression resistance, resistance due to soil shear strength and the soil-metal friction resistance between the blade and the soil. The decrease in the magnitude of the torque values after reaching the peak is attributed to the decreasing soil resistance due to the decreasing cross section of the cut soil slice as the blades moves through the soil (§3.2.4 & 3.2.5), and the continuous decrease in the rake angle of the blade.

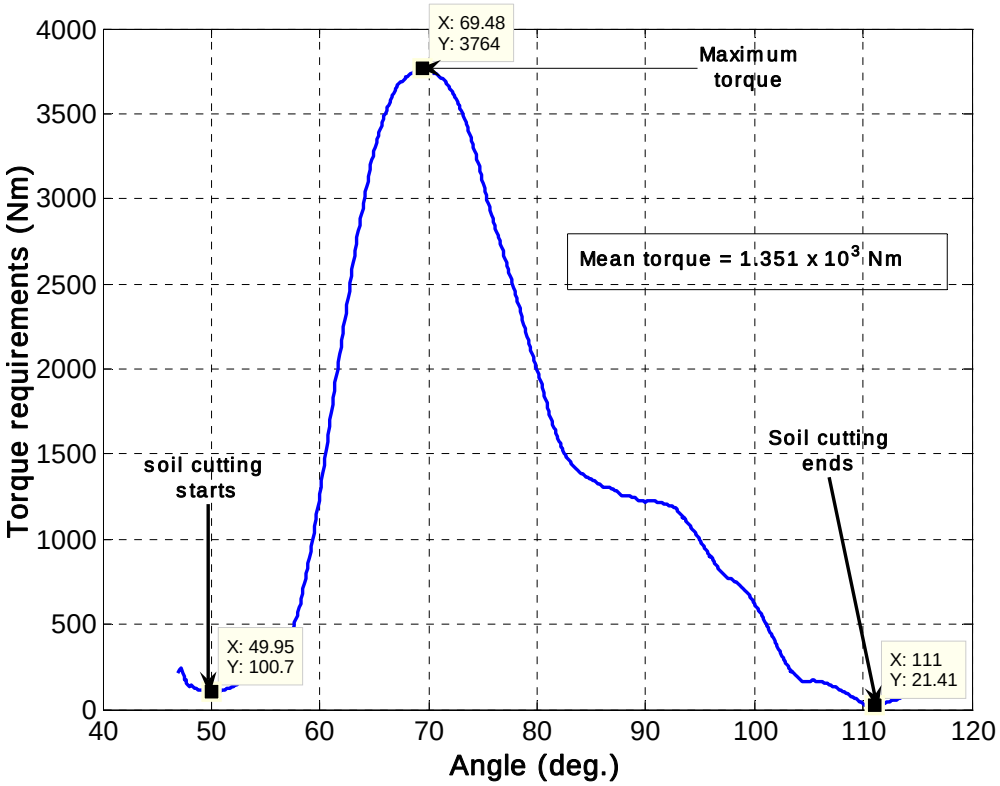

Figure 6.4: Typical variation of torque requirements with rotational angle for a single blade between the start and end of soil cutting process *[X-value = angle turned through by the rotavator blade from the horizontal position; Y-value = torque requirement value at position X]*

At the end of the soil cutting process by a single blade and before the start of soil cutting by a subsequent blade, the torque requirement values recorded/measured should be zero. However, measurement taken during rotary tillage test trials with the experimental rotavator show that the rotavator requires some torque, even when there is no blade cutting the soil (Figures 6.3 & 6.4). This observation was attributed to the presence of friction and other parasitic forces in the rotor assembly of the experimental rotavator.

The somewhat greater than zero torque requirement values recorded in-between successive blade cutting operations is associated with the turning effort required to overcome motion resistance of the rotor assembly, and to overcome the intrinsic parasitic forces in the rotavator assembly.

The response curves for the forces recorded on the top and the two lower links (Fig. 6.6) indicates that these forces are in opposite directions. Subsequently, at an instantaneous moment of time, the direction and magnitude of the resultant horizontal force is the difference between the sum of the forces on the two lower links and the force on the top link. Depending on the magnitudes of the respective instantaneous time moment forces in the three links, the resultant force can be positive or negative with respect to the forward travel direction of the rotavator.

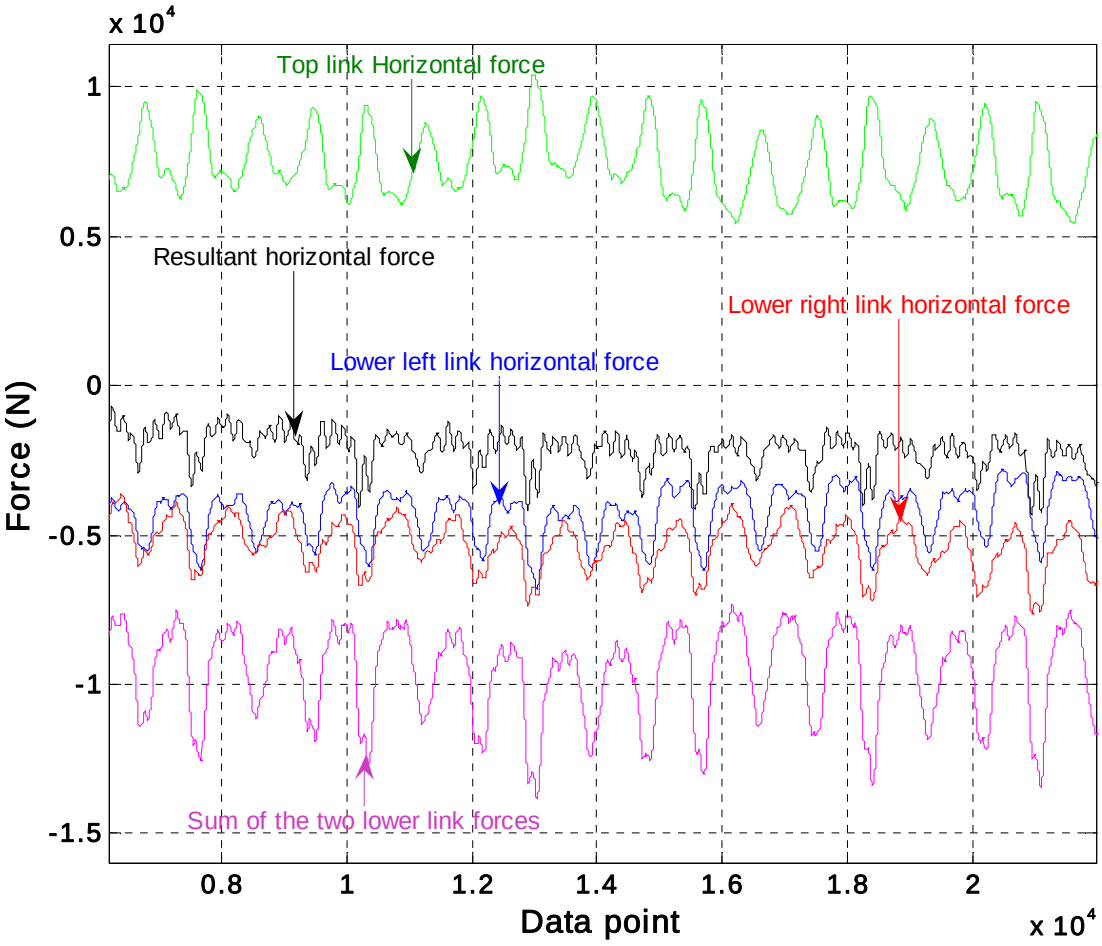

Figure 6.5: A section of a graph showing the variation of the horizontal forces recorded on the three links, the sum of the lower link forces and the resultant horizontal thrust force

At any instantaneous time moment, if the instantaneous time moment sum of the forces on the two lower links is greater than the instantaneous time moment force on the top link, the instantaneous time moment resultant force exerts a push. Similarly, if the instantaneous time moment force on the top link is greater than the sum of the instantaneous time moment forces on the two lower links, the instantaneous time moment resultant force exerts a draft or a pull force, like is the case, with passive tillage tools.

The magnitudes of the measured reaction horizontal forces on the two lower links were unequal (Figures 6.4 & 6.6). The horizontal force on the lower left link, on average, was about twice that on the lower right link. This difference was due to the unequal distances from the centre of the cutting force to the points at which the strain gauges measuring the thrust forces are placed on the tiller tool-frame. This observation, however, has no effect on the magnitude of the resultant thrust force generated during the operation of the experimental rotavator. The magnitude of the thrust force generated was the instantaneous difference between the instantaneous sum of forces of the two lower links and instantaneous force on the top link.

In Figure 6.5, the resultant force is a push, since the sum of instantaneous forces recorded by the two lower links is greater than the force recorded by the top link. The direction of the resultant horizontal force is important in the performance of rotary tillage tools because it affects the energy requirements during the tool's tillage operation. Consequently, in this study, the magnitude of the resultant thrust force and torque requirement was used to assess the performance of the experimental deep-tilling rotavator for different sets of operational conditions (§6.4 below).

6.4 Performance evaluation of the experimental rotavator

Literature reviewed (Chapter 2) revealed that there is dearth of information on the performance of the rotavators in deep tillage, i.e., tillage at depths greater than 200 mm. Consequently, field experiments were done to evaluate the performance of the experimental rotavator described in Chapter 4 in the 200 mm – 500 mm tillage depth

range. The performance factors measured were the torque requirements and the resultant horizontal force generated for the following rotavator operational conditions:

- Effect of depth at a constant kinematic parameter, λ, on the torque requirements and the resultant horizontal force generated
- Effect of bite length, i.e., different values of the kinematic parameter, λ, on torque requirements and the resultant horizontal force generated.

6.4.1 Effect of set tillage depth at constant kinematic parameter, λ

Figure 6.6 shows the variation in torque requirements curves for single cutting blades at tillage depths of 250 mm, 300mm and 450 mm. These curves indicate that rotavator torque requirements increase with the tillage depth. In terms of the rates of increase, it is apparent from the curves that torque requirements increase at a rate higher than the rate of increments in depth. A number of previous researchers (Hendrick & Gill, 1971a; Shibusawa, 1993; Manian & Kathirvel, 2001) made similar observations for rotavators operated within the 'normal' set tillage depth range, i.e., set tillage depths not exceeding 250 mm.

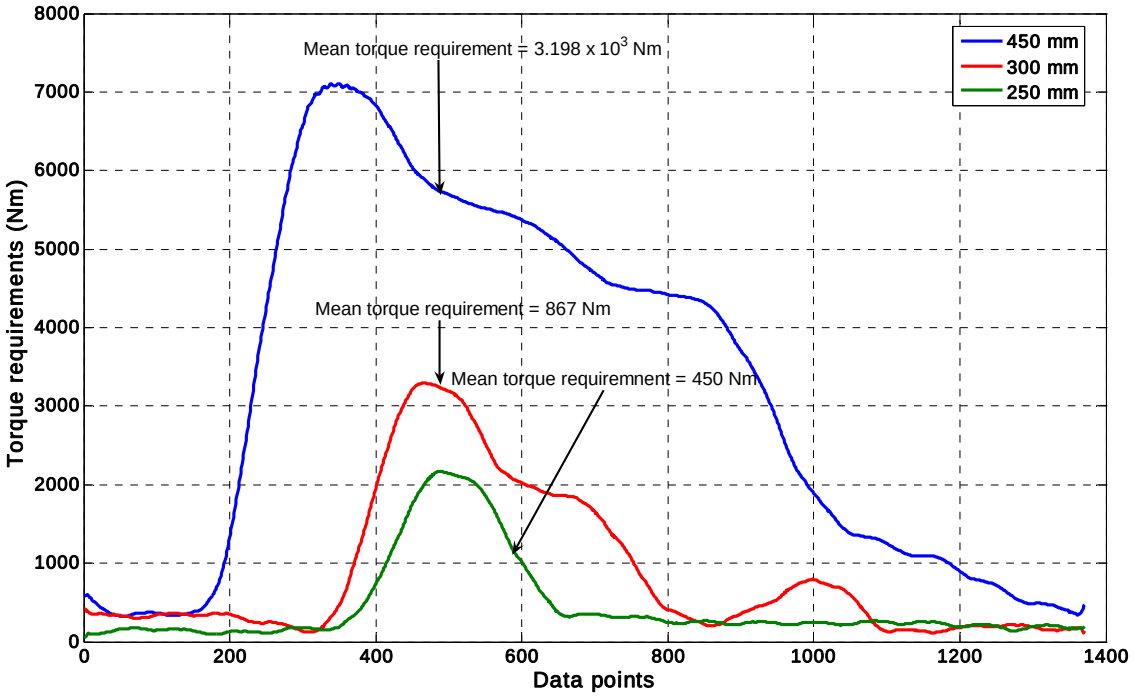

Figure 6.6: A graph showing the typical effect of depth on torque requirements for a down-cut tillage test-run for a given soil condition and fixed kinematic parameter, λ

Table 6.4 is a summary of the percentage increments in depth and associated mean torque requirements for the single blade data presented in Figure 6.6. From this data, excessive torque requirements accompany relatively small increments in the depth of tillage. This observation is consistent to that made by other researchers (Hendrick & Gill, 1971a; Shibusawa, 1993); and is responsible for the lack of adoption of the rotavator as an alternative primary tillage tool (Marenya, du Plessis & Musonda, 2003).

The causes of this excessive energy consumption by rotavators in deep tillage are many and varied, but the reported studies did not attempt to address them. The objective of such studies focused on the comparison of energy demanded or consumed by different primary tillage tools under specified conditions. In this study, the causes of the excessive energy consumption by the deep-tilling experimental rotavator were addressed by an analysis of the theoretical equations and the rotary motion of the rotavator during tillage. In this regard, two physical factors are considered to be responsible for observations made regarding the effect of tillage depth on torque requirements. These two physical factors are the tilling route length and the volume of the soil processed by a rotavator blade for different set tillage depths.

Table 6.4: Comparison of the percentage increases in depth and mean torque requirements for a fixed rotavator configuration and operational conditions; and a fixed soil condition

Tillage depth		Torque requirements	
Depth, mm	% increase	Mean torque requirement, Nm	% increase
250	0	450	0
300	20	876	93
450	80	3198	611

Increasing the set tillage depth, resulted in increased tilling route length and increased volume of soil processed by a blade. The increase in torque requirement values with increasing depth is possibly caused by the increase in both the tilling route length and the volume of the soil chips cut by a blade. As the set tillage depth is increased, both the tilling route length and the volume of the cut soil chips increased at constant kinematic parameter, λ.

The increase in the volume of cut soil slice is caused by the increase in depth (Equation 3.33) since the width of the blade (w) and the bite length (L_b) are fixed at a given level of the kinematic parameter, λ. Increasing the depth of tillage also decreases the angle (α_i), from the horizontal position, at which the blades starts cutting the soil, while increasing the angle at which the soil cutting stops (α_e). This results in increased length of cut (the tilling route length) as given by Equation (3.40). For the results presented in Figure 6.6, the increase in the tilling route length is reflected in the form of the increasing range of data points over which the values of torque is substantially greater than zero for different depths of tillage.

6.4.2 Effect of the bite length

The different bite lengths, L_b, were calculated using Equation (3.8) with three and six blades on the same side of the flange for two forward travel gears. The two forward travel gears resulted in two different forward speeds, V_f. Since the rotavator rotational speed was fixed, the combination of the two forward travel speeds and the two sets of the number of blades on one side of the flange, resulted in four different values of the kinematic parameter, and hence four different bite lengths. The forward travel speeds and the rotational speed used to calculated the different bite length using Equation (3.8) were presented in §5.2.2 The calculated bite lengths for the four different values of the kinematic parameter λ, are given in Table 6.5.

Table 6.5: Calculated bite lengths for different number of blades on the flange, z and the forward travel speeds, V_f

Combination of number of blades and forward travel speed	Bite length, m
1. Forward travel on gear I and 3 blades on the flange	0.323
2. Forward travel on gear I and 6 blades on the flange	0.162
3. Forward travel on gear II and 3 blades on the flange	0.392
4. Forward travel on gear II and 6 blades on the flange	0.196

The field experiments for investigating the effect of the bite length were done as outlined in §5.3.2. Figure 6.7 shows the variation of torque requirements for bite lengths of 0.323 m and 0.162 m (Table 6.5), respectively, with the rotavator traveling at a

forward speed of 0.425 m/s (§5.2.2) ,and processing the soil at a set tillage depth of 250 mm. The comparison of the mean torque requirement values for the two bite lengths at the tillage depth of 250 mm indicate increasing the bite length by 0.162 m, resulted in more than 100 % increase in the mean torque requirement value for the experimental rotavator.

The observed effect of changing bite length on the torque requirement can be explained by Equation (3.20) and Equation (3.33), since they relate the area of the cross-section and volume, respectively, of the soil slice cut by a blade to the bite length. From these expressions, changing the bite length by either reducing the number of the blades on the flange, or increasing the forward travel speed, while holding the rotor rotational speed constant results in increased cross-section area and volume of the soil slice processed by a blade. The increase in cross-sectional area and greater volume of the processed soil translates to greater torque requirements and longer time durations during which a blade processes the soil.

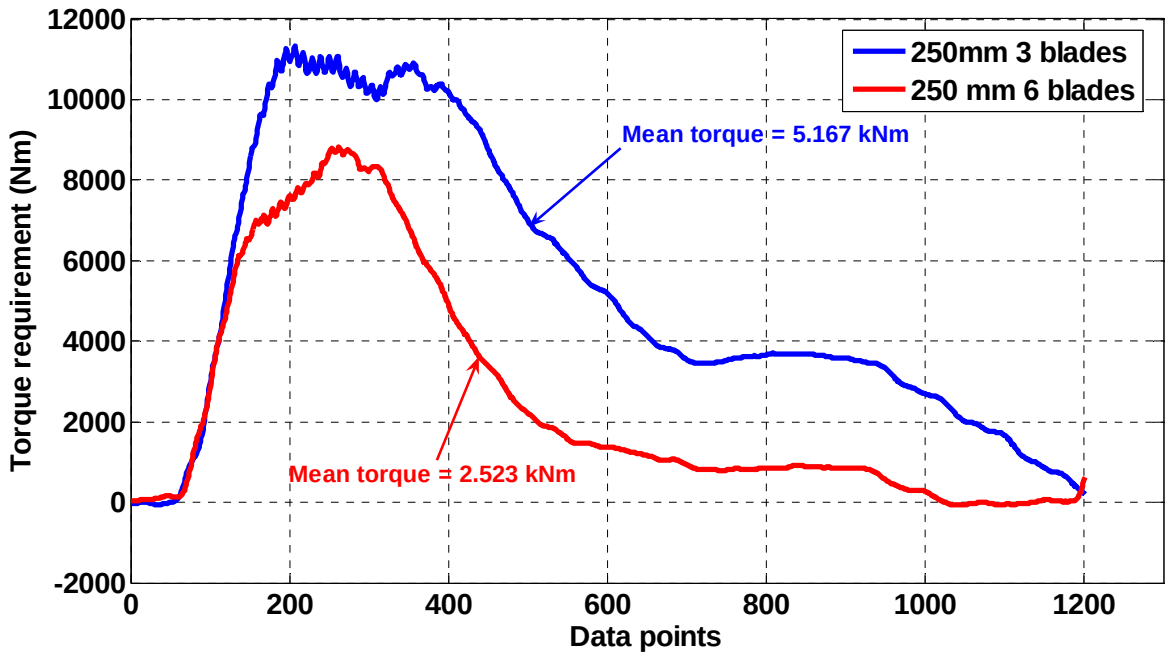

Figure 6.7: Effect of bite length on torque requirements

The sensitivity of torque to changing bite length, necessitates for a tighter control of this parameter in rotavator tillage. Since under practical conditions, the number of blades on

a flange, depth of tillage and the rotational speed of the rotor can be held constant, the only possibility of changing the bite length during rotavator tillage is by operating at a varying forward travel speed. Lack of operating at the desired constant forward travel speed also results in tilth quality changes. This is because changes in forward travel speed results in changes in the resulting clod size and its distribution. Consequently, it is crucial that rotavator prime-movers are operated at a uniform forward travel speed in order to control both the torque requirement and the resultant tilth quality.

6.4.3 The generated resultant horizontal force

The magnitude of the thrust or pull forces generated is important in analyzing the overall power requirements and performance in rotavator tillage operations. This is because the resultant horizontal thrust force generated may assists in the traction of the prime mover. In the literature reviewed there was no information on the variation of the resultant horizontal forces generated for different rotavator configurations and tiller operational conditions. In addition, the literature reviewed revealed that studies on rotavator tillage has been limited to a tillage depth of 300 mm or less. This section, therefore, presents and analyzes the data on the thrust forces generated by the experimental rotavator in the 200 mm – 500 mm depth range i.e., deep tillage.

Figure 6.8 shows the variation of the magnitude of the resultant thrust forces generated for different bite lengths and different set rotavator tillage depths, for field experiments conducted on the same date. The purpose of conducting these experiments on the same date was to ensure that all the tests, for analyzing the resultant generated thrust, were done at approximately the same soil condition; which in this study was defined by the soil water content. The soil water content affects the soil dynamic and strength parameters (Marenya & du Plessis, 2006).

In Figure 6.8, the resultant horizontal thrust force generated for each combination of forward travel gear and number of blades on the rotor, increased with depth to a maximum value, and thereafter decreased with increasing set tillage depth. The depth at which the maximum generated horizontal thrust force occurred, is dependent on

combination of the number of blades on the rotor and the forward travel speed, determined by the forward travel gear. The combination of these two parameters determines the bite length; and therefore, bite length has significant influence on the resultant thrust forces generated. Increasing the bite length, resulted in a decrease in depth, at which the maximum resulted horizontal thrust forces generated occurred.

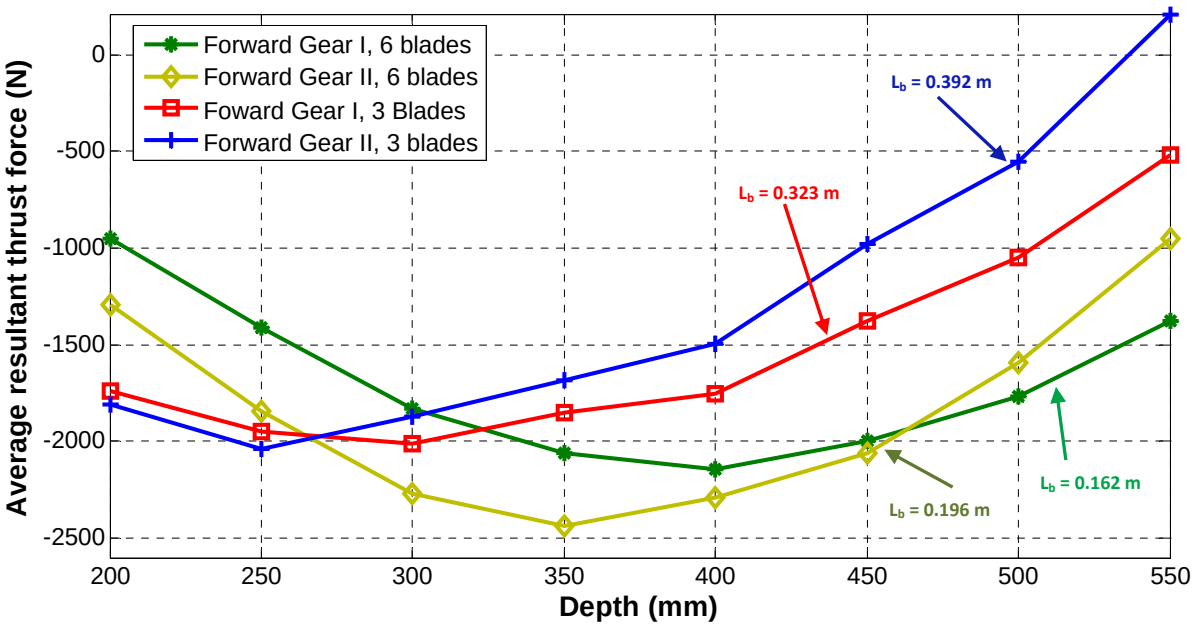

Figure 6.8: Variation of the resultant horizontal thrust forces generated at different tillage depths and different bite lengths at a constant soil condition (soil water content of 13.97 %)

The decrease in the magnitude of the maximum horizontal thrust force generated show that for the experimental blade used in this study, there exist a bite length at which increasing the set tillage depth will be accompanied by a decrease in the magnitude of the resultant horizontal thrust force. The respective curves (Figure 6.8) for the different rotavator operational parameter combinations indicate that there exists a set tillage depth at which the generation of the forward thrust force ceases. The results further indicate that as the set tillage depth increased, the magnitude of the resultant horizontal thrust generated decreased, and that operating the rotavator at increasingly deeper set tillage depths, may result in the exertion of a draft force instead. For example, operating the experimental operation on forward travel gear I with three blades on the same side

of the flange at a set tillage depth of 550 mm, resulted in a draft force being exerted, on the prime-mover by the rotavator. A similarly shaped curve was obtained by Hendrik (1980) for draft power in a study of a powered rotary chisel for the downward direction.

6.4.4 Analysis of torque and power requirements

The reviewed literature (Chapter 2) indicated lack of information on torque and power requirements of rotavators at set tillage depths greater than 250 mm. Accordingly, one of the objectives of this study was to characterize the torque and power requirements of rotavators at set tillage depths in excess of 250 mm. This section reports the findings of the measured experimental results, undertaken with the experimental rotavator described in Chapter 4. Both the rotary and the linear power requirements, which constitute the total rotavator power requirements were calculated for a given soil condition and different rotavator configurations and operational parameters.

The rotary power requirement at a given depth and level of the kinematic parameter, λ was calculated using Equating (6.1).

$$P_{sp} = T\omega \qquad \text{... (6.3)}$$

where:

P_{sp} = average power requirement for processing the soil (kW)

T = average torque requirement (kNm)

ω = average angular velocity (rad/s)

The power due to the resultant horizontal force was also determined for each field test using the standard force-velocity relationship (Srivastava, *et al.*, 1993; Goering, 1992). The volumes of soil slices cut by individual blades for different rotavator operational conditions tested in this study are presented in Table 6.6. The calculation of the soil slice volumes was done using Equation 3.35 (see §3.2.6), which approximates the actual volume of the soil slice volumes cut by individual rotavator blades. As expected, tillage depth had a direct and significant influence on the volume of soil processed for constant kinematic parameter levels.

Table 6.6: Theoretical actual soil chip volumes processed by the experimental rotavator for different experimental setups

Tillage depth (mm)	Soil volume processed (m^3)			
	$\lambda_I = 6.026$		$\lambda_{II} = 4.944$	
	6 blades	*3 blades*	*6 blades*	*3 blades*
250	0.0032	0.0065	0.0039	0.0078
300	0.0039	0.0078	0.0047	0.0094
350	0.0045	0.0091	0.0055	0.0109
400	0.0052	0.0103	0.0062	0.0125
450	0.0058	0.0116	0.0070	0.0140
500	0.0065	0.0129	0.0078	0.0156
550	0.0071	0.0142	0.0086	0.0172

Table 6.7 presents a summary of the results obtained for using the approach highlighted above. The calculated parameters for analyzing the performance of the experimental deep-tilling rotavator included the average linear power generated by the resultant horizontal thrust force, the rotary power required for processing the soil slice, and the specific energy requirements at different depths for different tests. In order to provide a basis for comparing the specific energy requirements of this tool with other tillage tools, its specific energy requirements were determined. Specific energy requirements is a standard approach for comparing the energy performance of tillage tools (Gill & Van den Berg, 1967). In this study, the specific energy requirements were expressed in terms of the energy units per volume of the soil processed.

The power performance of the experimental tiller was determined by calculating the rotary and linear power requirements (see §3.4). The specific rotary tillage energy was calculated from the rotary power by determining the energy required for 10 complete revolutions for different conditions and then dividing this by the total volume of the soil processed. The total volume was obtained as the product of the number of blades on the flange and the respective theoretical volumes presented in Table 6.6 for a particular set tillage depth, multiplied by the number of complete revolutions.

The results presented in Table 6.7 indicate that increasing both the set tillage depth and bite length, influences the rotary power requirements and the specific energy. In general, change in bite length has a greater influence on power requirements and specific energy than the change in set tillage depth. These findings are consistent with

those of previous researchers (Salokke & Ramalingam, 2001; Balock *et al.*, 1986; Bukhari *et al.*, 1996; Shibusawa, 1993) for relatively shallow tilling rotavators. A comprehensive review on literature, particularly from the then USSR by Hendrick and Gill (1971b) also revealed that both the set depth of tillage and the bite length affects the power requirements and the specific energy.

Table 6.7: Summary of average thrust, torque, power requirements, and specific energy requirements for down-cut deep rotary tillage test-runs (soil water content of 13.97 %)

Rotavator configuration (Travel gear and number of blades on the flange)	Depth (mm)	Thrust (N)	Torque (Nm)	Power requirements (kW)		Specific energy (kJm^{-3})
				Linear	Rotary	
1. Forward gear I with six (6) blade on the flange	200	- 936	360	- 0.398	0.991	105.554
	250	- 1409	401	- 0.599	1.104	117.734
	300	- 1807	581	- 0.768	1.600	107.604
	350	- 2092	632	- 0.889	1.741	135.117
	400	- 2100	870	- 0.892	2.396	127.192
	450	- 2020	941	- 0.856	2.591	156.978
	500	- 1798	1130	- 0.764	3.112	151.504
	550	- 1415	1318	- 0.601	3.629	166.559
2. Forward gear II with six (6) blades on the flange	200	- 1295	604	- 0.667	1.663	187.109
	250	- 1945	712	- 1.002	1.960	191.057
	300	- 2497	975	- 1.286	2.685	217.097
	350	- 2890	1062	- 1.488	2.924	202.073
	400	- 2905	1462	- 1.496	4.026	246.776
	450	- 2783	1581	- 1.433	4.360	236.663
	500	- 2478	1902	- 1.276	5.235	255.056
	550	- 1947	2211	- 1.003	6.083	268.810
3. Forward gear I with three (3) blades on the flange	200	- 1736	960	- 0.738	2.643	327.657
	250	- 1946	1059	- 0.827	2.999	350.664
	300	- 2010	1512	- 0.854	4.164	405.728
	350	- 1851	1685	- 0.786	4.640	387.557
	400	- 1750	2409	- 0.743	6.634	489.528
	450	- 1379	2509	- 0.586	6.909	452.710
	500	- 1050	3031	- 0.446	8.297	488.863
	550	- 517	3552	- 0.220	9.782	523.555
4. Forward gear II with three (3) blades on the flange	200	-1805	1598	- 0.930	4.397	615.145
	250	-2040	1820	- 1.051	5.008	642.133
	300	-1870	2555	- 0.963	7.031	717.486
	350	-1686	2778	- 0.868	7.645	707.381
	400	-1495	3998	- 0.769	11.002	880.200
	450	-979	4212	- 0.504	11.591	827.959
	500	-549	5063	- 0.283	13.933	893.165
	550	210*	6036	0.108	16.611	965.760

* - For this setting, a draft force is exerted on Tractor 2

The greater influence of changes in bite length on the specific energy is attributed to changes in several factors that lead to the increase in volume of the cut soil slices. Changes in bite length have significant effects on the tilling route length, the maximum soil chip thickness, and the absolute velocity of the rotor blade tip. All these three factors individually affect the torque requirement and therefore any changes in bite length, in combination with any of them, would significantly impact the rotavator torque and power requirements. From Table 6.6, change in volume of the worked soil, owing to increase in depth, is relatively small in comparison to the change in the worked volume due to bite length changes. Hence change in torque and power requirements owing to changes in depth, in general are lower than changes due to an equivalent change in bite length.

The foregoing analysis indicate that changing bite length affects a number of factors with a combined effect of greater torque and power requirements when compared to changes in depth for a fixed level of the kinematic parameter, λ. Thus, it is important that the kinematic parameter is maintained constant after the set tillage depth at which the rotavator is to be operated at, has been decided. As is evident from the presented results, any change in the kinematic parameters would result in increased torque and power requirement of rotavators. However, the findings indicated that minor changes in depth, for example due to unevenness of the ground surface can be tolerated well in rotavator tillage. It is therefore vital that the ratio of the forward travel speed to the rotational speed, which determines λ, is maintained constant throughout a rotavator tillage operation.

6.5 Model verification and validation

The proposed analytical model (Chapter 3) is validated by comparing the measured and calculated (model generated) torque requirements. Owing to the complexity of the calculations required to calculate a single torque requirement value at a specified rotavator blade position from the horizontal (α = 0°, Fig. 3.11), a computer program based on the developed mathematical expressions (§3.4) was coded in MATLAB

(*Mathworks Inc., USA*) to solve the model. The steps used in this process and the resulting outputs obtained are presented in the subsequent subsections.

6.5.1 Model inputs

The model inputs required to calculate the torque requirements were identified in §3.4. They can be categorized into two types, namely 'constant' and 'varying' inputs. The constant model inputs remain unchanged, whereas the varying inputs change with regard to the position of the blade from the horizontal position during the rotavator operations. The constant and varying model inputs were derived from both the soil and rotavator operational parameters.

The constant model inputs that are dependent on the soil type and condition were further categorized as soil or rotavator input.

- Inputs that are dependent on the soil condition, i.e., the soil water content. These include the soil strength parameters of cohesion, internal angle of friction, soil/metal adhesion, soil and metal friction angle, soil bulk density, and the calculated dimensionless N-factors, i.e. $N_c^{'}$ and $N_q^{'}$. The N-factors were determined using the graphical approach (Godwin & Spoor, 1977). Variation of these factors with the internal angle of friction is presented in Figure 6.9.

- Input variables obtained by measurement of different rotavator dimensions or predetermined levels, and remain constant throughout a rotary tillage process. These include input variables such as the set tillage depth and pertinent rotavator dimensions including the rotavator radius, blade cutting width, and blade thickness.

- Rotavator operational inputs that remain unchanged during rotary tillage operations. These include the set depth of tillage, the forward travel and the rotor rotational speeds, the bite length, blade thickness, the number of blades on the rotavator flange, and the kinematic parameter, λ.

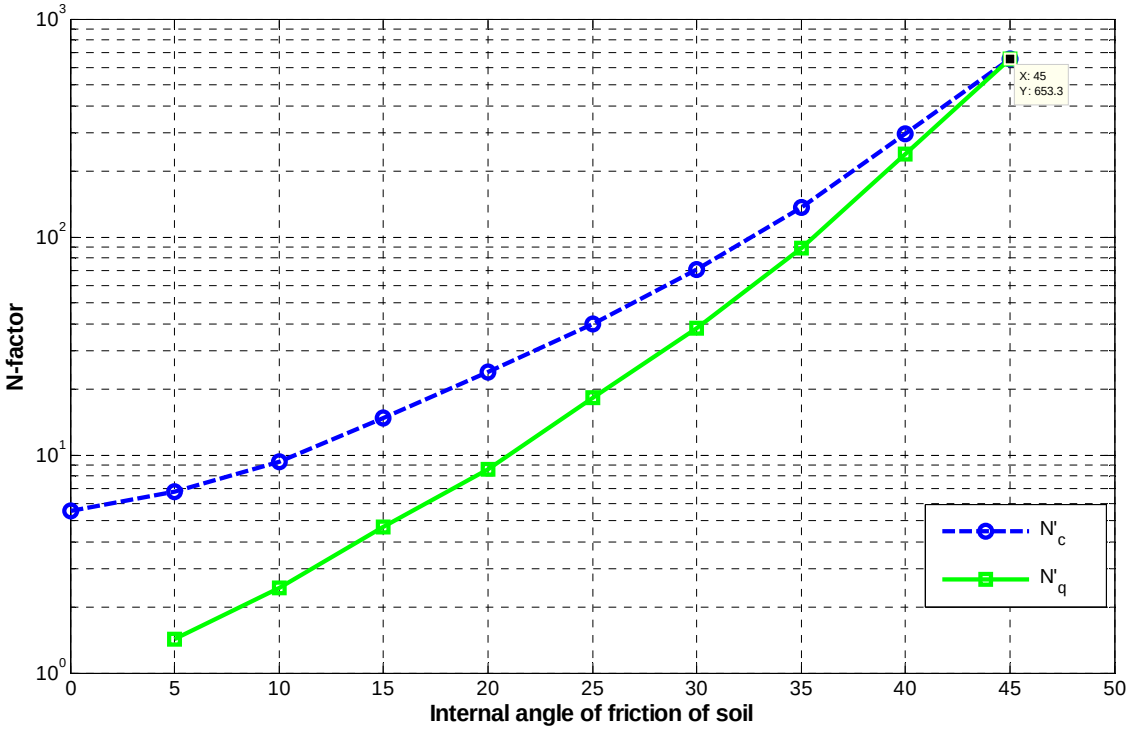

Figure 6.9: Graph used for the determination of dimensionless N-factors for lateral soil failure (Godwin & Spoor, 1977).

Table 6.8 gives the constant model input variables; their notations and numerical values assigned to the respective variables. Owing to the sensitivity of the soil related inputs to the soil water content, all the 'constant' model input variables affecting the soil's strength and dynamic parameters were determine at an overall average soil water content level of 13.97 %, for the 200 – 550 mm tillage depth range. The 13.97 % was the average soil water content, at the experimental site, at which the field experiments for assessing the performance of the experimental deep-tilling rotavator were undertaken.

The varying model inputs arise from the varying portions of the blade that interact with the soil between the angle of blade entry and exit during rotavator tillage (Figure 3.10). This soil-blade interaction results in the change of the values of the rake angle (β) and the rupture angle (ρ) as shown in Figure 3.15 and Figure 3.16 in §3.4.2. These two angles vary with the position of the rotavator blade from the horizontal position (Figure 3.11) during the soil cutting process. At any position from the horizontal, the blade rake angle for the span of the L-shaped blade was given by Equation 6.4.

$$\beta = 2\pi - \left(\alpha + \frac{\pi}{2}\right) \tag{6.4}$$

Table 6.8: Listing of the model input variables and their assigned values

Description of the model input variable	Notation	Value(s)
Soil dynamics and strength parameters:		
Angle of internal soil friction (°)	ϕ	38.86
Soil cohesion (kN/m²)	C_c	15.8
Soil-metal friction angle (°)	δ	32.06
Soil-metal adhesion (kN/m²)	C_a	7.93
Set depths of tillage (m)	d	0.250, 0.350, 0.500
Soil bulk density (kN/m³)	γ	17.200
Rotavator parameters		
Rotor radius (m)	R	0.93
Width of blade (m)	w	0.130
Leg length of the blade (m)	L	0.100
Thickness of the blade (m)	t	0.007
Forward travel speed (m/s)	V_f	0.425, 0.515
Rotor speed (rad/s)	ω	2.754
Number of blades on flange	z	3 or 6
Bite length (m)*	L_b	0.323, 0.162; 0.392, 0.196
Kinematic parameter (dimensionless)	λ	6.026, 4.944
Calculated N-factor soil strength parameters:		
Cohesion N-factor (dimensionless)	$N_c^{'}$	257.52
Surcharge N-factor (dimensionless)	$N_q^{'}$	203.94

* Bite length was calculated using Equation (3.8) as explained in §5.3.2.

After determining the rake angle, the rupture angle (ρ) was calculated using the approach of Perumpral *et al*. (1983). These two angles were calculated and utilized by the computer program internally, in the computation of the total resultant force P_s (Equation 3.57). With the model inputs determined and the computer program developed, the next step was to verify the proposed model.

6.5.2 Model and computer program verification

The computer program developed for solving the proposed analytical model performed all the required computations, and produced several outputs using, the values assigned to the inputs (Table 6.8) and the derived mathematical expressions (Chapter 3). The outputs from the program are also used as a means of verifying that both the program itself and the analytical model are producing the expected outputs. Selected program outputs required to build confidence in its computational process and assess the suitability of the derived mathematical expressions are discussed in this section.

One of the important outputs of the program is the trochoidal path followed by the tip of the rotavator blade during field operations (Figure 6.10). The graph plots the (*x, y*) coordinates of the tip of the blade from the horizontal position at predetermined time intervals. The inputs required to generate the coordinates of the tip of the blade at different angular blades are the rotor radius, the rotational and the forward travel speeds. The ability of the program to trace the path followed by the tip of the blade for different set tillage depths is important because it serves as the basis for the other computations required to predict the torque requirements at different blade positions. The graphical output also included additional important data required in the calculation of the torque requirements. The additional outputs included the following:

- A - The position of the centre of the rotor when the cutting edge of the blade comes into contact with the ground surface.
- B - The point at which the cutting edge of the blade comes into contact with the ground surface, i.e α_i. The set depth of tillage is then the difference between the y-coordinate at this point and the y-coordinate of the lowest point on the cutting path. In the case shown in Figure 6.10, the y-coordinate at point B is -580 m, which correspond to the set depth of tillage of 350 mm. By simultaneously taking the (*x, y*) coordinates at points A and B, respectively, the program computes the angle at which the tip of span part of the blade comes into contact with the ground surface.

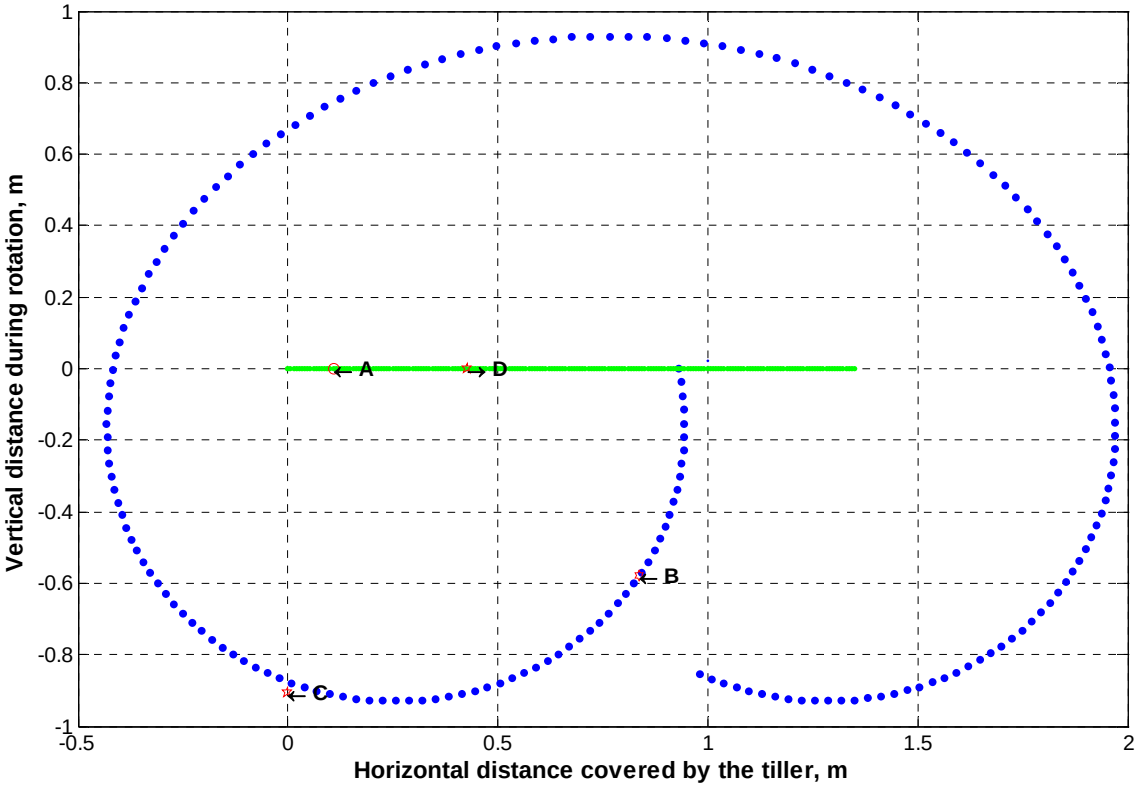

Figure 6.10: A typical graphical output of the path followed by tip of the span of the blade produced by the computer program for a set tillage depth

- C – This is the point at which the cutting edge of the blade stops cutting the soil. It is the point that forms the crest (Figure 3.4). By taking the coordinates of this point and those of point D, which is the position of the centre of the rotor at the end of the soil processing by the blade, the program calculates the angle α_e, the angle at which blade stops processing the soil. With these two angles, i.e., α_i and α_e, the tilling route length is determined for the set depth of tillage.

- The other important parameter determined using the pairs of *(x, y)* coordinates is the instantaneous length of the blade in contact with the soil. This calculation is necessary because the length of the blade in contact with the soil at different time moments, which varies instantaneously for a given set depth of tillage, is the basis for the computation of the total instantaneous soil-tool interaction forces P_s (Figure 3.15, p70). This force is then used to calculate the torque

requirements for single blades at predetermined positions of the rotor between the angle of entry (α_i) and exit (α_e). The weight of the soil supported by the span of the blade depends on the length of the blade in contact with the soil.

- The final program output is a tabulation of the angle, α and the torque requirements at different positions of the tip of the blade during the soil cutting process. The program also generated a graphical output of these two parameters for different set depths of tillage and rotavator operational parameters. Figure 6.11 is a typical graphical output for the torque requirements for a single rotavator blade at different angular rotor positions from the horizontal during the soil cutting process for a 350 mm set tillage depth.

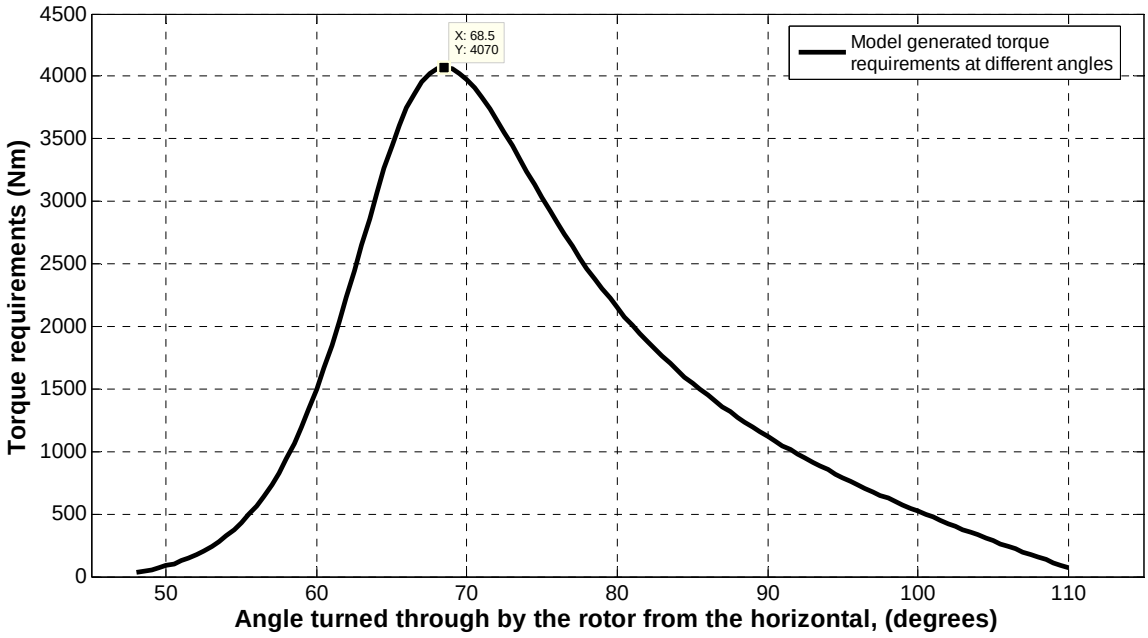

Figure 6.11 Model generated torque requirement values at different angular positions of the tip of the blade during soil processing at set tillage depth of 350 mm.

From Figure 6.11, it is evident that the shape of the graphical output of the model generated torque requirements at different angular rotor positions, closely resembles, Figure 6.4. The choice of set tillage depth of 350 mm for the verification of the model was based on the fact that Figure 6.4 was used for analyzing the measured torque requirement. Therefore, it allows for the visual comparisons and the general verification of the proposed model. Like is the case of the measured (experimental) torque

requirements, the model graphical output shows that immediately after the commencement of the soil processing, there is a steep increase in torque requirements, before a peak value is reached after about 20 degrees. This is followed by a decrease in torque requirements at a decreasing rate until up to the point where the soil processing by a blade stops.

The model was tested with different set tillage depths and bites but similar soil conditions; and in all cases a similar shape (Figure 6.11) was obtained for all the conditions. This is different for the measured torque requirements data for single blades which showed differences, particularly after the peak torque requirements values had been reached. The measured torque requirements curve, after the peak value had been reached, was not as smooth as that of Figure 6.11. There appeared to be some increase or in some cases the torque requirements values being constant with increasing angular position towards the end of the soil cutting process by a blade (Figure 6.4).

6.5.3 Model validation and evaluation

The proposed model is validated by comparing the model generated and measured (field experiments) torque requirement values as explained in §5.4.2. The validation and evaluation of the model is done for selected set tillage depths of 250 mm, 350 mm and 500 mm at a constant average soil water content of 13.97 %. In addition to the statistical analysis techniques described in §5.4.2, visual comparisons of the measured and model generated torque requirements is also used to assess the degree of agreement between the two sets of data.

The visual comparison is used to compare the variation of both the measured and model generated (predicted) torque requirement values, at different angular rotavator blade positions during the soil cutting process. This was done by plotting the model generated and measured torque requirements on the same axes at specified angular rotavator blade positions, for a given set tillage depth. The selected set tillage depths used for these comparisons are 250 mm, 350 mm and 500 mm, respectively. The measured torque requirements used for the visual comparison are averages of soil processing by an individual blade at five different positions along the cut furrow.

6.5.3.1 Measured and predicted torque at 250 mm set tillage depth

Figure 6.12 is a combined graph showing the measured and model generated torque requirement values for 250 mm set tillage depth at different angular rotavator blade positions during the soil cutting process. Visual comparison between the measured and predicted torque requirements (Figure 6.12) indicated that in general the predicted torque requirements are greater than the corresponding measured torque values.

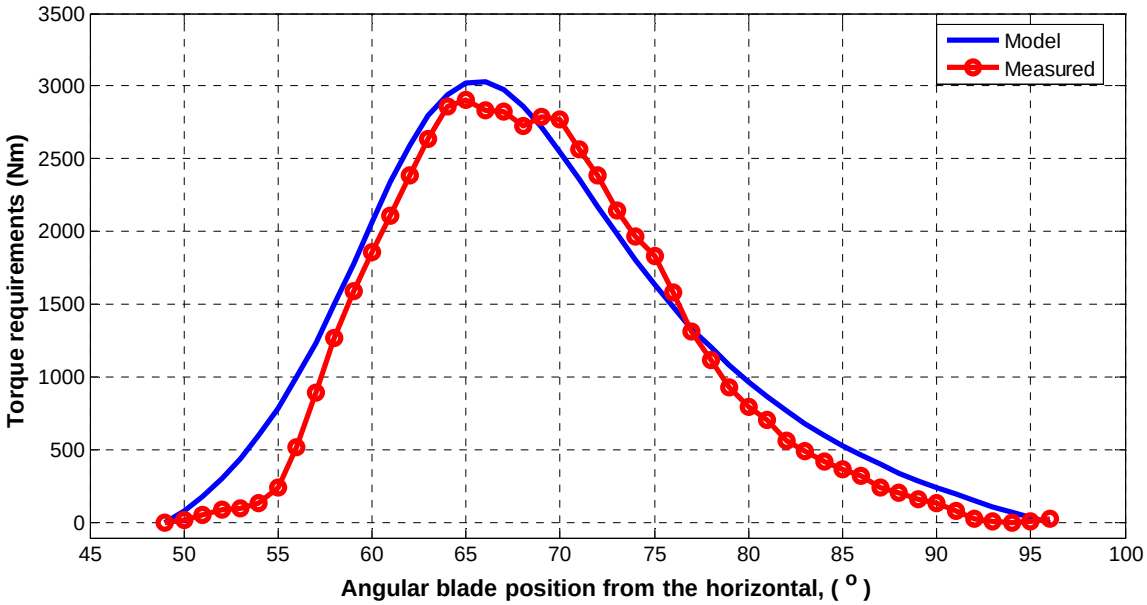

Figure 6.12: Comparison of predicted and measured torque requirement at 250 mm set tillage depth

Two statistical tests, namely, the least squares regression analysis and the paired t-test was effected on the model and torque generated data to evaluate the agreement between the two sets of data (see §5.4.2). The results obtained for this set tillage depth are presented in Figure 6.13, and Tables 6.10 and 6.11. From the paired t-test, the mean generated and measured torque values are 1.269 kNm and 1.15 kNm, respectively. The respective standard deviations are 1.007 kNm and 1.063 kNm. The large standard deviation values returned for both the predicted and the corresponding measured torque requirements is due to the large variations in torque requirements between the initiation and end of the soil cutting process by a rotavator blade.

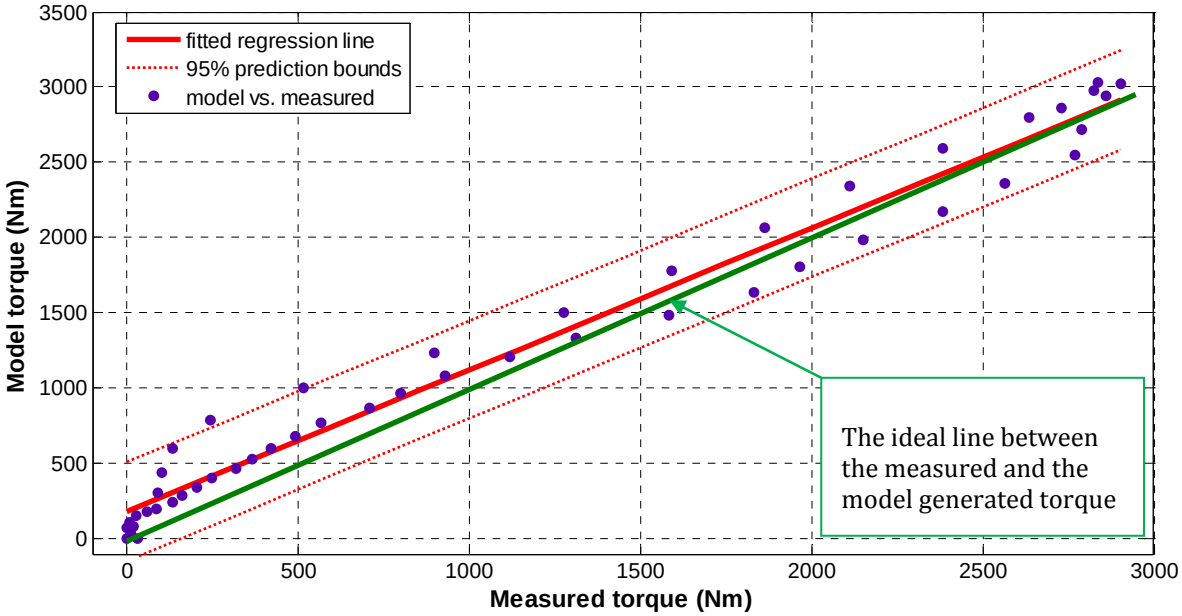

Figure 6.13: Results of the least squares linear regression of the model and measured torque requirements at different angular blade positions for 250 mm set tillage depth

The statistical analyses performed (Tables 6.10 and 6.11) on the two sets of torque requirements indicated that the difference between the measured and predicted torque requirements for this set tillage depth is statistically significant ($p < 0.05$). This result implies that the model and measured torque requirements at the same angular rotavator blade positions, for this set tillage depth, are different at the 0.05 level of significance. This finding confirms the wide disparities that are evident from Figure 6.12 at different angular rotor positions.

The results of the least square regression analysis for predicted and measured torque requirements for the set tillage depth of 250 mm are presented in Figure 6.13 and Table 6.11. If there was no discrepancy between the measured and the predicted torque requirements, all the point would lie on a straight line with a slope of one (1), and pass through the origin, i.e., a zero (0) vertical intercept. In Figure 6.13, the fitted regression line between the measured and predicted torque requirements has a slope of 0.936 and an intercept of 0.192 with an R^2 value of 97.5 %. The tabulated linear regression analysis results are given in Table 6.11, and indicate that both the slope and the vertical intercept are significantly different from one and zero, respectively ($p < 0.05$). These results

indicate that at the significance level of $\alpha = 0.05$, the measured and the model generated torque requirements for this set tillage depth are significantly different.

Table 6.10: Paired *t*-test results for torque requirement for the 250 mm set tillage depth

	N	*Mean (kNm)*	*SD**	*SE Mean***
Model torque, kNm	47	1.269	1.007	0.147
Measured torque, kNm	47	1.150	1.063	0.155
Difference	47	0.1183	0.1699	0.0248
95 % CI for mean (0.0684, 0.1681)				
T-Test for mean difference = 0 (vs not = 0): T-value = 4.77, p-value = 0.000				

T_{mod} = model generated or predicted torque requirements; T_{meas} = measured torque requirements;
*SD** - Standard deviation (kNm); *SE Mean*** - Standard error mean

Table 6.11: Results of the least squares regression of the model generated torque requirements on the measured torque for 250 mm set tillage depth

The least-squares regression equation is: $T_{mod}(kNm) = 0.192 + 0.936 \bullet T_{meas}(kNm)$

Predictor	*Coef*	*SE Coef*	*T*	*P*
Constant	0.19188	0.03402	5.64	0.000
Measured, kNm	0.93600	0.02183	42.88	0.000

S = 0.1574 R^2 = 97.6 % $R^2_{adj} = 97.6\%$

Analysis of Variance

Source	*df*	*SS*	*MS*	*F*	*P*
Regression	1	45.561	45.561	1838.93	0.000
Residual Error	45	1.115	0.25		
Total	46	46.676			

Unusual observations

Observation	T_{meas}, *kNm*	T_{mod}, *kNm*	*Fit*	*SE Fit*	*Residual*	*SE Residual*
7	0.25	0.788	0.4220	0.0303	0.3661	2.37R
8	0.52	1.0003	0.6753	0.0268	0.3250	2.10R

R denotes an observation with a large standardized residual

Coef – coefficient; **SS** – Sum of Squares; ***df*** – degree of freedom ***P*** – p-value, ***T*** – t-value

The foregoing findings of the least squares linear regression test is in agreement with the paired Student t-test results (Table 6.10), i.e., the model and measured torque requirement values for the set tillage depth of 250 mm are significantly different. The least square linear regression results (Table 6.11) indicate that observations 7 and 8 fall outside the 95 % confidence interval; and are, therefore outliers. According to Montgomery and Runger (2003) outliers can significantly influence the outcome of selected statistical tests. Probably the significant results obtained for the two test statistics reported for this set depth of tillage was partly due to the presence of outliers between the two sets of torque requirements data.

The conclusion that can be drawn from the analysis of the measured and predicted torque requirements data for the 250 mm set tillage depth is that the two sets of data are significantly different at the 0.05 level of significance. This is evident from both the visual comparisons and the two statistical analyses test effected on the two sets of data. The possible causes of these disparities are the unsteady interaction between the soil-tool at the commencement and toward the end of the soil cutting process and the variations in soil strength parameters owing to variation in the soil water content with depth.

6.5.3.2 Measured and predicted torque at 350 mm set tillage depth

Figure 6.14 is a combined graph showing the measured and model generated torque requirement values for 350 mm set tillage depth at different angular positions of the rotavator during the soil cutting process. Compared to the graph for the 250 mm set tillage depth, there is a better agreement between the measured and the predicted torque requirements for this set tillage depth. Since the field tests for verifying the model were done on the same day, and at almost the same time, the relatively better agreement between the measured and the predicted torque requirement results, for this set depth, compared to that for 250 mm set depth is attributed to a more uniform soil strength in the portion of the land tilled when the verifications test was done.

The variation in the soil strength at the experimental site at different locations was possible because the soil at the selected site was not conditioned. Conditioning the soil however, is not a guarantee for the uniformity in soil strength as this phenomenon was reported in tillage studies conducted in conditioned soil (Girma, 1989; Owende & Ward, 1996). Soil strength variations, even within the short distance such as the bite lengths encountered in rotary tillage, for set test conditions, are not unusual under field conditions, because the soil is not a homogeneous material.

The results of the statistical analysis done on the model generated and measured torque requirements at this set tillage depth, are presented in Tables 6.12 and 6.13, and Figure 6.15. The paired student's t-test statistic for the difference between the measured and predicted torque requirements for this set tillage depth indicate that there is no

statistical difference at $\alpha = 0.05$ significance level. This result confirms the closeness of the two predicted and measured torque requirement curves presented in Figure 6.14.

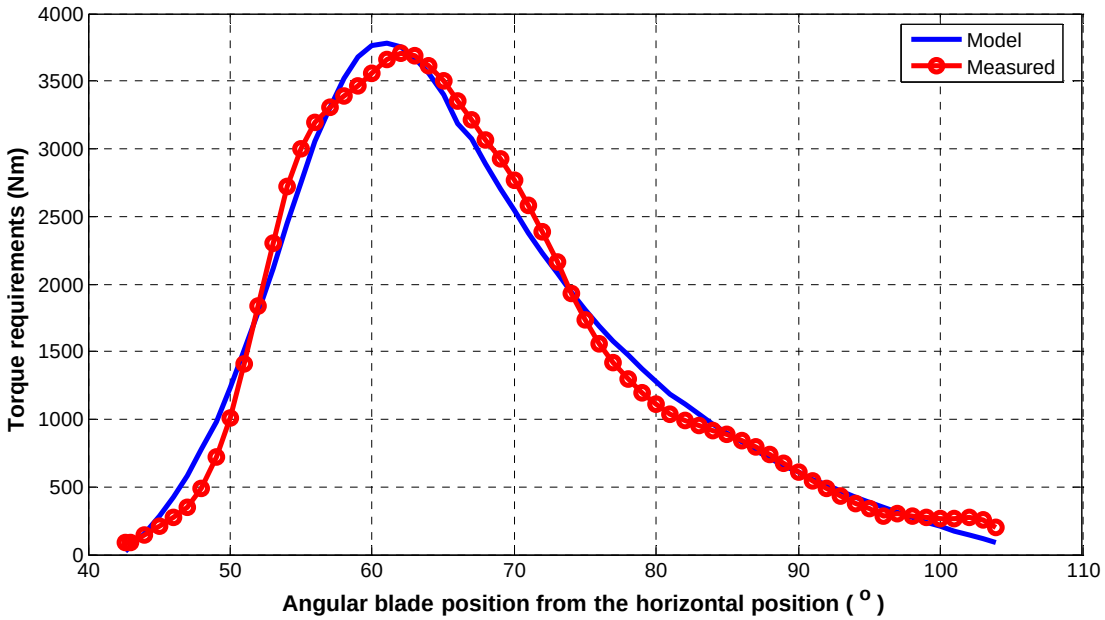

Figure 6.14: Comparison of the predicted and measured torque requirement at 350 mm set tillage depth

Table 6.12: Paired t-test results for torque requirement for the 350 mm set tillage depth

	N	*Mean (kNm)*	*SD**	*SE Mean*
Model torque, kNm	63	1.521	1.219	0.154
Measured torque, kNm	63	1.515	1.248	0.157
Difference	63	0.006	0.1353	0.017
95 % CI for mean (-0.0280, 0.0401)				
T-Test for mean difference = 0 (vs not = 0): T-value = 0.35, p-value = 0.725				

The least squares linear regression results (Table 6.13), however indicate that the slope between measured and predicted torque requirements are not a perfect replica of one another at the same angular positions. The values of the slope of 0.972 though close to 1, has a p-value = 0.00, which indicates that the measured and model generated torque requirements at the same, angular blade positions is statistically significant. The analysis of variance for the least squares regression also indicated that the measured and predicted torque requirements are significantly different for this tillage depth, as was the case for the 250 mm set tillage depth.

Table 6.13: Results of the least squares regression for the predicted versus the measured torque requirements for 350 mm set tillage depth

The least-squares regression equation is: $T_{\mathrm{mod}}(kNm) = 0.0488 + 0.972 \bullet T_{meas}(kNm)$

Predictor	*Coef*	*SE Coef*	*T*	*P*
Constant	0.0488	26.23	1.86	0.067
Measured, kNm	0.972	0.0134	72.48	0.000

S = 0.132 R^2 = 98.9 % $R^2_{adj} = 98.8\%$

Analysis of Variance

Source	*df*	*SS*	*MS*	*F*	*P*
Regression	1	91.46	91.146	5253.97	0.000
Residual Error	61	1.058	0.017		
Total	62	92.204			

Unusual observations

Observation	T_{meas}, *kNm*	T_{mod}, *kNm*	*Fit*	*SE Fit*	*Residual*	*SE Residual*
18	3.47	3.68	3.4184	0.0310	0.2616	2.04R

R denotes an observation with a large standardized residual

In Figure 6.15, minor disparities between the ideal line and the fitted regression line are noted at the low- and high-end torque requirement values. In the in the 500 – 2500 Nm torque requirements range, the fitted linear regression and the ideal line more or less coincide. The observed deviations between the ideal and the regression line indicated that the model under- and over- predicted the torque requirement values at the start and towards the end of the soil cutting process by a rotavator blade for the 350 mm set tillage depth.

Although the foregoing analyses indicate that the two sets of torque requirements data are significantly different, both the visual comparison and the results of the least square linear regression show that the deviations are minor. In general, the shapes (Figure 6.14) of the curves for the measured and predicted torque requirements, at different angular blade position, followed the same trend. The minor differences in these curves can be attributed to lack of uniformity in the soil strength parameters within the set tillage depth. The difference noted in the torque value at the commencement and towards the end of the soil cutting process; and which were the major causes of the disparities observed between the measured and predicted torque requirements for this set tillage depth, could be due to dynamic instability between the soil and the blade. At both ends

during the rotavator tillage, there is a continual change in the mass of the soil in contact with the blade. In conclusion, the model generated torque requirements for this depth are comparable to the measured values; save for the inevitable minor differences noted.

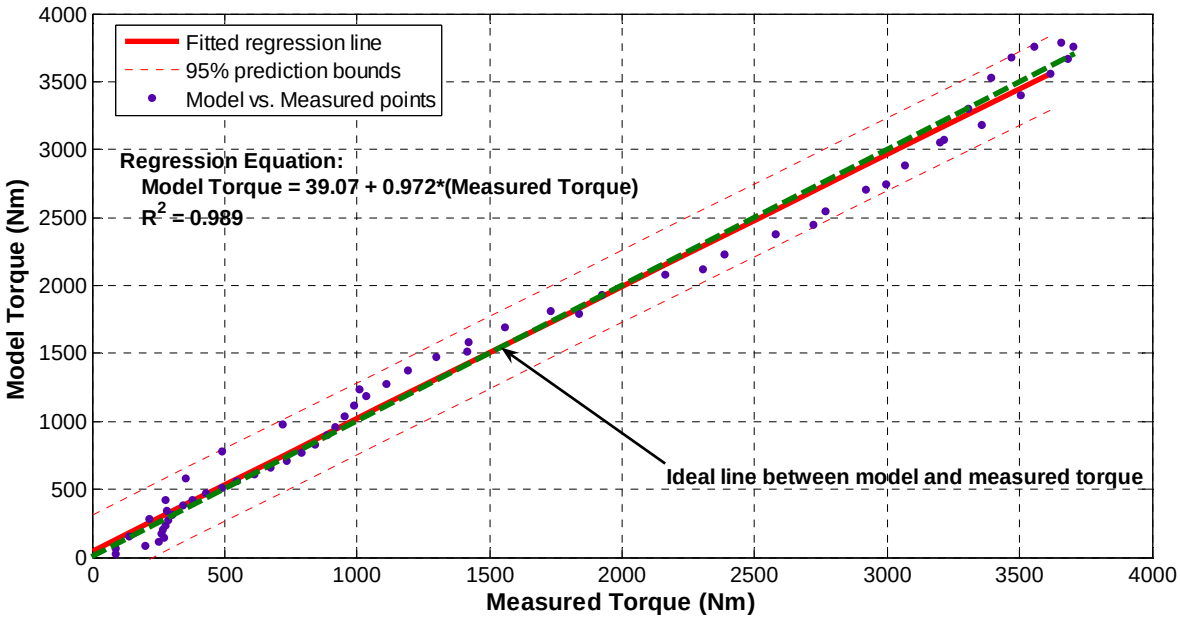

Figure 6.15: Results of the least squares linear regression of the model and measured torque requirements at different angular blade positions for 350 mm set tillage depth

6.5.3.3 Measured and predicted torque at 500 mm set tillage depth

Figure 6.16 shows the variation of the measured and model generated torque requirement curves for the 500 mm set tillage depth at different angular positions of the rotavator blade during the soil cutting process. Compared to similar graphs for the 250 mm and 350 mm set tillage depths, there appear to be greater disparities between the measured and model generated torque requirements, at this set tillage depth. In particular, the inconsistency between the predicted and the measured torque requirements are greatest at the blade angular positions in the 35^{o} – 50^{o} range, after the commencement of soil cutting. Within this angular position range, the measured torque requirements curve indicated a sudden drop in the torque requirements, followed by a sudden increase in torque requirements which persists until the peak value is reached.

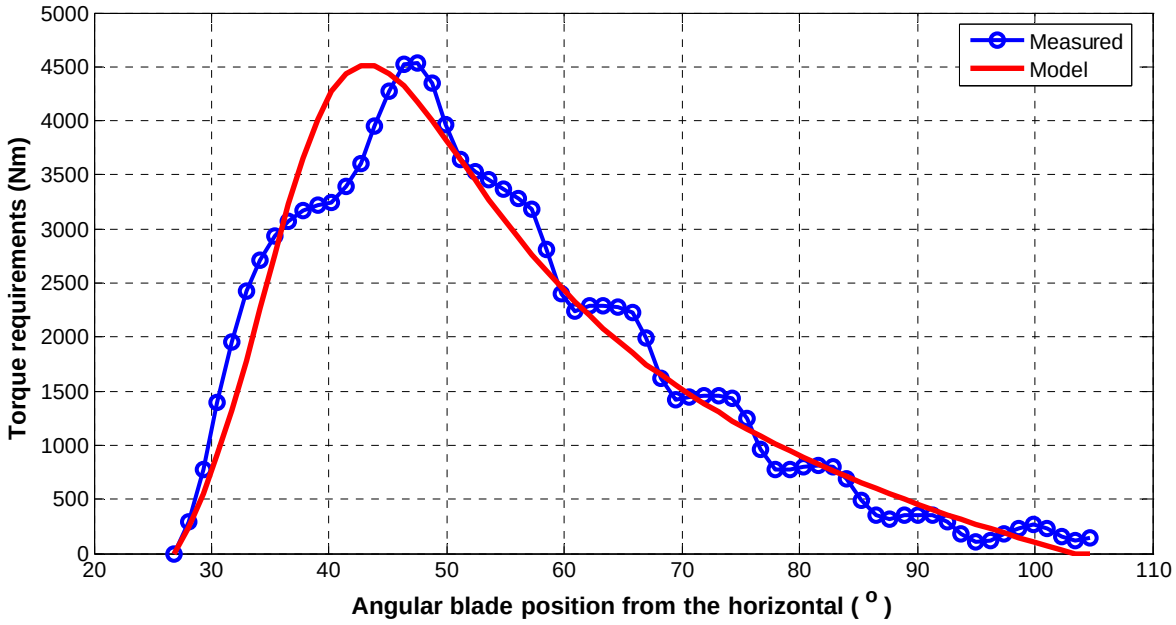

Figure 6.16: Comparison of the predicted and measured torque requirement at 500 mm set tillage depth

Given that measured data curve (Figure 6.16) is for an average cutting by the same blade at five different locations along the tilled path, this observation cannot be explained by the inconsistencies due to the soil strength. The possible explanation of the observation made could be the instability of the test equipment (tool-frame carrier onto which the rotavator was mounted) at set depths of tillage in excess of 450 mm. It was noted beyond this depth, the entire test equipment became unsteady and the degree of unsteadiness increased with further increase in depth.

After the peak torque requirement value has been reached, for this set tillage depth, an interesting observation in the form of vacillations in the measured torque requirement is apparent until the end of the soil cutting process by a blade. The nature of the observed vacillations is such that constant torque requirement levels are maintained at seemingly regular blade angular position intervals to the end of the soil cutting process. In some instances, relatively greater torque requirements, relative to previous angular blade positions, were observed. The maintenance of constant torque requirements or its increment with the increase in the blade angular position (blade advancement), after a peak torque requirement level has been registered reached, resulted in higher average

torque requirements values for this set tillage depth. Some of the possible causes of this behaviour are analyzed below, based on the findings by Shibusawa (1993).

In the said study by Shibusawa (1993) it was reported that deep rotavator tillage demanded excessive energy owing to the possibility of re-tilling of soil massed that fall back into the furrow. While this was not visually observable during the field experiments undertaken in this study, the observed vacillations in the measured torque requirements after the peak value has been reached (Figure 6.16) are an indication of an increase in resistance to cutting of the soil by a blade. From the kinematics of rotavators fitted with L-shaped blades (Chapter 3), as the blade moves through the soil, the cross-section of the soil slice initially increases to a maximum value and thereafter decreases until the end of the soil cutting process. Therefore, possible and logical explanation for observation made in Figure 6.16, could be due the falling-back of the already cut and thrown soil mass onto the blade cutting path. The effect of this would be the increase in the dynamic mass of the soil in contact with the blade, increased soil cutting resistance, and increased soil chip thickness. All these three would result in the overall increase in resistance, which would manifest itself as increased torque requirements.

The predicted and measured torque requirement data obtained for this set tillage depth was also subjected to the two statistical tests (§5.3.2) in order to compare the degree of agreement between the measured and the predicted torque requirements. The results of the paired t-test and the least squares linear regression are presented in Table 6.14 and 6.16, and Figure 6.17. The paired t-test results indicated that the difference between the two sets of torque requirements data for this set tillage depth was statistically insignificant ($p > 0.05$).

Table 6.14: Paired t-test results for torque requirement for the 500 mm set tillage depth

	N	*Mean (kNm)*	*SD**	*SE Mean*
Model torque , kNm	65	1.796	1.407	0.174
Measured torque, kNm	65	1.792	1.458	0.181
Difference	65	0.0045	0.3358	0.0417
95 % CI for mean (-0.0787, 0.0877)				
T-Test for mean difference = 0 (vs not = 0): T-value = 0.11, p-value = 0.914				

The results of the least square linear regression (Table 6.15), between the measure and predicted torque requirements data, showed that the intercept was not significantly different from zero, while the slope was significantly different from 1. The regression analysis of the predicted and measured torque requirement data, for this set tillage depth, indicated some of the data sets (corresponding data) were outliers. Specifically, there were four pairs of data that fell outside the 95 % confidence interval (95 % CI, Figure 6.17). These points are identified in Table 6.15 under unusual observations.

Although the least square regression results for the model and measured torque requirements for this set tillage depth are inconclusive, it is noteworthy that the fitted and ideal line are difficult to separate visually. In addition, given that the intercept of the regression equation is not statistically different from zero, it can justifiably be concluded that the model gives a good approximation of the torque requirements for the experimental rotavator at this set depth of tillage. The significant difference from 1, of the slope of the regression line between the two sets of torque requirement data, for this set tillage depth predicted torque is probably due to the presence of outliers.

Table 6.15: Results of the least squares regression of the model generated torque requirements on the measured torque for 500 mm set tillage depth

The least-squares regression equation is: $T_{\mathrm{mod}}(kNm) = -0.0204 + 1.01 \bullet T_{meas}(kNm)$

Predictor	*Coef*	*SE Coef*	*T*	*P*
Constant	-0.0204	0.0684	-0.30	0.767
Measured, kNm	1.00885	0.03006	33.56	0.000

S = 0.338244 R^2 = 94.7 % $R^2_{adj} = 94.6\%$

Analysis of Variance

Source	*df*	*SS*	*MS*	*F*	*P*
Regression	1	128.86	128.86	1126.32	0.000
Residual Error	63	7.21	0.11		
Total	64	136.07			

Unusual observations

Observation	T_{meas}, kNm	T_{mod}, kNm	*Fit*	*SE Fit*	*Residual*	*SE Residual*
11	3.22	4.0094	3.2280	0.0599	0.7814	2.35R
12	3.24	4.2705	3.2521	0.0605	1.0184	3.06R
13	3.39	4.4363	3.3976	0.0636	1.0387	3.13R
14	3.61	4.5133	3.6215	0.0688	0.8898	2.69R

R denotes an observation with a large standardized residual

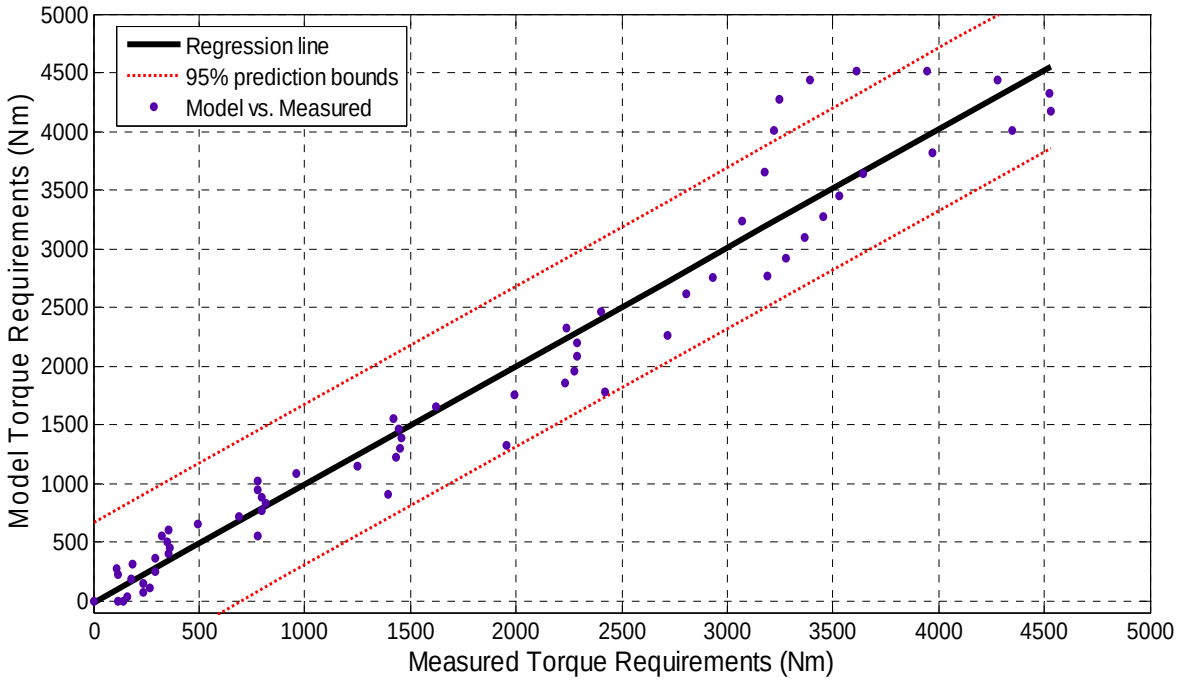

Figure 6.17: Results of the least squares linear regression of the predicted and measured torque requirements at different angular rotavator blade positions for 500 mm set tillage depth

6.6 Chapter Summary

In this chapter, the results of the field measurements and proposed model were presented. The field experiments indicated that the soil at the experimental site is sandy loam. The results also indicated that the soil strength properties could be satisfactorily characterized using the torsional shear apparatus.

Characterization of the deep-tilling experimental rotavator was only done for the down-cut direction of rotation. The results indicated that torque and power requirements as well as the specific energy increased with depth. On the generated forward thrust the results indicated that the magnitude of the thrust forces generated was dependent on the set tillage depth for a given rotavator configuration and operational conditions.

The torque requirements prediction model proposed on Chapter 3 was verified, validated and evaluated. The model was solved using a specially developed computer program, written in MATLAB. The model was validated and evaluated by comparing the

model generated and measured torque requirement data. Model validation was done for 250 mm, 350 mm and 500 mm set tillage depths by comparing the torque requirement values at chosen suitable rotavator blade angular positions from the horizontal position, during the soil cutting process. The results for the 250 mm and 350 mm set tillage depths were statistically different at the 0.05 level of significance for the paired t-test and the least squares regression, statistical tests. For the 500 mm set tillage depth, the paired t-test produced results that were not statistically different, while least square regression results produced inconclusive results at the 0.05 level of significance.

In general, it was observed that the graphs for the model and measured torque requirements for the three set tillage depths of 250 mm, 350 mm and 500 mm had similar shapes. However, some discrepancies in the measured torque requirement values at the same rotavator blade angular position were noted. The likely causes for the noted discrepancies could be the assumptions regarding the constancy of the soil dynamic and strength parameters used in the model; and the unsteady interaction between the soil-tool interface arising from tool-frame instability and the soil movement over the blade during the rotavator tillage operations.

CHAPTER 7

SUMMARY, CONCLUSIONS AND RECOMMENDATIONS

7.1 Summary

From literature, it was evident that no studies had been undertaken in the past that documented the performance of rotavators in deep tillage. In addition, the literature reviewed revealed that there are no analytical models for predicting the torque requirements of rotavators. There is also a lack of suitable research equipment and techniques for studying the performance of deep tilling rotavators, particularly under field conditions. This study was therefore designed to provide information on the performance of rotavators in deep tillage under field conditions, and to develop an analytical model capable of predicting the torque requirements. The predicted torque requirement is precursory for the prediction of power and specific energy requirement of rotavators.

In order to accomplish the research goals, two instrumented tool-frame carriers; one carrying an experimental deep-tilling rotavator and the other carrying the soil strength characterisation apparatus were developed. The tool-frame carrier, onto which the experimental rotavator was mounted, was instrumented for the measurement of the instantaneous tillage depth, the thrust or pull forces on the tractor three-point links, the angular position of the rotavator blade, the forward distance travelled and speed, the rotor rotational speed and the instantaneous rotavator blade torque requirements.

Soil strength characterisation and soil/steel frictional characteristics was facilitated by measuring the normal and shearing torque using a torsional shearing device fitted, alternatively, with a circular grouser head and a smooth circular flat steel plate. The recorded loads when the torsional shearing device was fitted with the circular grouser head and the circular plate, respectively, was used for the determination of the soil shear strength and soil-metal frictional parameters, respectively. For all field experiments, soil water content and the soil bulk density were also determined using standard procedures at different depth ranges.

A computerized data acquisition system (DAS), comprising the two instrumented tool-frame carriers, a eight-channel commercial data logger and a personal computer, was used to acquire the measured data under field conditions. The combination of the DAS and the instrumented tool-frame carrier used for soil characterisation enabled the measurement and recording of the normal, shear and frictional loads; and the storage of the measured data for the determination of the soil strength and friction parameters directly into the hard disk of a computer. Soil strength parameters are some of the inputs required by the proposed torque requirements analytical model. Using the same DAS and the tool-frame carrier onto which the rotavator was mounted, measurement of the rotavator torque requirements, the forces on the three tractor link points, the rotational speed of the rotor, the angular position of the rotavator blade, the forward distance travelled and the times was made. From the time-distance relation, the speed of tillage trial-test run was determined.

From literature, it was possible to modify existing models for passive blades and apply the basic soil-tool equilibrium analysis to develop an analytical model for predicting the torque requirements of a rotavator fitted with L-shaped blades. This possibility was based on the fact that, at an instantaneous time moment, the soil-tool interaction between the span of the L-shaped rotavator blade is similar to that of a passive tool when processing the soil. The modification effected considered the continually changing tillage depth of a rotavator blade and the changing rake angle of the blade, while processing the soil and the presence of the leg part of the blade.

Through field measurements, the performance of the experimental deep tilling rotavator was evaluated for different rotavator operational conditions. The performance was evaluated in terms of the variations in the magnitude of the resultant thrust force generated for different rotavator configuration and operational conditions; and the torque and power requirements, and the specific energy under the stated conditions.

Finally, the proposed analytical model and the computer program developed to solve it was verified and evaluated. The evaluation was done by comparing the experimental and model generated torque requirements for the same angular rotavator blade positions using appropriate statistical analyses and graphical presentation techniques.

Considering the inherent variability of both the soil water content and the soil bulk density under field conditions; and the fact that the experimental site was not conditioned prior to the experimentation, the torque requirements prediction results obtained are promising.

The study addressed the performance characteristics of the experimental rotavator for the 200 mm - 550 mm tillage depth range. The application of the model data proved that the adoption and modification of existing analytical models for passive blades produced a model that was capable of predicting the torque requirement of a down-cutting rotavator fitted with L-shaped blades. Based on the measured torque requirements and resultant horizontal thrust forces generated, it was possible to quantify the performance of the experimental deep tilling rotavator. The analysis of the thrust forces generated under different experimental conditions and rotavator configurations indicated the existence of an optimum depth, for each set of operational conditions. Consequently, all the study hypotheses postulated could not be rejected.

7.2 Conclusions

Based on the field experimental results for characterising the performance of the experimental deep tilling rotavator, and performance of the proposed analytical torque requirements prediction model, the following conclusions were drawn:

1. The field tests undertaken with the soil characterisation apparatus for the determination of soil strength parameters produced acceptable results. The apparatus could therefore be used confidently for the determination of the soil shear strength and soil-metal friction parameters required by the proposed torque requirements prediction model.

2. The instrumented tool-frame carrier, onto which the experimental deep-tilling rotavator was mounted, is suitable for studying the performance of rotavators for a wide range of set tillage depths. In combination with the computerized DAS, this tool-frame carrier provided a suitable means for acquiring all the pertinent data necessary for characterising the experimental deep tilling rotavator. In

particular the ability of the DAS to accurately acquire the measured data at a frequency of 2.4 kHz suits it for the measurement of the instantaneous rotavator blade angular position and torque data, which can be problematic if the systems used cannot record data at frequencies in excess of 2 kHz.

3. The accuracy of the measured data recorded using the computerised DAS from the two tool-frame carriers together with the measured soil bulk density is adequate as model inputs for the prediction of soil-tool interaction resistance forces and the prediction of torque requirements for a rotavator fitted with L-shaped blades.

4. The soil bulk density and the soil water content at the experimental site significantly changed with depth from the soil surface. The soil water content increased with depth while bulk density decreased.

5. Since the soil shear strength and the soil-metal frictional characteristics are affected by the soil water content, the use of fixed values for these parameters, as model inputs introduced some error.

6. The magnitude and variations of the resultant forward thrust force generated for a down-cut tillage operation depended on bite length, set tillage depth, and the kinematic parameter, λ. Therefore, the rotavator configuration and operational parameters must be controlled precisely in order to realize and maintain the desirable resultant thrust force for a down-cut rotavator.

7. There exist a unique depth for each rotavator configuration and operational condition at which the thrust force generated is greatest. This depth is influenced by the bite length, and decreased as the bite length is increased. Therefore the realisation and maintenance of the maximum forward thrust generation, where required, can only be realised by strictly operating a rotavator at the correct set tillage depth for a given set of rotavator configuration and operational conditions.

8. In general, the specific energy requirements of the rotavator increased with increment in both the set tillage depth and bite length. However, bite length had a greater influence on the specific energy requirements than the set tillage depth. Therefore, operating a down-cutting rotavator at greater bite lengths, even at relatively shallow set tillage depths required excessive energy, and hence excessive input power requirements than operations done at relatively deeper set tillage depths at lower values of the bite length.

9. The computer program developed for solving the proposed analytical torque requirements model, accurately generated the path followed by the tip of the rotavator blade, the blade leg length and blade span in contact with the soil, the location of the centre of the rotor as the soil processing by a blade progressed, and torque requirement values at specified angular rotavator blade positions.

10. Based on the statistical and visual evaluation, effected between the measured and predicted torque requirements data, the proposed model generated acceptable torque requirements at selected rotavator blade angular positions for a rotavator fitted with L-shaped blades when operated in the concurrent (down-cut) direction.

7.3 Recommendations

The following recommendations based on findings of this study are made for possible future studies on rotavators in deep tillage:

1. Only the L-shaped blade was used with the experimental deep-tilling rotavator, characterised in this study. The other types of blades, particularly those currently used in the Asian sub-continent should also be tested for deep rotavator tillage. The performance results of the experimental deep-tilling rotavator, when fitted with different types of blades can, thereafter be compared and the blade type(s) with better performance characteristics recommended.

2. There is need to develop a method for measuring only the torque required by the blade for the processing of the soil, that does not involve the use of the Torque Arm. The torque requirements measured by the approach used in this study, included the torque required to overcome the hydraulic motor parasitic forces and the inherent friction forces in the rotavator assembly. The parasitic torque component was considered to be responsible for the non-zero torque requirements recorded when there was no blade processing the soil during the trial test-runs.

3. There may be a need to undertake similar studies in a conditioned soil to avoid the variations noted in the measured torque requirements and the resultant push/pull forces. These variations were difficult to explain, particularly when they occurred between subsequent blade cuttings within a test-run block. Soil conditioning of the experimental site should result in the creation of a uniform condition within the experimental site. This would reduce the variations of the differences in the magnitudes of both the rotavator torque requirements and the thrust forces generated for different blade cuttings for a set tillage depth within a test-run block. This would result in a more realistic performance characterisation of the experimental deep-tilling rotavator.

4. The tool-frame carrier on which the rotavator is mounted should be adjusted to ensure that the magnitude of the thrust forces on the lower left and lower right links are balanced. The imbalance noted in the data recorded for these two links, was suspected to be the cause of the instability of this tool-frame carrier, particularly during field test-run for set tillage depths beyond 350 mm.

5. The application of the proposed rotavator torque prediction model required the availability of accurate soil dynamic, soil/steel frictional and soil strength parameters. The collection and processing of such data for the determination of these parameters was laborious and time consuming. Therefore, better experimental techniques and faster data processing methods should be developed. This can be achieved by employing real-time methods for the

determination of the soil water content and soil bulk density; and developing computer program modules that would read and process the data immediately upon the completion of an experiment.

6. Some rotavator performance characteristics, such as the effect of the operational conditions and rotavator configuration on the ridge heights at the bottom of the tilled furrow, were not evaluated. An additional computer program module should be developed, and integrated with computer program developed for solving the proposed rotavator torque requirements prediction model, to evaluate the effect of rotavator kinematics on the irregularities produced at the bottom of the cut furrow for different configurations and values of kinematic parameter, λ. The bottom-of-the furrow irregularity produced by rotavators are important performance indicators for rotavator tillage, but was not evaluated in this study deep rotavator tillage.

7. The tool-frame carrier, onto which the rotavator was mounted, should be used to study the performance of alternative experimental rotavators with different radii, and blade configurations, and number of blades on the same side of the flange; and assess their performance characteristics in the concurrent (down-cut) direction of rotation. This may lead to the optimization of the performance characteristics of the down-cutting rotavator in deep tillage.

8. The proposed analytical model should serve as a basis for the development of improved models for predicting the performance of down-cutting rotavators fitted with L-shaped blades. Modifications can also be made in the current model to develop a torque requirements prediction model for the up-cut (reverse) direction of rotation for rotavators fitted with the same type of blades. The model can also serve as a basis for developing torque predictions models for the types of rotavator blades.

9. Although preliminary observations made ruled out further investigations of the performance characteristics of the experimental rotavator, when operated in the

reverse direction of rotation, studies should be undertaken to evaluate both the torque requirements and the generation of thrust forces in this tillage direction. Additional investigation for this direction of rotation of the rotavator should include an investigation of the tool's soil amendment materials mixing, and the mixing of tilled soil from different soil depth ranges.

LIST OF REFERENCES

Anonymous. California trenching and shoring manual (CTSM) Chapter 4: Earth pressure theory and application. Retrieved 27th Nov. 2004, from the World Wide Web: http://www.dot.ca.gov/hq/esc/construction/Maual/TrenchingandShoring/ch4_earth.pdf.

Aref, K. S., W. J. Chancellor and D. R. Nielson. 1975. Dynamic shear strength properties of unsaturated soils. *Transactions of the ASAE,* 18: 818 – 823.

ASAE 1994. *ASAE Monograph No. 12*. Pamela De Vore-Hansen Ed. American Society of Agricultural Engineers, 2950 Niles Road, St Joseph, Michigan, USA.

ASAE Standards. 2000. *ASAE Standards* (47th Ed.). ASAE EP291.2 DEC98: Terminology and definitions for soil tillage and soil-tool relationships. American Society of Agricultural Engineers. St. Joseph, Mich. USA.

Ayers, P. D. 1987. Moisture and bulk density effects on soil shear strength parameters for coarse grained soils. *Transactions of the ASAE,* 31: pp. 1282–1287.

Azyamova, E. N. 1963. Studies of dynamics of deformation of soil. Trudy (TSNIIMESKH) Minsk 1:131-139. (Translated by W.R. Gill, National Tillage Machinery Laboratory, USDA-ARS, Auburn, AL).

Bailey, A. C. and J. A. Weber. 1965 : Comparison of methods of measuring soil shear strength using artificial soils. Trans. ASAE 8(2), 153-156,

Baloch, J. M., S. B. Bukhari., J. Kilgour and A.Q.A. Mughal. 1986. Performance of power tiller blades. *Agricultural Mechanisation in Asia, Africa and Latin America*, 17(1):22 – 26.

Bardet, J. 1997. *Experimental Soil Mechanics*. Prentice Hall. ISBN: 0133749355.

Beeny, J. M. and D. J Greig. 1965. The efficiency of a rotary cultivator. *Journal of Agricultural Engineering Research*, 10(1):5 – 12.

Beeny, J. N. 1973. Rotary cultivation of wet land-comparison of blade shapes. *Journal of Agricultural Engineering Research*, 18(3):224 – 251.

Beeny, J. N. and D.C.P Khoo. 1970. Preliminary investigations into the performance of different shaped blades for rotary tillage of wet rice soil. *Journal of Agricultural Engineering Research*, 15(1):27 – 33.

Bentley, J. P. 1995. *Principles of measurement systems.* Longman Scientific & Technical, Longman Group UK Limited.

Bernacki, H., J. Haman and Cz. Kanafojski. 1972. *Agricultural machines, theory and construction*. US Department of Commerce, National Technical Information Service, Springfield, Virginia 22151.

Bosoi, E. S., O. V. Verniev, I. I. Smirnov and E. G. Sultan-Shakh. 1988. *Theory construction and calculations of agricultural machine. Volume* 1. Russian Translation series 66. A.A. Balkema Rotterdam.

Bukhari, K. H., S. Bukhari, M. M. Leghari and M. S. Memon. 1996. The effect of speed and rear shield on the performance of rotary tiller. *Agricultural Mechanization in Asia, Africa and Latin America* 27(2):9 - 14.

Butterfield, R. and K. Z. Andrawes. 1972. On the angles of friction between sand and plane surfaces. *Journal of Terramechanics*, 8(4): 15 – 23.

Camp, C. R and W. R. Gill. 1969. The effect of drying on soil strength parameters. Soil Sci. Am. Proc. 33: 641 – 644.

Chamen, W. C. T., R. E. Cope and D. E. Patterson. 1979. Development and performance of a high output rotary digger. *Journal of Agricultural Engineering Research* 24: 301 – 308.

Chancellor, W. J. 1994. Chapter 2 - Soil physical properties. In: *Advances in Soil Dynamics Volume 1*. ASAE Monograph Number 12.

Chancellor, W. J. and J. A. Vomicil. 1971. The relation of moisture content to failure strength of seven agricultural soils. *Transactions of the ASAE,* 13(1): 9 – 13, 17

Chi, L. and R. L. Kushwaha. 1989. Finite element analysis of forces on a plane soil blade. *Canadian Agricultural Engineering* 31(2): 135 – 140.

Chi, L. and R. L. Kushwaha. 1990. A nonlinear 3-D finite element analysis of soil failure for tillage tools. *Journal of Terramechanics* 27(4):343 – 366.

Chi, L. and R. L. Kushwaha. 1991a. Finite element analysis of forces on two shapes tillage tools. *Canadian Agricultural Engineering* 33(1): 39 – 45.

Chi, L. and R.L. Kushwaha. 1991b. Three-dimensional, finite element interaction between soil and simple tillage tool. *Transactions of the ASAE,* 34(2): 361-366.

Destan, M. F. and K. Houmy. 1990. Effects of design and kinematic parameters of rotary cultivators on soil structure. *Soil & Tillage Research*, 17 (1990): 291 – 301.

Doebelin, E. O. 2004. *Measurement systems. Applications and design*. 5th Edition. Tata McGraw-Hill Publishing. ISBN 0-07-058203-3.

du Plessis, H. L. M. 2004. Personal communication. Department of Civil and Biosystems Engineering, University of Pretoria, Pretoria, South Africa.

El-Domiaty, A. M. and W. J. Chancellor. 1970. Stress-strain characteristics of a saturated clay soil at various rates of strain. *Transactions of the ASAE,* 13: 685 – 689.

Erbach, D. C. 1987. Measurement of soil bulk density and moisture. *Transactions of the ASAE,* 30(4):922 – 932.

Fielke, J. M. 1999. Finite element modelling of the interaction of the cutting edge of tillage implements with soil. *Journal of Agricultural Engineering Research* 74: 91-101

Fleniken, J. M, R. E. Hefner and J. A. Weber. 1977. Dynamic soil strength parameters from unconfined compression tests. *Transactions of the ASAE,* 20: 21 – 29.

Gardner, W. H. 1986. Water Content. In *Methods of soil analysis, Part I. Physical and Mineralogical Methods*, 2nd Ed., ed. A Klute, 493 – 544. Madison, Wis.: American Society of Agronomy.

Ghosh, B. N. 1967. The power requirement of a rotary cultivator. *J. Agric. Eng. Res.* 12(1): 5 – 12.

Gill, W. R. and G. E. Vanden Berg. 1967. *Soil dynamics in tillage and traction*. Agricultural Handbook No. 316. Washington D.C., US GPO.

Girma, G. 1989. Measurement and prediction of forces on plough bodies. I – Measurement of forces and soil dynamic parameters. *Proceedings of the Eleventh International Congress on Agricultural Engineering*. Dublin, Sept. 4 – 9, pp 1539 – 1546.

Gitau, A. N., Gumbe, L. O. and Biamah E. K. (2006). Influence of soil water on stress strain behaviour of a compacting soil in semi-arid Kenya. Soil and Tillage Res. 89 (2006): 144 – 154.

Glancey, J. L., S. K. Upadhyaya, W. J. Chancellor and J. W. Rumsey. 1996. Prediction of agricultural implement draft using an instrumented analog tillage tool. *Soil and Tillage Research,* 37: 47 – 65.

Godwin, R. J. and M. J. O'Dogherty. 2006. Integrated soil tillage force prediction models. *Journal of Terramechanics*, 44: 3 – 14.

Godwin, R. J., Spoor, G., 1977. Soil failure with narrow tine. *Journal of Agricultural Engineering Research*. 22(3): 213 – 228.

Goering, C. E. 1992. *Engine and tractor power*. ASAE Textbook No. 3. American Society of Agricultural Engineers 2950 Niles Road, St Joseph, Michigan, USA.

Grisso, R. D. and J. V. Perumpal. 1985. Review of Models for Predicting Performance of Narrow Tillage Tools. *Transactions of the ASAE*, 28(4): 1062 – 1067.

Gupta, C. P., and R. Visvanathan. 1993a. Dynamic behaviour of saturated soil under impact loading. *Transactions of the ASAE*, 36(4): 1001 – 1007.

Gupta, C. P., and R. Visvanathan. 1993b. Power requirements of a rotary tiller in saturated soil. *Transactions of the ASAE*, 36(4): 1009 – 1012.

Hendrick, J. G. 1980. A rotary chisel. *Transactions of the ASAE,* pp 1349 – 1352.

Hendrick, J. G. and A. C. Bailey. 1982. Determining components of soil-metal friction sliding resistance. *Transactions of the ASAE,* 25(4): 845 – 849

Hendrick, J. G. and W. R. Gill. 1978. Rotary tiller design parameters, V: Kinematics. *Transactions of the ASAE*, 21(4): 658 – 660.

Hendrick, J.G. and W.R. Gill. 1971a. Rotary tiller design parameters: Part I - Direction of rotation. *Transactions of the ASAE,* 14(4): 669-674, 683.

Hendrick, J.G. and W.R. Gill. 1971b. Rotary tiller design parameters: Part II – Depth of tillage. *Transactions of the ASAE,* 14(4): 675-678.

Hendrick, J.G. and W.R. Gill. 1974. Rotary tiller design parameters: Part IV – blade clearance angle. *Transactions of the ASAE,* 17(1): 4 – 7.

Hendrick, J.G. and W.R. Gill. 1976. The irregularities of soil disturbance depth by circular and rotating tillage tools. *Transactions of the ASAE,* 19(2): 230– 233.

Hendrick, J.G. and W.R. Gill. 197lc. Rotary tiller design parameters: Part III-Ratio of peripheral and forward velocities. *Transactions of the ASAE,* 14(4): 679 – 683

Hettiaratchi, D.R.P. and A.R. Reece. 1967. Symmetrical three-dimensional soil failure. *Journal of Terramechanics* 4(3): 45-67.

Hettiaratchi, D.R.P. and A.R. Reece. 1974. The calculation of passive soil resistance. *Geotechnique* 24(3): 289-310.

Hettiaratchi, D.R.P., B.D. Witney and A.R. Reece. 1966. The calculation of passive pressure in two dimensional soil failure. *Journal of Agricultural Engineering Research* 11(2): 89-107.

Hillel, D. 1980. *Fundamentals of Soil Physics 1st Ed.* New York, NY: Academic Press, Inc.

Hottinger Baldwin Messtechik. 1999. *Spider8 operating manual*. PC measurement electronics, Spider8 and Spider8-30. HBM Mess-und Systemtechnik GmbH, Germany

Hryciw, R. D., S. A. Raschke, A. M. Ghalib, D. A. Horner and J. F. Peters. 1997. Videotracking for experimental validation of discrete element simulations of large discontinuous deformations. *Computer and Geotechnics*. 21(3): 235-253.

Johns, R. A. 2000. *Probability and statistics for engineers*. Pearson Education. ISBN 81-780-529-1.

Johnson, C. E., R. D. Grisso, T. A. Nichols and A. C. Bailey. 1987. Shear measurement of agricultural soil – a review. *Transaction of the ASAE,* 30(4):935 – 938.

Karmakar, S. and R. L. Kushwaha. 2005a. Simulation of soil deformation around a tillage tool using computational fluid dynamics. *Transactions of the ASAE,* 48(3): 923 – 932.

Karmakar, S. and R. L. Kushwaha. 2005b. CFD Simulation of soil forces on a flat tillage tool. ASABE paper No. 051160. St Joseph, ASABE.

Kataoka, T. and S. Shibusawa. 2002. Soil-blade dynamics in up-cut-rotational rotary tillage. *Journal of Terramechanics*, 39(2002): 95 – 113.

Kataoka, T., K. Onodera, S. Shibusawa and Y. Ota,. 1998. Layer mixing of different blades of reverse-rotational rotary tiller. *Proceedings of the 5th Asia-Pacific Regional Conference of the ISTVS,* Seoul Korea, October 20 – 21, pp 233 – 240.

Kataoka, T., K. Onodera, S. Shibusawa and Y. Ota. 1995. A model for backward throwing of sliced soil clods by a reverse-rotational rotary tiller using rigid body kinetics. *Proceedings of the 4th Asia-Pacific Regional Conference of the ISTVS,* Okinawa, Japan, November 20 – 21, pp 339 – 346.

Katsygin, V. V. 1964. Relation of draft of agricultural machines to operation speeds. *Voprosy Sel'skohozyaistvennoi Mekhaniki*, Section 2, 96-119, Vol. XII. (Translated by W.R. Gill, National Tillage Machinery Laboratory, USDA-ARS, Auburn, AL).

Kepner, R. A., R. Bainer and E. L. Barger. 1978. *Principles of farm machinery*. Westport, Conn.: AVI Publishing Inc.

Khat, L. R., V. M. Salokhe and H. Jayasuriva. 2005. Experimental validation of distinct element simulation for dynamic wheel-soil interaction. ASAE Paper No. 053120. Presented in Annual International Meeting, 17-20 July, 2005, Tampa Convocation Center, Tampa, Florida, USA.

Kinzel, G. L., R. Holmes and S. Huber. 1981. Computer graphics analysis of rotary tillers. *Transactions of the ASAE,* 1392 – 1395 & 1399.

Koolen, A. J. and H. Kuipers. 1983. *Agricultural soil mechanics*. Spinger-Verlag. ISBN 3-540-12257-5.

Kuipers, H. and B. Kroesbergen. 1966. The significance of moisture content, pore space, method of sample preparation and type of shear annulus use on laboratory torsional shear testing of soil. *Journal of Terramechanics*, 3(4): 17 – 28.

Kushwaha, R. L. and J. Shen. 1995. Finite element analysis of the dynamic interaction between soil and tillage tool. *Transactions of the ASAE,* 37(5): 1315-1319.

Kushwaha, R. L., L. Chi and J. Shen. 1993. Analytical and numerical models for predicting soil forces on narrow tillage tools – A review. *Canadian Agricultural Engineering*, 35(3): 184 – 193.

Lambe, T. W. 1951. *Soil testing for civil engineers*. John Wiley & Sons. ISBN 0-471-51183-8.

Lee, K. S., S. H. Park, W. Y. Park and C. S. Lee. 2003. Strip tillage characteristics of rotary tiller blades for use in a dryland direct rice seeder. *Soil & Tillage Research* 71(2003): 25 – 32.

Levine, D. M., P. Ramsey and R. Smidt. 2000. *Applied statistics for engineers and scientists: using Microsoft Excel & Minitab*. Prentice Hall. ISBN**:** 0134888014

Mandal, J. N. and D.G ***Divshikar. 1994****. Soil testing in civil engineering*. India Book House Limited. ISBN**:** 8120409035

Manian, R. and K. Kathirvel. 2001. Development and evaluation of an active-passive tillage machine. *Agricultural Mechanization in Asia, Africa and Latin America*, 32(1): 9 – 18.

Marenya, M. O. and H. L. M. du Plessis. 2006. Torque Requirements and Forces Generated by a Deep Tilling Down-Cut Rotary Tiller. ASABE Paper No. 061096. St Joseph, Michigan, USA.

Marenya, M. O., H. L. M. du Plessis and N. G. Musonda. 2003. Theoretical force and power prediction models for rotary tillers – a review. *Journal of Engineering in Agriculture and the Environment* 3(1): 1 – 10.

Marenya M. O. and G. O. Nyakiti. 2000. Compaction of acrisols as influenced by incorporation of fresh sugarcane factory filter-press mud. *Agricultural Engineering in South Africa*, Vol 31 No. 1 pp 56 – 61.

McKyes, E. 1989. *Agricultural engineering soil mechanics*. Developments in Agricultural Engineering 10. Elsevier Publishing Co.

McKyes, E., 1985. In: *Soil Cutting and Tillage*, Elsevier, Amsterdam, the Netherlands, p. 217.

McKyes, E. and Ali, O.S., 1977. The cutting of soil by narrow blades. *Journal of Terramechanics.* 14 2, pp. 43–58

Meyerhof, G. G. 1951. The ultimate bearing capacity of foundations. *Geotechnique* 2: pp 301 – 332.

Misczak, M., 2005. A torque evaluation for a rotary subsoiler. *Soil & Tillage Research.* 84(2): 178-183.

Meriam, J. L and L. G. Kraige. 1987. Engineering mechanics: dynamics, Volume 2. John Wiley & Sons. ISBN: 13-978-0471 739 319.

Montgomery, D. C. and G. C. Runger. 2003. *Applied probability and statistics for engineers*. 3rd Edition. John Wiley & Sons, Inc.

Mouazen, A. M. and H. Ramon. 2002. A numerical–statistical hybrid modelling scheme for evaluation of draught requirements of a subsoiler cutting a sandy loam soil, as affected by moisture content, bulk density and depth, *Soil Tillage Research* 63 (2002), pp. 155–165.

Mouazen, A. M. and M. Nemenyi. 1999. Finite element analysis of subsoiler cutting in non-homogeneous sandy loam soil. *Soil & Tillage Research* 51: 1-15.

Neal, M. S. 1966. Friction and adhesion between soil and rubber. *Journal of Agricultural Engineering Research*, 12(1): 83 – 87.

O'Callaghan, J. R. and K. M. Farrelly. 1964. Cleavage of soil by tined implements. *Journal of Agricultural Engineering Research*. 9 (3): 259–270.

Olsen, H. J. 1984. A torsional shearing device for field tests. *Soil &Tillage Research* 4(6):599 – 611.

Osman, J. S. 1964. The mechanics of soil cutting blades. *Journal of Agricultural Engineering Research*. 9(4): 313 – 328.

Owende, P. M. O. and S. M. Ward. 1996. Characteristic loading of light mouldboard ploughs at slow speed. *Journal of Terramechanics*, 33 (1):29-53

Payne, P. C. J. 1956. The relationship between the mechanical properties of soil and the performance of simple cultivation implements. *Journal of Agricultural Engineering Research* 1(1): 23-50.

Payne, P. C. J. and D.W. Tanner. 1959. The relationship between rake angle and the performance of simple cultivation implements. *Journal of Agricultural Engineering Research* 4(4): 312-325.

Perumpal, J. V., R. D. Grisso and C. S. Desai. 1983. A Soil-Tool Model Based on Limit Equilibrium Analysis. *Transactions of the ASAE*, 26(4): 991 – 995.

Prasad, J. 1996. A comparison between a rotavator and conventional tillage equipment for wheat-soybean rotations on a vertisol in Central India. *Soil & Tillage Research*, 37 (1996): 191 – 199.

Raper, R. L. 2000. The influence of implement type, and tillage timing on residue burial. *Transaction of the ASAE,* 45(5):1281 – 186.

Reece, A. R. 1965. The fundamental equation of earth-moving mechanics. In: *Symposium on Earth Moving MachineryProc. Inst. Mech. Eng.* 179, pp. 16–22.

Robinson, D. H., R. L. Schafer, and C. E. Johnson. 1988. Minimizing tillage energy due to sliding resistance. *ASAE Paper No. 87-1580. St Joseph, Michigan: ASAE.*

Romig, B. E. 1971. Performance of rotary tiller blades. *Transactions of the ASAE*, 14(1): 10 -13.

Ros, V., R. J. Smith, S. J. Marley and D. C. Erbach. 1995. Mathematical modeling and computer-aided design of passive tools. *Transaction of the ASAE,* 38(3):675 – 683.

Salokhe, V. M. and N. Ramalingam. 2001. Effects of direction of rotary tiller on properties of Bangkok clay soil. *Soil & Tillage Research*, 63(1): 64 – 74.

Salokhe, V. M., M. Hanif and M. Hoki. 1993. Effect of blade type on power requirement and puddling quality of a rotavator in wet clay. *Journal of Terramechanics*, 30(5): 337 – 350.

Schafer, R. L., C. W. Bockop and W. G. Lovely. 1963. Vane and torsion for measuring soil shear strength. *Transactions of the ASAE*: 57 – 59.

Schjønning, P. 1986. Shear strength determination in undisturbed soil at controlled water potential. *Soil & Tillage Research,* 8 (1986):171 – 179.

Shen, J and L. R. Kushwaha. 1998. *Soil–Machine Interaction: a Finite Element Perspective*, Marcel Dekker Inc., New York. USA.

Shibusawa, S. 1993. Reverse-rotational rotary tiller for reduced power requirements in deep tillage. *Journal of Terramechanics,* 30(3): 205 – 217.

Shinners, K. J., J. M. Wilkes and T. D. England. 1993. Performance characteristics of tillage machine with active-passive components. *Journal of Agricultural Engineering Research*, 55: 277 – 297.

Sineokov, G. N. and I. M. Panov. 1978. *Theory and calculation of soil working machines*. Translated for the U.S Department of Agriculture, Agricultural Research Service and the National Science Foundation, Washington D.C.

Smith, J. L. 1964. *Strength-moisture relations of fine-grained soil in vehicle mobility research*. U.S. Army Engineers Waterways Experiment Station, Technical Report No. 3 - 636. Vicksburg, MS.

Spoor, G and R. J. Godwin. 1978. An experimental investigation into the deep loosening of soil by rigid tines. J. Agric. Eng. Res. 23(3): 243 – 258.

Spoor, G. and R. J. Godwin. 1979. Soil deformation and shear strength characteristics of some clay soils at different soil moisture content. *Journal of Soil Science,* 30: 483 – 498.

Srivastava, A. K., C. E. Goering and R. P. Rőhrbach. 1993. *Engineering principles of agricultural machines*. ASAE Textbook No. 6. American Society of Agricultural Engineers 2950 Niles Road, St Joseph, Michigan, USA.

Stafford, J. V. 1979. The performance of rigid tine in relation to soil properties and speed. *Journal of Agricultural Engineering Research* 24(1): 41-56.

Stafford, J. V. and D. W. Tanner. 1977. The frictional characteristics of steel sliding on soil. *Journal of Soil Science*, 28: 541 – 553.

Stafford, J. V. and D. W. Tanner. 1983b. Effect of rate on soil shear strength and soil-metal friction. II. Soil-metal friction. *Soil & Tillage Research*, 3(4): 321 – 330.

Stafford, J. V. and D. W. Turner. 1983a. Effect of rate on soil shear strength and soil-metal friction. I. Shear Strength. *Soil and Tillage Research,* 3(3): 245 – 260.

Terzaghi, K. 1959. *Theoretical soil mechanics.* John Wiley and Sons, Inc. New York.

Thakur, T. C. and R. J. Godwin. 1989. The present state of force prediction models for rotary powered tillage tools. *Journal of Terramechanics.* 27(2):121 – 138.

Thakur, T. C. and R. J. Godwin, 1990. The mechanics of cutting by a rotating wire. *Journal of Terramechanics.* 27(4):291 – 305.

Vetrov, Y. A. and V. P. Stanevski. 1972. The investigation of the factors of the speed of cutting soils. *Mining Construction and Highway Machines* 8: 21-26. Translated by W.R. Gill, National Tillage Machinery Laboratory, Auburn, AL.

Walters, T. and R. Owen. 1996. *A collection of technical formulae*. 8th English Edition. Giek Verlag, D – 82110, Germering.

Wells, L. G. and O. Treesuwan. 1978. The response of soil strength indices to changing water content and bulk density. *Transactions of the ASAE:* 854 – 861.

Yong, R. N. and A.W. Hanna. 1977. Finite element analysis of plane soil cutting. *Journal of Terramechanics* 14(3): 103-125.

Zeng, D. and Y. Yao. 1992. A dynamic model for soil cutting by blade and tine. *Journal of Terramechanics* 29(3): 317-327.

Zhang, J. and R. L. Kushwaha. 1995. A modified model to predict soil cutting resistance. Soil and Tillage Res. 34: 157 – 168.

Zhang, Z. X. and R. L. Kushwaha. 1999. Operating speed effect on the advancing soil failure zone in tillage operation. *Canadian Agricultural Engineering* 41(2): 87-92.